

DEVELOPMENT OF FLUORINATED RHODACYANINE ANALOGUES FOR ANTI-  
LEISHMANIASIS



A Thesis Submitted in Partial Fulfillment of the Requirements  
for the Degree of Master of Science in Chemistry  
Department of Chemistry  
Faculty of Science  
Chulalongkorn University  
Academic Year 2019  
Copyright of Chulalongkorn University

การพัฒนาสารกลุ่มโรตาไฮยานีนที่มีฟลูออรีนสำหรับการต้านโรคลิซมาเนีย



วิทยานิพนธ์นี้เป็นส่วนหนึ่งของการศึกษาตามหลักสูตรปริญญาวิทยาศาสตรมหาบัณฑิต  
สาขาวิชาเคมี ภาควิชาเคมี  
คณะวิทยาศาสตร์ จุฬาลงกรณ์มหาวิทยาลัย  
ปีการศึกษา 2562  
ลิขสิทธิ์ของจุฬาลงกรณ์มหาวิทยาลัย



ฐิติยา ลาสิงห์ : การพัฒนาสารกลุ่มโรดาไซยานินที่มีฟลูออรีนสำหรับการต้านโรคไลชมาเนีย. ( DEVELOPMENT OF FLUORINATED RHODACYANINE ANALOGUES FOR ANTI-LEISHMANIASIS) อ.ที่ปรึกษาหลัก : อ. ดร.ธนธรณ์ ขอทวีวัฒนา, อ.ที่ปรึกษาร่วม : ศ. ดร.ธีรยุทธ วิไลวัลย์

เมื่อไม่นานมานี้มีการรายงานว่าโรดาไซยานินที่มีฟลูออรีนมีประสิทธิภาพในการยับยั้งเชื้อไลชมาเนียสปีชีส์ *Leishmania donovani* จากรายงานพบว่าการแทนที่อะตอมไฮโดรเจนด้วยอะตอมฟลูออรีนเพียง 1 อะตอมบนวงเบนโซโทเอโซลส่งผลต่อฤทธิ์การยับยั้งเชื้อไลชมาเนียอย่างมีนัยสำคัญ อย่างไรก็ตาม ยังไม่พบว่ามี การรายงานถึงบทบาทของหมู่แทนที่ที่มีฟลูออรีนในสารกลุ่มนี้และที่สำคัญคือกลไกการออกฤทธิ์ของสารกลุ่มนี้ยังไม่ได้รับการศึกษา ดังนั้นในงานวิจัยนี้ สารกลุ่มโรดาไซยานินที่มีฟลูออรีนซึ่งประกอบไปด้วยสารใหม่จำนวน 15 ชนิดและสารที่ถูกรายงานแล้วจำนวน 3 ชนิด (10c และ 11a-11q) ถูกนำไปทดสอบฤทธิ์ต้านเชื้อไลชมาเนียระยะ promastigote และระยะ axenic amastigote ซึ่งสปีชีส์ *L. martiniquensis* และ *L. orientalis* เป็นสปีชีส์ที่ พบมากในประเทศไทย จากผลการศึกษาความสัมพันธ์ระหว่างการออกฤทธิ์และโครงสร้างของสารกลุ่มนี้ (SAR) การแทนที่ด้วยอะตอมฟลูออรีนที่คาร์บอนตำแหน่งที่ 5 6 5' และ 6' บนวงเบนโซโทเอโซลส่งผลให้การยับยั้งเชื้อ ชนิดนี้มีประสิทธิภาพมากขึ้นอย่างมีนัยสำคัญ ซึ่งมีความสัมพันธ์กับคุณสมบัติทางเคมีไฟฟ้าโดยพบว่าสารที่มีฤทธิ์ การยับยั้งที่มีประสิทธิภาพจะมีความสามารถในการเกิดปฏิกิริยารีดักชัน (ปฏิกิริยาการรับอิเล็กตรอน) ได้ดีด้วย เช่นกัน แต่เมื่อสารกลุ่มนี้ถูกแทนที่ด้วยหมู่  $-CF_3$  และ  $-OCF_3$  ส่งผลให้ฤทธิ์การยับยั้งเชื้อลดลงอย่างชัดเจน เหตุที่ เป็นเช่นนี้สามารถอธิบายได้ด้วยการทำนายสมบัติทางยาโดยใช้โปรแกรมทางคอมพิวเตอร์ (ADMET) แสดงให้เห็น ว่าสารดังกล่าวมีความสามารถในการละลายน้ำต่ำกว่าสารอื่น ๆ จากกลุ่มเดียวกัน จึงส่งผลต่อฤทธิ์การยับยั้งเชื้อลิ ชมาเนียที่ไม่ดีนัก ถึงแม้ว่าสารกลุ่มนี้จะสามารถทนทานต่อการเกิดเมตาบอลิซึมจากไมโครโซมในตับของมนุษย์ ได้ไม่มากนัก แต่จากการทำนายคุณสมบัติทางยาอื่น ๆ พบว่าสารกลุ่มนี้มีความเป็นไปได้ที่จะพัฒนาเป็นยากินและยัง ไปกว่านั้น จากการทำนายสมบัติทางยาโดยใช้โปรแกรมคอมพิวเตอร์พบว่าสารกลุ่มนี้อาจมีความสามารถต่อการ ต้านเชื้อไลชมาเนียที่เกี่ยวกับสมองหรือโรคทางระบบประสาทอื่นได้อีกด้วย ทั้งนี้ข้อมูลที่ได้จากงานวิจัยนี้สามารถ นำไปใช้เป็นความรู้เบื้องต้นต่อการพัฒนาสารกลุ่มโรดาไซยานินสำหรับใช้เป็นยาในการรักษาโรคไลชมาเนียในอนาคต ต่อไป

สาขาวิชา เคมี  
ปีการศึกษา 2562

ลายมือชื่อนิสิต .....  
ลายมือชื่อ อ.ที่ปรึกษาหลัก .....  
ลายมือชื่อ อ.ที่ปรึกษาร่วม .....

# # 6071928823 : MAJOR CHEMISTRY

KEYWORD: anti-leishmanial activity, drug discovery, fluorine, rhodacyanine

Thitiya Lasing : DEVELOPMENT OF FLUORINATED RHODACYANINE ANALOGUES FOR ANTI-LEISHMANIASIS. Advisor: Dr. Tanatorn Khotavivattana, Ph.D. Co-advisor: Prof. Dr. TIRAYUT VILAVAN, Ph.D.

Recently, fluorinated rhodacyanine has been disclosed as a highly effective agent against *Leishmania donovani*; it was shown that replacement of hydrogen with a fluorine atom on a benzothiazole unit significantly enhanced the anti-leishmanial activity. However, the role of the fluorine substituent in this analogue has not yet been clarified and mechanism of actions remains unclear. In this research, fifteen novel and three known fluorine-containing rhodacyanine analogues (10c, and 11a-11q) were synthesized and tested the anti-leishmanial activity against promastigote and axenic amastigote stages of *L. martiniquensis* and *L. orientalis*, the indigenous *Leishmania* species of Thailand. The SAR knowledge of this series reveals that the introduction of fluorine atom(s) at different positions on the benzothiazole units, including C-5, 6, 5', or 6', led to enhance the activities, which correlates with the less negative reduction potentials of the fluorinated analogues confirmed by the electrochemical study. In contrast, the introduction of  $-CF_3$  and  $-OCF_3$  led to a dramatic decrease in the bioactivity due to the poor solubility confirmed by the predicted ADMET properties. Although these analogues seem to be rapidly metabolized in human liver microsomes, other predicted properties indicate that this series could be potential for an administrated orally anti-leishmanial drug. Moreover, these analogues may be suitable for treating cerebral leishmaniasis or other nervous system diseases. This information could become valuable for the drug discovery for the development of cyanine-base anti-leishmanial drug in the future.

Field of Study: Chemistry

Academic Year: 2019

Student's Signature .....

Advisor's Signature .....

Co-advisor's Signature .....

## ACKNOWLEDGEMENTS

This thesis becomes successful with the utmost guidance, kind support, and assistance of many individuals. I would like to express my sincere thanks to all whom have contributed to making this thesis possible.

First and foremost, I would like to express the deepest and sincere gratitude towards my supervisor, Dr. Tanatorn Khotavivattana, who has the attitude and substance of a genius: he always conveys a spirit of the adventure regarding research and accomplishment, and an enthusiasm in regard to teaching and living. His motivation, sincerity, encouragement, empathy, and excellent scientific guidance have deeply inspired me. Furthermore, I am extremely grateful to express my warmest appreciation to my joint supervisor, Professor Dr. Tirayut Vilaivan, who always kindly provides me his support, suggestion, encouragement, and strong academic guidance. Without their supervisions and persistent assistances, this thesis would not have been accomplished.

I would also like to sincerely express my deepest appreciation to Associate Professor Dr. Vudhichai Parasuk for his constant guidance throughout the thesis work and being a chair for this thesis defense. I would also like to thank my committee members, Associate Professor Dr. Khanitha Pudhom and Assistant Professor Dr. Chaturong Suparpprom, for their encouragement, insightful comments, and suggestions.

My deepest appreciation to Professor Dr. Padet Siriyasatien, M.D., Ph.D., and Dr. Atchara Phumee, Department of Parasitology, Faculty of Medicine, Chulalongkorn University, for providing me an opportunity to experience with the biological test, especially for anti-leishmanial evaluation. Their kind suggestion, helpfulness, and guidance greatly enriched my knowledge and sharpened my view.

Special thanks to Associate Professor Dr. Ng Chew Hee and Miss Mak Kit-Kay, a lecturer, School of Pharmacy, International Medical University (IMU), Malaysia, for their kind support on the in silico ADMET analysis section. Moreover, I would also like to special thanks to Dr. Muruges Kandasamy, a lecturer at IMU for his timely assistance and guidance for collection the metabolic stability investigation.

I am very much indebted and grateful to Dr. Parichatr Vanalabhpatana, for providing me valuable suggestion and support in the electrochemical analysis. Special thanks to Miss Kantima Chitchak who provided me the inestimable cyclic voltammetry data, and analysed all result for this part.

I would also like to sincerely thank to the Research Grant for New Scholar, [MRG6280024] from the Thailand Research Fund and the Office of the Higher Education Commission; the

Development and Promotion of Science and Technology Talents Project (Royal Government of Thailand scholarship); and Ratchadaphiseksomphot Endowment Fund, for all support.

Finally, I would also like to take this opportunity to thank my family's members: my father Mr. Boonmee Lasing, mother Mrs. Nisa Lasing, and brother Mr. Wattana Lasing who were continuously supporting me throughout my life and leaving me free in all my decisions. Many thanks to all colleagues and TK-lab members at the Department of Chemistry, Faculty of Science, Chulalongkorn University, all whom involved in the project for their moral support, helpfulness, and willingness to listen all the problems during this project.

Thitiya Lasing



## TABLE OF CONTENTS

	Page
ABSTRACT (THAI).....	iii
ABSTRACT (ENGLISH).....	iv
ACKNOWLEDGEMENTS .....	v
TABLE OF CONTENTS.....	vii
LIST OF TABLES.....	xiv
LIST OF FIGURES .....	xv
CHAPTER I INTRODUCTION.....	1
1. Background and significance of research.....	1
2. Literature review .....	2
2.1 Leishmaniasis.....	2
2.2 The clinical manifestations of leishmaniasis.....	3
2.2.1 Cutaneous leishmaniasis (CL) .....	3
2.2.2 Mucocutaneous leishmaniasis (MCL).....	4
2.2.3 Visceral leishmaniasis (VL).....	4
2.3 Current medications for the treatment of leishmaniasis .....	5
2.3.1 Pentavalent Antimonials .....	5
2.3.2 Pentamidine .....	6
2.3.3 Paromomycin.....	6
2.3.4 Amphotericin B.....	7
2.3.5 Miltefosine.....	7
2.4 Leishmaniasis in Thailand.....	7



2.5	Rhodacyanine dyes .....	9
2.5.1	Rhodacyanines in anticancer drug discovery .....	9
2.5.2	Rhodacyanines and their antimalarial activities.....	11
2.5.3	Rhodacyanine analogues as anti-leishmaniasis.....	13
2.6	Fluorine in drug discovery .....	14
3.	Objectives.....	16
4.	Scope of research.....	16
5.	Beneficial outcome .....	16
CHAPTER II EXPERIMENTS.....		17
1.	Chemical synthesis .....	17
1.1	Materials for chemical synthetic section.....	19
1.2	General procedure .....	19
1.2.1	General procedure A.....	19
1.2.2	General procedure B.....	20
1.2.3	General procedure C.....	20
1.2.4	General procedure D.....	21
1.2.5	General procedure E .....	21
1.2.6	General procedure F .....	21
1.2.7	General procedure G.....	22
1.2.8	General procedure H.....	22
1.2.9	General procedure I.....	22
1.3	Synthesis of benzothiazolium building blocks (6a-6h).....	23
1.3.1	2,3-Dimethylbenzo[d]thiazol-3-ium 4-methylbenzenesulfonate (6a) .....	23

1.3.2	4-Fluoro-2,3-dimethylbenzo[d]thiazol-3-ium 4-methylbenzenesulfonate (6b).....	23
1.3.3	5-Fluoro-2,3-dimethylbenzo[d]thiazol-3-ium 4-methylbenzenesulfonate (6c).....	24
1.3.4	6-Fluoro-2,3-dimethylbenzo[d]thiazol-3-ium 4-methylbenzenesulfonate (6d).....	25
1.3.5	7-Fluoro-2,3-dimethylbenzo[d]thiazol-3-ium 4-methylbenzenesulfonate (6e).....	26
1.3.6	2,3-Dimethyl-6-(trifluoromethyl)benzo[d]thiazol-3-ium 4-methylbenzenesulfonate (6f).....	26
1.3.7	2,3-Dimethyl-6-(trifluoromethoxy)benzo[d]thiazol-3-ium 4-methylbenzenesulfonate (6g).....	27
1.3.8	5,6-Difluoro-2,3-dimethylbenzo[d]thiazol-3-ium 4-methylbenzenesulfonate (6h).....	28
1.4	Synthesis of fluorinated rhodacyanine analogues (10c, 11a-11q).....	29
1.4.1	N-((3-Ethyl-4-oxo-2-thioxothiazolidin-5-ylidene)methyl)-N-phenylpropionamide (7).....	29
1.4.2	2-(3-Ethyl-5-(2-(3-methylbenzo[d]thiazol-2(3H)-ylidene)ethylidene)-4-oxothiazolidin-2-ylidene)methyl)-3-methylbenzo[d]thiazol-3-ium chloride (11a).....	30
1.4.3	2-(3-Ethyl-5-(2-(3-methylbenzo[d]thiazol-2(3H)-ylidene)ethylidene)-4-oxothiazolidin-2-ylidene)methyl)-4-fluoro-3-methylbenzo[d]thiazol-3-ium chloride (11b).....	31
1.4.4	2-(3-Ethyl-5-(2-(3-methylbenzo[d]thiazol-2(3H)-ylidene)ethylidene)-4-oxothiazolidin-2-ylidene)methyl)-5-fluoro-3-methylbenzo[d]thiazol-3-ium 4-methylbenzenesulfonate (10c). 31	

1.4.5	2-(3-Ethyl-5-(2-(3-methylbenzo[d]thiazol-2(3H)-ylidene)ethylidene)-4-oxothiazolidin-2-ylidene)methyl)-5-fluoro-3-methylbenzo[d]thiazol-3-ium chloride (11c).....	32
1.4.6	2-(3-Ethyl-5-(2-(3-methylbenzo[d]thiazol-2(3H)-ylidene)ethylidene)-4-oxothiazolidin-2-ylidene)methyl)-6-fluoro-3-methylbenzo[d]thiazol-3-ium chloride (11d) .....	33
1.4.7	2-(3-Ethyl-5-(2-(3-methylbenzo[d]thiazol-2(3H)-ylidene)ethylidene)-4-oxothiazolidin-2-ylidene)methyl)-7-fluoro-3-methylbenzo[d]thiazol-3-ium chloride (11e) .....	34
1.4.8	2-(3-Ethyl-5-(2-(4-fluoro-3-methylbenzo[d]thiazol-2(3H)-ylidene)ethylidene)-4-oxothiazolidin-2-ylidene)methyl)-3-methylbenzo[d]thiazol-3-ium chloride (11f) .....	34
1.4.9	2-(3-Ethyl-5-(2-(5-fluoro-3-methylbenzo[d]thiazol-2(3H)-ylidene)ethylidene)-4-oxothiazolidin-2-ylidene)methyl)-3-methylbenzo[d]thiazol-3-ium chloride (11g).....	35
1.4.10	2-(3-Ethyl-5-(2-(6-fluoro-3-methylbenzo[d]thiazol-2(3H)-ylidene)ethylidene)-4-oxothiazolidin-2-ylidene)methyl)-3-methylbenzo[d]thiazol-3-ium chloride (11h) .....	36
1.4.11	2-(3-Ethyl-5-(2-(7-fluoro-3-methylbenzo[d]thiazol-2(3H)-ylidene)ethylidene)-4-oxothiazolidin-2-ylidene)methyl)-3-methylbenzo[d]thiazol-3-ium chloride (11i).....	37
1.4.12	2-(3-Ethyl-5-(2-(3-methylbenzo[d]thiazol-2(3H)-ylidene)ethylidene)-4-oxothiazolidin-2-ylidene)methyl)-3-methyl-6-(trifluoromethyl)benzo[d]thiazol-3-ium chloride (11j).....	38
1.4.13	2-(3-Ethyl-5-(2-(3-methylbenzo[d]thiazol-2(3H)-ylidene)ethylidene)-4-oxothiazolidin-2-ylidene)methyl)-3-methyl-6-(trifluoromethoxy)benzo[d]thiazol-3-ium chloride (11k).....	39

1.4.14	2-(3-Ethyl-5-(2-(3-methylbenzo[d]thiazol-2(3H)-ylidene)ethylidene)-4-oxothiazolidin-2-ylidene)methyl)-5,6-difluoro-3-methylbenzo[d]thiazol-3-ium chloride (11l) .....	40
1.4.15	2-(3-Ethyl-5-(2-(5-fluoro-3-methylbenzo[d]thiazol-2(3H)-ylidene)ethylidene)-4-oxothiazolidin-2-ylidene)methyl)-5-fluoro-3-methylbenzo[d]thiazol-3-ium chloride (11m).....	41
1.4.16	2-(3-Ethyl-5-(2-(6-fluoro-3-methylbenzo[d]thiazol-2(3H)-ylidene)ethylidene)-4-oxothiazolidin-2-ylidene)methyl)-6-fluoro-3-methylbenzo[d]thiazol-3-ium chloride (11n) .....	42
1.4.17	2-(3-Ethyl-5-(2-(5-fluoro-3-methylbenzo[d]thiazol-2(3H)-ylidene)ethylidene)-4-oxothiazolidin-2-ylidene)methyl)-6-fluoro-3-methylbenzo[d]thiazol-3-ium chloride (11o) .....	43
1.4.18	2-(3-Ethyl-5-(2-(6-fluoro-3-methylbenzo[d]thiazol-2(3H)-ylidene)ethylidene)-4-oxothiazolidin-2-ylidene)methyl)-5-fluoro-3-methylbenzo[d]thiazol-3-ium chloride (11p) .....	44
1.4.19	2-(3-Ethyl-5-(2-(3-methyl-6-(trifluoromethyl)benzo[d]thiazol-2(3H)-ylidene)ethylidene)-4-oxothiazolidin-2-ylidene)methyl)-5-fluoro-3-methylbenzo[d]thiazol-3-ium chloride (11q) .....	44
2.	Biological evaluation.....	45
2.1	Materials for biological section.....	45
2.2	Cell culture .....	46
2.3	Cell counting method .....	46
2.4	The <i>in vitro</i> anti-leishmanial assays.....	46
2.4.1	The percentage of promastigote proliferation inhibition.....	46
2.4.2	The half maximal inhibitory concentration (IC <sub>50</sub> ) evaluation of promastigote proliferation inhibition .....	47
2.4.3	The percentage of axenic amastigote proliferation inhibition .....	47

2.4.4	The half maximal inhibitory concentration (IC <sub>50</sub> ) evaluation of axenic amastigote proliferation inhibition.....	47
2.4.5	Colorimetric assay.....	47
2.5	Cytotoxicity.....	48
3.	Pharmacological properties.....	48
3.1	The <i>in silico</i> ADMET prediction analysis.....	48
3.2	The <i>in vitro</i> microsomal metabolic stability.....	48
4.	Electrochemistry.....	50
CHAPTER III RESULTS & DISCUSSIONS.....		51
1.	Synthesis of benzothiazolium building blocks.....	51
2.	Synthesis of fluorinated rhodacyanine analogues.....	59
3.	The biological results.....	64
4.	The <i>in silico</i> ADMET properties.....	68
5.	Metabolic stability.....	71
5.1	Metabolic stability of verapamil.....	71
5.2	Metabolic stability of 11a.....	73
5.3	Metabolic stability of 11c.....	74
5.4	A comparison of the metabolic stabilities between three compounds...	76
6.	Electrochemistry.....	76
CHAPTER IV CONCLUSION.....		81
REFERENCES.....		82
APPENDICES.....		91
APPENDIX A.....		92
APPENDIX B.....		109

VITA..... 177



จุฬาลงกรณ์มหาวิทยาลัย  
**CHULALONGKORN UNIVERSITY**

## LIST OF TABLES

	Page
Table 1 The autochthonous leishmaniasis cases reported in Thailand during 1996-2013 <sup>44</sup> .....	8
Table 2 The anti-malarial activity and the toxicity to normal cells .....	12
Table 3 The <i>N</i> -acetylation of <i>o</i> -bromoanilines and anilines containing fluorine or perfluoroalkyl group using General procedure A.....	51
Table 4 The thionation of compounds 1a-1e and 3a, and 3b using Lawesson's reagent.....	53
Table 5 The synthesis of benzothiazoles using a palladium-catalysed intramolecular cyclization of <i>o</i> -bromoarylthioamides .....	54
Table 6 The synthesis of benzothiazoles via Jacobson cyclization using potassium ferricyanide.....	56
Table 7 <i>N</i> -Methylation of benzothiazoles for the formation of fluorine-containing benzothiazolium building blocks (6a-6h) .....	58
Table 8 The synthesis of fluorine-containing rhodanine 8a-8f .....	60
Table 9 The synthesis of the tosylate salt 9a-9f .....	60
Table 10 Synthesis of fluorinated rhodacyanine 10a-10q .....	61
Table 11 Synthesis of fluorinated rhodacyanine analogue 11a-11q .....	62
Table 12 The <i>in vitro</i> anti-leishmanial activities of eighteen rhodacyanine analogues against promastigotes of <i>L. martiniquensis</i> compared to the reference drugs. ....	65

## LIST OF FIGURES

	Page
Figure 1 The life-cycle of Leishmania parasites, consisting of the sandfly and mammalian stages <sup>13</sup> .....	3
Figure 2 The clinical manifestations of leishmaniasis. (a) Cutaneous leishmaniasis (CL), (b) mucocutaneous leishmaniasis (MCL), (c) visceral leishmaniasis (VL), and (d) post-Kalar aza dermal VL <sup>21</sup> .....	5
Figure 3 Drugs currently used in the treatment of leishmaniasis .....	6
Figure 4 The skeleton of rhodacyanines (a) class I (a general structure of rhodacyanine), (b) class II, (c) class III (A=CH) and class V (A=N), and (d) class IV rhodacyanine .....	9
Figure 5 MKT-077 and its analog JG-98 are allosteric inhibitors of Hsp70 that bind in the NBD. (a) Modification of metabolically labile positions led to more a potent and stable analogue, JG-98. (b) Model of JG-98 binding to an allosteric pocket in Hsp70, based on NMR and mutagenesis. JG-98 carbons coloured in cyan and Hsp70 carbons coloured in green <sup>52</sup> .....	11
Figure 6 (a) The structure of MKH-57; (b) the structure of SSJ-183. (a) The synthesised Fused Rhodacyanines as Fluorescent Probes: (c) compound 42; (d) compound 43... ..	12
Figure 7 (a) The general structure of rhodacyanine; (b) the enhancement of <i>in vitro</i> activity against <i>L. donovani</i> of the fluorinated rhodacyanine .....	14
Figure 8 (a) The prevention from metabolic oxidation in the presence of fluorine substituent; (b) an enhanced lipophilicity of trifluoromethyl group in sitagliptin; ED <sub>50</sub> = median effective dose; Log D = distribution coefficient; F = bioavailability.....	15
Figure 9 An overview of the research methodology.....	17
Figure 10 The synthesis procedures of fluorinated benzothiazolium tosylate (a) pathway 1; (b) pathway 2 .....	18



Figure 11 The synthesis of fluorine-containing rhodacyanines .....	18
Figure 12 The proposed mechanism of thionation using Lawesson's reagent <sup>80</sup> .....	52
Figure 13 The proposed mechanism of a palladium-catalysed cyclization <sup>81</sup> .....	55
Figure 14 The proposed mechanism of Jacobson synthesis of the fluorinated benzothiazoles through a single electron transfer.....	56
Figure 15 The synthesis of benzothiazole via a one-pot synthesis .....	57
Figure 16 The proposed mechanism of the benzothiazole formation through a one-pot synthesis <sup>83</sup> .....	57
Figure 17 The synthesis of compound 7.....	59
Figure 18 The proposed mechanism of the synthesis of 11c.....	63
Figure 19 Metabolic stability of verapamil in human liver microsomes expressed in graph of percentage remaining (%) against time (minute).....	72
Figure 20 Metabolic stability of 11a in human liver microsomes expressed in graph of percentage remaining (%) against time (minute).....	73
Figure 21 Metabolic stability of 11c in human liver microsomes expressed in graph of percentage remaining (%) against time (minute).....	75
Figure 22 The percentage remaining of each compound against the incubation times in the presence of human liver microsomes.....	76
Figure 23 Cyclic voltammograms recorded with a glassy carbon electrode (area = 0.071 cm <sup>2</sup> ) at 100 mV·s <sup>-1</sup> for DMF containing 0.10 M TBAP in the presence of 1.0 mM (a) 11a (solid lines) and DMF containing only 0.10 M TBAP (dashed lines); (b) 11c and 11g. Potential scans go from -0.70 to -1.80 to -0.70 V and -0.70 to +0.90 to -0.70 V..	78
Figure 24 Cyclic voltammograms recorded with a glassy carbon electrode (area = 0.071 cm <sup>2</sup> ) from -0.70 to -1.80 to -0.70 V at 10-800 mV·s <sup>-1</sup> in DMF containing 0.10 M TBAP and 1.0 mM (A) 11a, (B) 11c, and (C) 11g. (D) to (F) depict the corresponding plots of cathodic peak current obtained from the cyclic voltammograms of 11a, 11c, and 11g, respectively, versus square root of scan rate.....	80

Figure 25 $^1\text{H}$ NMR spectrum of 6a.....	93
Figure 26 $^{13}\text{C}$ NMR spectrum of 6a.....	93
Figure 27 HRMS spectrum of 6a.....	94
Figure 28 $^1\text{H}$ NMR spectrum of 6b.....	95
Figure 29 $^{13}\text{C}$ NMR spectrum of 6b.....	95
Figure 30 $^{19}\text{F}$ NMR spectrum of 6b.....	96
Figure 31 HRMS spectrum of 6b.....	96
Figure 32 $^1\text{H}$ NMR spectrum of 6c.....	97
Figure 33 $^{13}\text{C}$ NMR spectrum of 6c.....	97
Figure 34 $^{19}\text{F}$ NMR spectrum of 6c.....	98
Figure 35 HRMS spectrum of 6c.....	98
Figure 36 $^1\text{H}$ NMR spectrum of 6d.....	99
Figure 37 $^{13}\text{C}$ NMR spectrum of 6d.....	99
Figure 39 $^{19}\text{F}$ NMR spectrum of 6d.....	100
Figure 38 HRMS spectrum of 6d.....	100
Figure 40 $^1\text{H}$ NMR spectrum of 6e.....	101
Figure 41 $^{13}\text{C}$ NMR spectrum of 6e.....	101
Figure 42 HRMS spectrum of 6e.....	102
Figure 43 $^{19}\text{F}$ NMR spectrum of 6e.....	102
Figure 44 $^1\text{H}$ NMR spectrum of 6f.....	103
Figure 45 $^{13}\text{C}$ NMR spectrum of 6f.....	103
Figure 46 HRMS spectrum of 6f.....	104
Figure 47 $^{19}\text{F}$ NMR spectrum of 6f.....	104
Figure 48 $^1\text{H}$ NMR spectrum of 6g.....	105

Figure 49 $^{13}\text{C}$ NMR spectrum of 6g.....	105
Figure 50 $^{19}\text{F}$ NMR spectrum of 6g.....	106
Figure 51 HRMS spectrum of 6g.....	106
Figure 52 $^1\text{H}$ NMR spectrum of 6h.....	107
Figure 53 $^{13}\text{C}$ NMR spectrum of 6h.....	107
Figure 54 $^{19}\text{F}$ NMR spectrum of 6h.....	108
Figure 55 HRMS spectrum of 6h.....	108
Figure 56 $^1\text{H}$ NMR spectrum of 7.....	110
Figure 57 $^{13}\text{C}$ NMR spectrum of 7.....	110
Figure 58 $^1\text{H}$ NMR spectrum of 11a.....	111
Figure 59 $^{13}\text{C}$ NMR spectrum of 11a.....	111
Figure 60 HRMS spectrum of 11a.....	112
Figure 61 $^1\text{H}$ NMR spectrum of 11b.....	113
Figure 62 $^{13}\text{C}$ NMR spectrum of 11b.....	113
Figure 63 $^{19}\text{F}$ NMR spectrum of 11b.....	114
Figure 64 2D NMR spectra of 11b (a) COSY; and (b) HSQC spectrum.....	115
Figure 65 HRMS spectrum of 11b.....	115
Figure 66 $^1\text{H}$ NMR spectrum of 10c.....	116
Figure 67 $^{13}\text{C}$ NMR spectrum of 10c.....	116
Figure 68 $^{19}\text{F}$ NMR spectrum of 10c.....	117
Figure 69 HRMS spectrum of 10c.....	117
Figure 70 $^1\text{H}$ NMR spectrum of 11c.....	118
Figure 71 $^{13}\text{C}$ NMR spectrum of 11c.....	118
Figure 72 $^{19}\text{F}$ NMR spectrum of 11c.....	119

Figure 73 2D NMR spectra of 11c (a) COSY; (b) HSQC; and (c) HMBC spectrum .....	120
Figure 74 HRMS spectrum of 11c .....	121
Figure 75 $^1\text{H}$ NMR spectrum of 11d .....	122
Figure 76 $^{13}\text{C}$ NMR spectrum of 11d .....	122
Figure 77 $^{19}\text{F}$ NMR spectrum of 11d.....	123
Figure 78 2D NMR spectra of 11d (a) COSY; (b) HSQC; and (c) HMBC spectrum .....	124
Figure 79 HRMS spectrum of 11d.....	125
Figure 80 $^1\text{H}$ NMR spectrum of 11e.....	126
Figure 81 $^{13}\text{C}$ NMR spectrum of 11e.....	126
Figure 82 $^{19}\text{F}$ NMR spectrum of 11e.....	127
Figure 83 2D NMR spectra of 11e (a) COSY; (b) HSQC; and (c) HMBC spectrum .....	128
Figure 84 HRMS spectrum of 11e.....	129
Figure 85 $^1\text{H}$ NMR spectrum of 11f.....	130
Figure 86 $^{13}\text{C}$ NMR spectrum of 11f.....	130
Figure 87 $^{19}\text{F}$ NMR spectrum of 11f.....	131
Figure 88 2D NMR spectra of 11f (a) COSY; (b) HSQC; and (c) HMBC spectrum .....	132
Figure 89 HRMS spectrum of 11f.....	133
Figure 90 $^1\text{H}$ NMR spectrum of 11g.....	134
Figure 91 $^{13}\text{C}$ NMR spectrum of 11g.....	134
Figure 92 $^{19}\text{F}$ NMR spectrum of 11g.....	135
Figure 93 2D NMR spectra of 11g (a) COSY; (b) HSQC; and (c) HMBC spectrum.....	136
Figure 94 HRMS spectrum of 11g .....	137
Figure 95 $^1\text{H}$ NMR spectrum of 11h.....	138
Figure 96 $^{13}\text{C}$ NMR spectrum of 11h .....	138

Figure 97 $^{19}\text{F}$ NMR spectrum of 11h.....	139
Figure 98 2D NMR spectra of 11h (a) COSY; (b) HSQC; and (c) HMBC spectrum .....	140
Figure 99 HRMS spectrum of 11h.....	141
Figure 100 $^1\text{H}$ NMR spectrum of 11i.....	142
Figure 101 $^{13}\text{C}$ NMR spectrum of 11i.....	142
Figure 102 $^{19}\text{F}$ NMR spectrum of 11i.....	143
Figure 103 2D NMR spectra of 11i (a) COSY; (b) HSQC; and (c) HMBC spectrum .....	144
Figure 104 HRMS spectrum of 11i.....	145
Figure 105 $^1\text{H}$ NMR spectrum of 11j.....	146
Figure 106 $^{13}\text{C}$ NMR spectrum of 11j.....	146
Figure 107 $^{19}\text{F}$ NMR spectrum of 11j.....	147
Figure 108 2D NMR spectra of 11j (a) COSY; (b) HSQC; and (c) HMBC spectrum .....	148
Figure 109 HRMS spectrum of 11j.....	149
Figure 110 $^1\text{H}$ NMR spectrum of 11k.....	150
Figure 111 $^{13}\text{C}$ NMR spectrum of 11k.....	150
Figure 112 $^{19}\text{F}$ NMR spectrum of 11k.....	151
Figure 113 2D NMR spectra of 11k (a) COSY; (b) HSQC; and (c) HMBC spectrum .....	152
Figure 114 HRMS spectrum of 11k.....	153
Figure 115 $^1\text{H}$ NMR spectrum of 11l.....	154
Figure 116 $^{13}\text{C}$ NMR spectrum of 11l .....	154
Figure 117 $^{19}\text{F}$ NMR spectrum of 11l.....	155
Figure 118 2D NMR spectra of 11l (a) COSY; (b) HSQC; and (c) HMBC spectrum.....	156
Figure 119 HRMS spectrum of 11l.....	157
Figure 120 $^1\text{H}$ NMR spectrum of 11m.....	158

Figure 121 $^{13}\text{C}$ NMR spectrum of 11m.....	158
Figure 122 $^{19}\text{F}$ NMR spectrum of 11m.....	159
Figure 123 2D NMR spectra of 11m (a) COSY; (b) HSQC; and (c) HMBC spectrum.....	160
Figure 124 HRMS spectrum of 11m.....	161
Figure 125 $^1\text{H}$ NMR spectrum of 11n.....	162
Figure 126 $^{13}\text{C}$ NMR spectrum of 11n.....	162
Figure 127 $^{19}\text{F}$ NMR spectrum of 11n.....	163
Figure 128 2D NMR spectra of 11n (a) COSY; (b) HSQC; and (c) HMBC spectrum.....	164
Figure 129 HRMS spectrum of 11n.....	165
Figure 130 $^1\text{H}$ NMR spectrum of 11o.....	166
Figure 131 $^{13}\text{C}$ NMR spectrum of 11o.....	166
Figure 132 $^{19}\text{F}$ NMR spectrum of 11o.....	167
Figure 133 2D NMR spectra of 11o (a) COSY; (b) HSQC; and (c) HMBC spectrum.....	168
Figure 134 HRMS spectrum of 11o.....	169
Figure 135 $^1\text{H}$ NMR spectrum of 11p.....	170
Figure 136 $^{13}\text{C}$ NMR spectrum of 11p.....	170
Figure 137 $^{19}\text{F}$ NMR spectrum of 11p.....	171
Figure 138 2D NMR spectra of 11p (a) COSY; (b) HSQC; and (c) HMBC spectrum.....	172
Figure 139 HRMS spectrum of 11p.....	173
Figure 140 $^1\text{H}$ NMR spectrum of 11q.....	174
Figure 141 $^{13}\text{C}$ NMR spectrum of 11q.....	174
Figure 142 $^{19}\text{F}$ NMR spectrum of 11q.....	175
Figure 143 2D NMR spectra of 11q (a) COSY; and (b) HSQC spectrum; and (c) HRMS spectrum.....	176



จุฬาลงกรณ์มหาวิทยาลัย  
**CHULALONGKORN UNIVERSITY**

# CHAPTER I

## INTRODUCTION

### 1. Background and significance of research

Leishmaniasis is a vector-borne disease caused by *Leishmania* parasites which results in almost 60,000 deaths annually.<sup>1</sup> It is estimated that over 350 million people across 98 countries including Thailand are currently at risk.<sup>2</sup> In Thailand, an increasing number of autochthonous leishmaniasis infections has been reported; the *Leishmania* species which are responsible for these cases include *L. martiniquensis*, *L. donovani*, *L. infantum*, as well as *L. siamensis* (or *L. orientalis*), the latter is a novel indigenous species of Thailand. Depending on the species of the parasite, there are various symptoms associated with leishmaniasis ranging from skin ulcers to life-threatening internal organ failure; hence, an effective medication is in high demand. However, the currently available medications suffer from various limitations such as high cost, lack of efficacy, serious side effects, low bioavailability and drug resistance.<sup>3,4</sup>

To date, several researches have introduced a variety of synthetic compounds as potential drug candidates for treating leishmaniasis,<sup>5</sup> one of which is a series of compounds belonging to the class of rhodacyanine dyes. It was reported that these compounds have a diverse range of bioactivity, including anti-cancer, anti-malarial and anti-leishmanial properties.<sup>6</sup> One of the most potent compounds among the series was reported by M. Ihara and co-workers in 2010;<sup>7</sup> the fluorinated rhodacyanine analogue, SJL-01, exhibited exceptionally high efficacy and excellent selectivity index (>15000) in the *in vivo* testing against *L. donovani*; although the exact role of the fluorine substituent in SJL-01 has not yet been clarified. Moreover, the development of SJL-01 as an anti-leishmanial drug was limited by the low bioavailability because the *in vivo* inhibiting percentage against *L. donovani* was decreased from 94.5% by intravenous injection to 28.0% by oral administration.<sup>7</sup> In this regard, we reasoned that these issues can be addressed by expanding the scope of the fluorinated rhodacyanine analogues.

Fluorine has found widespread applications in drug discovery and development owing to its unique properties such as high electronegativity, low polarizability and the extremely strong C-F bond strength. Installation of fluorine or perfluoroalkyl groups at the correct position in drug molecules could lead to various beneficial effects, for instance, the increase in the potency, metabolic stability, and membrane permeability.<sup>8</sup> According to these reasons, we hypothesise that the low bioavailability, which is the major drawback of SJL-01 could be improved by installing perfluoroalkyl groups onto the molecule to increase its lipophilicity. In addition, it is possible to gain more understanding on the exact roles of fluorine by studying the structure-



activity relationship of the rhodacyanine analogues with different types of the fluorine-containing groups at different positions on the molecule. The knowledge from this study is crucial for further development of rhodacyanine-based anti-leishmanial drugs in the future.

## 2. Literature review

### 2.1 Leishmaniasis

Leishmaniasis is a tropical and subtropical disease caused by over 20 species of the protozoan parasites belonging to the genus *Leishmania* which are transmitted between mammalian hosts by blood-sucking sand flies.<sup>9</sup> According to the World Health Organization (WHO), leishmaniasis was classified as one of the major neglected tropical diseases (NTDs) caused by protozoan infection, ranking second only after malaria.<sup>10</sup> It is particularly prevalent in underdeveloped and developing countries. Currently, there are more than 12 million people across 98 countries infected by leishmaniasis and it is estimated that approximately 2 million new cases will occur each year, with more than 350 million people being at risk of contracting the disease.<sup>11</sup>

*Leishmania* parasites alternate between two major forms throughout their life cycle (**Figure 1**), involving a mammalian and a sandfly stage.<sup>12</sup> Inside the sandfly's digestive tract, *Leishmania* parasites occur as the **promastigotes** (the infective form). Once the promastigotes are transferred into mammal hosts through the bite of the infected female sand flies, they are phagocytized by macrophages and transformed into **amastigotes**. The tissue-stage amastigotes multiply and divide asexually through a simple division inside the host cells until bursting out and infect the other tissues. Ultimately, new sandflies becomes infected again after taking the blood meal through either with a skin lesion or a capillary of the mammal host. The leishmanial infection leads to various symptoms depending on the type of the infecting *Leishmania* parasites.

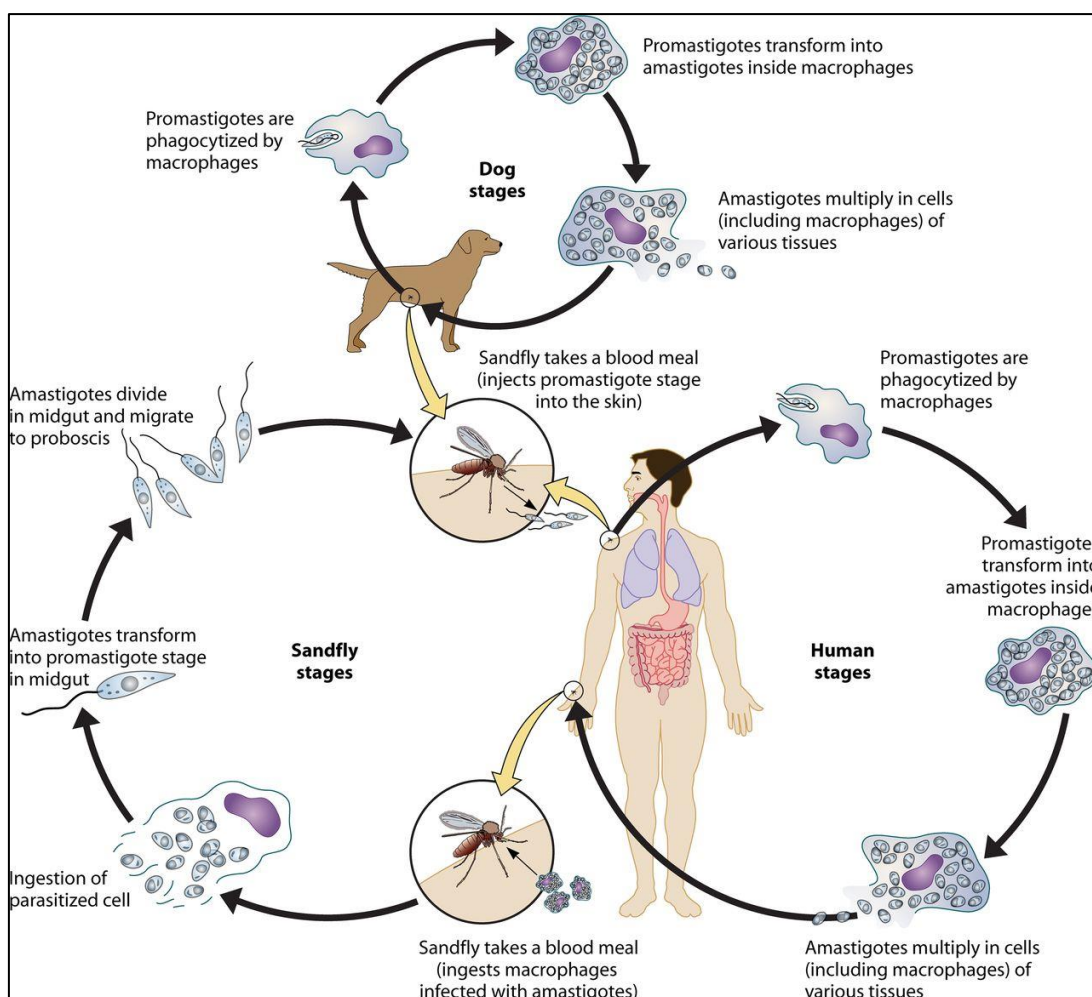


**Figure 1** The life-cycle of *Leishmania* parasites, consisting of the sandfly and mammalian stages<sup>13</sup>

## 2.2 The clinical manifestations of leishmaniasis

Depending on the clinical presentation of the disease, leishmaniasis can be divided into three dominant clinical syndromes. The different clinical manifestations are defined by the species of infecting parasite and the genetic susceptibility of the host.<sup>14</sup>

### 2.2.1 Cutaneous leishmaniasis (CL)

Cutaneous leishmaniasis is the most common form of leishmaniasis, displaying single or multiple skin ulcers at the bite sites (**Figure 2a**). This symptom is caused by several *Leishmania* species, such as *Leishmania major*, *L. mexicana*, *L. tropica*, *L. amazonensis*, *L. panamensis*, *L. guyanensis*, and *L. braziliensis*. Moreover, satellite lesions or nodular lymphangitis are also observed in many CL cases. Although simple CL is often self-healing, full recovery typically takes up to several months. During this period, the patients usually suffer from function impairment, the development of permanent scars and susceptibility to secondary infection or even progression to infect mucocutaneous tissue.<sup>15</sup>

### 2.2.2 Mucocutaneous leishmaniasis (MCL)

Mucocutaneous leishmaniasis is the less common type and usually found in CL cases where the secondary infection occurs through metastatic spread to reach the upper respiratory tract mucosa. Although several *Leishmania* species can cause CL, only *Leishmania braziliensis* can cause mucosal leishmaniasis. This could lead to extensive tissue destruction and ulceration at the throat and mouth organs (Figure 2b). In some cases, MCL could be fatal by secondary super-infections and/or malnutrition.<sup>16</sup>

### 2.2.3 Visceral leishmaniasis (VL)

Visceral leishmaniasis, also known as Kala-azar or black fever, is the most severe type with the fatality rate as high as 100% if left untreated. Several *Leishmania* protozoan parasites that are responsible for causing VL, such as *Leishmania donovani*, *L. infantum*, and *L. tropica*, lead to a systemic disease that affects internal organs, especially the spleen, liver, and bone marrow (Figure 2c).<sup>17</sup>

Furthermore, many reports demonstrated that VL has emerged as a significant opportunistic infection associated with human immunodeficiency virus (HIV).<sup>18</sup> Both VL and HIV are mutually reinforcing:<sup>19</sup> HIV infection increases the risk of developing active VL by 100 to 2320 times, while VL accelerates HIV replication and progression to AIDS. As a result, the emerging problem of HIV/VL co-infection is one of the major concerns according to the WHO. Moreover, in some patients who have successfully treated for VL, a secondary syndrome called **post-Kala-azar dermal leishmaniasis (PKDL)** may also develop. PKDL is usually associated with chronic maculopapular or nodular rash which occurs months to years after apparently successful VL treatment (Figure 2d).<sup>20</sup>



**Figure 2** The clinical manifestations of leishmaniasis. **(a)** Cutaneous leishmaniasis (CL), **(b)** mucocutaneous leishmaniasis (MCL), **(c)** visceral leishmaniasis (VL), and **(d)** post-Kalar aza dermal VL<sup>21</sup>

### 2.3 Current medications for the treatment of leishmaniasis

Since the disease occurs in various forms, the anti-leishmanial therapy is highly dependent on the species of the *Leishmania* parasite, symptoms and geographical regions.<sup>22</sup> CL will often self-heal; however, treatment can speed healing, reduce scarring, and decrease the risk of further disease. MCL and VL, on the other hand, always require treatment. The current drugs that have been used for the treatment of VL, the most severe form for leishmaniasis, include pentavalent antimonials, pentamidine, paromomycin, amphotericin B, and miltefosine (**Figure 3**).<sup>23</sup> Some of these drugs can also be used for the treatment of both CL and MCL.<sup>24</sup>

#### 2.3.1 Pentavalent Antimonials

Pentavalent Antimonials ( $Sb^V$ )<sup>25</sup> (meglumine antimoniate [Glucantime<sup>®</sup>, Aventis] and sodium stibogluconate [Pentostam<sup>®</sup>, GlaxoSmithKline]) have been used since the 1940s for the treatment both VL and CL cases. These compounds appear to inhibit bioenergetic pathways such as glycolysis and fatty acid oxidation in *Leishmania* amastigotes. However, the drawback lies in their significant toxicities; the  $Sb^V$ -induced hyperamylasemia and pancreatitis are common can be fatal, especially in those co-infected with HIV.<sup>26</sup>

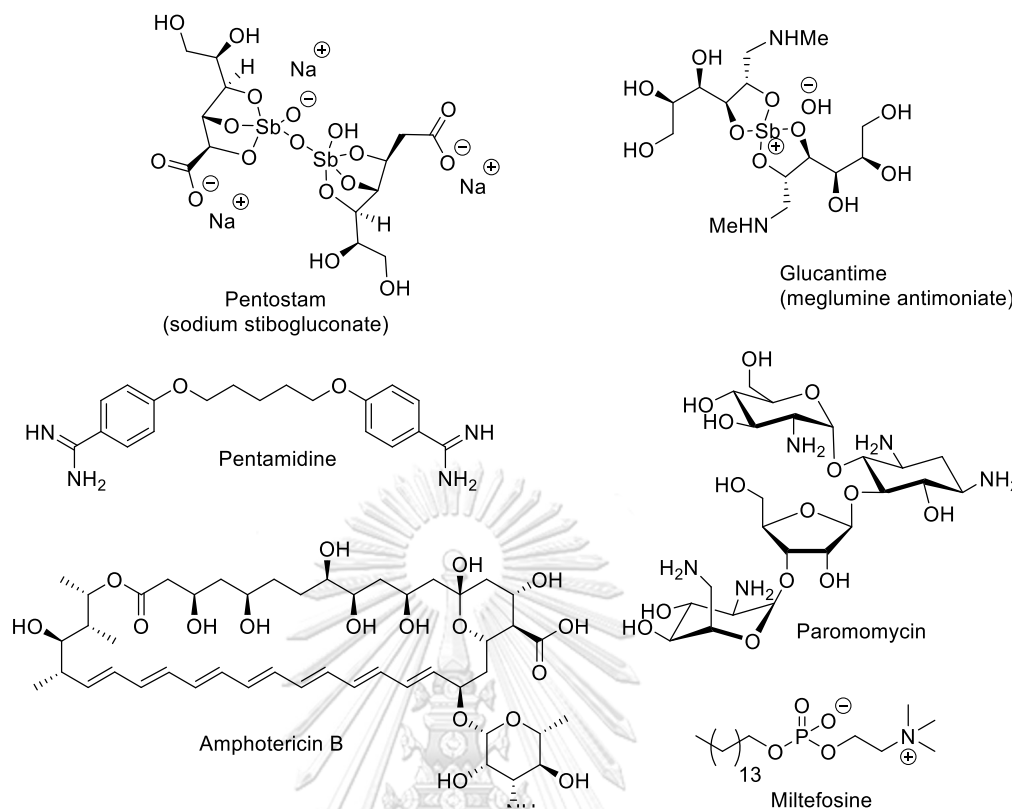


**Figure 3** Drugs currently used in the treatment of leishmaniasis

### 2.3.2 Pentamidine

Pentamidine was discovered in the 1960s, is typically used for the treatment of amebiasis (parasitic infection of the intestines) as well as both VL and CL.<sup>27, 28</sup> Pentamidine is known as an antibiotic since it can reversibly inhibit trypanosomal *S*-adenosyl-*L*-methionine decarboxylase, thereby reducing the synthesis of polyamines. However, various side effects have been reported such as hypoglycaemia and kidney problems.<sup>29</sup> In addition, there has been a report demonstrating that its efficacy for VL in India has progressively declined with current cure rates of approximately 70%.<sup>30</sup> Therefore, the use of pentamidine for the treatment of VL is now discouraged, although it is still be used under strict precaution for treatment CL.<sup>31</sup>

### 2.3.3 Paromomycin

Paromomycin, also known as aminosidine, is an aminoglycoside which is a highly effective and cheap anti-leishmanial drug for VL, though it shows little efficacy in CL or MCL.<sup>32</sup> However, it was reported that paromomycin can induce acute renal failure, deafness, and cataract formation in cats; as a result, its use has been limited, especially in human.<sup>33</sup>

### 2.3.4 Amphotericin B

Amphotericin B (AmB) is an active agent against most fungi and some protozoa.<sup>34</sup> It was first isolated from *Streptomyces nodosus* in 1955. The mechanisms of action are related with binding to ergosterol and cholesterol of the cell membrane of most protozoa species and induced the cell damage through a cascade of oxidative reactions with formation of free radicals. In order to reduce toxicity and improve the tolerability of amphotericin, several lipid formulations have been developed; for examples, amphotericin deoxycholate is a powerful anti-leishmanial drug and relatively non-toxic.<sup>35</sup> However, since it requires a slow intravenous injection, patients are needed to be hospitalised and hence limiting the medication at rural sites. Although it is very effective to treat many systematic fungal infections and visceral leishmaniasis, the microbial production is very complicated due to the impurity named Amphotericin A which is a severely toxic compound.<sup>36</sup> Therefore, the biosynthesis to produce AmB needs some modifications of both chemical and engineered biosynthesis to reduce its toxicity (i.e. using polypeptide synthase components)<sup>37</sup> which reflects by its high cost (cost per death ranging from 53 to 527 USD).<sup>38</sup>

### 2.3.5 Miltefosine

Miltefosine is the first oral drug to treat VL patients. It activates proteases in *Leishmania spp.* and causes apoptotic death of the parasite.<sup>39</sup> The mechanism may involve a combination of several mechanism of actions, including the phospholipid metabolism and induction of mitochondrial dysfunction. Although it is one of the most effective and safest medicines for leishmaniasis, the access to miltefosine remains limited due to inefficient supply chains, which ultimately links to its high cost. The price for one full adult course of miltefosine treatment is ranging from 117 to 164 USD in the developing countries purchased by non-profit organisations Médecins Sans Frontières (MSF) and 33000 to 51000 USD in USA.<sup>40</sup>

## 2.4 Leishmaniasis in Thailand

Prior to the year 1999, leishmaniasis was considered as an imported disease in Thailand.<sup>41</sup> However, an increasing number of autochthonous leishmaniasis (both CL and VL) has recently been reported in many regions, mainly the northern, southern and central Thailand. In several cases, the patients are also co-infected with HIV/AIDS, although immunocompetent patients with the age ranging from 3 to 81 years old were also reported (**Table 1**).<sup>42</sup> Among these CL and VL cases, many *Leishmania* species have been identified including *L. donovani*, as well as the new species, *L. siamensis* (recently renamed to *L. orientalis*) and *L. martiniquensis*, which were first discovered in Thailand.<sup>43</sup>

**Table 1** The autochthonous leishmaniasis cases reported in Thailand during 1996-2013<sup>44</sup>

Year	Age (years)	Province	Clinical forms	<i>Leishmania</i> species	Treatment
1996	3	Surat Thani	VL	N/A	Pentamidine
2005	40	Nan	VL	<i>L. donovani</i>	Amphotericin B
2006	55	Phang Nga	VL	<i>L. martiniquensis</i>	Amphotericin B
2007	66	Bangkok	VL	<i>L. infantum</i>	Amphotericin B
2007	81	Songkhla	VL	<i>L. donovani</i>	Amphotericin B
2008	37	Chanthaburi	VL	<i>L. martiniquensis</i>	Amphotericin B
2008	45	Chiang Rai	CL, VL	<i>L. martiniquensis</i>	No treatment
2009	46	Songkhla	CL, VL	<i>L. martiniquensis</i>	Amphotericin B
2010	32	Trang	VL	<i>L. siamensis</i>	Amphotericin B
2010	5	Satun	VL	<i>L. martiniquensis</i>	Amphotericin B
2011	30	Trang	VL	<i>L. martiniquensis</i>	Amphotericin B
2011	34	Yangon (Myanmar)	CL	<i>L. martiniquensis</i>	Amphotericin B
2011	22		Asymptomatic	<i>L. martiniquensis</i>	No treatment
2013	60		CL	<i>L. martiniquensis</i>	Amphotericin B
2012	3	Lopburi	CL	N/A	Itraconazole
2012	52	Lamphun	VL	<i>L. martiniquensis</i>	Amphotericin B
2012	48	Chiang Mai	CL	<i>L. martiniquensis</i>	Amphotericin B
2012	38	Lamphun	CL	<i>L. martiniquensis</i>	Amphotericin B
2013	28	Songkhla	Asymptomatic	<i>L. martiniquensis</i>	No treatment

CL: cutaneous leishmaniasis, VL: visceral leishmaniasis. N/A means data is not available.

Regarding to the treatment of leishmaniasis in Thailand, amphotericin B was the only available medication to treat both VL and CL during 1996-2016.<sup>44</sup> There are significant drawbacks associated with amphotericin B including the high tendency for parasite resistance as well as its relatively high cost. For these reasons, the leishmaniasis treatment in Thailand is not fully effective, leading to an increasing number of leishmaniasis cases.

## 2.5 Rhodacyanine dyes

In the past few decades, numerous heteroaromatic compounds has emerged as potential anti-leishmanial drug candidates,<sup>10</sup> one of which that have gained recent attention is the rhodacyanine dye. It was originally used in textile industry as a synthetic dye and photographic industry as a silver halide sensitizer.<sup>45</sup> Rhodacyanine is one of the polynuclear cyanine dyes containing three heterocyclic rings: a central rhodanine ring (4-oxothiazolidine) and two heteroaromatic rings at both ends linked by methine groups with various lengths. There are five major classes of rhodacyanines containing the  $\pi$ -electron delocalised lipophilic cations (DCLs).<sup>46</sup> Class I ([0, 0] rhodacyanine), a general structure of rhodacyanine, contains 2 terminal heteroaromatic rings (A, C) and one center rhodanine (4-oxothiazolidine, B) (**Figure 4a**). Class II ([1, 0] rhodacyanine) is similar to those general structures but it has an additional methine group (**Figure 4b**) while class III ([0, 0, 0] rhodacyanine, A=CH) and class V ([0, 0, 0] azarhodacyanine, A=N) has two rhodanine rings (**Figure 4c**). Class IV ([0, 0] azarhodacyanine) is considered when CH at methine group of a general structure of rhodacyanine is replaced by N atom (**Figure 4d**).<sup>47</sup>

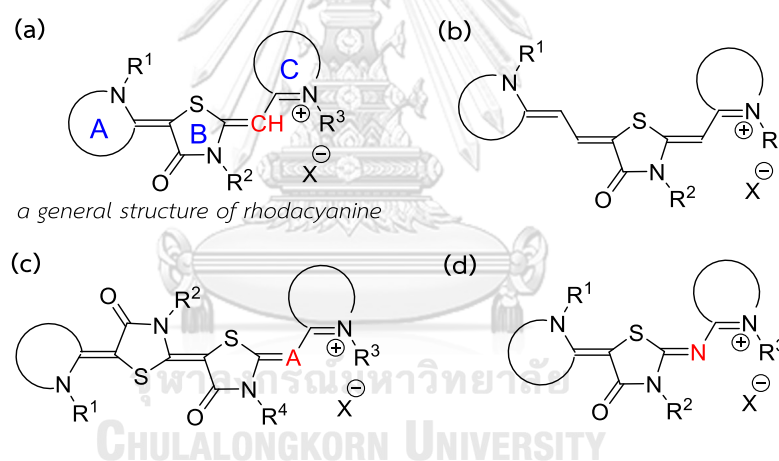


**Figure 4** The skeleton of rhodacyanines (a) class I (a general structure of rhodacyanine), (b) class II, (c) class III (A=CH) and class V (A=N), and (d) class IV rhodacyanine

### 2.5.1 Rhodacyanines in anticancer drug discovery

In 1996, the rhodacyanine in class I named MKT-077 (**Figure 5a**) (formerly known as FJ-776) was first discovered and studied its anti-cancer activity by Len Bo Chen from Harvard Medical School in USA and the scientists from FUJIFILM Co. in Japan.<sup>48</sup> According to their results, MKT-077 displayed significant growth-inhibitory activity against five human cancer cell lines, including colon cancer CX-1, breast cancer MCF-7, pancreatic cancer CRL 1420, bladder transitional cell cancer U, and melanoma LOX. It showed the  $IC_{50}$  values in a range from 0.35 to 1.2  $\mu$ M and has a low toxicity to normal cell line (CV-1 from monkey normal kidney epithelial). Furthermore, it also exhibits high water-solubility (>200 mg/mL). For Phase I clinical trial, 30



patients with refractory cancer were treated with 48 mg/m<sup>2</sup>/day of MKT-077 for 3 weeks. There were no serious side effects, including cardiac toxicity and myelotoxicity in these patients.

MKT-077 was then considered to be a new candidate as an anti-cancer agent and its mechanism of action was studied. Moreover, Chen and his co-worker also revealed that MKT-077 inhibits ADP-stimulated and DNP-stimulated mitochondrial respiration and relates to the electron transfer reaction at the mitochondrial membrane. The result also showed that MKT-077 has the sensitivity to inhibit glutamate plus malate vs succinate stimulated respiration (the energy in mitochondria) but not inhibit NADH vs succinate linked electron transport reactions. Interestingly, the loss of mtDNA between cancer cells (CRL 1420, CX-1) and normal cells (CV-1) in the presence of MKT-077 correlated with its low toxicity to normal cells (CRL 1420 > CX-1 >> CV-1).<sup>49</sup> However, ten patients with advanced solid cancer were treated by MKT-077 at three dose levels, including 30, 40 and 50 mg/m<sup>2</sup>/day. The result showed that MKT-077 was slightly effective for cancer treatment; however, side effects such as renal toxicity was observed.<sup>50</sup>

The mechanism of action of MKT-077 was unclear until in 2000 when Wadhwa and co-workers reported that MKT-077 binds to an Hsp70 family member, mortalin (mot-2), and abrogates its interactions with the tumour suppressor protein, p53.<sup>51</sup> In 2013, Gestwicki and co-workers from United States discovered a novel MKT-077 analogue named JG-98 (**Figure 5a**), which showed improved anti-cancer activity against MDA-MB-231 cells as well as enhanced affinity for Hsp70 *in vitro* approximately 80-fold (KD = 90 nM).<sup>52</sup> The optimizing interaction framed by Y148, V81, P146 and F149 (**Figure 5b**) while the pyridinium was predicted to interact with a region formed by Asp223, Thr224, and His225. Furthermore, the disadvantage of MKT-077 is its rapid metabolism in liver by P450 enzyme ( $t_{1/2} \sim 5$  min). The metabolite identification showed that the benzothiazole and pyridinium rings of MKT-077 are the major sites of attack by the P450 enzymes.<sup>53</sup>

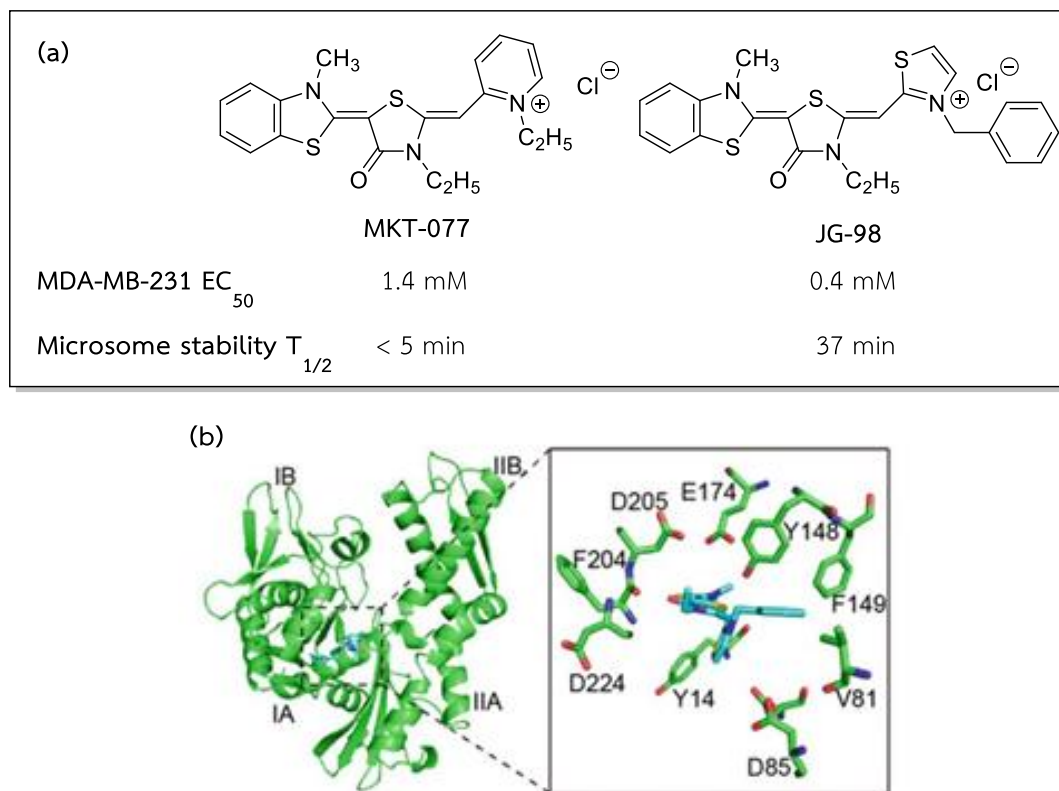


**Figure 5** MKT-077 and its analog JG-98 are allosteric inhibitors of Hsp70 that bind in the NBD. (a) Modification of metabolically labile positions led to more a potent and stable analogue, JG-98. (b) Model of JG-98 binding to an allosteric pocket in Hsp70, based on NMR and mutagenesis. JG-98 carbons coloured in cyan and Hsp70 carbons coloured in green<sup>52</sup>

### 2.5.2 Rhodacyanines and their antimalarial activities

The broad screening of numerous carbohydrates and heterocycles by Ihara and his colleagues also indicated that many compounds containing DLC moiety showed the moderate to good anti-malarial activity while MKT-077 showed a strong anti-malarial activity ( $EC_{50} = 70$  nM) against erythrocyte of *Plasmodium falciparum* and moderate selective toxicity (selectivity index = 210) (**Table 2**).<sup>54</sup> Furthermore, they synthesised several novel rhodacyanine derivatives to improve the activity and to decrease the toxicity. The  $EC_{50}$  values of the *in vitro* anti-malarial activity against *P. falciparum* were in the range from 4 to 300 nM. The most active agent was MKH-57 (**Figure 6a**) with the  $EC_{50} = 12$  nM and the selective toxicity of  $EC_{50}$  values for L-6/ $EC_{50}$  for *P. falciparum* was 1000.<sup>55</sup>

**Table 2** The anti-malarial activity and the toxicity to normal cells

compounds	EC <sub>50</sub> (M)		selective toxicity <sup>c</sup>
	<i>P. falciparum</i> <sup>a</sup>	FM3A <sup>b</sup>	
quinine	1.1 × 10 <sup>-7</sup>	1.0 × 10 <sup>4</sup>	910
chloroquine	1.8 × 10 <sup>-8</sup>	3.2 × 10 <sup>-5</sup>	1800
Methylene blue	1.7 × 10 <sup>-8</sup>	1.1 × 10 <sup>-6</sup>	65
rhodamine 123	3.0 × 10 <sup>-7</sup>	1.0 × 10 <sup>-5</sup>	33
MKT-077	7.0 × 10 <sup>-8</sup>	1.5 × 10 <sup>-5</sup>	210
MKH-57	1.2 × 10 <sup>-8</sup>	1.2 × 10 <sup>-5</sup>	1000

<sup>a</sup>Chloroquine sensitive strain (FCR-3). <sup>b</sup>Mouse mammary tumor FM3A cells representing a model of host. <sup>c</sup>Selective toxicity = EC<sub>50</sub> value for FM3A/EC<sub>50</sub> for *P. falciparum*.

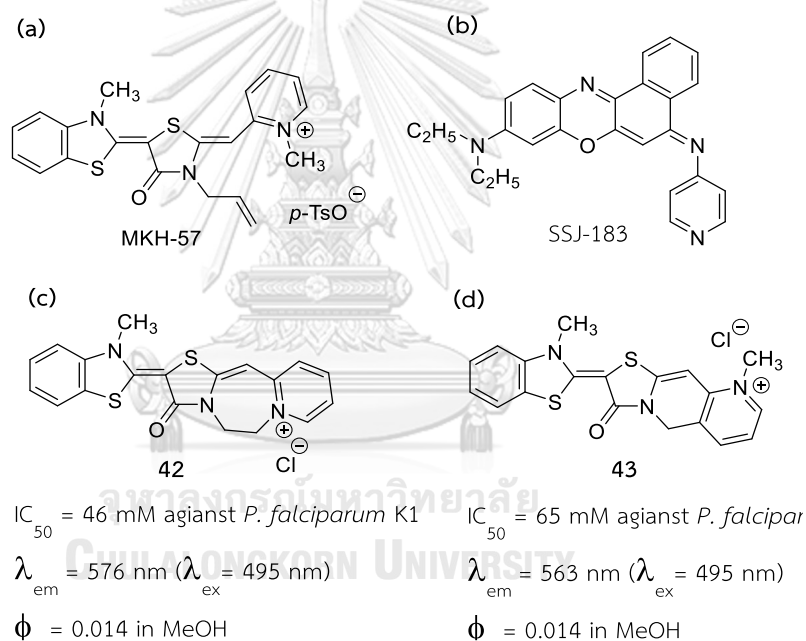


**Figure 6** (a) The structure of MKH-57; (b) the structure of SJJ-183. (c) The synthesised Fused Rhodacyanines as Fluorescent Probes: (c) compound **42**; (d) compound **43**.

The mechanism of action of rhodacyanines for anti-malarial activity was investigated by using the synthesised probes with stronger fluorescence than the original rhodacyanine (MKT-077). They synthesised the new rhodacyanines **42** and **43** (Figures 6c and 6d) which displayed the anti-malarial activities comparable to MKT-077 but fluorescence intensity was improved more than 70 times. Compound **43** clearly showed the fluorescence localization among parasite organelles and the lowest concentration = 5 × 10<sup>-8</sup> M could be detected. Then they studied the double stains of *P. berghei*-infected erythrocytes co-incubated with compound **43** and selective fluorescent markers of subcellular organelles, including marker of nucleus (DAPI) and

mitochondria (Mitotracker Red CMXRos®). The fluorescent microscopic images of the intracellular distribution of **43** with DAPI was found among different organelles. In contrast, the localised fluorescence of compound **43** was consistent with CMXRos® signal which indicated that the rhodacyanine **43** selectively accumulated within the plasmodium mitochondria. Thus, the uptake of rhodacyanines in mitochondria plays an important role in anti-malaria.<sup>46</sup> In addition, the benzophenoxazine dye SSJ-183 (**Figure 6b**) was also discovered by the same group to show a good *in vitro* anti-malarial activity against *P. falciparum* ( $IC_{50}$  = 7.6 nM, selectivity index >7300) and an excellent *in vivo* safety test for oral doses (highest concentration = 2000 mg/kg).<sup>56</sup>

### 2.5.3 Rhodacyanine analogues as anti-leishmaniasis

Apart from the anti-cancer and antimalarial property, M. Ihara and co-workers later found that the rhodacyanine dyes were also effective as other anti-parasitic agents, especially the anti-leishmaniasis. In 2004, the same group reported the anti-leishmanial property of rhodacyanine dyes against *Leishmania major*,<sup>57</sup> and later in 2010, the activity against *Leishmania donovani* was also reported.<sup>7</sup> The evaluation of the structure-activity relationships revealed numerous features contributing to the drug effectiveness. First, it was found that the molecules containing benzothiazole rings at both ends exhibited greater activities comparing to other types of heterocycles. In addition, the  $\pi$ -electron delocalised lipophilic cations (DLCs) feature is highly emphasized and the optimum lengths of the methine bridges were found to be  $m = 2$  and  $n = 1$  (**Figure 7a**). Strikingly, replacing a hydrogen atom on the C-5 position of the benzothiazole ring with a fluorine atom (SJL-01) enhances the *in vitro* activity for almost 10 times (even surpass that of miltefosine as a drug reference) and the selectivity was improved for over 200 times (**Figure 7b**). The animal testing revealed that SJL-01 also exhibits high *in vivo* *L. donovani* inhibition via intravenous administration (injected directly into the vein). However, it showed no bioavailability when administered subcutaneously (injected into the part between the skin and muscle), potentially due to the low membrane permeability. In addition, it also showed poor activities when administered orally.

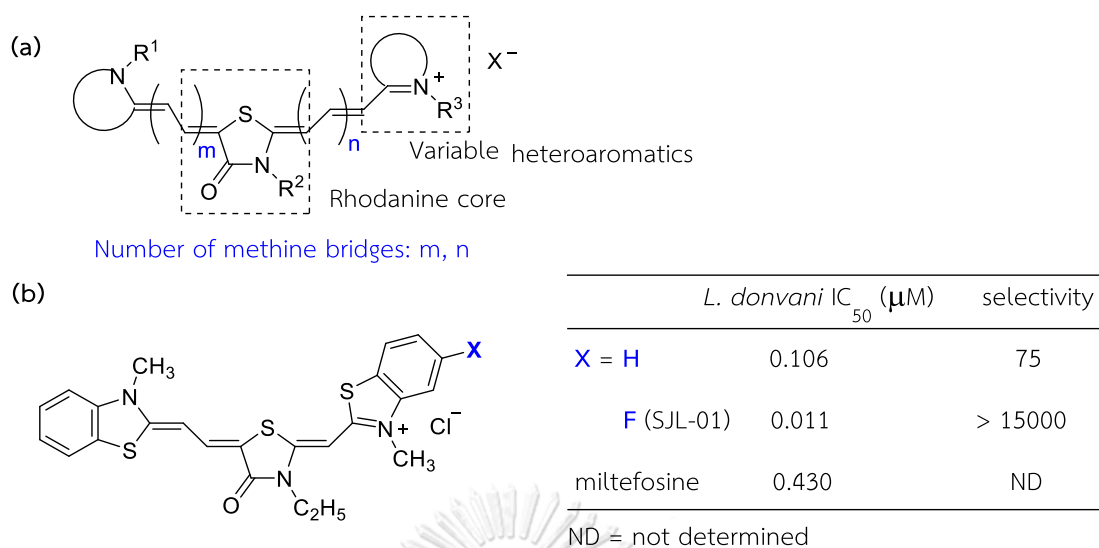


**Figure 7** (a) The general structure of rhodacyanine; (b) the enhancement of *in vitro* activity against *L. donovani* of the fluorinated rhodacyanine

## 2.6 Fluorine in drug discovery

Fluorine or fluorine-containing groups such as difluoromethyl ( $-\text{CF}_2\text{H}$ ), trifluoromethyl ( $-\text{CF}_3$ ), difluoromethoxy ( $-\text{OCF}_2\text{H}$ ), trifluoromethoxy ( $-\text{OCF}_3$ ), and trifluoromethyl thiol ( $-\text{SCF}_3$ ) have found many applications in medicinal chemistry, especially in drug design and development.<sup>58</sup> It was estimated that these motifs appeared in over 30 % of newly approved drugs, as well as in many top-selling drugs such as atorvastatin (trade name: Lipitor), the most profitable drug to date.<sup>59</sup> The installation of fluorine substituent at a suitable position on drug molecules can dramatically improve pharmaceutical effectiveness, biological half-life, and bioabsorption of the drug due to the unique properties of fluorine.

Among all of the elements, fluorine has the highest electronegativity ( $\chi_p = 4$ ),<sup>60</sup> which can lower the  $pK_a$  of its neighbouring functional groups; hence affecting the pharmacokinetic properties as well as the binding affinities of drug molecules.<sup>61</sup> The small size of a fluorine atom (van der Waals radius = 1.47 Å)<sup>62</sup> is very convenient for replacing a hydrogen atom in drug molecules since it will cause only a minor steric demand at receptor sites.<sup>63</sup> Additionally, the exceptionally high C–F bond strength (homolytic bond dissociation enthalpy = 441 kJ/mol) can be exploited for preventing metabolic oxidation of drug molecules (usually by P450 enzymes in the liver) which is one of the major problems in drug design.<sup>64, 65</sup> Blocking the metabolic labile sites with fluorine atoms can significantly increase the half-life of the drug *in vivo* as demonstrated by the development of the cholesterol inhibitor, ezetimibe (**Figure 8a**);<sup>66</sup> introduction of fluorine atoms enhanced drug effectiveness for over 50 times.

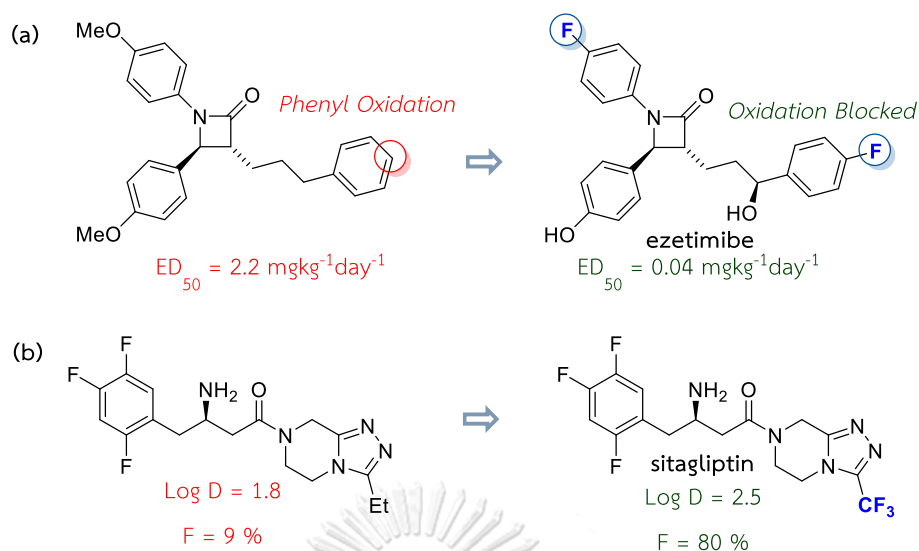


**Figure 8** (a) The prevention from metabolic oxidation in the presence of fluorine substituent; (b) an enhanced lipophilicity of trifluoromethyl group in sitagliptin;  $ED_{50}$  = median effective dose; Log D = distribution coefficient; F = bioavailability.

Another major concern associated with drug design is the drug absorption, which directly affects the bioavailability (F) of the drug, especially when the drug is administered orally (as a reference, F = 100 % when a medication is administered intravenously).<sup>67</sup> Drug molecules can enter living cell *via* two mechanisms: the active transport (a process that requires energy) and a passive transport (a process that does not require energy). The passive transport is the more common route and it is largely influenced by the drug permeability through cell membrane; therefore, the lipophilicity (usually quantified by the distribution coefficient, log D) of drug molecules is a crucial factor in this process.

Typically, the drug must be lipophilic enough to be able to enter the lipid bilayer membrane but not too lipophilic to be permanently trapped in it. In this context, fluorine-containing groups can be employed to fine-tune the lipophilicity of the drug molecules.<sup>68</sup> The introduction a fluorine atom may lead to the decrease in the lipophilicity since the molecules become more polar due to the strong C–F bond dipoles.<sup>69</sup> On the other hand, perfluoroalkyl groups such as trifluoromethyl ( $-CF_3$ ) can significantly increase lipophilicity due to the low polarizability of fluorine (the same principle as largely employed in the super-hydrophobic surface of Teflon).<sup>70</sup> For example, the enhanced lipophilicity of sitagliptin (Junavia<sup>®</sup>), a drug for treatment of type II diabetes mellitus, was achieved by replacement of an ethyl group with the trifluoromethyl group (Log D increases from 1.8 to 2.5), leading to a dramatic increase in

bioavailability from 9% to 80% (**Figure 8b**).<sup>71</sup> In particular, SJL-01 also experienced the similar problem, which could potentially be fixed by the introduction of these fluorine-containing motifs.

### 3. Objectives

- 3.1 To design, synthesise and characterise novel fluorinated analogues of rhodacyanine
- 3.2 To evaluate the anti-leishmanial activity of the synthesised rhodacyanine analogues against indigenous Leishmania in Thailand and establish the structure-activity relationship (SAR)
- 3.3 To investigate the mechanism of action of the synthesised rhodacyanine analogues on the anti-leishmanial activity

### 4. Scope of research

- 4.1 Synthesise fluorinated analogues of rhodacyanine
- 4.2 Evaluate the bioactivity of the synthesised fluorinated rhodacyanine analogues
- 4.3 Establish the structure-activity relationship (SAR)
- 4.4 Clarify the mechanism of action of the fluorinated rhodacyanines

### 5. Beneficial outcome

New fluorinated rhodacyanine analogues for anti-leishmaniasis with improved activities, the structure-activity relationship (SAR) and mechanism of action will be obtained.

## CHAPTER II EXPERIMENTS

The methodology for this research project is divided into 4 stages (**Figure 9**). First, various fluorine-containing building blocks (fluorinated benzothiazolium tosylate) were prepared. Next, the fluorinated rhodacyanine analogues were synthesised starting from the prepared building blocks. After that, those compounds were evaluated their anti-leishmanial activities against the proliferation of promastigote and amastigote forms of *Leishmania orientalis* and *L. martiniquensis*. Finally, the selected rhodacyanine analogues were investigated for their mechanism of action.

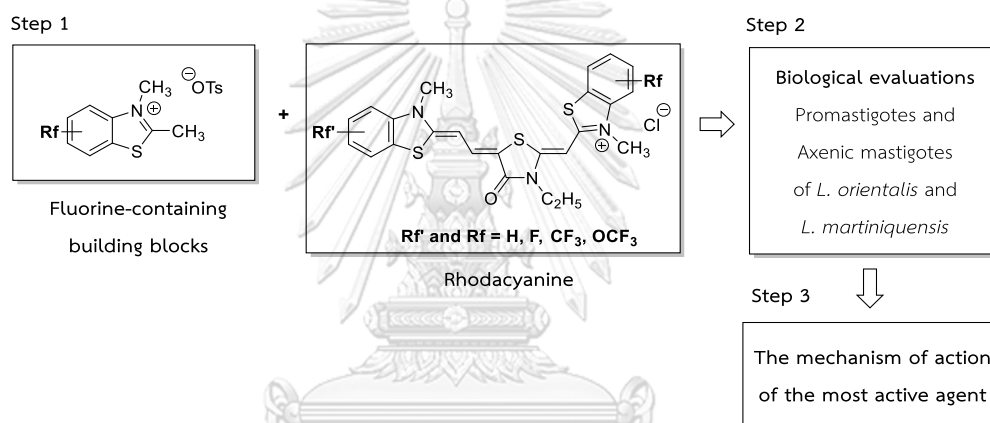


**Figure 9** An overview of the research methodology

### 1. Chemical synthesis

The fluorinated rhodacyanine analogues were designed and synthesised using the following procedures according to the previous reports by M. Ihara and co-workers,<sup>7, 57</sup> which were divided into 2 major steps, including the synthesis of fluorinated-containing building blocks (**Figure 10**), and the synthesis of the fluorinated rhodacyanine analogues (**Figure 11**).



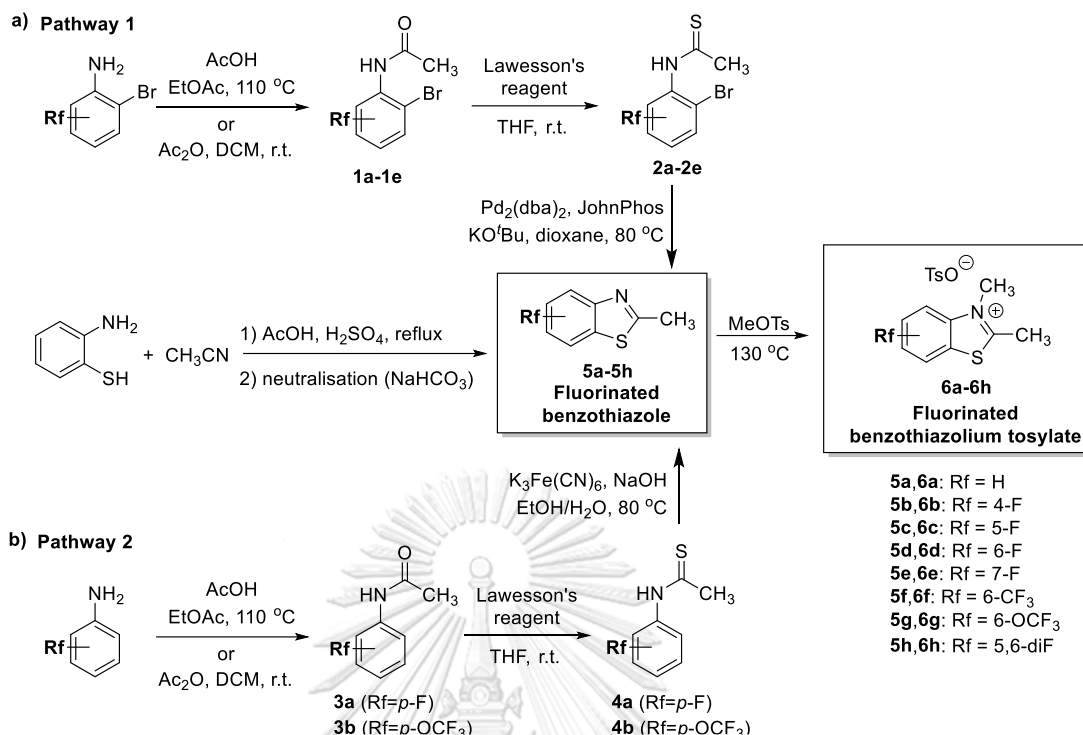


Figure 10 The synthesis procedures of fluorinated benzothiazolium tosylate (a) pathway 1; (b) pathway 2

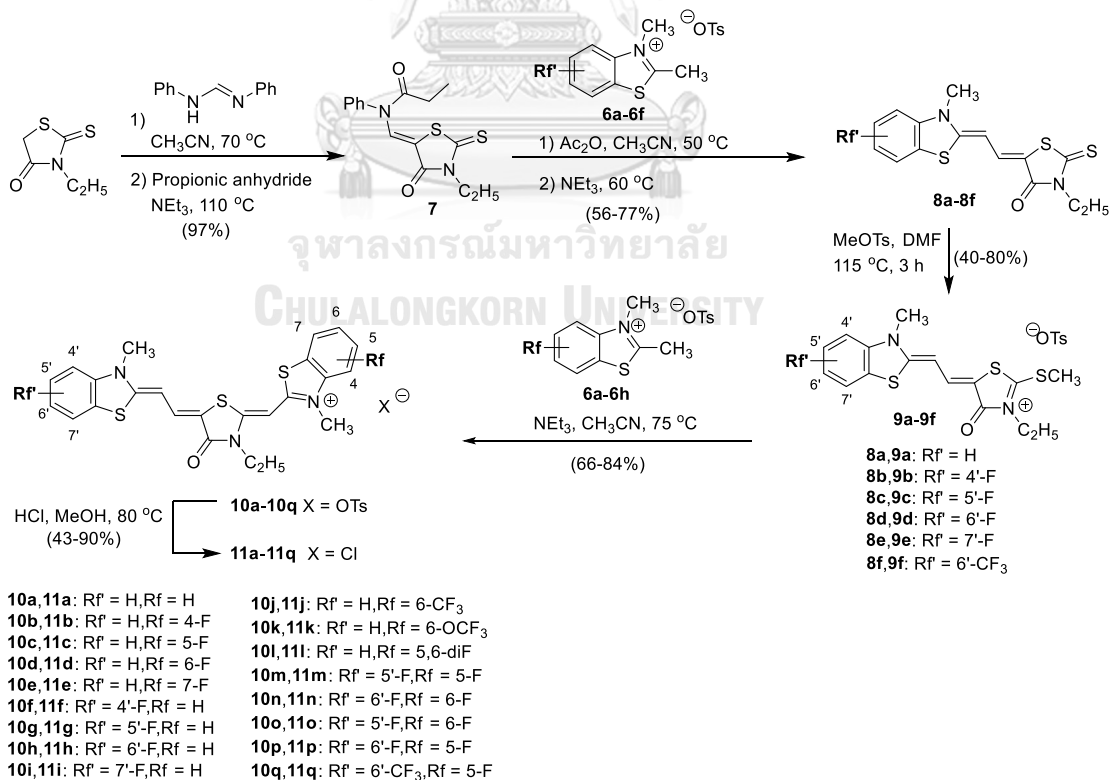


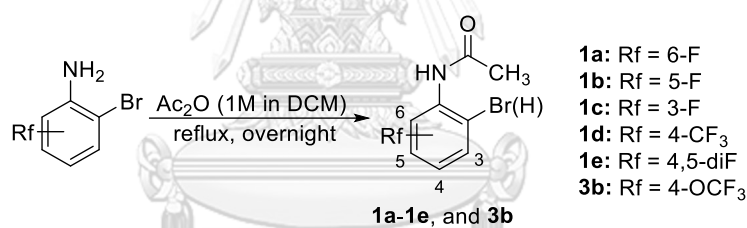
Figure 11 The synthesis of fluorine-containing rhodacyanines

### 1.1 Materials for chemical synthetic section

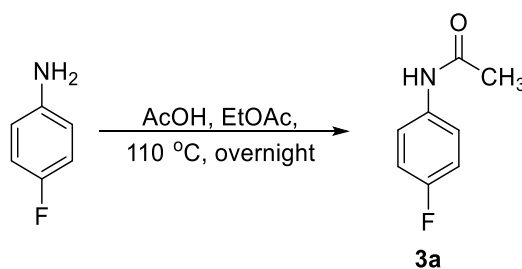
All reagents and solvents were obtained from Sigma-Aldrich (St. Louis, MO, USA), TCI Chemicals (Tokyo, Japan), Fluorochem (Hadfield, Derbyshire, UK) and Merck (Darmstadt, Germany). All solvents for column chromatography from RCI Labscan (Samutsakorn, Thailand) were distilled before use. Reactions were monitored by thin-layer chromatography (TLC) using aluminium Merck TLC plates coated with silica gel 60 F<sub>254</sub>. Normal phase column chromatography was performed using silica gel 60 (0.063-0.200 mm, 70-230 mesh ASTM, Merck, Darmstadt, Germany). Proton, carbon, fluorine and two-dimensional nuclear magnetic resonance (<sup>1</sup>H, <sup>13</sup>C, <sup>19</sup>F and 2D NMR) spectra were recorded on a Bruker Avance (III) 400WB spectrometer. Chemical shifts were expressed in parts per million (ppm), *J* values were in Hertz (Hz). High-resolution mass spectra (HRMS) were obtained with a micrOTOF-Q II mass spectrometer (Bruker Daltonics) with electrospray ionization. IR spectra were recorded using the Thermo Scientific™ Nicolet™ iS50 FTIR spectrometer with ATR module. Melting points (Mp) were determined using a Stuart SMP20 melting point apparatus.

### 1.2 General procedure

#### 1.2.1 General procedure A



*Method I.* Compounds **1a-1e** and **3b** were synthesised using a modified procedure.<sup>72</sup> Substituted aniline (1.0 equiv.) was added to a round-bottom flask. The flask was fitted with a rubber septum and purged with nitrogen gas, and acetic anhydride (1M in CH<sub>2</sub>Cl<sub>2</sub>, 1.1 equiv.) was added at room temperature. The reaction was refluxed overnight and monitored by TLC. Upon completion the reaction mixture was quenched with H<sub>2</sub>O. The resulting mixture was extracted with CH<sub>2</sub>Cl<sub>2</sub>. The combined organic layers were washed with brine, dried over anh. Na<sub>2</sub>SO<sub>4</sub>, filtered, then concentrated *in vacuo* to give the product.



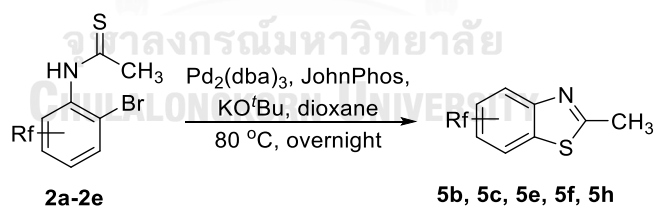
*Method II.* Compound **3a** was synthesised using a modified procedure.<sup>73</sup> To a solution of substituted aniline (1.0 equiv.) in EtOAc was added acetic acid (5.0 equiv.). The mixture was refluxed at 110 °C overnight then cooled to room temperature. After the crude mixture was concentrated *in vacuo*, the resulting solid was recrystallised in EtOAc/hexanes. The solid was collected and washed with hexanes to give the product.

### 1.2.2 General procedure B



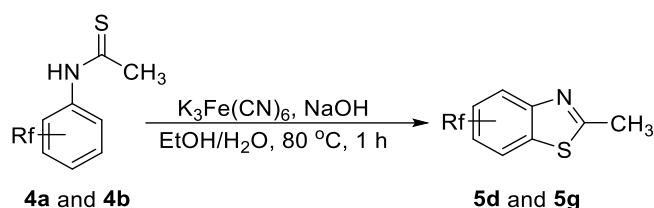
Compounds **2a-2e**, **4a**, and **4b** were synthesised using a modified procedure.<sup>72</sup> Compound **1a-1e**, **3a**, or **3b** (1.0 equiv.) was added to a round-bottom flask. The flask was fitted with a rubber septum, purged with nitrogen gas, then dry THF was added. Lawesson's reagent (0.7 equiv.) was added then the mixture was stirred at room temperature for 24 h and monitored by TLC. Upon completion the reaction mixture was quenched with H<sub>2</sub>O and the resulting mixture was extracted with EtOAc. The combined organic layers were washed with brine, dried over anhydrous Na<sub>2</sub>SO<sub>4</sub>, filtered then concentrated *in vacuo*. The crude mixture was purified by silica gel column chromatography to give the product.

### 1.2.3 General procedure C



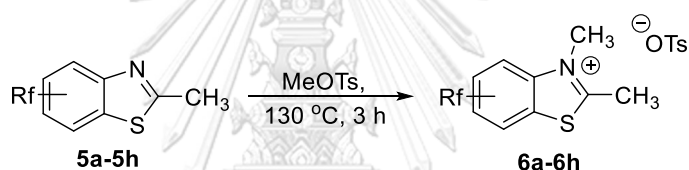
The compounds **5b**, **5c**, **5e**, **5f** and **5h** were synthesised using a modified procedure.<sup>72</sup> To a solution of **2a-2e** (1.0 equiv.) in 1,4-dioxane under nitrogen atmosphere; Pd<sub>2</sub>(dba)<sub>3</sub> (5 mol%), JohnPhos (7.5 mol%) and potassium *tert*-butoxide (1.5 equiv.) were added. The resulting mixture was stirred at 80 °C overnight then cooled to room temperature. The reaction mixture was filtered through Celite<sup>®</sup>, washed with EtOAc, and the filtrate was concentrated *in vacuo*. The crude mixture was purified by silica gel column chromatography to provide the product.

## 1.2.4 General procedure D



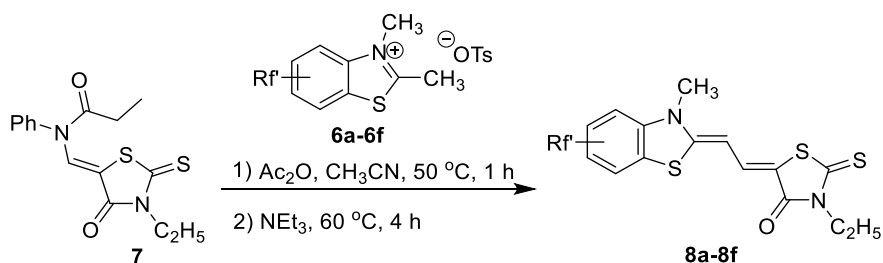
Compounds **5d** and **5g** were synthesised using a modified procedure.<sup>74</sup> A solution of potassium hexacyanoferrate(III) (3.0 equiv.) in H<sub>2</sub>O was added to a round bottom flask followed by dropwise addition of a solution of **4a** or **4b** (1.0 equiv.) in the mixture of EtOH and 10% NaOH (8.0 equiv.). The mixture was refluxed at 80 °C for 1 h or until the starting material was completely consumed. After that, the mixture was extracted with EtOAc. The combined organic layers were washed with brine, dried over anhydrous Na<sub>2</sub>SO<sub>4</sub>, filtered then concentrated *in vacuo*. The crude mixture was purified by silica gel column chromatography to provide the product.

## 1.2.5 General procedure E



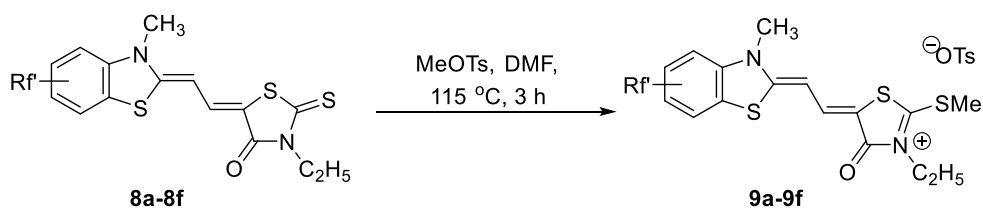
Compounds **6a-6h** were synthesised using a modified procedure.<sup>75</sup> A solution of **5a-5h** (1.0 equiv.) in methyl *p*-toluenesulfonate (1.3 equiv.) was stirred at 130 °C for 3 h then cooled to room temperature. Acetone was added, and the resulting mixture was stirred at room temperature for 1 h to allow precipitation. Then, the solid was collected using vacuum filtration and washed with cold acetone. The solid was dried *in vacuo* to obtain the product.

## 1.2.6 General procedure F



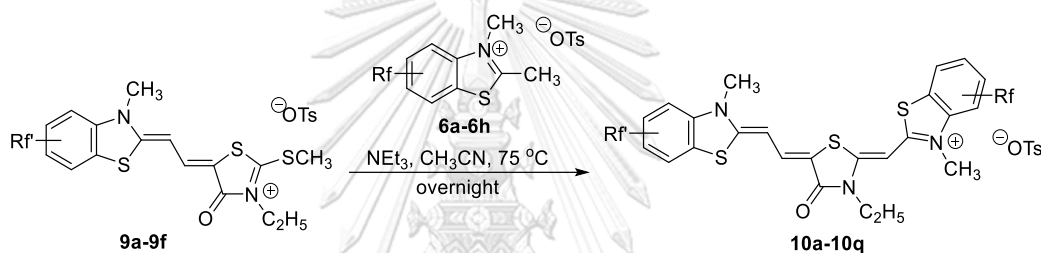
Compounds **8a-8f** were synthesised using the previous method.<sup>55</sup> A mixture of **7** (1 equiv.) and **6a-6f** (1 equiv.) in acetonitrile was added acetic anhydride (1.4 equiv.). After stirring at 50 °C for 1 h, triethylamine (3.7 equiv.) was added and the resulting mixture was stirred at 60 °C for an additional 4 h. Then, the solution was cooled to room temperature. The precipitate was filtered and washed with acetonitrile. The solid was dried *in vacuo* to obtain the product.

## 1.2.7 General procedure G



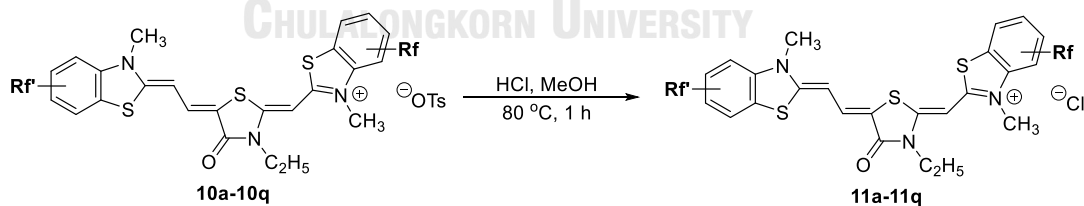
Compounds **9a-9f** were synthesised using the previous method.<sup>55</sup> A mixture of **8a-8f** (1 equiv.) and methyl *p*-toluenesulfonate (3 equiv.) in dimethylformamide was stirred at 115 °C for 3 h. After being cooled to room temperature, the mixture was stirred with acetone for further 30 min to allow precipitation. The solid formed was collected and washed with acetone to give the product.

## 1.2.8 General procedure H



Compounds **10a-10q** were synthesised using a modified method.<sup>7</sup> To a mixture of **9a-9f** (1.0 equiv.) and **6a-6h** (1.0 equiv.) in acetonitrile was added triethylamine (3.0 equiv.). The mixture was stirred at 75 °C overnight. After being cooled to room temperature, the precipitate formed was collected and washed with acetonitrile to give the product.

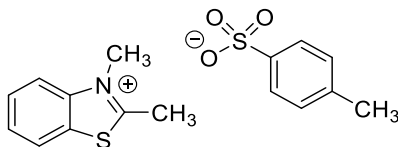
## 1.2.9 General procedure I



Compounds **11a-11q** were synthesised using the previous method.<sup>7</sup> The tosylate salts, **10a-10q**, (1.0 equiv.) were dissolved in methanol. The resulting solution was stirred at 80 °C for 30 min before slowly adding conc. HCl. The mixture was stirred for an additional 30 min. After cooling to room temperature, the precipitate formed was filtered and washed with methanol to yield **11a-11q**.

### 1.3 Synthesis of benzothiazolium building blocks (6a-6h)

#### 1.3.1 2,3-Dimethylbenzo[d]thiazol-3-ium 4-methylbenzenesulfonate (6a)

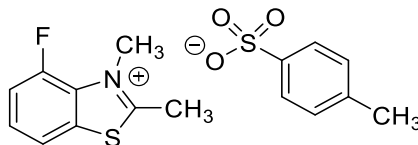


The title compound was synthesised using the modified method.<sup>76</sup> The mixture of 2-aminothiophenol (4.28 mL, 40 mmol, 1.0 equiv.), acetonitrile (6.23 mL, 120 mmol, 3.0 equiv.), glacial acetic acid (40 mL), and conc. H<sub>2</sub>SO<sub>4</sub> (0.43 mL, 20 mol%) was stirred under reflux overnight. After being cooled to room temperature, the mixture was neutralised by sat. NaHCO<sub>3</sub>(aq) and extracted with EtOAc (3 x 20 mL). The combined organic layers were washed with brine, dried with anh. Na<sub>2</sub>SO<sub>4</sub>, filtered and concentrated *in vacuo*. The crude product was purified by silica gel column chromatography (eluent: EtOAc/hexanes = 1:4) to give 2-methylbenzo[d]thiazole (**5a**) (3.85 g, 26 mmol, 64% yield). Then **6a** was synthesised following the **General procedure E** using **5a** (3.77 g, 25.3 mmol), methyl *p*-toluenesulfonate (5.06 mL, 32.8 mmol), to give the title compound (6.06 g, 72% yield) as a light-green solid.

<sup>1</sup>H NMR (400 MHz, DMSO-*d*<sub>6</sub>) δ 8.40 (d, *J* = 8.1 Hz, 1H, ArH), 8.26 (d, *J* = 8.4 Hz, 1H, ArH), 7.88 (t, *J* = 7.8 Hz, 1H, ArH), 7.79 (t, *J* = 7.7 Hz, 1H, ArH), 7.46 (d, *J* = 7.8 Hz, 2H, ArH), 7.08 (d, *J* = 7.6 Hz, 2H, ArH), 4.18 (s, 3H, CH<sub>3</sub>), 3.15 (s, 3H, CH<sub>3</sub>), 2.26 (s, 3H, CH<sub>3</sub>); <sup>13</sup>C NMR (101 MHz, DMSO-*d*<sub>6</sub>) δ 177.49, 145.80, 141.81, 137.93, 129.49, 128.92, 128.30, 128.28, 125.68, 124.61, 116.98, 36.33, 20.98, 17.19; IR (neat): 1585 (C=N), 1524 (C=N), 1218 (SO<sub>3</sub>), 1187 (SO<sub>3</sub>), 1116 (C-S), 1030 (SO<sub>3</sub>), 819 (C-S), 680 (C-S) cm<sup>-1</sup>; HRMS (ESI<sup>+</sup>): *m/z* calcd for C<sub>9</sub>H<sub>10</sub>NS<sup>+</sup> [M]<sup>+</sup> 164.0528, found 164.0537; Mp: 185-187 °C.

Data consistent with the literature values<sup>75</sup>

#### 1.3.2 4-Fluoro-2,3-dimethylbenzo[d]thiazol-3-ium 4-methylbenzenesulfonate (6b)

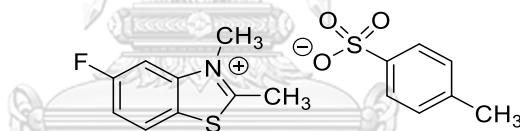


The title compound was synthesised following **General procedure A, method I** using 2-bromo-6-fluoroaniline (2.3 mL, 20 mmol) and acetic anhydride (1M in dichloromethane, 22 mL, 22 mmol) to give *N*-(2-bromo-6-fluorophenyl)acetamide (**1a**) (4.68 g, 100% yield) as a white solid. Next, **1a** (4.52 g, 19.5 mmol) was thionated *via* **General procedure B** using dry THF (70 mL) and Lawesson's reagent (6.17 g, 14 mmol). The crude product was purified by silica gel column chromatography (eluent: EtOAc/hexanes = 1:20-1:4) to give *N*-(2-bromo-6-fluorophenyl)

thioacetamide (**2a**) (4.13 g, 85% yield) as a yellow solid. Then, **2a** (4.12 g, 16.6 mmol) was subjected to **General procedure C** using 1,4-dioxane (60 mL), Pd<sub>2</sub>(dba)<sub>3</sub> (0.76 g, 0.83 mmol), JohnPhos (0.37 g, 1.25 mmol) and potassium *tert*-butoxide (2.79 g, 24.9 mmol). The crude product was purified by silica gel column chromatography (eluent: EtOAc/hexanes = 1:20-1:4) to provide 5-fluoro-2-methylbenzo[*d*]thiazole (**5b**) (1.84 g, 66% yield) as a pale-yellow oil. Finally, **5b** (1.84 g, 11 mmol) was subjected to **General procedure E** using methyl *p*-toluenesulfonate (2.2 mL, 14.3 mmol) to give the desired product **6b** (2.19 g, 56% yield) as a yellow solid.

<sup>1</sup>H NMR (400 MHz, DMSO-*d*<sub>6</sub>) δ 8.24 (dd, *J* = 6.3, 2.7 Hz, 1H, ArH), 7.91 – 7.68 (m, 2H, ArH), 7.45 (d, *J* = 8.0 Hz, 2H, ArH), 7.09 (d, *J* = 7.8 Hz, 2H, ArH), 4.28 (s, 3H, CH<sub>3</sub>), 3.15 (s, 3H, CH<sub>3</sub>), 2.27 (s, 3H, CH<sub>3</sub>); <sup>13</sup>C NMR (101 MHz, DMSO-*d*<sub>6</sub>) δ 178.52, 150.77 (d, <sup>1</sup>*J*<sub>CF</sub> = 253.4 Hz), 145.76, 137.48, 131.27, 130.27 (d, <sup>2</sup>*J*<sub>CF</sub> = 10.6 Hz), 129.04 (d, <sup>3</sup>*J*<sub>CF</sub> = 7.6 Hz), 127.94, 125.40, 120.73 (d, <sup>3</sup>*J*<sub>CF</sub> = 4.5 Hz), 115.98 (d, <sup>2</sup>*J*<sub>CF</sub> = 19.3 Hz), 39.18, 20.70, 16.94; <sup>19</sup>F NMR (376 MHz, DMSO-*d*<sub>6</sub>) δ -125.36; IR (neat): 1588 (C=N), 1521 (C=N), 1262 (C-F), 1216 (SO<sub>3</sub>), 1191 (SO<sub>3</sub>), 1116 (C-S), 1027 (SO<sub>3</sub>), 919 (C-F), 810 (C-S), 677 (C-S) cm<sup>-1</sup>; HRMS (ESI<sup>+</sup>): *m/z* calcd for C<sub>9</sub>H<sub>9</sub>FNS<sup>+</sup> [M]<sup>+</sup> 182.0434, found 182.0438; Mp: 203-206 °C.

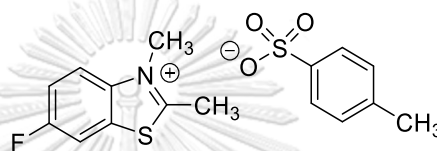
### 1.3.3 5-Fluoro-2,3-dimethylbenzo[*d*]thiazol-3-ium 4-methylbenzenesulfonate (**6c**)



The title compound was synthesised following **General procedure A, method I** using 2-bromo-5-fluoroaniline (4.75 g, 25 mmol) and acetic anhydride (1M in dichloromethane, 28 mL, 27.5 mmol) to give *N*-(2-bromo-5-fluorophenyl)acetamide (**1b**) (5.62 g, 24 mmol, 96% yield) as a white solid. Next, **1b** (5.57 g, 24 mmol) was thionated *via* **General procedure B** using dry THF (80 mL) and Lawesson's reagent (7.49 g, 17 mmol). The crude product was purified by silica gel column chromatography (eluent: EtOAc/hexanes = 1:10-1:4) to give *N*-(2-bromo-5-fluorophenyl)thioacetamide (**2b**) (4.95 g, 20 mmol, 83% yield) as a yellow solid. Then, **2b** (4.91 g, 19.8 mmol) was subjected to **General procedure C** using 1,4-dioxane (66 mL), Pd<sub>2</sub>(dba)<sub>3</sub> (0.91 g, 0.99 mmol), JohnPhos (0.45 g, 1.49 mmol) and potassium *tert*-butoxide (3.33 g, 29.7 mmol). The crude product was purified by silica gel column chromatography (eluent: EtOAc/hexanes = 1:10) to provide 4-fluoro-2-methylbenzo[*d*]thiazole (**5c**) (2.01 g, 12 mmol, 61% yield) as an orange oil. After that, **5c** (1.95 g, 11.7 mmol) was subjected to **General procedure E** using methyl *p*-toluenesulfonate (2.3 mL, 15.2 mmol) to give the title product **6c** (2.23 g, 6.3 mmol, 54% yield) as a light-green solid.

$^1\text{H}$  NMR (400 MHz, DMSO- $d_6$ )  $\delta$  8.46 (dd,  $J$  = 9.0, 5.1 Hz, 1H, ArH), 8.31 (dd,  $J$  = 9.5, 2.2 Hz, 1H, ArH), 7.73 (td,  $J$  = 9.0, 2.3 Hz, 1H, ArH), 7.44 (d,  $J$  = 7.9 Hz, 2H, ArH), 7.08 (d,  $J$  = 7.7 Hz, 2H, ArH), 4.15 (s, 3H,  $\text{CH}_3$ ), 3.15 (s, 3H,  $\text{CH}_3$ ), 2.27 (s, 3H,  $\text{CH}_3$ );  $^{13}\text{C}$  NMR (101 MHz, DMSO- $d_6$ )  $\delta$  179.53, 162.33 (d,  $^1J_{\text{CF}}$  = 246.6 Hz), 145.76, 142.73 (d,  $^3J_{\text{CF}}$  = 12.7 Hz), 137.48, 127.94, 126.44 (d,  $^3J_{\text{CF}}$  = 10.1 Hz), 125.40, 124.68, 116.71 (d,  $^2J_{\text{CF}}$  = 25.0 Hz), 104.15 (d,  $^2J_{\text{CF}}$  = 28.7 Hz), 36.36, 20.70, 17.18;  $^{19}\text{F}$  NMR (376 MHz, DMSO- $d_6$ )  $\delta$  -110.17; IR (neat): 1615, (C=N), 1596 (C=N), 1268 (C-F), 1197 ( $\text{SO}_3$ ), 1119 (C-S), 1037 ( $\text{SO}_3$ ), 921 (C-F), 825 (C-S), 678 (C-S)  $\text{cm}^{-1}$ ; HRMS (ESI $^+$ ):  $m/z$  calcd for  $\text{C}_9\text{H}_9\text{FNS}^+$  [ $\text{M}$ ] $^+$  182.0434, found 182.0474; Mp: 181-184  $^\circ\text{C}$ .

#### 1.3.4 6-Fluoro-2,3-dimethylbenzo[*d*]thiazol-3-ium 4-methylbenzenesulfonate (6d)

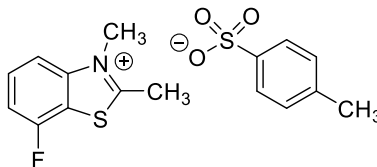


The title compound was synthesised following **General procedure A, method II** using 4-fluoroaniline (4.74 mL, 50 mmol) using EtOAc (25 mL) and acetic acid (7.15 mL, 125 mmol) to give *N*-(4-fluorophenyl)acetamide (**3a**) (5.49 g, 36 mmol, 72% yield) as an off-white solid. Next, **3a** (5.48 g, 36 mmol) was thionated via **General procedure B** using dry THF (120 mL) and Lawesson's reagent (11.03 g, 25 mmol). The crude product was purified by silica gel column chromatography (eluent: EtOAc/hexanes = 1:9-1:1) to give *N*-(4-fluorophenyl)thioacetamide (**4a**) (4.44 g, 26 mmol, 73% yield) as a yellow solid. Then, **4a** (4.44 g, 26 mmol) was subjected to **General procedure D** using potassium hexacyanoferrate(III) (25.44 g, 79 mmol),  $\text{H}_2\text{O}$  (75 mL), EtOH (10 mL) and 10% NaOH(aq) (84 mL, 210 mmol). The crude product was purified by silica gel column chromatography (eluent: EtOAc/hexanes = 1:5-1:3) to provide 6-fluoro-2-methylbenzo[*d*]thiazole (**5d**) (1.29 g, 7.7 mmol, 29% yield) as a yellow solid. After that, **5d** (7 mmol) was subjected to **General procedure E** using methyl *p*-toluenesulfonate (1.4 mL, 9.3 mmol) to give the title product **6d** (1.65 g, 4.7 mmol, 65% yield) as a gray solid.

$^1\text{H}$  NMR (400 MHz, DMSO- $d_6$ )  $\delta$  8.49 – 8.15 (m, 2H, ArH), 7.82 (td,  $J$  = 9.0, 2.5 Hz, 1H, ArH), 7.45 (d,  $J$  = 8.0 Hz, 2H, ArH), 7.09 (d,  $J$  = 7.8 Hz, 2H, ArH), 4.18 (s, 3H,  $\text{CH}_3$ ), 3.14 (s, 3H,  $\text{CH}_3$ ), 2.27 (s, 3H,  $\text{CH}_3$ );  $^{13}\text{C}$  NMR (101 MHz, DMSO- $d_6$ )  $\delta$  177.79, 160.70 (d,  $^1J_{\text{CF}}$  = 247.3 Hz), 145.78, 138.47, 137.49, 130.26 (d,  $^3J_{\text{CF}}$  = 12.2 Hz), 127.96, 125.42, 118.76 (d,  $^3J_{\text{CF}}$  = 9.7 Hz), 117.89 (d,  $^2J_{\text{CF}}$  = 25.7 Hz), 110.81 (d,  $^2J_{\text{CF}}$  = 28.6 Hz), 36.41, 20.71, 17.08;  $^{19}\text{F}$  NMR (376 MHz, DMSO- $d_6$ )  $\delta$  -111.72; IR (neat): 1600 (C=N), 1540 (C=N), 1241 (C-F), 1205 ( $\text{SO}_3$ ), 1190 ( $\text{SO}_3$ ), 1122 (C-F), 1022 (C-S), 910 (C-F), 887 (C-F), 820 (C-S), 691 (C-S)  $\text{cm}^{-1}$ ; HRMS (ESI $^+$ ):  $m/z$  calcd for  $\text{C}_9\text{H}_9\text{FNS}^+$  [ $\text{M}$ ] $^+$  182.0434, found 182.0433; Mp: 173-175  $^\circ\text{C}$ .



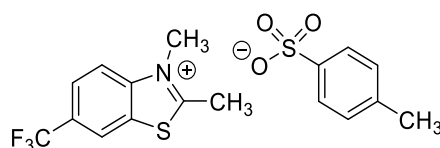
1.3.5 7-Fluoro-2,3-dimethylbenzo[d]thiazol-3-ium  
4-methylbenzenesulfonate (6e)



The title compound was synthesised following **General procedure A, method I** using 2-bromo-3-fluoroaniline (1.9 g, 10 mmol) and acetic anhydride (1M in dichloromethane, 11 mL, 11 mmol) to give *N*-(2-bromo-3-fluorophenyl)acetamide (**1c**) (2.44 g, 10 mmol, 100% yield) as a white solid. Next, **1c** (10 mmol) was thionated *via* **General procedure B** using dry THF 20 mL and Lawesson's reagent (3.1 g, 7.0 mmol). The crude product was purified by silica gel column chromatography (eluent: EtOAc/hexanes = 1:10) to give *N*-(2-bromo-3-fluorophenyl)thioacetamide(**2c**) (1.35 g, 5.4 mmol, 54% yield) as a yellow oil. Then, **2c** (1.34 g, 5.4 mmol, 1.0 equiv.) was subjected to **General procedure C** using 1,4-dioxane (20 mL), Pd<sub>2</sub>(dba)<sub>3</sub> (0.25 g, 0.27 mmol), JohnPhos (0.12 g, 0.41 mmol) and potassium *tert*-butoxide (0.91 g, 8.1 mmol). The crude product was purified by silica gel column chromatography (eluent: EtOAc/hexanes = 1:9-1:4) to provide 7-fluoro-2-methylbenzo[d]thiazole (**5e**) (0.61 g, 3.6 mmol, 67% yield) as an orange oil. After that, **5e** (1.0 g, 6.0 mmol, 1 equiv.) was subjected to **General procedure E** using methyl *p*-toluenesulfonate (1.2 mL, 7.8 mmol) to give the title product **6e** (0.83 g, 2.3 mmol, 39% yield) as a dark-brown solid.

<sup>1</sup>H NMR (400 MHz, DMSO-*d*<sub>6</sub>) δ 8.19 (d, *J* = 8.5 Hz, 1H, ArH), 7.95 (td, *J* = 8.3, 5.4 Hz, 1H, ArH), 7.76 (t, *J* = 8.9 Hz, 1H, ArH), 7.44 (d, *J* = 8.0 Hz, 2H ArH), 7.08 (d, *J* = 7.8 Hz, 2H, ArH), 4.23 (s, 3H, CH<sub>3</sub>), 3.22 (s, 3H, CH<sub>3</sub>), 2.27 (s, 3H, CH<sub>3</sub>); <sup>13</sup>C NMR (101 MHz, DMSO-*d*<sub>6</sub>) δ 178.41, 155.80 (d, <sup>1</sup>*J*<sub>CF</sub> = 250.2 Hz), 145.75, 143.84 (d, <sup>3</sup>*J*<sub>CF</sub> = 5.3 Hz), 137.51, 131.44 (d, <sup>3</sup>*J*<sub>CF</sub> = 7.6 Hz), 127.97, 125.41, 116.40 (d, <sup>2</sup>*J*<sub>CF</sub> = 23.0 Hz), 114.04 (d, <sup>2</sup>*J*<sub>CF</sub> = 17.5 Hz), 113.59 (d, <sup>4</sup>*J*<sub>CF</sub> = 3.9 Hz), 36.97, 20.72, 17.37; <sup>19</sup>F NMR (376 MHz, DMSO-*d*<sub>6</sub>) δ -113.61; IR (neat): 1585 (C=N), 1254 (C-F), 1216 (SO<sub>3</sub>), 1194 (SO<sub>3</sub>), 1032 (SO<sub>3</sub>), 908 (C-F), 816 (C-S), 675 (C-S) cm<sup>-1</sup>; HRMS (ESI<sup>+</sup>): *m/z* calcd for C<sub>9</sub>H<sub>9</sub>FNS<sup>+</sup> [M]<sup>+</sup> 182.0434, found 182.0446; Mp: 171-173 °C.

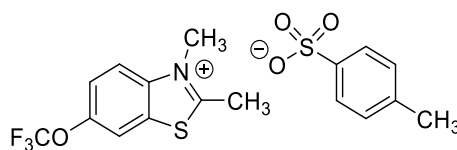
1.3.6 2,3-Dimethyl-6-(trifluoromethyl)benzo[d]thiazol-3-ium 4-methylbenzenesulfonate (6f)



The title compound was synthesised following **General procedure A, method I** using 2-bromo-4-(trifluoromethyl)aniline (2.40 g, 10 mmol) and acetic anhydride (1M in dichloromethane, 11 mL, 11 mmol) to give *N*-(2-bromo-4-(trifluoromethyl)phenyl)acetamide (**1d**) (2.75 g, 9.7 mmol, 97% yield) as a white solid. Next, **1d** (2.68 g, 9.5 mmol, 1 equiv.) was thionated *via* **General procedure B** using dry THF (35 mL) and Lawesson's reagent (2.93 g, 6.6 mmol). The crude product was purified by silica gel column chromatography (eluent: EtOAc/hexanes = 1:10) to give *N*-(2-bromo-4-(trifluoromethyl)phenyl)thioacetamide (**2d**) (2.68 g, 9.0 mmol, 95% yield) as a pale-yellow solid. Then, **2d** (2.65 g, 4.4 mmol) was subjected to **General procedure C** using 1,4-dioxane (30 mL), Pd<sub>2</sub>(dba)<sub>3</sub> (0.41 g, 0.45 mmol), JohnPhos (0.20 g, 0.67 mmol) and potassium *tert*-butoxide (1.50 g, 13.4 mmol) were added. The crude product was purified by silica gel column chromatography (eluent: EtOAc/hexanes = 1:10) to provide 2-methyl-6-(trifluoromethyl)benzo[*d*]thiazole (**5f**) (0.52 g, 2.8 mmol, 63% yield) as a yellow solid. After that, **5f** (0.49 g, 2.6 mmol) was subjected to **General procedure E** using methyl *p*-toluenesulfonate (0.5 mL, 3.4 mmol) to give the title product **6f** (0.34 g, 0.9 mmol, 35% yield) as a brown solid.

<sup>1</sup>H NMR (400 MHz, DMSO-*d*<sub>6</sub>) δ 8.91 (s, 1H), 8.49 (d, *J* = 8.9 Hz, 1H, ArH), 8.22 (d, *J* = 8.9 Hz, 1H, ArH), 7.44 (d, *J* = 8.0 Hz, 2H, ArH), 7.08 (d, *J* = 7.9 Hz, 2H, ArH), 4.23 (s, 3H, CH<sub>3</sub>), 3.21 (s, 3H, CH<sub>3</sub>), 2.26 (s, 3H, CH<sub>3</sub>); <sup>13</sup>C NMR (101 MHz, DMSO-*d*<sub>6</sub>) δ 181.13, 145.54, 143.92, 137.64, 129.49, 128.02 (q, <sup>2</sup>*J*<sub>CF</sub> = 32.8 Hz), 128.00, 125.89 (q, <sup>3</sup>*J*<sub>CF</sub> = 3.3 Hz), 125.41, 123.57 (q, <sup>1</sup>*J*<sub>CF</sub> = 272.7 Hz), 122.49 (q, <sup>3</sup>*J*<sub>CF</sub> = 4.3 Hz), 118.15, 36.48, 20.70, 17.38; <sup>19</sup>F NMR (376 MHz, DMSO-*d*<sub>6</sub>) δ -60.43; IR (neat): 1593 (C=N), 1535 (C=N), 1316 (C-CF<sub>3</sub>), 1213 (SO<sub>2</sub>), 1174 (SO<sub>2</sub>), 1077 (C-CF<sub>3</sub>), 1030 (SO<sub>2</sub>), 919 (C-F), 808 (C-S), 675 (C-S) cm<sup>-1</sup>; HRMS (ESI<sup>+</sup>): *m/z* calcd for C<sub>10</sub>H<sub>9</sub>F<sub>3</sub>NS<sup>+</sup> [M]<sup>+</sup> 232.0402, found 232.0428; Mp: 171-173 °C.

### 1.3.7 2,3-Dimethyl-6-(trifluoromethoxy)benzo[*d*]thiazol-3-ium 4-methylbenzenesulfonate (**6g**)

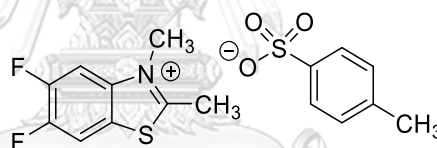


The title compound was synthesised following **General procedure A, method I** using 4-(trifluoromethoxy)aniline (1.78 mL, 20 mmol) and acetic anhydride (1M in dichloromethane, 22 mL, 22 mmol) to give *N*-(4-(trifluoromethoxy)phenyl)acetamide (**3b**) (3.12 g, 14 mmol, 71% yield) as an off-white solid. Next, **3b** (3.09 g, 14 mmol) was thionated *via* **General procedure B** using dry THF (120 mL) and Lawesson's reagent (11.03 g, 25 mmol). The crude product was purified by silica gel column chromatography (eluent: EtOAc/hexanes = 1:4-1:1) to give *N*-(4-(trifluoromethoxy)phenyl)thioacetamide (**4b**) (2.68 g, 11 mmol, 81% yield) as a yellow solid. Then, **4b** (4.44 g, 26 mmol) was subjected to **General procedure D** using potassium

hexacyanoferrate(III) (25.44 g, 79 mmol), H<sub>2</sub>O (75 mL), EtOH (10 mL) and 10% NaOH(aq) (84 mL, 210 mmol). The crude product was purified by silica gel column chromatography (eluent: EtOAc/hexanes = 1:20-1:10) to provide 2-methyl-6-(trifluoromethoxy)benzo[d]thiazole (**5g**) (1.53 g, 6.5 mmol, 59% yield) as an orange solid. After that, **5g** (1.50 g, 6.4 mmol) was subjected to **General procedure E** using methyl *p*-toluenesulfonate (1.3 mL, 8.3 mmol). The crude product was purified by silica gel column chromatography (eluent: methanol/EtOAc = 1:5-1:1) to give the title product **6g** (1.50 g, 3.6 mmol, 56% yield) as a dark-brown solid.

R<sub>f</sub> 0.4 (1:1 methanol:EtOAc); <sup>1</sup>H NMR (400 MHz, DMSO-*d*<sub>6</sub>) δ 8.54 (s, 1H, ArH), 8.40 (d, *J* = 9.2 Hz, 1H, ArH), 7.91 (d, *J* = 9.0 Hz, 1H, ArH), 7.44 (d, *J* = 7.7 Hz, 2H, ArH), 7.07 (d, *J* = 7.8 Hz, 2H, ArH), 4.19 (s, 3H, CH<sub>3</sub>), 3.17 (s, 3H, CH<sub>3</sub>), 2.26 (s, 3H, CH<sub>3</sub>); <sup>13</sup>C NMR (101 MHz, DMSO-*d*<sub>6</sub>) δ 179.14, 146.79, 145.47, 140.20, 137.35, 129.99, 127.75, 125.19, 122.65, 119.76 (q, <sup>1</sup>*J*<sub>CF</sub> = 258.2 Hz), 118.55, 116.57, 36.24, 20.48, 16.99; <sup>19</sup>F NMR (376 MHz, DMSO-*d*<sub>6</sub>) δ -57.11; IR (neat): 1672 (C=N), 1604 (C=N), 1258 (C-F), 1170 (C-O-CF<sub>3</sub>), 1121 (SO<sub>3</sub>), 1038 (SO<sub>3</sub>), 817 (C-S), 680 (C-S) cm<sup>-1</sup>; HRMS (ESI<sup>+</sup>): *m/z* calcd for C<sub>10</sub>H<sub>9</sub>F<sub>3</sub>NOS<sup>+</sup> [M]<sup>+</sup> 248.0351, found 248.0388; Mp: 75-77 °C.

### 1.3.8 5,6-Difluoro-2,3-dimethylbenzo[d]thiazol-3-ium 4-methylbenzenesulfonate (6h)

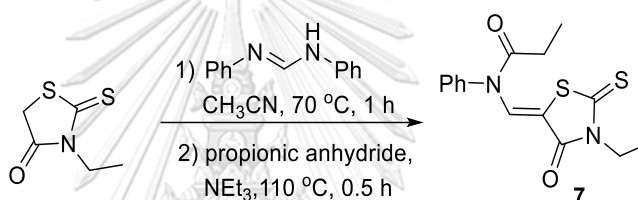


The title compound was synthesised following **General procedure A, method I**, using 2-bromo-4,5-difluoroaniline (2.1 g, 10 mmol) and acetic anhydride (1M in dichloromethane, 11 mL, 11 mmol) to give *N*-(2-bromo-4,5-difluorophenyl)acetamide (**1e**) (2.4 g, 9.6 mmol, 96% yield) as a white solid. Next, **1e** (1.54 g, 6.2 mmol, 1 equiv.) was thionated *via* **General procedure B** using dry THF 25 mL and Lawesson's reagent (1.94 g, 4.4 mmol). The crude product was purified by silica gel column chromatography (eluent: EtOAc/hexanes = 1:20) to give *N*-(2-bromo-4,5-difluorophenyl)thioacetamide (**2e**) (1.20 g, 4.5 mmol, 73% yield) as a yellow oil. Then, **2e** (1.18 g, 4.4 mmol, 1.0 equiv.) was subjected to **General procedure C** using 1,4-dioxane (15 mL), Pd<sub>2</sub>(dba)<sub>3</sub> (0.20 g, 0.22 mmol), JohnPhos (0.10 g, 0.33 mmol) and potassium *tert*-butoxide (0.75 g, 6.7 mmol). The crude product was purified by silica gel column chromatography (eluent: EtOAc/hexanes = 1:20) to provide 5,6-difluoro-2-methylbenzo[d]thiazole (**5h**) (0.52 g, 2.8 mmol, 63% yield) as a yellow solid. After that, **5h** (0.49 g, 2.6 mmol) was subjected to **General procedure E** using methyl *p*-toluenesulfonate (0.5 mL, 3.4 mmol) to give the title product **6h** (0.34 g, 0.92 mmol, 35% yield) as a brown solid.

$^1\text{H}$  NMR (400 MHz, DMSO- $d_6$ )  $\delta$  8.62 (dd,  $J = 10.7, 6.7$  Hz, 1H, ArH), 8.53 (dd,  $J = 9.4, 7.9$  Hz, 1H, ArH), 7.45 (d,  $J = 7.9$  Hz, 2H, ArH), 7.09 (d,  $J = 7.8$  Hz, 2H, ArH), 4.15 (s, 3H,  $\text{CH}_3$ ), 3.14 (s, 3H,  $\text{CH}_3$ ), 2.28 (s, 3H,  $\text{CH}_3$ );  $^{13}\text{C}$  NMR (101 MHz, DMSO- $d_6$ )  $\delta$  179.38, 150.63 (dd,  $^1J_{\text{CF}} = 249.7, ^2J_{\text{CF}} = 15.0$  Hz), 149.29 (dd,  $^1J_{\text{CF}} = 250.3, ^2J_{\text{CF}} = 14.6$  Hz), 145.66, 138.27 (d,  $^3J_{\text{CF}} = 9.9$  Hz), 137.58, 127.99, 125.42, 124.97 (dd,  $^3J_{\text{CF}} = 10.1, ^4J_{\text{CF}} = 2.2$  Hz), 112.78 (d,  $^2J_{\text{CF}} = 23.9$  Hz), 106.39 (d,  $^2J_{\text{CF}} = 24.2$  Hz), 36.70, 20.72, 17.24;  $^{19}\text{F}$  NMR (376 MHz, DMSO- $d_6$ )  $\delta$  -132.91 (d,  $J = 21.9$  Hz, 1F), -134.71 (d,  $J = 22.0$  Hz, 1F). IR (neat): 1601 (C=N), 1532 (C=N), 1271 (C-F), 1185 ( $\text{SO}_2$ ), 1116 ( $\text{SO}_2$ ), 1030 ( $\text{SO}_2$ ), 882 (C-F), 810 (C-S), 683 (C-S)  $\text{cm}^{-1}$ ; HRMS (ESI $^+$ ):  $m/z$  calcd for  $\text{C}_9\text{H}_8\text{F}_2\text{NS}^+$  [M] $^+$  200.0340, found 200.0347; Mp: 203-206  $^\circ\text{C}$ .

#### 1.4 Synthesis of fluorinated rhodacyanine analogues (10c, 11a-11q)

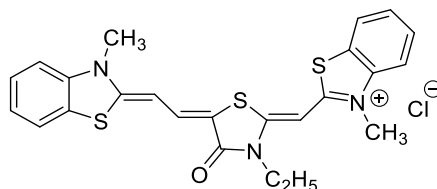
##### 1.4.1 *N*-((3-Ethyl-4-oxo-2-thioxothiazolidin-5-ylidene)methyl)-*N*-phenylpropionamide (7)



The title compound was synthesised using the modified method.<sup>77</sup> A mixture of 3-ethylrhodanine (8.06 g, 50.0 mmol, 1 equiv.) and *N,N'*-diphenylformamidinium (9.81 g, 50.0 mmol, 1 equiv.) in acetonitrile (50 mL) was heated at 70  $^\circ\text{C}$  for 1 h. After cooling to room temperature, the resulting precipitates were filtered and washed with cold acetone to give the intermediate named 3-ethyl-5-((phenylamino)methylene)-2-thioxothiazolidin-4-one (9.67 g, 37 mmol, 73% yield) as a yellow solid. The intermediate (9.67 g, 37 mmol, 1 equiv.) was dissolved in propionic anhydride (20 mL, 157 mmol, 4.2 equiv.) and triethylamine (0.4 mL, 12 mol%). The mixture was stirred at 110  $^\circ\text{C}$  for 30 min. The solution was concentrated *in vacuo* at 75  $^\circ\text{C}$  and allowed to cool to room temperature. After adding methanol into the cold solution over ice bath, the precipitation occurred. The precipitate was collected *via* vacuum filtration and washed with methanol to obtain the desired product (11.41 g, 36 mmol, 97% yield) as a yellow solid.

R<sub>f</sub>: 0.33 (1:4 EtOAc:hexanes);  $^1\text{H}$  NMR (400 MHz, DMSO- $d_6$ )  $\delta$  8.72 (s, 1H, methine CH), 7.70 – 7.52 (m, 3H, ArH), 7.28 (d,  $J = 4.8$  Hz, 2H, ArH), 4.09 (q,  $J = 7.1$  Hz, 2H,  $\text{CH}_2\text{CH}_3$ ), 2.25 (q,  $J = 7.2$  Hz, 2H,  $\text{CH}_2\text{CH}_3$ ), 1.21 (t,  $J = 7.1$  Hz, 3H,  $\text{CH}_2\text{CH}_3$ ), 1.13 (t,  $J = 7.3$  Hz, 3H,  $\text{CH}_2\text{CH}_3$ );  $^{13}\text{C}$  NMR (101 MHz, DMSO- $d_6$ )  $\delta$  194.12, 173.48, 168.40, 136.46, 131.32, 131.20, 130.75, 129.70, 106.07, 39.61, 28.65, 12.22, 8.94; IR (neat): 1718 (C=O of amide), 1604 (cyclic C=O), 1443 (C-N), 1330 (C-N), 1298 (C-N), 1102 (C=S), 883 (C-S)  $\text{cm}^{-1}$ ; Mp: 172-174  $^\circ\text{C}$ .

1.4.2 2-(3-Ethyl-5-(2-(3-methylbenzo[d]thiazol-2(3*H*)-ylidene)ethylidene)-4-oxothiazolidin-2-ylidene)methyl)-3-methylbenzo[d]thiazol-3-ium chloride (11a)

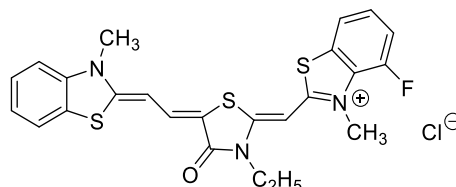


The title compound was synthesised following **General procedure F** using **7** (3.20 g, 10 mmol), **6a** (3.35 g, 10 mmol), acetonitrile (50 mL), acetic anhydride (1.32 mL, 14 mmol) and triethylamine (975  $\mu$ L, 37 mmol) to give 3-ethyl-5-(2-(3-methylbenzo[d]thiazol-2(3*H*)-ylidene)ethylidene)-2-thioxothiazolidin-4-one (**8a**) as a brown solid (1.88 g, 5.6 mmol, 56% yield). Next, **8a** (1.68 g, 5.0 mmol) was subjected to **General procedure G** using methyl *p*-toluenesulfonate (2.3 mL, 15.0 mmol) and DMF (6.7 mL) to give 3-ethyl-5-(2-(3-methylbenzo[d]thiazol-2(3*H*)-ylidene)ethylidene)-2-(methylthio)-4-oxo-4,5-dihydrothiazol-3-ium 4-methylbenzenesulfonate (**9a**) as a green solid (2.08 g, 3.4 mmol, 80% yield). A mixture of **9a** (100 mg, 0.19 mmol) and **6a** (65 mg, 0.19 mmol) was subjected to **General procedure H** using acetonitrile (4.2 mL) and triethylamine (80  $\mu$ L, 0.57 mmol) to give 2-(3-ethyl-5-(2-(3-methylbenzo[d]thiazol-2(3*H*)-ylidene)ethylidene)-4-oxothiazolidin-2-ylidene)methyl)-3-methylbenzo[d]thiazol-3-ium 4-methylbenzenesulfonate (**10a**) as a dark-green solid (91 mg, 0.14 mmol, 74% yield). Finally, **10a** (66 mg, 0.1 mmol) was subjected to **General procedure I** using methanol (6.6 mL) and conc. HCl (0.3 mL) to give the title product **11a** as a dark-green solid (31 mg, 0.062 mmol, 62% yield).

$^1\text{H NMR}$  (400 MHz, DMSO- $d_6$ )  $\delta$  8.24 (d,  $J = 8.0$  Hz, 1H, ArH), 7.90 (d,  $J = 8.1$  Hz, 1H, ArH), 7.84 (d,  $J = 7.8$  Hz, 1H, ArH), 7.74 – 7.62 (m, 2H, ArH, methine CH), 7.60 – 7.51 (m, 1H, ArH), 7.50 – 7.38 (m, 2H, ArH), 7.32 – 7.24 (m, 1H, ArH), 6.75 (s, 1H, methine CH), 5.94 (d,  $J = 13.3$  Hz, 1H, methine CH), 4.17 (q,  $J = 6.8$  Hz, 2H,  $\text{CH}_2\text{CH}_3$ ), 4.06 (s, 3H,  $\text{CH}_3$ ), 3.72 (s, 3H,  $\text{CH}_3$ ), 1.27 (t,  $J = 7.0$  Hz, 3H,  $\text{CH}_2\text{CH}_3$ );  $^{13}\text{C NMR}$  (101 MHz, DMSO- $d_6$ )  $\delta$  163.62, 162.95, 162.88, 156.94, 141.89, 140.37, 134.55, 128.83, 127.57, 126.05, 125.80, 124.15, 123.95, 123.42, 122.58, 114.66, 112.40, 101.83, 90.70, 86.32, 39.52, 34.69, 32.89, 12.38 (s); IR (neat): 1673 (C=N), 1562 (C=N), 1512 (C=C), 1471 (C=O), 1342 (C-N), 1181 (C-N), 1019 (C-S), 812 (C-S)  $\text{cm}^{-1}$ ; HRMS (ESI $^+$ ):  $m/z$  calcd for  $\text{C}_{24}\text{H}_{22}\text{N}_3\text{OS}_3^+$  [M] $^+$  464.0920, found 464.0909; Mp: 254-256  $^\circ\text{C}$ .

Data consistent with the literature values<sup>7</sup>

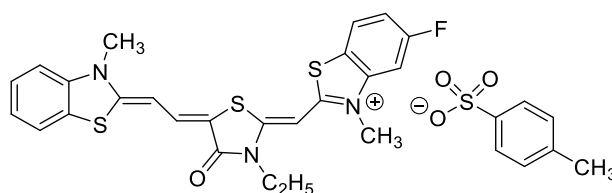
1.4.3 2-(3-Ethyl-5-(2-(3-methylbenzo[d]thiazol-2(3*H*)-ylidene)ethylidene)-4-oxothiazolidin-2-ylidene)methyl)-4-fluoro-3-methylbenzo[d]thiazol-3-ium chloride (11b)



The title compound was synthesised following **General procedure H** using **9a** (156 mg, 0.3 mmol, synthesised as described in the synthesis of **11a**), **6b** (106 mg, 0.3 mmol), acetonitrile (7.0 mL) and triethylamine (125  $\mu$ L, 0.9 mmol) to provide 2-(3-ethyl-5-(2-(3-methylbenzo[d]thiazol-2(3*H*)-ylidene)ethylidene)-4-oxothiazolidin-2-ylidene)methyl)-4-fluoro-3-methylbenzo[d]thiazol-3-ium 4-methylbenzenesulfonate (**10b**) as a dark-green solid (151 mg, 0.23 mmol, 77% yield). Finally, **10b** (93 mg, 0.18 mmol) was subjected to **General procedure I** using methanol (9.0 mL) and conc. HCl (0.6 mL) to give the title product **11b** as a dark-green solid (68 mg, 0.13 mmol, 72% yield).

$^1\text{H NMR}$  (400 MHz, DMSO- $d_6$ )  $\delta$  8.04 (d,  $J$  = 8.9 Hz, 1H, ArH), 7.88 (d,  $J$  = 7.2 Hz, 1H, ArH), 7.72 (d,  $J$  = 13.0 Hz, 1H, methine CH), 7.58 – 7.43 (m, 4H, ArH), 7.32 (t,  $J$  = 6.9 Hz, 1H, ArH), 6.72 (s, 1H, methine CH), 6.03 (d,  $J$  = 13.1 Hz, 1H, methine CH), 4.20 – 4.12 (m, 5H,  $\text{CH}_2\text{CH}_3$ ,  $\text{CH}_3$ ), 3.75 (s, 3H,  $\text{CH}_3$ ), 1.26 (t,  $J$  = 7.1 Hz, 3H,  $\text{CH}_2\text{CH}_3$ );  $^{13}\text{C NMR}$  (101 MHz, DMSO- $d_6$ )  $\delta$  163.58, 163.17, 161.40, 161.35 (d,  $^1J_{\text{CF}}$  = 235.1 Hz), 157.98, 150.76, 145.54, 141.89, 135.11, 127.69, 124.39, 123.31 (d,  $^2J_{\text{CF}}$  = 25.1 Hz), 122.65, 119.70, 116.04 (d,  $^2J_{\text{CF}}$  = 20.5 Hz), 115.99, 112.59, 110.01, 91.17, 86.02, 39.02, 37.29, 33.00, 12.36;  $^{19}\text{F NMR}$  (376 MHz, DMSO- $d_6$ )  $\delta$  -126.65; IR (neat): 1688 (C=N), 1556 (C=N), 1516 (C=C), 1469 (C=O), 1349 (C-N), 1224 (C-F), 1185 (C-N), 1021 (C-S), 921 (C-F), 808 (C-S)  $\text{cm}^{-1}$ ; HRMS (ESI $^+$ ):  $m/z$  calcd for  $\text{C}_{24}\text{H}_{21}\text{FN}_3\text{OS}_3^+$  [M] $^+$  482.0825, found 482.0834; Mp: 231-233  $^\circ\text{C}$ .

1.4.4 2-(3-Ethyl-5-(2-(3-methylbenzo[d]thiazol-2(3*H*)-ylidene)ethylidene)-4-oxothiazolidin-2-ylidene)methyl)-5-fluoro-3-methylbenzo[d]thiazol-3-ium 4-methylbenzenesulfonate (10c)



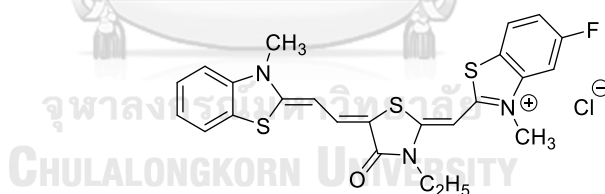
The title compound was synthesised following **General procedure H** using **9a** (100 mg, 0.19 mmol, synthesised as described in the synthesis of **11a**), **6c** (68 mg, 0.19 mmol), acetonitrile

(4.2 mL) and triethylamine (80  $\mu$ L, 0.57 mmol) to provide 2-(3-ethyl-5-(2-(3-methylbenzo[d]thiazol-2(3*H*)-ylidene)ethylidene)-4-oxothiazolidin-2-ylidene)methyl)-5-fluoro-3-methylbenzo[d]thiazol-3-ium 4-methylbenzenesulfonate (**10c**) as a dark-green solid (97 mg, 0.14 mmol, 74% yield).

$^1\text{H NMR}$  (400 MHz, DMSO- $d_6$ )  $\delta$  8.22 (dd,  $J = 5.6$  Hz, 1H, *ArH*), 7.94 – 7.69 (m, 2H, *ArH*), 7.63 (d,  $J = 12.8$  Hz, 1H, methine *CH*), 7.48 (d,  $J = 7.8$  Hz, 2H, *ArH*), 7.45 – 7.33 (m, 3H, *ArH*), 7.28 (s, 1H, *ArH*), 7.11 (d,  $J = 7.9$  Hz, 2H, *ArH*), 6.70 (s, 1H, methine *CH*), 5.92 (d,  $J = 13.1$  Hz, 1H, methine *CH*), 4.16 (q,  $J = 6.9$  Hz, 2H,  $\text{CH}_2\text{CH}_3$ ), 3.97 (s, 3H,  $\text{CH}_3$ ), 3.69 (s, 3H,  $\text{CH}_3$ ), 2.28 (s, 3H,  $\text{CH}_3$ ), 1.28 (t,  $J = 6.9$  Hz, 3H,  $\text{CH}_2\text{CH}_3$ );  $^{13}\text{C NMR}$  (126 MHz, DMSO- $d_6$ )  $\delta$  164.14, 163.22, 162.73 (d,  $^1J_{\text{CF}} = 250.2$  Hz), 157.69, 145.38, 141.74, 138.33, 128.46, 127.81, 126.34, 125.77, 125.09, 124.54, 123.99, 123.30 (d,  $^3J_{\text{CF}} = 9.7$  Hz), 122.77, 122.19 (d,  $^3J_{\text{CF}} = 9.5$  Hz), 121.64, 114.64 (d,  $^2J_{\text{CF}} = 24.7$  Hz), 112.53, 108.59 (d,  $^2J_{\text{CF}} = 27.2$  Hz), 102.18, 91.35, 86.66, 39.19, 34.88, 33.03, 21.04, 12.60;  $^{19}\text{F NMR}$  (376 MHz, DMSO- $d_6$ )  $\delta$  -111.16; IR (neat): 1679 (C=N), 1560 (C=N), 1493 (C=C), 1463 (C=O), 1341 ( $\text{SO}_3$ ), 1190 (C-N), 1124 (C-S) 1030 ( $\text{SO}_3$ ), 1058 (C-S), 915 (C-F), 816 (C-S), 680 (C-S)  $\text{cm}^{-1}$ ; HRMS (ESI $^+$ ):  $m/z$  calcd for  $\text{C}_{24}\text{H}_{21}\text{FN}_3\text{OS}_3^+$  [M] $^+$  482.0825, found 482.0808; Mp: 293-295  $^\circ\text{C}$ .

Data consistent with the literature values<sup>7</sup>

#### 1.4.5 2-(3-Ethyl-5-(2-(3-methylbenzo[d]thiazol-2(3*H*)-ylidene)ethylidene)-4-oxothiazolidin-2-ylidene)methyl)-5-fluoro-3-methylbenzo[d]thiazol-3-ium chloride (**11c**)



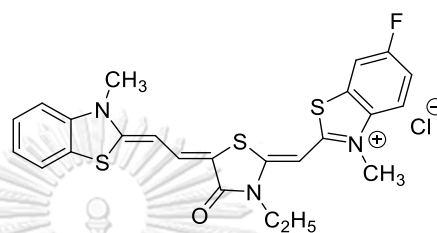
**10c** (65 mg, 0.1 mmol) was subjected to **General procedure I** using methanol (6.6 mL) conc. HCl (0.3 mL) to give the title product **11c** as a dark-green solid (40 mg, 0.07 mmol, 77% yield).

$^1\text{H NMR}$  (400 MHz, DMSO- $d_6$ )  $\delta$  8.25 (dd,  $J = 8.8, 5.1$  Hz, 1H, *ArH*), 7.82 (d,  $J = 7.7$  Hz, 1H, *ArH*), 7.74 (d,  $J = 8.3$  Hz, 1H, *ArH*), 7.59 (d,  $J = 13.1$  Hz, 1H, methine *CH*), 7.42 – 7.32 (m, 3H, *ArH*), 7.30 – 7.22 (m, 1H, *ArH*), 6.71 (s, 1H, methine *CH*), 5.89 (d,  $J = 13.2$  Hz, 1H, methine *CH*), 4.16 (q,  $J = 7.1$  Hz, 2H,  $\text{CH}_2\text{CH}_3$ ), 3.98 (s, 3H,  $\text{CH}_3$ ), 3.68 (s, 3H,  $\text{CH}_3$ ), 1.29 (t,  $J = 7.1$  Hz, 3H,  $\text{CH}_2\text{CH}_3$ );  $^{13}\text{C NMR}$  (101 MHz, DMSO- $d_6$ )  $\delta$  163.68, 163.44, 163.06, 162.66 (d,  $^1J_{\text{CF}} = 285.4$  Hz), 157.31, 141.76, 141.68, 134.63, 127.52, 125.01 (d,  $^3J_{\text{CF}} = 10.1$  Hz), 124.21, 123.85, 122.56, 121.54, 113.53 (d,  $^2J_{\text{CF}} = 24.7$  Hz), 112.37, 102.18 (d,  $^2J_{\text{CF}} = 28.9$  Hz), 101.72, 90.91, 86.49, 39.00, 34.81, 32.87, 12.35;  $^{19}\text{F NMR}$  (376 MHz,

DMSO- $d_6$ )  $\delta$  -111.13; IR (neat): 1668 (C=N), 1560 (C=N), 1513 (C=C), 1466 (C=O), 1191 (C-N), 1127 (C-S), 1055 (C-S), 944 (C-F), 824 (C-S)  $\text{cm}^{-1}$ ; HRMS (ESI<sup>+</sup>):  $m/z$  calcd for  $\text{C}_{24}\text{H}_{21}\text{FN}_3\text{OS}_3^+$  [M]<sup>+</sup> 482.0825, found 482.0841; Mp: 275-277 °C.

Data consistent with the literature values<sup>7</sup>

**1.4.6 2-(3-Ethyl-5-(2-(3-methylbenzo[d]thiazol-2(3H)-ylidene)ethylidene)ethylidene)-4-oxothiazolidin-2-ylidene)methyl)-6-fluoro-3-methylbenzo[d]thiazol-3-ium chloride (11d)**

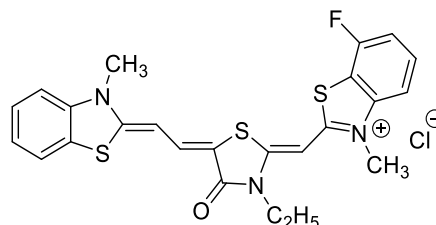


The title compound was synthesised following **General procedure H** using **9a** (100 mg, 0.19 mmol, synthesised as described in the synthesis of **11a**), **6d** (68 mg, 0.19 mmol), acetonitrile (5.0 mL) and triethylamine (80  $\mu\text{L}$ , 0.57 mmol) to give 2-(3-ethyl-5-(2-(3-methylbenzo[d]thiazol-2(3H)-ylidene)ethylidene)ethylidene)-4-oxothiazolidin-2-ylidene)methyl)-6-fluoro-3-methylbenzo[d]thiazol-3-ium 4-methylbenzenesulfonate (**10d**) as a dark-green solid (87 mg, 0.13 mmol, 68% yield). Finally, **10d** (65 mg, 0.1 mmol) was subjected to **General procedure I** using methanol (6.6 mL) and conc. HCl (0.3 mL) to give the title product **11d** as a dark-green solid (32 mg, 0.062 mmol, 62% yield).

<sup>1</sup>H NMR (400 MHz, DMSO- $d_6$ )  $\delta$  8.16 (dd,  $J = 7.9, 1.9$  Hz, 1H, ArH), 7.80 (d,  $J = 8.1$  Hz, 2H, ArH), 7.64 – 7.46 (m, 2H, ArH, methine CH), 7.37 (s, 2H, ArH), 7.24 (s, 1H, ArH), 6.68 (s, 1H, methine CH), 5.87 (d,  $J = 12.9$  Hz, 1H, methine CH), 4.15 (q,  $J = 6.9$  Hz, 2H,  $\text{CH}_2\text{CH}_3$ ), 4.01 (s, 3H,  $\text{CH}_3$ ), 3.69 (s, 3H,  $\text{CH}_3$ ), 1.28 (t,  $J = 7.0$  Hz, 3H,  $\text{CH}_2\text{CH}_3$ ); <sup>13</sup>C NMR (101 MHz, DMSO- $d_6$ )  $\delta$  163.53, 163.09, 162.96, 159.30 (d,  $^1J_{\text{CF}} = 244.8$  Hz), 157.02, 141.80, 137.18, 134.51, 127.58, 124.05 (d,  $^2J_{\text{CF}} = 27.6$  Hz), 122.57, 116.83 (d,  $^2J_{\text{CF}} = 27.2$  Hz), 116.70, 116.17, 112.34, 110.39, 110.10, 101.69, 90.76, 86.43, 38.96, 34.95, 32.88, 12.36; <sup>19</sup>F NMR (376 MHz, DMSO- $d_6$ )  $\delta$  -114.81; IR (neat): 1685 (C=N), 1574 (C=N), 1524 (C=C), 1477 (C=O), 1308 (C-N), 1202 (C-F), 1191 (C-N), 1124 (C-S), 1052 (C-S), 810 (C-S)  $\text{cm}^{-1}$ ; HRMS (ESI<sup>+</sup>):  $m/z$  calcd for  $\text{C}_{24}\text{H}_{21}\text{FN}_3\text{OS}_3^+$  [M]<sup>+</sup> 482.0825, found 482.0831; Mp: 264-266 °C.



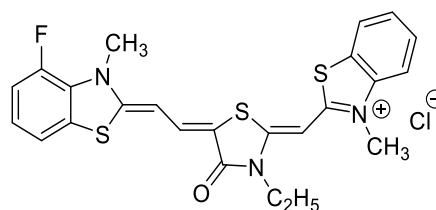
1.4.7 2-(3-Ethyl-5-(2-(3-methylbenzo[d]thiazol-2(3H)-ylidene)ethylidene)-4-oxothiazolidin-2-ylidene)methyl)-7-fluoro-3-methylbenzo[d]thiazol-3-ium chloride (11e)



The title compound was synthesised following **General procedure H** using **9a** (130 mg, 0.25 mmol, synthesised as described in the synthesis of **11a**), **6e** (88 mg, 0.25 mmol), acetonitrile (6.25 mL) and triethylamine (105  $\mu$ L, 0.75 mmol) to give 2-(3-ethyl-5-(2-(3-methylbenzo[d]thiazol-2(3H)-ylidene)ethylidene)-4-oxothiazolidin-2-ylidene)methyl)-7-fluoro-3-methylbenzo[d]thiazol-3-ium 4-methylbenzenesulfonate (**10e**) as a dark-green solid (121 mg, 0.185 mmol, 74% yield). Finally, **10e** (109 mg, 0.17 mmol) was subjected to **General procedure I** using methanol (8.5 mL) to give the title product **11e** as a dark-green solid (73 mg, 0.14 mmol, 82% yield).

$^1\text{H NMR}$  (400 MHz,  $\text{DMSO-}d_6$ )  $\delta$  7.86 (d,  $J = 7.3$  Hz, 1H, ArH), 7.81 – 7.66 (m, 3H, ArH, methine CH), 7.54 (d,  $J = 8.3$  Hz, 1H, ArH), 7.45 (dd,  $J = 16.7, 8.6$  Hz, 2H, ArH), 7.29 (t,  $J = 7.2$  Hz, 1H, ArH), 6.76 (s, 1H, methine CH), 6.25 (d,  $J = 13.7$  Hz, 1H, methine CH), 4.18 (q,  $J = 6.4$  Hz, 2H,  $\text{CH}_2\text{CH}_3$ ), 4.07 (s, 3H,  $\text{CH}_3$ ), 3.80 (s, 3H,  $\text{CH}_3$ ), 1.27 (t,  $J = 6.4$  Hz, 3H,  $\text{CH}_2\text{CH}_3$ );  $^{13}\text{C NMR}$  (101 MHz,  $\text{DMSO-}d_6$ )  $\delta$  164.04, 163.49, 162.01, 159.39, 158.38, 156.01 (d,  $^1J_{\text{CF}} = 247.2$  Hz), 143.04 (d,  $^3J_{\text{CF}} = 5.3$  Hz), 141.94, 139.63, 135.52, 130.80 (d,  $^3J_{\text{CF}} = 7.6$  Hz), 127.63, 124.30 (d,  $^2J_{\text{CF}} = 22.0$  Hz), 122.62, 112.71, 111.54 (d,  $^2J_{\text{CF}} = 18.0$  Hz), 110.97, 101.24, 91.80, 86.25, 39.53, 35.25, 33.25, 12.47;  $^{19}\text{F NMR}$  (376 MHz,  $\text{DMSO-}d_6$ )  $\delta$  -114.99; IR (neat): 1663 (C=N), 1556 (C=N), 1511 (C=C), 1474 (C=O), 1323 (C-N), 1245 (C-F), 1188 (C-N), 1062 (C-S), 939 (C-F), 810 (C-S)  $\text{cm}^{-1}$ ; HRMS (ESI $^+$ ):  $m/z$  calcd for  $\text{C}_{24}\text{H}_{21}\text{FN}_3\text{OS}_3^+$  [M] $^+$  482.0825, found 482.0825; Mp: 268-271  $^\circ\text{C}$ .

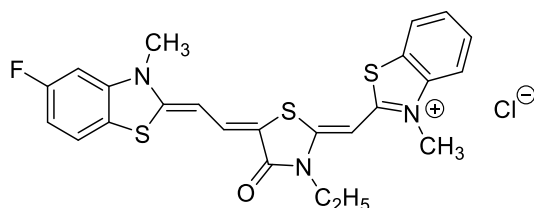
1.4.8 2-(3-Ethyl-5-(2-(4-fluoro-3-methylbenzo[d]thiazol-2(3H)-ylidene)ethylidene)-4-oxothiazolidin-2-ylidene)methyl)-3-methylbenzo[d]thiazol-3-ium chloride (11f)



The title compound was synthesised following **General procedure F** using **7** (0.48 g, 1.5 mmol), **6b** (0.53 g, 1.5 mmol), acetonitrile (8.0 mL), acetic anhydride (200  $\mu$ L, 21 mmol) and triethylamine (775  $\mu$ L, 5.5 mmol) to give 3-ethyl-5-(2-(4-fluoro-3-methylbenzo[d]thiazol-2(3H)-ylidene)ethylidene)-2-thioxothiazolidin-4-one (**8b**) as a red solid (0.35 g, 1.0 mmol, 67% yield). Next, **8b** (0.35 g, 1.0 mmol) was subjected to **General procedure G** using methyl *p*-toluenesulfonate (0.5 mL, 3.0 mmol) and DMF (2.0 mL) to give 3-ethyl-5-(2-(4-fluoro-3-methylbenzo[d]thiazol-2(3H)-ylidene)ethylidene)-2-(methylthio)-4-oxo-4,5-dihydrothiazol-3-ium 4-methylbenzenesulfonate (**9b**) as a green solid (0.29 g, 0.5 mmol, 50% yield). A mixture of **9b** (108 mg, 0.2 mmol) and **6a** (68 mg, 0.2 mmol) was subjected to **General procedure H** using acetonitrile (5.0 mL) and triethylamine (85  $\mu$ L, 0.6 mmol) to give 2-(3-ethyl-5-(2-(4-fluoro-3-methylbenzo[d]thiazol-2(3H)-ylidene)ethylidene)-4-oxothiazolidin-2-ylidene)methyl)-3-methylbenzo[d]thiazol-3-ium 4-methylbenzenesulfonate (**10f**) as a dark-green solid (64 mg, 0.1 mmol, 50% yield). Finally, **10f** (58 mg, 0.09 mmol) was subjected to **General procedure I** using methanol (4.5 mL) and conc. HCl (0.28 mL) to give the title product **11f** as a dark-green solid (39 mg, 0.07 mmol, 78% yield).

$^1\text{H NMR}$  (400 MHz, DMSO- $d_6$ )  $\delta$  8.26 (d,  $J$  = 7.8 Hz, 1H, ArH), 7.81 (d,  $J$  = 8.0 Hz, 1H, ArH), 7.64 (dd,  $J$  = 15.5, 7.7 Hz, 2H, ArH), 7.60 – 7.50 (m, 2H, ArH, methine CH), 7.31 – 7.13 (m, 2H, ArH), 6.75 (s, 1H, methine CH), 5.85 (d,  $J$  = 13.1 Hz, 1H, methine CH), 4.17 (q,  $J$  = 6.8 Hz, 2H,  $\text{CH}_2\text{CH}_3$ ), 4.04 (s, 3H,  $\text{CH}_3$ ), 3.78 (s, 3H,  $\text{CH}_3$ ), 1.29 (t,  $J$  = 6.8 Hz, 3H,  $\text{CH}_2\text{CH}_3$ );  $^{13}\text{C NMR}$  (101 MHz, DMSO- $d_6$ )  $\delta$  163.62, 163.11, 162.19, 156.90, 148.37 (d,  $^1J_{\text{CF}}$  = 246.6 Hz), 140.21, 134.22, 129.53 (d,  $^3J_{\text{CF}}$  = 9.1 Hz), 128.81, 127.90, 126.23 (d,  $^2J_{\text{CF}}$  = 26.8 Hz), 125.88, 124.69 (d,  $^3J_{\text{CF}}$  = 7.2 Hz), 123.35, 118.80, 115.04 (d,  $^2J_{\text{CF}}$  = 20.5 Hz), 114.66, 103.52, 90.40, 86.66, 39.52, 35.49, 34.72, 12.26;  $^{19}\text{F NMR}$  (376 MHz, DMSO- $d_6$ )  $\delta$  -130.05; IR (neat): 1688 (C=N), 1504 (C=C), 1479 (C=O), 1337 (C-N), 1190 (C-N), 1122 (C-F), 1055 (C-S), 918 (C-F), 810 (C-S)  $\text{cm}^{-1}$ ; HRMS (ESI $^+$ ):  $m/z$  calcd for  $\text{C}_{24}\text{H}_{21}\text{FN}_3\text{OS}_3^+$  [M] $^+$  482.0825, found 482.0800; Mp: 270-273  $^\circ\text{C}$ .

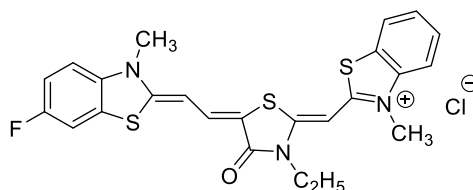
**1.4.9 2-(3-Ethyl-5-(2-(5-fluoro-3-methylbenzo[d]thiazol-2(3H)-ylidene)ethylidene)-4-oxothiazolidin-2-ylidene)methyl)-3-methylbenzo[d]thiazol-3-ium chloride (11g)**



The title compound was synthesised following **General procedure F** using **7** (0.32 g, 1.0 mmol), **6c** (0.35 g, 1.0 mmol), acetonitrile (5.0 mL), acetic anhydride (135  $\mu$ L, 1.4 mmol) and triethylamine (515  $\mu$ L, 3.7 mmol) to give 3-ethyl-5-(2-(5-fluoro-3-methylbenzo[d]thiazol-2(3H)-ylidene)ethylidene)-2-thioxothiazolidin-4-one (**8c**) as a red solid (0.27 g, 0.77 mmol, 77% yield). Next, **8c** (0.26 g, 0.75 mmol) was subjected to **General procedure G** using methyl *p*-toluenesulfonate (0.35 mL, 2.25 mmol) and DMF (1.1 mL) to give 3-ethyl-5-(2-(5-fluoro-3-methylbenzo[d]thiazol-2(3H)-ylidene)ethylidene)-2-(methylthio)-4-oxo-4,5-dihydrothiazol-3-ium 4-methylbenzenesulfonate (**9c**) as a green solid (168 mg, 0.3 mmol, 41% yield). A mixture of **9c** (108 mg, 0.2 mmol) and **6a** (68 mg, 0.2 mmol) was subjected to **General procedure H** using acetonitrile (5.0 mL) and triethylamine (85  $\mu$ L, 0.6 mmol) to give 2-(3-ethyl-5-(2-(5-fluoro-3-methylbenzo[d]thiazol-2(3H)-ylidene)ethylidene)-4-oxothiazolidin-2-ylidene)methyl)-3-methylbenzo[d]thiazol-3-ium 4-methylbenzenesulfonate (**10g**) as a dark-green solid (91 mg, 0.14 mmol, 70% yield). Finally, **10g** (65 mg, 0.1 mmol) was subjected to **General procedure I** using methanol (6.6 mL) and conc. HCl (0.3 mL) to give the title product **11g** as a dark-green solid (31 mg, 0.06 mmol, 60% yield).

$^1\text{H NMR}$  (400 MHz, DMSO- $d_6$ )  $\delta$  8.25 (d,  $J$  = 9.2 Hz, 1H, ArH), 7.92 (dd,  $J$  = 17.3, 8.4 Hz, 1H, ArH), 7.83 (dd,  $J$  = 8.8, 5.6 Hz, 1H, ArH), 7.78 – 7.64 (m, 1H, ArH), 7.65 – 7.50 (m, 2H, ArH, methine CH), 7.50 – 7.36 (m, 1H, ArH), 7.12 (t,  $J$  = 8.1 Hz, 1H, ArH), 6.76 (s, 1H, methine CH), 5.92 (d,  $J$  = 12.6 Hz, 1H, methine CH), 4.17 (q,  $J$  = 7.1 Hz, 2H,  $\text{CH}_2\text{CH}_3$ ), 4.07 (s, 3H,  $\text{CH}_3$ ), 3.67 (s, 3H,  $\text{CH}_3$ ), 1.28 (t,  $J$  = 7.1 Hz, 3H,  $\text{CH}_2\text{CH}_3$ );  $^{13}\text{C NMR}$  (101 MHz, DMSO- $d_6$ )  $\delta$  163.74, 163.63, 162.02 (d,  $^1J_{\text{CF}}$  = 231.5 Hz), 156.92, 140.39, 134.19, 128.87, 126.15, 125.94, 123.80 (d,  $^3J_{\text{CF}}$  = 10.5 Hz), 123.45, 119.38, 114.79, 111.11 (d,  $^2J_{\text{CF}}$  = 24.5 Hz), 105.08, 104.92, 103.01, 100.38 (d,  $^2J_{\text{CF}}$  = 29.0 Hz), 90.97, 86.61, 39.53, 34.77, 33.06, 12.34;  $^{19}\text{F NMR}$  (376 MHz, DMSO- $d_6$ )  $\delta$  -113.59; IR (neat): 1668 (C=N), 1513 (C=C), 1468 (C=O), 1332 (C-N), 1183 (C-N), 1055 (C-S), 927 (C-F), 830 (C-S)  $\text{cm}^{-1}$ ; HRMS (ESI $^+$ ):  $m/z$  calcd for  $\text{C}_{24}\text{H}_{21}\text{FN}_3\text{OS}_3^+$  [M] $^+$  482.0825, found 482.0836; Mp: 265-267  $^\circ\text{C}$ .

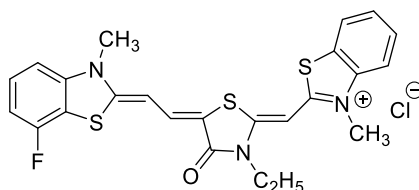
**1.4.10 2-(3-Ethyl-5-(2-(6-fluoro-3-methylbenzo[d]thiazol-2(3H)-ylidene)ethylidene)-4-oxothiazolidin-2-ylidene)methyl)-3-methylbenzo[d]thiazol-3-ium chloride (11h)**



The title compound was synthesised following **General procedure F** using **7** (0.32 g, 1.0 mmol), **6d** (0.35 g, 1.0 mmol), acetonitrile (5.0 mL), acetic anhydride (135  $\mu$ L, 1.4 mmol) and triethylamine (515  $\mu$ L, 3.7 mmol) to give 3-ethyl-5-(2-(6-fluoro-3-methylbenzo[d]thiazol-2(3H)-ylidene)ethylidene)-2-thioxothiazolidin-4-one (**8d**) as a red solid (0.27 g, 0.75 mmol, 75% yield). Next, **8d** (0.25 g, 0.72 mmol) was subjected to **General procedure G** using methyl *p*-toluenesulfonate (335  $\mu$ L, 2.2 mmol) and DMF (1.0 mL) to give 3-ethyl-5-(2-(6-fluoro-3-methylbenzo[d]thiazol-2(3H)-ylidene)ethylidene)-2-(methylthio)-4-oxo-4,5-dihydrothiazol-3-ium 4-methylbenzenesulfonate (**9d**) as a green solid (108 mg, 0.2 mmol, 28% yield). A mixture of **9d** (100 mg, 0.18 mmol) and **6a** (61 mg, 0.18 mmol) was subjected to **General procedure H** using acetonitrile (4.5 mL) and triethylamine (75  $\mu$ L, 0.54 mmol) to give 2-(3-ethyl-5-(2-(6-fluoro-3-methylbenzo[d]thiazol-2(3H)-ylidene)ethylidene)-4-oxothiazolidin-2-ylidene)methyl)-3-methylbenzo[d]thiazol-3-ium 4-methylbenzenesulfonate (**10h**) as a dark-green solid (77 mg, 0.12 mmol, 66% yield). Finally, **10h** (70 mg, 0.11 mmol) was subjected to **General procedure I** using methanol (5.0 mL) and conc. HCl (0.35 mL) to give the title product **11h** as a dark-green solid (40 mg, 0.077 mmol, 70% yield).

$^1\text{H NMR}$  (400 MHz, DMSO- $d_6$ )  $\delta$  8.21 (d,  $J$  = 8.0 Hz, 1H, ArH), 7.87 (d,  $J$  = 8.8 Hz, 1H, ArH), 7.77 (d,  $J$  = 8.4 Hz, 1H, ArH), 7.66 (t,  $J$  = 7.7 Hz, 1H, ArH), 7.62 – 7.45 (m, 2H, ArH, methine CH), 7.39 (s, 1H, ArH), 7.27 (dd,  $J$  = 22.5, 13.7 Hz, 1H, ArH), 6.72 (s, 1H, methine CH), 5.89 (d,  $J$  = 12.8 Hz, 1H, methine CH), 4.15 (q,  $J$  = 7.0 Hz, 2H,  $\text{CH}_2\text{CH}_3$ ), 4.05 (s, 3H,  $\text{CH}_3$ ), 3.68 (s, 3H,  $\text{CH}_3$ ), 1.27 (t,  $J$  = 7.0 Hz, 3H,  $\text{CH}_2\text{CH}_3$ );  $^{13}\text{C NMR}$  (101 MHz, DMSO- $d_6$ )  $\delta$  163.60, 162.87, 158.68 (d,  $^1J_{\text{CF}}$  = 242.0 Hz), 156.94, 140.29, 138.65, 134.32, 128.83, 128.00, 126.02, 125.81, 125.47, 123.37, 114.79 (d,  $^2J_{\text{CF}}$  = 24.7 Hz), 114.60, 113.32 (d,  $^3J_{\text{CF}}$  = 8.8 Hz), 109.85 (d,  $^2J_{\text{CF}}$  = 28.8 Hz), 102.17, 90.84, 86.34, 38.91, 34.67, 33.12, 12.34;  $^{19}\text{F NMR}$  (376 MHz, DMSO- $d_6$ )  $\delta$  -117.86; IR (neat): 1657 (C=N), 1562 (C=N), 1505 (C=C), 1474 (C=O), 1335 (C-N), 1185 (C-S), 1063 (C-S), 905 (C-F), 805 (C-S)  $\text{cm}^{-1}$ ; HRMS (ESI $^+$ ):  $m/z$  calcd for  $\text{C}_{24}\text{H}_{21}\text{FN}_3\text{OS}_3^+$  [M] $^+$  482.0825, found 482.0825; Mp: 231-234  $^\circ\text{C}$ .

**1.4.11 2-(3-Ethyl-5-(2-(7-fluoro-3-methylbenzo[d]thiazol-2(3H)-ylidene)ethylidene)-4-oxothiazolidin-2-ylidene)methyl)-3-methylbenzo[d]thiazol-3-ium chloride (11i)**

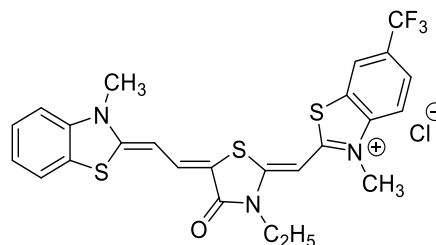


The title compound was synthesised following **General procedure F** using **7** (0.48 g, 1.5 mmol), **6e** (0.53 g, 1.5 mmol), acetonitrile (7.5 mL), acetic anhydride (200  $\mu$ L, 2.1 mmol) and

triethylamine (775  $\mu\text{L}$ , 5.5 mmol) to give 3-ethyl-5-(2-(7-fluoro-3-methylbenzo[*d*]thiazol-2(3*H*)-ylidene)ethylidene)-2-thioxothiazolidin-4-one (**8e**) as a red solid (0.34 g, 0.96 mmol, 64% yield). Next, **8e** (0.31 g, 0.87 mmol) was subjected to **General procedure G** using methyl *p*-toluenesulfonate (405  $\mu\text{L}$ , 2.6 mmol) and DMF 1.5 mL to give 3-ethyl-5-(2-(7-fluoro-3-methylbenzo[*d*]thiazol-2(3*H*)-ylidene)ethylidene)-2-(methylthio)-4-oxo-4,5-dihydrothiazol-3-ium 4-methylbenzenesulfonate (**9e**) as a green solid (303 mg, 0.56 mmol, 65% yield). A mixture of **9e** (108 mg, 0.2 mmol) and **6a** (67 mg, 0.2 mmol) was subjected to **General procedure H** using acetonitrile (5.0 mL) and triethylamine (84  $\mu\text{L}$ , 0.6 mmol) to give 2-(3-ethyl-5-(2-(7-fluoro-3-methylbenzo[*d*]thiazol-2(3*H*)-ylidene)ethylidene)-4-oxothiazolidin-2-ylidene)methyl)-3-methylbenzo[*d*]thiazol-3-ium 4-methylbenzenesulfonate (**10i**) as a dark-green solid (100 mg, 0.15 mmol, 76% yield). Finally, **10i** (93 mg, 0.14 mmol) was subjected to **General procedure I** using methanol (7.0 mL) conc. HCl (0.46 mL) to give the title product **11i** as a dark-green solid (31 mg, 0.06 mmol, 43% yield).

$^1\text{H NMR}$  (400 MHz,  $\text{DMSO-}d_6$ )  $\delta$  8.25 (d,  $J = 8.1$  Hz, 1H, *ArH*), 7.96 (d,  $J = 8.2$  Hz, 1H, *ArH*), 7.71 (t,  $J = 7.7$  Hz, 1H, *ArH*), 7.68 – 7.53 (m, 2H, *ArH*, methine *CH*), 7.45 (dd,  $J = 14.1, 8.3$  Hz, 2H, *ArH*), 7.31 (d,  $J = 8.2$  Hz, 1H, *ArH*), 7.27 – 7.01 (m, 1H, *ArH*), 6.79 (s, 1H, methine *CH*), 5.96 (d,  $J = 13.0$  Hz, 1H, methine *CH*), 4.16 (q,  $J = 7.1$  Hz, 2H,  $\text{CH}_2\text{CH}_3$ ), 4.10 (s, 3H,  $\text{CH}_3$ ), 3.71 (s, 3H,  $\text{CH}_3$ ), 1.26 (t,  $J = 7.1$  Hz, 3H,  $\text{CH}_2\text{CH}_3$ );  $^{13}\text{C NMR}$  (101 MHz,  $\text{DMSO-}d_6$ )  $\delta$  163.72, 163.36, 161.10, 156.85, 155.76 (d,  $^1J_{\text{CF}} = 244.9$  Hz), 144.56 (d,  $^3J_{\text{CF}} = 6.0$  Hz), 140.36, 133.93, 130.92, 129.56 (d,  $^3J_{\text{CF}} = 7.9$  Hz), 128.92, 126.13 (d,  $^2J_{\text{CF}} = 20.3$  Hz), 123.45, 114.85, 110.16 (d,  $^2J_{\text{CF}} = 22.5$  Hz), 108.59 (d,  $^4J_{\text{CF}} = 2.9$  Hz), 104.24, 90.92, 89.03, 86.84, 39.13, 34.87, 33.36, 12.35;  $^{19}\text{F NMR}$  (376 MHz,  $\text{DMSO-}d_6$ )  $\delta$  -115.98; IR (neat): 1658 (C=N), 1507 (C=C), 1476 (C=O), 1344 (C-N), 1193 (C-S), 1054 (C-S), 927 (C-F)  $\text{cm}^{-1}$ ; HRMS (ESI $^+$ ):  $m/z$  calcd for  $\text{C}_{24}\text{H}_{21}\text{FN}_3\text{OS}_3^+$  [M] $^+$  482.0825, found 482.0825; Mp: 276-277  $^\circ\text{C}$ .

**1.4.12 2-(3-Ethyl-5-(2-(3-methylbenzo[*d*]thiazol-2(3*H*)-ylidene)ethylidene)-4-oxothiazolidin-2-ylidene)methyl)-3-methyl-6-(trifluoromethyl)benzo[*d*]thiazol-3-ium chloride (11j)**

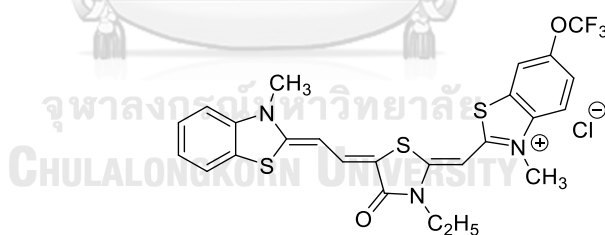


The title compound was synthesised following **General procedure H** using **9a** (104 mg, 0.2 mmol), synthesised as described in the synthesis of **11a**, **6f** (81 mg, 0.2 mmol), acetonitrile

(5.0 mL) and triethylamine (80  $\mu$ L, 0.6 mmol) to provide 2-(3-ethyl-5-(2-(3-methylbenzo[d]thiazol-2(3*H*)-ylidene)ethylidene)-4-oxothiazolidin-2-ylidene)methyl)-3-methyl-6-(trifluoromethyl)benzo[d]thiazol-3-ium 4-methylbenzenesulfonate (**10j**) as a dark-green solid (93 mg, 0.136 mmol, 68% yield). Finally, **10j** (68 mg, 0.1 mmol) was subjected to **General procedure I** using methanol (5.0 mL) and conc. HCl (0.35 mL) to give the title product **11j** as a dark-green solid (43 mg, 0.076 mmol, 76% yield).

$^1\text{H NMR}$  (400 MHz, DMSO- $d_6$ )  $\delta$  8.69 (s, 1H, ArH), 8.08 – 7.92 (m, 2H, ArH), 7.85 (d,  $J = 7.8$  Hz, 1H, ArH), 7.69 (d,  $J = 12.9$  Hz, 1H, methine CH), 7.52 – 7.34 (m, 2H, ArH), 7.29 (t,  $J = 7.6$  Hz, 1H, ArH), 6.77 (s, 1H, methine CH), 6.00 (d,  $J = 13.1$  Hz, 1H, methine CH), 4.20 (q,  $J = 7.0$  Hz, 2H,  $\text{CH}_2\text{CH}_3$ ), 4.07 (s, 3H,  $\text{CH}_3$ ), 3.76 (s, 3H,  $\text{CH}_3$ ), 1.28 (t,  $J = 7.1$  Hz, 3H,  $\text{CH}_2\text{CH}_3$ );  $^{13}\text{C NMR}$  (101 MHz, DMSO- $d_6$ )  $\delta$  164.22, 163.95, 163.66, 158.52, 143.35, 142.01, 135.44, 127.88, 126.92, 124.71, 124.65, 124.56 (q,  $^1J_{\text{CF}} = 259.5$  Hz), 124.30, 122.88, 121.37 (q,  $^3J_{\text{CF}} = 4.2$  Hz), 115.39, 114.64 (q,  $^2J_{\text{CF}} = 27.0$  Hz), 112.83, 101.45, 91.58, 86.88, 39.10, 35.07, 33.25, 12.67;  $^{19}\text{F NMR}$  (376 MHz, DMSO- $d_6$ )  $\delta$  -59.96; IR (neat): 1691 (C=N), 1516 (C=C), 1469 (C=O), 1352 (C-N), 1316 (C-CF<sub>3</sub>), 1191 (C-N), 1074 (C-CF<sub>3</sub>), 819 (C-S), 799 (C-F)  $\text{cm}^{-1}$ ; HRMS (ESI<sup>+</sup>):  $m/z$  calcd for  $\text{C}_{25}\text{H}_{21}\text{F}_3\text{N}_3\text{OS}_3^+$  [M]<sup>+</sup> 532.0793, found 532.0790; Mp: 244–247  $^\circ\text{C}$ .

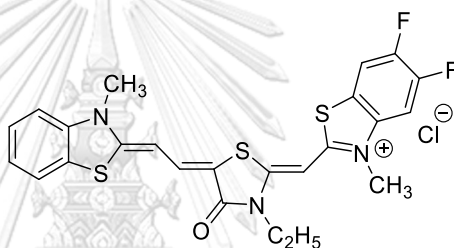
**1.4.13 2-(3-Ethyl-5-(2-(3-methylbenzo[d]thiazol-2(3*H*)-ylidene)ethylidene)-4-oxothiazolidin-2-ylidene)methyl)-3-methyl-6-(trifluoromethoxy)benzo[d]thiazol-3-ium chloride (**11k**)**



The title compound was synthesised following **General procedure H** using **9a** (156 mg, 0.3 mmol), synthesised as described in the synthesis of **11a**, **6g** (126 mg, 0.3 mmol), acetonitrile (7.0 mL) and triethylamine (125  $\mu$ L, 0.9 mmol) to provide 2-(3-ethyl-5-(2-(3-methylbenzo[d]thiazol-2(3*H*)-ylidene)ethylidene)-4-oxothiazolidin-2-ylidene)methyl)-3-methyl-6-(trifluoromethoxy)benzo[d]thiazol-3-ium 4-methylbenzenesulfonate (**10k**) as a dark-green solid (145 mg, 0.2 mmol, 67% yield). Finally, **10k** (72 mg, 0.1 mmol) was subjected to **General procedure I** using methanol (5.0 mL) and conc. HCl (0.35 mL) to give the title product **11k** as a dark-green solid (46 mg, 0.08 mmol, 80% yield).

$^1\text{H}$  NMR (400 MHz, DMSO- $d_6$ )  $\delta$  8.39 (s, 1H, ArH), 7.99 – 7.74 (m, 2H, ArH), 7.73 – 7.53 (m, 2H, ArH, methine CH), 7.44 – 7.19 (m, 3H, ArH), 6.72 (s, 1H, methine CH), 5.90 (d,  $J$  = 13.4 Hz, 1H, methine CH), 4.17 (q,  $J$  = 6.8 Hz, 2H,  $\text{CH}_2\text{CH}_3$ ), 4.02 (s, 3H,  $\text{CH}_3$ ), 3.70 (s, 3H,  $\text{CH}_3$ ), 1.29 (t,  $J$  = 6.9 Hz, 3H,  $\text{CH}_2\text{CH}_3$ );  $^{13}\text{C}$  NMR (101 MHz, DMSO- $d_6$ )  $\delta$  163.67, 163.48, 163.11, 157.59, 145.04, 141.79, 141.68, 139.44, 139.33, 134.78, 127.60, 125.41, 124.83 (q,  $^1J_{\text{CF}}$  = 249.4 Hz), 124.29, 122.61, 122.19 (q,  $^3J_{\text{CF}}$  = 6.8 Hz), 116.45, 112.40, 101.48, 90.96, 86.55, 39.11, 34.91, 32.91, 12.38;  $^{19}\text{F}$  NMR (376 MHz, DMSO- $d_6$ )  $\delta$  -57.10; IR (neat): 1690 (C=N), 1515 (C=C), 1468 (C=O), 1352 (C-N), 1243 (C-F), 1193 (C-O-CF<sub>3</sub>), 1021 (C-S), 808 (C-S)  $\text{cm}^{-1}$ ; HRMS (ESI<sup>+</sup>):  $m/z$  calcd for  $\text{C}_{25}\text{H}_{21}\text{F}_3\text{N}_3\text{O}_2\text{S}_3^+$  [M]<sup>+</sup> 548.0743, found 548.0730; Mp: 243-246 °C.

**1.4.14 2-(3-Ethyl-5-(2-(3-methylbenzo[d]thiazol-2(3H)-ylidene)ethylidene)ethylidene)-4-oxothiazolidin-2-ylidene)methyl)-5,6-difluoro-3-methylbenzo[d]thiazol-3-ium chloride (11l)**

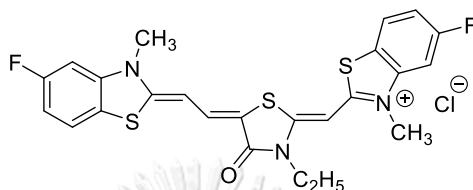


The title compound was synthesised following **General procedure H** using **9a** (156 mg, 0.3 mmol, synthesised as described in the synthesis of **11a**), **6h** (111 mg, 0.3 mmol), acetonitrile (7.0 mL) and triethylamine (125  $\mu\text{L}$ , 0.9 mmol) to give 2-(3-ethyl-5-(2-(3-methylbenzo[d]thiazol-2(3H)-ylidene)ethylidene)ethylidene)-4-oxothiazolidin-2-ylidene)methyl)-5,6-difluoro-3-methylbenzo[d]thiazol-3-ium 4-methylbenzenesulfonate (**10l**) as a dark-green solid (132 mg, 0.2 mmol, 67% yield). Finally, **10l** (87 mg, 0.13 mmol) was subjected to **General procedure I** using methanol (6.5 mL) and conc. HCl (0.4 mL) to give the title product **11l** as a dark-green solid (65 mg, 0.097 mmol, 75% yield).

$^1\text{H}$  NMR (400 MHz, DMSO- $d_6$ )  $\delta$  8.41 (dd,  $J$  = 9.2, 8.0 Hz, 1H, ArH), 8.19 (dd,  $J$  = 10.8, 6.5 Hz, 1H, ArH), 7.87 (d,  $J$  = 8.1 Hz, 1H, ArH), 7.70 (d,  $J$  = 13.3 Hz, 1H, methine CH), 7.56 – 7.43 (m, 2H, ArH), 7.31 (t,  $J$  = 7.7 Hz, 1H, ArH), 6.74 (s, 1H, methine CH), 5.97 (d,  $J$  = 13.4 Hz, 1H, methine CH), 4.18 (q,  $J$  = 6.9 Hz, 2H,  $\text{CH}_2\text{CH}_3$ ), 4.03 (s, 3H,  $\text{CH}_3$ ), 3.75 (s, 3H,  $\text{CH}_3$ ), 1.27 (t,  $J$  = 6.9 Hz, 3H,  $\text{CH}_2\text{CH}_3$ );  $^{13}\text{C}$  NMR (101 MHz, DMSO- $d_6$ )  $\delta$  163.95, 163.51, 163.35, 157.33, 151.32 (dd,  $^1J_{\text{CF}}$  = 271.2,  $^2J_{\text{CF}}$  = 29.8 Hz), 150.46 (dd,  $^1J_{\text{CF}}$  = 249.5,  $^2J_{\text{CF}}$  = 28.3 Hz), 142.52, 141.88, 137.36, 134.89, 127.62, 124.32, 124.03, 122.68, 112.54, 112.14 (dd,  $^2J_{\text{CF}}$  = 23.6, 1.9 Hz), 104.16, 101.41, 91.00, 86.65, 39.01, 35.20, 32.96, 12.38;  $^{19}\text{F}$  NMR (376 MHz, DMSO- $d_6$ )  $\delta$  -134.60 (d,  $J$  = 22.2 Hz, 1F), -138.72 (d,  $J$  = 22.1 Hz, 1F); IR

(neat): 1665 (C=N), 1554 (C=N), 1518 (C=C), 1468 (C=O), 1340 (C-N), 1224 (C-F), 1182 (C-N), 1026 (C-S), 819 (C-S)  $\text{cm}^{-1}$ ; HRMS (ESI<sup>+</sup>):  $m/z$  calcd for  $\text{C}_{24}\text{H}_{20}\text{F}_2\text{N}_3\text{OS}_3^+$  [M]<sup>+</sup> 500.0731, found 500.0721; Mp: 266-268 °C.

**1.4.15 2-(3-Ethyl-5-(2-(5-fluoro-3-methylbenzo[d]thiazol-2(3H)-ylidene)ethylidene)-4-oxothiazolidin-2-ylidene)methyl)-5-fluoro-3-methylbenzo[d]thiazol-3-ium chloride (11m)**

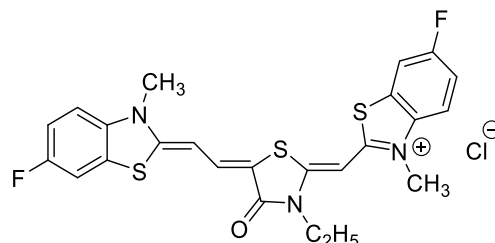


The title compound was synthesised following **General procedure H** using **9c** (102 mg, 0.19 mmol, synthesised as described in the synthesis of **11g**), **6c** (68 mg, 0.19 mmol), acetonitrile (5.0 mL) and triethylamine (80  $\mu\text{L}$ , 0.57 mmol) to give 2-(3-ethyl-5-(2-(5-fluoro-3-methylbenzo[d]thiazol-2(3H)-ylidene)ethylidene)-4-oxothiazolidin-2-ylidene)methyl)-5-fluoro-3-methylbenzo[d]thiazol-3-ium 4-methylbenzenesulfonate (**10m**) as a dark-green solid (107 mg, 0.16 mmol, 84% yield). Finally, **10m** (88 mg, 0.13 mmol) was subjected to **General procedure I** using methanol (6.0 mL) and conc. HCl (0.4 mL) to give the title product **11m** as a dark-green solid (61 mg, 0.11 mmol, 87% yield).

<sup>1</sup>H NMR (400 MHz, DMSO-*d*<sub>6</sub>)  $\delta$  8.27 (dd,  $J$  = 8.8, 5.1 Hz, 1H, ArH), 7.79 (dd,  $J$  = 8.6, 5.2 Hz, 1H, ArH), 7.68 (dd,  $J$  = 9.8, 1.9 Hz, 1H, ArH), 7.49 (d,  $J$  = 13.1 Hz, 1H, methine CH), 7.42 – 7.34 (m, 1H, ArH), 7.19 (dd,  $J$  = 10.0, 1.6 Hz, 1H, ArH), 7.08 (td,  $J$  = 8.9, 2.1 Hz, 1H, ArH), 6.69 (s, 1H, methine CH), 5.83 (d,  $J$  = 13.1 Hz, 1H, methine CH), 4.15 (q,  $J$  = 7.1 Hz, 2H, CH<sub>2</sub>CH<sub>3</sub>), 3.95 (s, 3H, CH<sub>3</sub>), 3.60 (s, 3H, CH<sub>3</sub>), 1.30 (t,  $J$  = 7.1 Hz, 3H, CH<sub>2</sub>CH<sub>3</sub>); <sup>13</sup>C NMR (101 MHz, DMSO-*d*<sub>6</sub>)  $\delta$  164.26, 163.60, 163.50, 162.49 (d, <sup>1</sup> $J_{\text{CF}}$  = 245.5 Hz), 162.03 (d, <sup>1</sup> $J_{\text{CF}}$  = 242.9 Hz), 157.33, 143.06 (d, <sup>3</sup> $J_{\text{CF}}$  = 12.2 Hz), 141.60 (d, <sup>3</sup> $J_{\text{CF}}$  = 12.3 Hz), 134.13, 125.09 (d, <sup>3</sup> $J_{\text{CF}}$  = 10.4 Hz), 123.78 (d, <sup>3</sup> $J_{\text{CF}}$  = 10.2 Hz), 121.56, 119.17, 113.65 (d, <sup>2</sup> $J_{\text{CF}}$  = 24.5 Hz), 111.18 (d, <sup>2</sup> $J_{\text{CF}}$  = 23.7 Hz), 102.97, 102.20 (d, <sup>2</sup> $J_{\text{CF}}$  = 29.0 Hz), 100.24 (d, <sup>2</sup> $J_{\text{CF}}$  = 28.7 Hz), 91.19, 86.76, 39.10, 34.84, 33.00, 12.30; <sup>19</sup>F NMR (376 MHz, DMSO-*d*<sub>6</sub>)  $\delta$  -111.17 (1F), -113.57 (1F); IR (neat): 1671 (C=N), 1518 (C=C), 1460 (C=O), 1327 (C-N), 1268, 1199 (C-N), 1060 (C-S), 932 (C-F)  $\text{cm}^{-1}$ ; HRMS (ESI<sup>+</sup>):  $m/z$  calcd for  $\text{C}_{24}\text{H}_{20}\text{F}_2\text{N}_3\text{OS}_3^+$  [M]<sup>+</sup> 500.0731, found 500.0724; Mp: 279-282 °C.



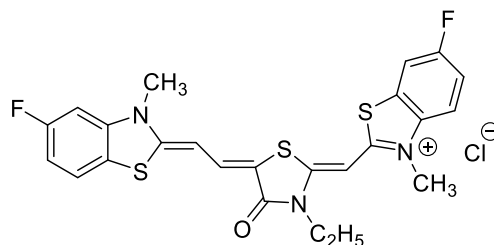
1.4.16 2-(3-Ethyl-5-(2-(6-fluoro-3-methylbenzo[d]thiazol-2(3*H*)-ylidene)ethylidene)-4-oxothiazolidin-2-ylidene)methyl)-6-fluoro-3-methylbenzo[d]thiazol-3-ium chloride (11n)



The title compound was synthesised following **General procedure H** using **9d** (102 mg, 0.19 mmol, synthesised as described in the synthesis of **11h**), **6d** (68 mg, 0.19 mmol), acetonitrile (5.0 mL) and triethylamine (80  $\mu$ L, 0.57 mmol) to give 2-(3-ethyl-5-(2-(6-fluoro-3-methylbenzo[d]thiazol-2(3*H*)-ylidene)ethylidene)-4-oxothiazolidin-2-ylidene)methyl)-6-fluoro-3-methylbenzo[d]thiazol-3-ium 4-methylbenzenesulfonate (**10n**) as a dark-green solid (86 mg, 0.13 mmol, 68% yield). Finally, **10n** (69 mg, 0.1 mmol) was subjected to **General procedure I** using methanol (5.0 mL) and conc. HCl (0.3 mL) to give the title product **11n** as a dark-green solid (54 mg, 0.09 mmol, 90% yield).

$^1\text{H NMR}$  (400 MHz, DMSO- $d_6$ )  $\delta$  8.21 (d,  $J = 7.6$  Hz, 1H, ArH), 7.89 (dd,  $J = 8.2, 4.3$  Hz, 1H, ArH), 7.68 – 7.51 (m, 3H, ArH, methine CH), 7.37–7.11 (m, 2H, ArH), 6.74 (s, 1H, methine CH), 5.86 (d,  $J = 13.1$  Hz, 1H, methine CH), 4.16 (q,  $J = 6.4$  Hz, 2H,  $\text{CH}_2\text{CH}_3$ ), 4.05 (s, 3H,  $\text{CH}_3$ ), 3.82 (s, 3H,  $\text{CH}_3$ ), 1.28 (t,  $J = 6.4$  Hz, 3H,  $\text{CH}_2\text{CH}_3$ );  $^{13}\text{C NMR}$  (101 MHz, DMSO- $d_6$ )  $\delta$  163.58, 162.28, 159.36 (d,  $^1J_{\text{CF}} = 245.3$  Hz), 156.98, 148.39 (d,  $^1J_{\text{CF}} = 246.9$  Hz), 137.11, 134.27, 129.56, 127.38, 126.39 (d,  $^4J_{\text{CF}} = 2.4$  Hz), 124.78 (d,  $^3J_{\text{CF}} = 7.5$  Hz), 118.88, 117.31 (d,  $^2J_{\text{CF}} = 20.7$  Hz), 116.89 (d,  $^2J_{\text{CF}} = 24.8$  Hz), 116.24 (d,  $^3J_{\text{CF}} = 10.0$  Hz), 115.09 (d,  $^2J_{\text{CF}} = 20.3$  Hz), 110.22 (d,  $^2J_{\text{CF}} = 28.6$  Hz), 103.34, 90.48, 86.81, 38.96, 35.53, 35.04, 12.29;  $^{19}\text{F NMR}$  (376 MHz, DMSO- $d_6$ )  $\delta$  -114.66 (1F), -130.18 (1F); IR (neat): 1662 (C=N), 1557 (C=N), 1499 (C=C), 1471 (C=O), 1313 (C-N), 1204 (C-N), 1021 (C-S), 910 (C-F)  $\text{cm}^{-1}$ ; HRMS (ESI $^+$ ):  $m/z$  calcd for  $\text{C}_{24}\text{H}_{20}\text{F}_2\text{N}_3\text{OS}_3^+$  [M] $^+$  500.0731, found 500.0689; Mp: 254–256  $^\circ\text{C}$ .

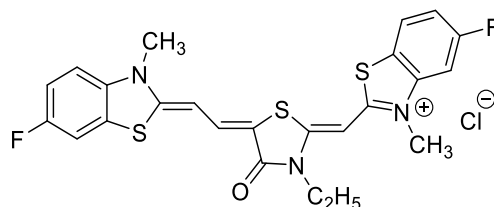
1.4.17 2-(3-Ethyl-5-(2-(5-fluoro-3-methylbenzo[d]thiazol-2(3*H*)-ylidene)ethylidene)-4-oxothiazolidin-2-ylidene)methyl)-6-fluoro-3-methylbenzo[d]thiazol-3-ium chloride (11o)



The title compound was synthesised following **General procedure H** using **9c** (102 mg, 0.19 mmol), synthesised as described in the synthesis of **11g**, **6d** (68 mg, 0.19 mmol), acetonitrile (5.0 mL) and triethylamine (80  $\mu$ L, 0.57 mmol) to give 2-(3-ethyl-5-(2-(5-fluoro-3-methylbenzo[d]thiazol-2(3*H*)-ylidene)ethylidene)-4-oxothiazolidin-2-ylidene)methyl)-6-fluoro-3-methylbenzo[d]thiazol-3-ium 4-methylbenzenesulfonate (**10o**) as a dark-green solid (96 mg, 0.14 mmol, 74% yield). Finally, **10o** (78 mg, 0.11 mmol) was subjected to **General procedure I** using methanol (5.5 mL) and conc. HCl (0.34 mL) to give the title product **11o** as a dark-green solid (47 mg, 0.085 mmol, 78% yield).

**<sup>1</sup>H NMR** (400 MHz, DMSO-*d*<sub>6</sub>)  $\delta$  8.18 (dd,  $J = 7.9, 2.0$  Hz, 1H, ArH), 7.94 (dd,  $J = 9.1, 4.0$  Hz, 1H, ArH), 7.82 (dd,  $J = 8.6, 5.2$  Hz, 1H, ArH), 7.64 – 7.56 (m, 2H, ArH, methine CH), 7.44 (dd,  $J = 9.4, 0.8$  Hz, 1H, ArH), 7.12 (td,  $J = 8.4, 1.4$  Hz, 1H, ArH), 6.73 (s, 1H, methine CH), 5.91 (d,  $J = 13.1$  Hz, 1H, methine CH), 4.17 (q,  $J = 6.9$  Hz, 2H, CH<sub>2</sub>CH<sub>3</sub>), 4.06 (s, 3H, CH<sub>3</sub>), 3.68 (s, 3H, CH<sub>3</sub>), 1.28 (t,  $J = 7.1$  Hz, 3H, CH<sub>2</sub>CH<sub>3</sub>); **<sup>13</sup>C NMR** (101 MHz, DMSO-*d*<sub>6</sub>)  $\delta$  163.62, 163.26, 162.09 (d,  $^1J_{CF} = 250.4$  Hz), 159.35 (d,  $^1J_{CF} = 245.0$  Hz), 156.95, 143.30 (d,  $^3J_{CF} = 12.1$  Hz), 137.20, 134.13, 127.94, 127.51, 123.79 (d,  $^3J_{CF} = 9.6$  Hz), 119.33 (d,  $^4J_{CF} = 2.2$  Hz), 116.85 (d,  $^2J_{CF} = 25.2$  Hz), 116.27 (d,  $^3J_{CF} = 9.3$  Hz), 111.12 (d,  $^2J_{CF} = 23.0$  Hz), 110.26 (d,  $^2J_{CF} = 28.6$  Hz), 102.80, 100.31 (d,  $^2J_{CF} = 29.3$  Hz), 90.99, 86.70, 39.10, 35.03, 33.03, 12.31; **<sup>19</sup>F NMR** (376 MHz, DMSO-*d*<sub>6</sub>)  $\delta$  -113.56 (1F), -114.64 (1F); **IR** (neat): 1690 (C=N), 1518 (C=C), 1476 (C=O), 1343 (C-N), 1202 (C-F), 1185 (C-N), 1060 (C-S), 932 (C-F) cm<sup>-1</sup>; **HRMS** (ESI<sup>+</sup>):  $m/z$  calcd for C<sub>24</sub>H<sub>20</sub>F<sub>2</sub>N<sub>3</sub>OS<sub>3</sub><sup>+</sup> [M]<sup>+</sup> 500.0731, found 500.0729; **Mp**: 271-274 °C.

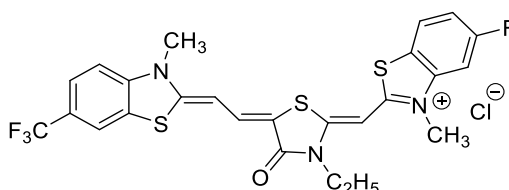
1.4.18 2-(3-Ethyl-5-(2-(6-fluoro-3-methylbenzo[d]thiazol-2(3*H*)-ylidene)ethylidene)-4-oxothiazolidin-2-ylidene)methyl)-5-fluoro-3-methylbenzo[d]thiazol-3-ium chloride (11p)



The title compound was synthesised following **General procedure H** using **9d** (102 mg, 0.19 mmol), synthesised as described in the synthesis of **11h**), **6c** (68 mg, 0.19 mmol), acetonitrile (5.0 mL) and triethylamine (80  $\mu$ L, 0.57 mmol) to give 2-(3-ethyl-5-(2-(6-fluoro-3-methylbenzo[d]thiazol-2(3*H*)-ylidene)ethylidene)-4-oxothiazolidin-2-ylidene)methyl)-5-fluoro-3-methylbenzo[d]thiazol-3-ium 4-methylbenzenesulfonate (**10p**) as a dark-green solid (89 mg, 0.13 mmol, 68% yield). Finally, **10p** (71 mg, 0.1 mmol) was subjected to **General procedure I** using methanol (5.0 mL) and conc. HCl (0.3 mL) to give the title product **11p** as a dark-green solid (48 mg, 0.087 mmol, 87% yield).

$^1\text{H NMR}$  (400 MHz, DMSO- $d_6$ )  $\delta$  8.29 (dd,  $J = 8.4, 5.4$  Hz, 1H, ArH), 7.82 (dd,  $J = 9.7, 1.3$  Hz, 1H, ArH), 7.65 (dd,  $J = 5.4, 3.2$  Hz, 1H, ArH), 7.57 (d,  $J = 13.1$  Hz, 1H, methine CH), 7.44 (td,  $J = 9.2, 1.8$  Hz, 1H, ArH), 7.24 (dd,  $J = 7.0, 6.3$  Hz, 2H, ArH), 6.75 (s, 1H, methine CH), 5.88 (d,  $J = 12.9$  Hz, 1H, methine CH), 4.16 (q,  $J = 6.9$  Hz, 2H,  $\text{CH}_2\text{CH}_3$ ), 4.01 (s, 3H,  $\text{CH}_3$ ), 3.81 (s, 3H,  $\text{CH}_3$ ), 1.29 (t,  $J = 6.9$  Hz, 3H,  $\text{CH}_2\text{CH}_3$ );  $^{13}\text{C NMR}$  (101 MHz, DMSO- $d_6$ )  $\delta$  164.57, 163.60, 162.48 (d,  $^1J_{\text{CF}} = 245.3$  Hz), 157.32, 148.46 (d,  $^1J_{\text{CF}} = 246.8$  Hz), 134.61, 129.57 (d,  $^3J_{\text{CF}} = 8.5$  Hz), 126.47 (d,  $^4J_{\text{CF}} = 2.7$  Hz), 125.47, 125.02 (d,  $^2J_{\text{CF}} = 24.1$  Hz), 124.93 (d,  $^2J_{\text{CF}} = 21.2$  Hz), 121.75, 118.91, 115.08 (d,  $^2J_{\text{CF}} = 21.1$  Hz), 113.74 (d,  $^2J_{\text{CF}} = 24.4$  Hz), 103.30, 102.49, 102.20, 90.63, 86.85, 39.10, 35.47, 34.95, 12.31;  $^{19}\text{F NMR}$  (376 MHz, DMSO- $d_6$ )  $\delta$  -110.98 (1F), -129.91 (1F); IR (neat): 1659 (C=N), 1556 (C=N), 1504 (C=C), 1455 (C=O), 1321 (C-N), 1200 (C-F), 1026 (C-S), 918 (C-F)  $\text{cm}^{-1}$ ; HRMS (ESI $^+$ ):  $m/z$  calcd for  $\text{C}_{24}\text{H}_{20}\text{F}_2\text{N}_3\text{O}_3$  $^+$  [M] $^+$  500.0731, found 500.0712; Mp: 274-276  $^\circ\text{C}$ .

1.4.19 2-(3-Ethyl-5-(2-(3-methyl-6-(trifluoromethyl)benzo[d]thiazol-2(3*H*)-ylidene)ethylidene)-4-oxothiazolidin-2-ylidene)methyl)-5-fluoro-3-methylbenzo[d]thiazol-3-ium chloride (11q)



The title compound was synthesised following **General procedure F** using **7** (0.48 g, 1.5 mmol), **6f** (0.61 g, 1.5 mmol), acetonitrile (7.5 mL), acetic anhydride (200  $\mu$ L, 2.1 mmol) and triethylamine (775  $\mu$ L, 5.5 mmol) to give 3-ethyl-5-(2-(3-methyl-6-(trifluoromethyl)benzo[*d*]thiazol-2(3*H*)-ylidene)ethylidene)-2-thioxothiazolidin-4-one (**8f**) as a red solid (0.43 g, 1.0 mmol, 67% yield). Next, **8f** (0.41 g, 1.0 mmol) was subjected to **General procedure G** using methyl *p*-toluenesulfonate (0.5 mL, 3.0 mmol) and DMF (2.0 mL) to give 3-ethyl-5-(2-(3-methyl-6-(trifluoromethyl)benzo[*d*]thiazol-2(3*H*)-ylidene)ethylidene)-2-(methylthio)-4-oxo-4,5-dihydrothiazol-3-ium 4-methylbenzene-sulfonate (**9f**) as a dark-green solid (234 mg, 0.4 mmol, 40% yield). A mixture of **9f** (234 mg, 0.4 mmol), **6c** (141 mg, 0.4 mmol) was subjected to **General procedure H** using acetonitrile (10.0 mL) and triethylamine (170  $\mu$ L, 1.2 mmol) to give 2-(3-ethyl-5-(2-(3-methyl-6-(trifluoromethyl)benzo[*d*]thiazol-2(3*H*)-ylidene)ethylidene)-4-oxothiazolidin-2-ylidene)methyl-5-fluoro-3-methyl-benzo[*d*]thiazol-3-ium 4-methylbenzenesulfonate (**10q**) as a dark-green solid (218 mg, 0.31 mmol, 77% yield). Finally, **10q** (105 mg, 0.15 mmol) was subjected to **General procedure I** using methanol (7.5 mL) and conc. HCl (0.5 mL) to the title product **11q** as a dark-green solid (77 mg, 0.13 mmol, 87% yield).

$^1\text{H NMR}$  (400 MHz, DMSO-*d*<sub>6</sub>)  $\delta$  8.28 (s, 2H, ArH), 7.94 (d, *J* = 8.3 Hz, 1H, ArH), 7.76 (d, *J* = 8.6 Hz, 1H, ArH), 7.65 (d, *J* = 12.9 Hz, 1H, methine CH), 7.60 (d, *J* = 8.5 Hz, 1H, ArH), 7.45 (t, *J* = 9.0 Hz, 1H, ArH), 6.79 (s, 1H, methine CH), 6.01 (d, *J* = 13.0 Hz, 1H, methine CH), 4.18 (q, *J* = 6.8 Hz, 2H, CH<sub>2</sub>CH<sub>3</sub>), 4.07 (s, 3H, CH<sub>3</sub>), 3.74 (s, 3H, CH<sub>3</sub>), 1.27 (t, *J* = 6.9 Hz, 3H, CH<sub>2</sub>CH<sub>3</sub>);  $^{13}\text{C NMR}$  (101 MHz, DMSO-*d*<sub>6</sub>)  $\delta$  172.24, 165.15, 163.03, 162.79 (d,  $^1J_{\text{CF}}$  = 252.5 Hz), 157.53, 145.13, 142.18, 134.64, 133.68, 130.85, 128.33, 125.29, 123.56 (q,  $^1J_{\text{CF}}$  = 253.4 Hz), 120.40, 120.27, 114.14 (d,  $^2J_{\text{CF}}$  = 24.7 Hz), 112.67, 104.50, 102.73 (d,  $^2J_{\text{CF}}$  = 27.4 Hz), 91.64, 87.31, 39.18, 35.32, 33.28, 12.56;  $^{19}\text{F NMR}$  (376 MHz, DMSO-*d*<sub>6</sub>)  $\delta$  -59.96 (3F), -111.03 (1F); IR (neat): 1670 (C=N), 1509 (C=C), 1468 (C=O), 1373 (C-CF<sub>3</sub>), 1311 (C-N), 1181 (C-N), 1065 (C-S), 941 (C-F) cm<sup>-1</sup>; HRMS (ESI<sup>+</sup>): *m/z* calcd for C<sub>25</sub>H<sub>20</sub>F<sub>4</sub>N<sub>3</sub>OS<sub>3</sub><sup>+</sup> [M]<sup>+</sup> 550.0699, found 550.0699; Mp: 255-258 °C.

## 2. Biological evaluation

### 2.1 Materials for biological section

Schneider's insect medium (Sigma-Aldrich, USA) containing 10% fetal bovine serum (FBS) was used for *Leishmania* cell culture. Dulbecco's modified Eagle's medium (DMEM) (Gibco, life technologies, USA) supplemented with 10% heat inactivated FBS was used for macrophages cell culture. Phosphate buffered saline (PBS) was purchased from Apsalagen, Bangkok, Thailand. The research grade of dimethyl sulfoxide (DMSO) (SERVA Electrophoresis GmbH, Heidelberg, Germany) was used for the preparation of compound solution. Resazurin sodium salt (TCI, Tokyo, Japan) was used as an indicator for colorimetric assay. Cells were inspected under an inverted

microscope (Olympus, Japan). The fluorescence intensities were obtained using the Thermo Scientific Varioskan® Flash microplate reader.

## 2.2 Cell culture

The biological evaluation was supported by Professor Dr. Padet Siriyasatien and Dr. Atchara Phumee, Department of Parasitology, Faculty of Medicine, Chulalongkorn University. The *Leishmania martiniquensis* strains, LSCM1, were isolated from the bone marrow of a Thai immunocompetent patient from Lamphun province, northern Thailand. The isolation of this strain was assigned WHO code MHOM/MQ/92/MAR; LEM2494. The *Leishmania orientalis* strains, PCM2, were isolated from the bone marrow of a Thai immunocompetent patient from Trang province, southern Thailand. The isolation of this strain was assigned WHO code MHOM/TH/2010/PCM2; Trang. One hundred  $\mu\text{L}$ s of thawing cells was loaded into 10 mL Schneider's insect medium + 10% FBS in a 25-cm<sup>3</sup> flask and maintained at  $25 \pm 2$  °C. As for *Cytotoxicity*: Murine macrophage J774A.1 cell was purchased from American Type Culture Collection and were cultured in DMEM + 10% FBS at 37 °C in 5% CO<sub>2</sub>.

## 2.3 Cell counting method

To the solution of 20  $\mu\text{L}$  of promastigote or macrophage cells in 20  $\mu\text{L}$  of trypan blue solution was gently mixed at a dilution factor of 2. Then, 10  $\mu\text{L}$  of the stained cell mixtures was transferred to the haemocytometer and incubated at room temperature for 5 min. Viable cells, unstained cells, were counted in 5 squares under a microscope at 40x magnification. The number of cells was calculated using the following equation:

$$\text{Number of cells (cells/mL)} = \text{Average cells} \times 10^4 \times \text{dilution factor}$$

## 2.4 The *in vitro* anti-leishmanial assays

### 2.4.1 The percentage of promastigote proliferation inhibition

The cultured solution of promastigotes of *L. martiniquensis* or *L. orientalis* ( $1 \times 10^6$  cells/mL, 90  $\mu\text{L}$ ) was transferred into 96-wells plate containing the fluorinated rhodacyanines at 0.1  $\mu\text{M}$  or 0.25  $\mu\text{M}$  (final concentration) with 1% DMSO in cultured solution. Cultures treated without the synthesised compounds were used as negative controls and medium without cells was used as blank. After adjusting the total volume to 100  $\mu\text{L}$  using Schneider's insect medium, the plates were incubated further for 72 h at  $25 \pm 2$  °C. Then, the living cells were quantified using the colorimetric assay (as described in Section 2.4.5, Chapter II).

#### **2.4.2 The half maximal inhibitory concentration (IC<sub>50</sub>) evaluation of promastigote proliferation inhibition**

The cultured solution of promastigotes of *L. martiniquensis* or *L. orientalis* ( $1 \times 10^6$  cells/mL, 90  $\mu$ L) was transferred into 96-wells plate containing two-fold dilution of the selected fluorinated rhodacyanines with 1% DMSO in cultured solution. Cultures treated without the synthesised compounds were used as negative controls and medium without cells was used as blank. After adjusting the total volume to 100  $\mu$ L using Schneider's insect medium, the plates were incubated further for 72 h at  $25 \pm 2$  °C. Then, the living cells were quantified using the colorimetric assay (as described in Section 2.4.5, Chapter II).

#### **2.4.3 The percentage of axenic amastigote proliferation inhibition**

The cultured solution of promastigotes of *L. martiniquensis* or *L. orientalis* ( $1 \times 10^7$  cells/mL, 90  $\mu$ L) was transferred into 96-wells plate containing fluorinated rhodacyanines at 0.25  $\mu$ M (final concentration) with 0.5% or 1% DMSO in cultured solution. Cultures treated without the synthesised compounds were used as negative controls and medium without cells was used as blank. After adjusting the total volume of 100  $\mu$ L using Schneider's insect medium, the plates were incubated further 72 h at 37 °C in 5% CO<sub>2</sub>. Then, the living cells were quantified using the colorimetric assay (as described in Section 2.4.5, Chapter II).

#### **2.4.4 The half maximal inhibitory concentration (IC<sub>50</sub>) evaluation of axenic amastigote proliferation inhibition**

The promastigotes of *L. martiniquensis* or *L. orientalis* ( $1 \times 10^7$  cells/mL, 90  $\mu$ L) were transferred into a 96-wells plate containing two-fold dilution of the selected fluorinated rhodacyanines with 0.5% or 1% DMSO in culture solution. Cultures treated without the synthesised compounds were used as negative controls and medium without cells was used as blank. After adjusting the total volume to 100  $\mu$ L using Schneider's insect medium, the plates were incubated further for 72 h at 37 °C in 5% CO<sub>2</sub>. Then, the living cells were quantified using the colorimetric assay (as described in Section 2.4.5, Chapter II).

#### **2.4.5 Colorimetric assay**

After incubation for 72 h, 10  $\mu$ L of 0.0125% resazurin in PBS was added to each well. The resazurin solution was prepared by dissolving 12.5 mg of resazurin sodium salt (TCI, Tokyo, Japan) in 100.00 mL of PBS, then stored at 4 °C. The plates were further incubated at 37 °C in 5% CO<sub>2</sub> for 2-3 h. The fluorescence intensities were calculated with a fluorescence plate reader using an excitation wavelength of 536 nm and an emission wavelength of 588 nm. The percentage of inhibition was calculated using the formula presented below:

$$\% \text{inhibition} = \frac{[\text{FI (control)} - \text{FI (blank)}] - [\text{FI (sample)} - \text{FI (blank)}]}{[\text{FI (control)} - \text{FI (blank)}]} \times 100$$

where FI means a fluorescence intensity

## 2.5 Cytotoxicity

Murine macrophage J774A.1 cell was purchased from American Type Culture Collection and were cultured in DMEM + 10% FBS at 37 °C in 5% CO<sub>2</sub> in a humidified atmosphere. The cultures were inspected for the parasites every 24 h under an inverted microscope (Olympus, Japan). After that, 200 µL of J774A.1 cells (2 x 10<sup>5</sup> cells/mL) was added into 96-wells plate and allowed cell adhesion by incubation at 37 °C in 5% CO<sub>2</sub> for 24 h. Cells were washed twice with DMEM and 99 µL of fresh medium was added followed by adding 1 µL of fluorinated rhodacyanines at the final concentration of 0.25 µM or 4.0 µM. Then, the plates were incubated at the same conditions for an additional 72 h. The percentages of viable cells were obtained using the mentioned colorimetric assay (as described in Section 2.4.5, Chapter II).

## 3. Pharmacological properties

### 3.1 The *in silico* ADMET prediction analysis

The analysis was performed with the assistance of Associate Professor Dr. Ng Chew Hee and Miss Mak Kit-Kay, School of Pharmacy, International Medical University, Malaysia. Briefly, QikProp v3.9 module of Maestro v9.7 interface of Schrödinger from Schrödinger Release 2019-2 was used to evaluate the *in silico* ADMET properties of the rhodacyanine analogues. Various physicochemical descriptors were calculated, including number of reactive functional groups (#rtvFG), octanol/water partition coefficient (QPlogPo/w), aqueous solubility level (QPlogS), brain/blood partition coefficient (QPlogBB), central nervous system activity (CNS), apparent gut-blood barrier permeability (QPpCaco), IC<sub>50</sub> value for blockage of HERG K<sup>+</sup> channels (QPlogHERG), number of likely metabolic reactions (#Metab), and percentage of human oral absorption level (Percentage of HOA). In addition, violation of the Lipinski's rule (vLRO5) was assessed using obtained values for the physicochemical descriptors.

### 3.2 The *in vitro* microsomal metabolic stability

The metabolic stability of the particular compounds (**11a** and **11c**) were measured.<sup>78</sup> This began with buffer preparation: 66.7 mM potassium phosphate buffer (PPB, pH 7.4) was prepared using the following procedures; (a) 1 M K<sub>2</sub>HPO<sub>4</sub> and 1 M KH<sub>2</sub>PO<sub>4</sub> in water was prepared, (b) 0.1 PPB was then prepared by adding 8.02 mL of 1 M K<sub>2</sub>HPO<sub>4</sub> into 1.98 mL of 1 M KH<sub>2</sub>PO<sub>4</sub> and the volume was adjusted to 100 mL with water, (c) 66.7 mL of 0.1 M PPB was diluted with water up to 100 mL, and (d) formic acid was used to adjust the pH value of the final buffer solution. Next,

0.2 mg/mL of all compounds were prepared by diluting a 10 mM of DMSO stock solution to 80% ACN in water. The mixtures were kept in the freezer until processing.

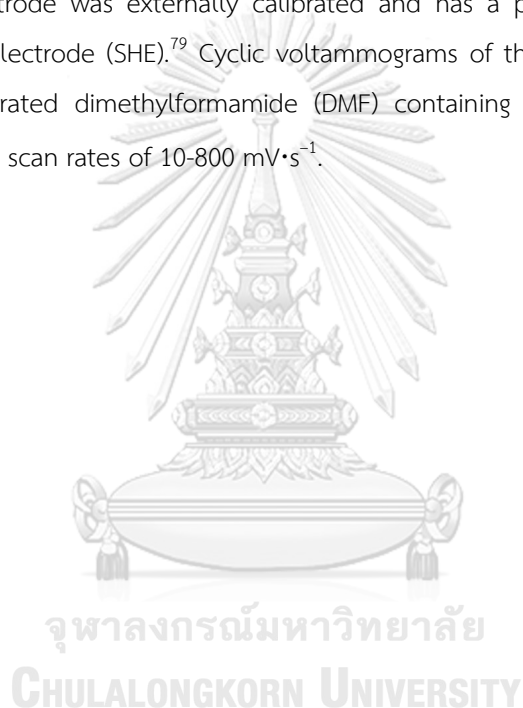
A pool of human liver microsomes was obtained from Gibco<sup>®</sup> by Life Technologies (Grand Island, NY, USA) and being kept at -80 °C. After thawing on the surface of ice bath, 110 µL microsomes (20 mg/mL) was withdrawn from the pool of microsomes and suspended in 3890 µL of 66.7 mM PPB (pH 7.4) in the polypropylene tube. Then, 900 µL of the previous solution was pipetted into three tubes. 5 µL of **11a**, **11c**, and verapamil (0.2 mg/mL in 80% ACN) was added into each tube. After that, 181 µL of the solution mixtures was transferred to 1.5 mL microcentrifuge tubes and those tubes were labelled as T<sub>c</sub>, T<sub>0</sub>, T<sub>5</sub>, T<sub>15</sub>, T<sub>30</sub> in which T<sub>c</sub> represents test tube control and the numeric numbers allocated for the other four remaining tubes indicate the incubation time. After that, all the tubes were pre-incubated together with NADPH (10 mM in water) at 37±2 °C for 5 minutes in Julabo model SW22 shaking water bath from Chemopharm<sup>®</sup> (Petaling Jaya, Selangor, MY). This is to mimic the body temperature to sustain microsomal viability. Next, 25 µL of NADPH was added into all tubes (excluding T<sub>c</sub>) and incubated according to their respective incubation time. NADPH serves as a co-factor to initiate the phase I enzymatic oxidation reaction. As for T<sub>c</sub>, instead of 25 µL of NADPH, 25 µL of PPB was added in tube T<sub>c</sub> and incubated for 30 min. T<sub>c</sub> serves as control to identify whether there is any non-NADPH enzymatic degradation. During the reaction, aliquots were collected and added 200 µL termination mixtures containing metronidazole, an internal standards (ISTD), at 0, 5, 15, and 30 min including T<sub>c</sub> to stop the reaction. The resulting samples were then centrifuged at 10000 rpm at 4 °C for 10 min.

Afterwards, 200 µL supernatant containing protein at the final concentration of 0.5 mg/mL were withdrawn to analyse for its metabolic stability using Agilent HPLC 1200 infinity series linked to a 1260 DAD VL detector (Agilent Technologies, Santa Clara, CA, USA). Aliquots (20 µL) were injected into a Shodex<sup>™</sup> C<sub>18</sub> packed column with particle size of 5 µm (4.6 mm × 150 mm, Tokyo, Japan). As in the separated experiments, **11a**, **11c**, and verapamil was eluted from the column using an isocratic elution with 80% ACN and formic acid buffer (0.2%v/v) at a flow rate of 0.5 mL/min. The DAD detector was set at 378 nm for **11a**, 383 nm for **11c**, 278 nm for verapamil, and 319 nm for ISTD.



#### 4. Electrochemistry

The electrochemical experiment was performed under the supervision of Dr. Parichat Vanalabhapatana, Department of Chemistry, Faculty of Science, Chulalongkorn University. With an assistance from Miss Kantima Chitchak, a doctoral student, the cyclic voltammetry measurements were obtained with an Autolab PGSTAT101 potentiostat/galvanostat (Eco Chemie, The Netherlands) using a three-electrode configuration. A glassy carbon electrode with a disk diameter of 3.0 mm was employed as a working electrode. Before use, the electrode was polished with an aqueous suspension of alumina powder. A platinum wire served as an auxiliary electrode. All potentials are quoted with respect to a non-aqueous silver/silver ion ( $\text{Ag}/\text{Ag}^+$ ) reference electrode. This electrode was externally calibrated and has a potential of 0.542 V *versus* a standard hydrogen electrode (SHE).<sup>79</sup> Cyclic voltammograms of the compounds (1.0 mM) were recorded in a deaerated dimethylformamide (DMF) containing 0.10 M tetrabutylammonium perchlorate (TBAP) at scan rates of 10-800  $\text{mV}\cdot\text{s}^{-1}$ .



## CHAPTER III

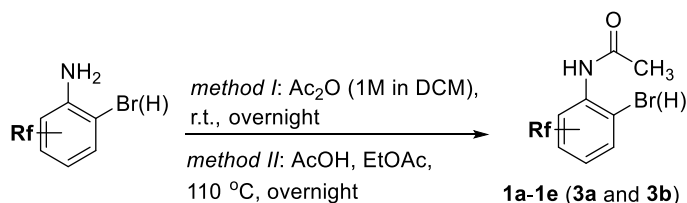
### RESULTS & DISCUSSIONS

#### 1. Synthesis of benzothiazolium building blocks

With slight modifications, the 18 fluorinated rhodacyanine analogues (**10c**, **11a-11q**) were synthesised using the procedures reported by M. Ihara and co-workers in 2010.<sup>7</sup> Firstly, the fluorine-containing benzothiazolium building blocks (**6a-6h**) were needed to be synthesised to control to position of fluorine or perfluoroalkyl group in the final products. There are four steps for this synthesis; (a) the *N*-acetylation of fluorine-containing *o*-bromoanilines, (b) the thionation of *o*-bromophenylacetamides to *o*-bromophenylthioacetamides; (c) the intramolecular cyclization to form the benzothiazole ring; and (d) the *N*-methylation of benzothiazoles to construct the corresponding benzothiazolium salts.

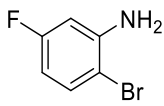
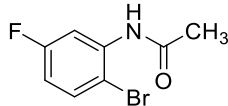
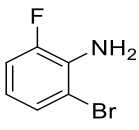
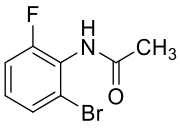
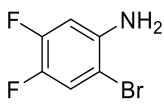
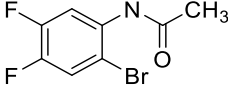
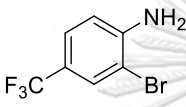
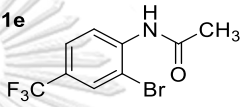
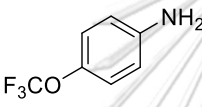
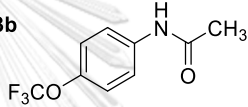
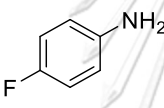
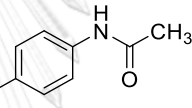
For the first step, the *N*-acetylation of *o*-bromoanilines, the simple and effective method was applied using acid anhydride ( $\text{Ac}_2\text{O}$ ). Unfortunately, concentrated  $\text{Ac}_2\text{O}$  is a highly regulated substance in Thailand because it is one of the important precursors to produce narcotics. To avoid this issue, the *N*-acetylation was performed using a commercially available 1 M solution of  $\text{Ac}_2\text{O}$  in DCM instead. Pleasingly, fluorine-containing *o*-bromophenylacetamides were obtained in excellent yields (**Table 3**, entries 1-6). Nonetheless, this pathway is relatively expensive due to cost of this reagent. In one instance, a more economical method was applied using acetic acid ( $\text{AcOH}$ ) in refluxing ethyl acetate ( $\text{EtOAc}$ ). Under this condition, the *p*-fluorophenylacetamide **3a** was successfully synthesised in excellent yield of 97% (**Table 3**, entry 7). Therefore, these two possible pathways can be adapted for further *N*-acetylation of the aromatic amines to obtain the desired acetamides in excellent yields.

**Table 3** The *N*-acetylation of *o*-bromoanilines and anilines containing fluorine or perfluoroalkyl group using **General procedure A**



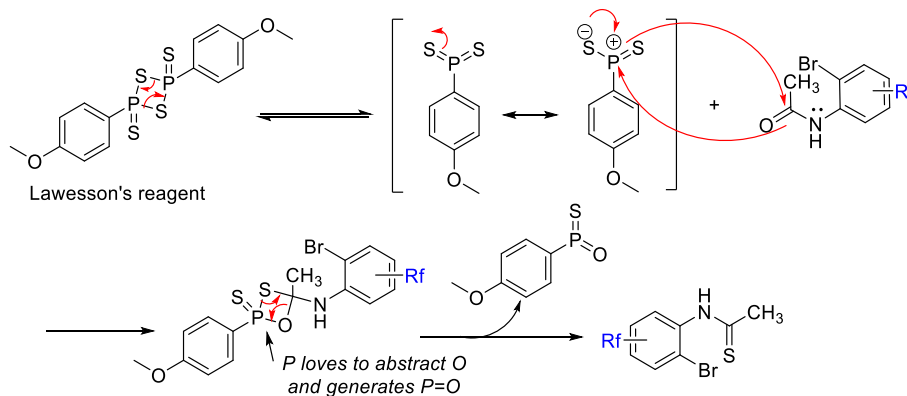
Entry	Starting material	Product	Yield (%)
1		<b>1a</b>	100 <sup>a</sup>

Table 3 (cont.)

Entry	Starting material	Product	Yield (%)
2		<b>1b</b> 	100 <sup>a</sup>
3		<b>1c</b> 	100 <sup>a</sup>
4		<b>1d</b> 	96 <sup>a</sup>
5		<b>1e</b> 	98 <sup>a</sup>
6		<b>3b</b> 	71 <sup>a</sup>
7		<b>3a</b> 	97 <sup>b</sup>

The product was performed using <sup>a</sup>method I and <sup>b</sup>method II.

Next, the resulting acetamides were then transformed to the corresponding thioacetamides using Lawesson's reagent. This reagent efficiently converts a carbonyl into a thiocarbonyl analogue through a mechanism that is closely related to Wittig reaction (**Figure 12**).<sup>80</sup> In this work, the thionation reaction was performed in anhydrous tetrahydrofuran (THF) overnight at room temperature under inert atmosphere to form the products (**2a-2e**) in moderate to excellent yields (**Table 4**).



**Figure 12** The proposed mechanism of thionation using Lawesson's reagent<sup>80</sup>

**Table 4** The thionation of compounds **1a-1e** and **3a**, and **3b** using Lawesson's reagent reagent

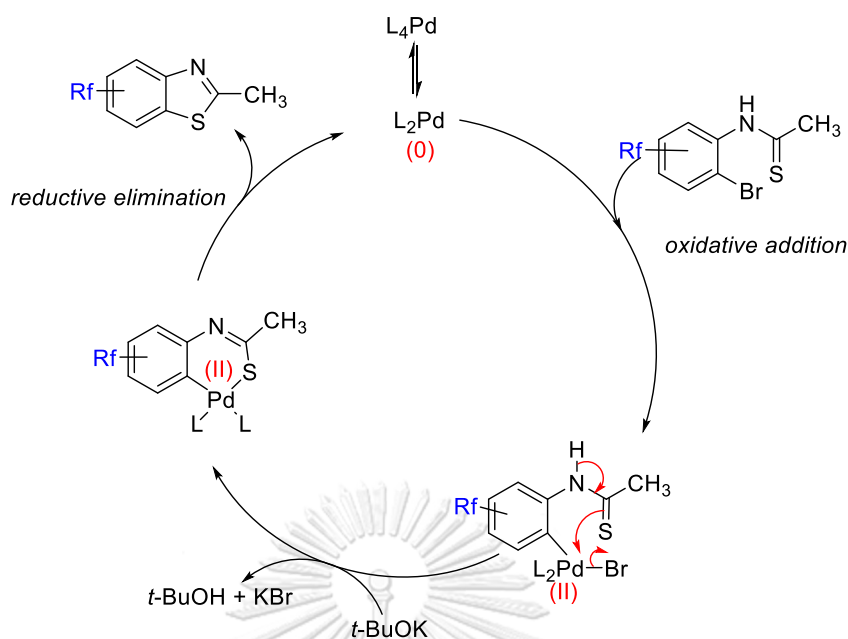


Entry	Starting material	Product	Yield (%)
1	<b>1a</b> 	<b>2a</b> 	54
2	<b>1b</b> 	<b>2b</b> 	89
3	<b>1c</b> 	<b>2c</b> 	85
4	<b>1d</b> 	<b>2d</b> 	73
5	<b>1e</b> 	<b>2e</b> 	95
6	<b>3a</b> 	<b>4a</b> 	71
7	<b>3b</b> 	<b>4b</b> 	81

After that, the intramolecular cyclization to produce benzothiazoles can be achieved using the two possible strategies, including the use of palladium (Pd) catalyst or the use of single electron cyclization. For the more popular method, the Pd-catalysed intramolecular cyclization of *o*-bromophenylthioacetamides (**2a-2e**) was performed using tris(dibenzylideneacetone) dipalladium(0) [Pd<sub>2</sub>(dba)<sub>3</sub>] in the presence of JohnPhos ligand and a base in 1,4-dioxane.<sup>72</sup> The corresponding benzothiazoles (**5b-5h**) were obtained in moderate to good yields (**Table 5**). Although this method requires expensive reagents, only a very small amounts are needed. The proposed mechanism of this reaction involves two key steps in the catalytic cycle; oxidative addition and reductive elimination (**Figure 13**). The oxidative addition involves the insertion of palladium into the carbon bearing the halides. Then, hydrogen of thioacetamide can be abstracted by the base to induce the insertion of thiol into the palladium(II). Finally, reductive elimination led to the formation of the desired benzothiazole.

**Table 5** The synthesis of benzothiazoles using a palladium-catalysed intramolecular cyclization of *o*-bromoarylthioamides

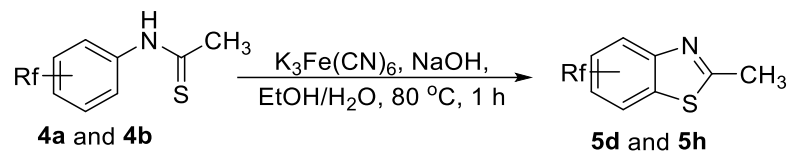
Entry	Starting material	Product	Yield (%)
	$\text{Rf}-\text{C}_6\text{H}_3(\text{Br})-\text{N}(\text{H})-\text{C}(=\text{S})\text{CH}_3 \xrightarrow[\text{KO}^t\text{Bu, dioxane, 80 }^\circ\text{C, overnight}]{\text{Pd}_2(\text{dba})_3 (5 \text{ mol}\%), \text{JohnPhos} (7.5 \text{ mol}\%)} \text{Rf}-\text{C}_6\text{H}_3(\text{N}=\text{C}(\text{CH}_3)\text{S})$		
1	<b>2c</b> 	<b>5b</b> 	70
2	<b>2b</b> 	<b>5c</b> 	43
3	<b>2a</b> 	<b>5e</b> 	67
4	<b>2e</b> 	<b>5f</b> 	72
5	<b>2d</b> 	<b>5h</b> 	63

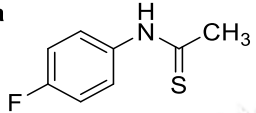
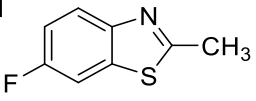
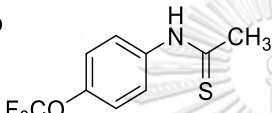
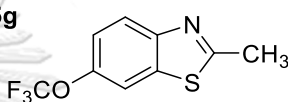


**Figure 13** The proposed mechanism of a palladium-catalysed cyclization<sup>81</sup>

Another strategy that can be applied to perform a similar intramolecular cyclization is Jacobson synthesis by oxidative cyclization of *N*-phenylthioamides carrying an unsubstituted *ortho* position, using potassium ferricyanide under basic conditions. The reaction can potentially yield two regioisomers that are difficult to separate if the two *ortho*-Hs are not chemically equivalent, and therefore this method is only applicable to symmetrical substrates. In this case, only the *N*-phenylthioacetamides bearing fluorine and trifluoromethyl ether at the *para* position (**4a** and **4b**) were used because they will give the identical products due to the symmetry of the molecule. According to the proposed mechanism reported by Y. A. Jackson and co-authors in 2004,<sup>82</sup> this reaction may involve the generation of a thiolate anion, which then undergoes one-electron oxidation by the potassium ferricyanide ( $K_3Fe(CN)_6$ ) to produce the thiol radical. The radical then attacks the unsubstituted *ortho* position followed by the second oxidation, then elimination of one proton to regain the aromaticity (**Figure 14**). The products **5d** and **5h** were synthesised according to this method in moderate yields (**Table 6**).

**Table 6** The synthesis of benzothiazoles via Jacobson cyclization using potassium ferricyanide



Entry	Starting material	Product	Yield (%)
1	<b>4a</b> 	<b>5d</b> 	50
2	<b>4b</b> 	<b>5g</b> 	59

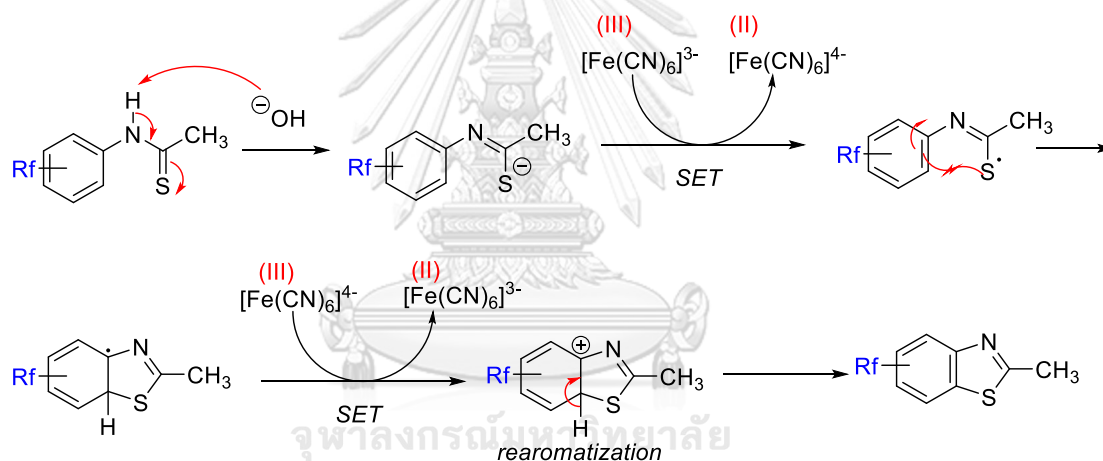


**Figure 14** The proposed mechanism of Jacobson synthesis of the fluorinated benzothiazoles through a single electron transfer

Additionally, the unsubstituted benzothiazole can be easily synthesised using an efficient one-pot synthesis reported by A. H. Zeniab and co-workers in 2017.<sup>83</sup> This environmentally friendly synthesis of benzothiazole was achieved by refluxing *o*-thioaniline with acetonitrile in glacial acetic acid (AcOH) containing a catalytic amount of concentrated sulfuric acid ( $\text{H}_2\text{SO}_4$ ). Finally, the benzothiazole (**5a**) was synthesised in good yield of 65% (**Figure 15**). The mechanism of this reaction could involve a nucleophilic attack of the aniline at the acid-activated acetonitrile then condensation with the loss of ammonia led to the benzothiazole ring formation (**Figure 16**).

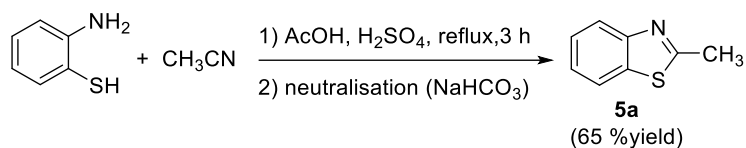


**Figure 15** The synthesis of benzothiazole via a one-pot synthesis

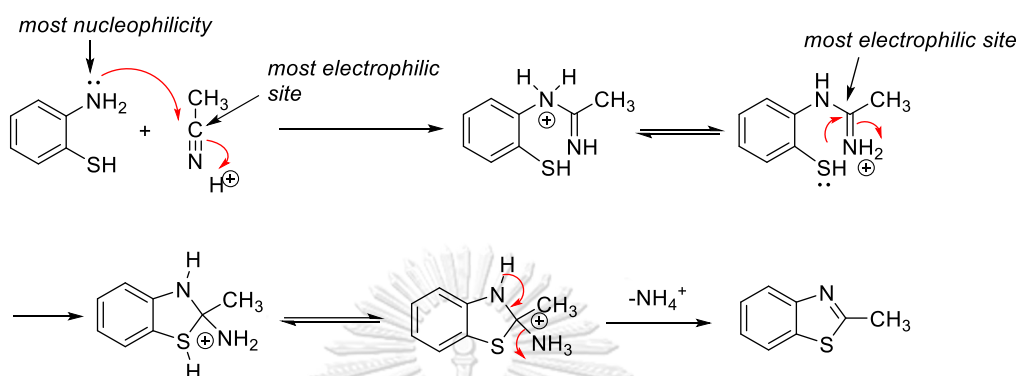


**Figure 16** The proposed mechanism of the benzothiazole formation through a one-pot synthesis<sup>83</sup>

Finally, all benzothiazole intermediates were then converted into *N*-methylbenzothiazolium *p*-toluenesulfonate using methyl *p*-toluenesulfonate. This reaction was operated at high-temperature under a solvent-free condition.<sup>55</sup> Simple precipitation yielded the desired products (**5a-5f**, and **5h**) in practically pure forms, except for **5g** which required purification by column chromatography. Generally, the benzothiazolium salts are very polar and impossible to be purified using chromatographic technique; however, the presence of  $-OCF_3$  in **5g** reduce its polarity and allow for such separation. All products were obtained in moderate to excellent yields (**Table 7**). The overall yields for the synthesis of the fluorine-containing benzothiazolium building blocks were also tabulated, which were in the range of 15-60 %. The major loss in the overall yields was in the cyclization step. Therefore, more reaction optimization on this cyclization step may be required to further improve the efficiency of the synthesis.



**Table 7** *N*-Methylation of benzothiazoles for the formation of fluorine-containing benzothiazolium building blocks (**6a-6h**)

$$\text{Rf-C}_6\text{H}_3\text{(S)-N(CH}_3\text{)=C(CH}_3\text{)-S} \xrightarrow[130\text{ }^\circ\text{C, 3h}]{\text{MeOTs}} \text{Rf-C}_6\text{H}_3\text{(S)-N}^+\text{(CH}_3\text{)(OTs)=C(CH}_3\text{)-S}$$

Entry	Substance	Product	Yield (%)	Overall yield (%)
1	<b>5a</b>	<b>6a</b>	72	47
2	<b>5b</b>	<b>6b</b>	39	23
3	<b>5c</b>	<b>6c</b>	65	25
4	<b>5d</b>	<b>6d</b>	51	18
5	<b>5e</b>	<b>6e</b>	56	27
6	<b>5f</b>	<b>6f</b>	89	60
7	<b>5g</b>	<b>6g</b>	56	19
8	<b>5h</b>	<b>6h</b>	35	15

## 2. Synthesis of fluorinated rhodacyanine analogues

After successful synthesis of the fluorine-containing benzothiazolium salts (**6a-6h**), they were then used as the building blocks for the synthesis of the rhodacyanines with variation on the position of fluorine atom or perfluoroalkyl group. According to the general structure of rhodacyanine class II, there are three main units connected by two methine carbons (**Figure 4b**). Throughout various rhodacyanine-based anti-leishmanial structure-activity relationship studies, the class of molecules that contain two benzothiazoles at both terminals of the 3-ethylrhodanine was found to be the most effective. The synthesis started with 3-ethylrhodanine as the central unit, which was then attached to a methine group using *N,N'*-diphenylformamidine followed by propionic anhydride at high temperature to form compound **7** (**Figure 17**).<sup>55</sup>

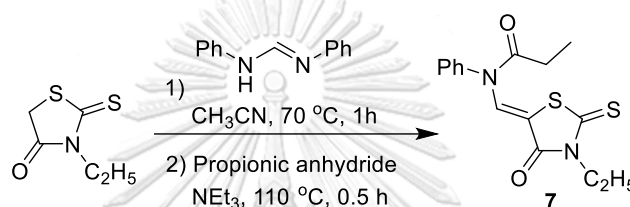


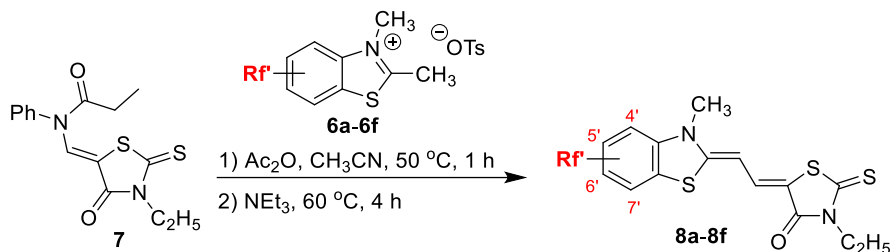
**Figure 17** The synthesis of compound **7**

Next, the intermediate **7** was treated with the corresponding benzothiazolium building blocks (**6a-6f**) in acetonitrile in the presence of acetic anhydride followed by adding triethylamine dropwise. During the addition of the base, the colour of the solution rapidly changed, most commonly resulted in a red solution. Then, the precipitate formed was filtered and washed with acetonitrile to give the desired compounds (**8a-8f**) in moderate to good yields (**Table 8**). Characterizations of these molecules were not possible due to their poor solubility in organic solvents; therefore, the next step was continued without further characterization. The tosylate compounds (**9a-9f**) were obtained in low to good yields (**Table 9**) via the *S*-methylation of the thiol group using methyl *p*-toluenesulfonate. Unfortunately, these compounds also gave complicated NMR spectra; therefore, they were subjected to the next reaction without additional characterizations. Next, the second benzothiazole unit was incorporated by the reaction of **9a-9f** with another benzothiazolium building block (**6a-6h**), giving **10a-10q** in moderate to excellent yields (**Table 10**).

Finally, the anion exchange was performed using concentrated hydrochloric acid to furnish the desired fluorinated rhodacyanine analogues (**11a-11q**) in moderate to excellent yields (**Table 11**). The overall yields were also tabulated in **Table 11**. The overall yields were relatively low, probably due to the poor solubility of those molecules. Moreover, performing the reaction in a small scale could exaggerate the product loss, especially during the filtration step. However, when the reaction was scaled up from 0.2 mmol to 0.5 mmol, the overall yield for the synthesis

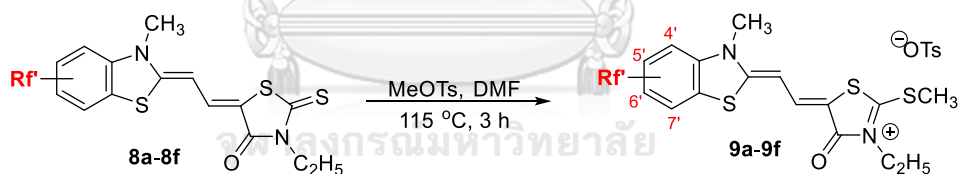
of compound **11c** was improved from 26% to 33%, respectively. With this believe, the scale-up for the synthesis of these analogues could increase the yields of the overall process with the easy synthetic protocol.

**Table 8** The synthesis of fluorine-containing rhodanine **8a-8f**



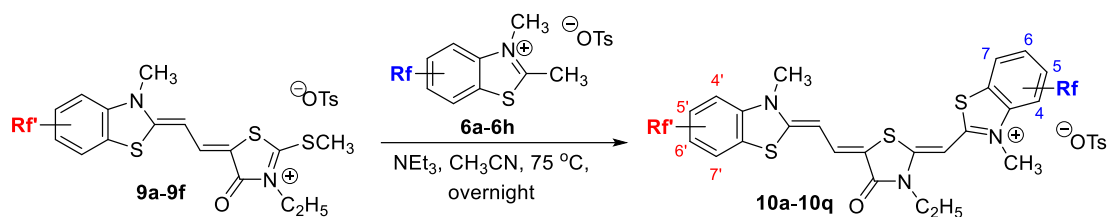
Entry	Reagent	Product	Rf'	Yield (%)
1	6a	8a	-	56
2	6b	8b	4'-F	67
3	6c	8c	5'-F	77
4	6d	8d	6'-F	75
5	6e	8e	7'-F	64
6	6f	8f	6'-CF <sub>3</sub>	67

**Table 9** The synthesis of the tosylate salt **9a-9f**



Entry	Starting material	Product	Rf'	Yield (%)
1	8a	9a	-	80
2	8b	9b	4'-F	50
3	8c	9c	5'-F	41
4	8d	9d	6'-F	28
5	8e	9e	7'-F	65
6	8f	9f	6'-CF <sub>3</sub>	40

Table 10 Synthesis of fluorinated rhodacyanine 10a-10q

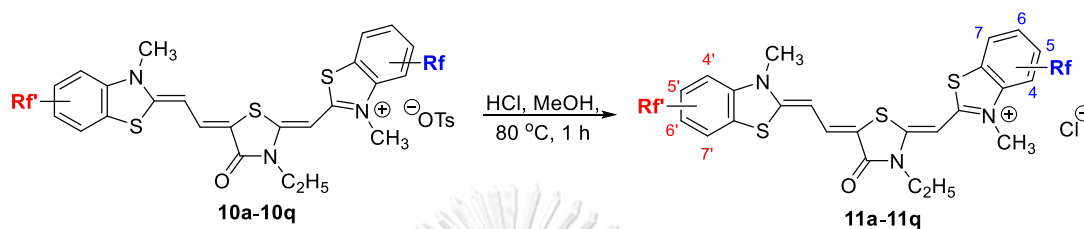


Entry	Starting material 1	Starting material 2	Product	Rf'	Rf	Yield (%)
1	9a	6a	10a	-	-	74
2	9a	6b	10b	-	4-F	77
3	9a	6c	10c	-	5-F	74
4	9a	6d	10d	-	6-F	68
5	9a	6e	10e	-	7-F	74
6	9b	6a	10f	4'-F	-	50
7	9c	6a	10g	5'-F	-	70
8	9d	6a	10h	6'-F	-	66
9	9e	6a	10i	7'-F	-	76
10	9a	6f	10j	-	6-CF <sub>3</sub>	68
11	9a	6g	10k	-	6-OCF <sub>3</sub>	67
12	9a	6h	10l	-	5,6-diF	67
13	9c	6c	10m	5'-F	5-F	84
14	9d	6d	10n	6'-F	6-F	68
15	9c	6d	10o	5'-F	6-F	74
16	9d	6c	10p	6'-F	5-F	68
17	9f	6c	10q	6'-CF <sub>3</sub>	5-F	77

Although the mechanism of this synthesis has not yet been reported, we propose that these reactions could involve E1cB elimination reaction and 1,4-addition/elimination reaction. The E1cB, the unimolecular elimination *via* conjugate base, generally occurs when a poor leaving group is involved. The first step is abstraction of the most acidic proton of 3-ethylrhodanine by NEt<sub>3</sub>, generating enolate which then further attack the central carbon of *N,N'*-diphenylformamidine. For the reaction to proceed to generate the methine bridge, aniline must act as a leaving group even though it is a poor leaving group, hence the E1cB mechanism is expected. This step generates  $\alpha,\beta$ -unsaturated ketone which can be attacked by the enamide intermediate of benzothiazole by a nucleophilic conjugate addition or 1,4-nucleophilic addition. The enolate then undergoes

subsequent elimination through the 1,4-conjugate elimination reaction to result in the second methine group. Similar reactions could occur in the step where compound **10a-10q** were synthesised. This reaction sequence lead to the formation of fully  $\pi$ -electron delocalised structures (**Figure 18**).

**Table 11** Synthesis of fluorinated rhodacyanine analogue **11a-11q**



Entry	Substance	Product	Rf'	Rf	Yield (%)	Overall yield (%)
1	10a	11a	-	-	62	21
2	10b	11b	-	4-F	72	25
3	10c	11c	-	5-F	77	26
4	10d	11d	-	6-F	62	19
5	10e	11e	-	7-F	82	27
6	10f	11f	4'-F	-	78	13
7	10g	11g	5'-F	-	60	13
8	10h	11h	6'-F	-	70	10
9	10i	11i	7'-F	-	43	14
10	10j	11j	-	6-CF <sub>3</sub>	76	23
11	10k	11k	-	6-OCF <sub>3</sub>	80	24
12	10l	11l	-	5,6-diF	75	23
13	10m	11m	5'-F	5-F	87	23
14	10n	11n	6'-F	6-F	90	13
15	10o	11o	5'-F	6-F	78	18
16	10p	11p	6'-F	5-F	87	12
17	10q	11q	6'-CF <sub>3</sub>	5-F	87	18

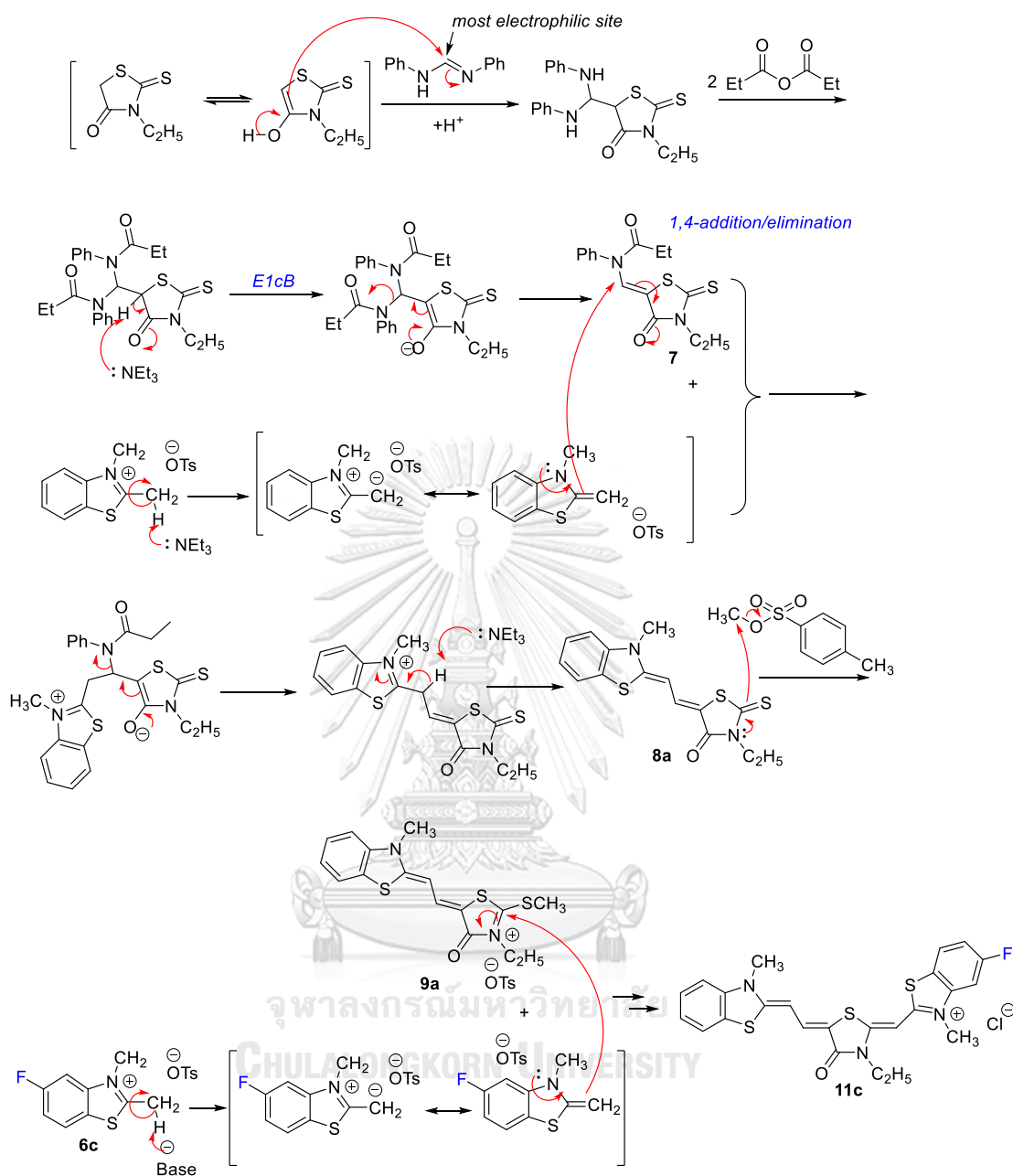


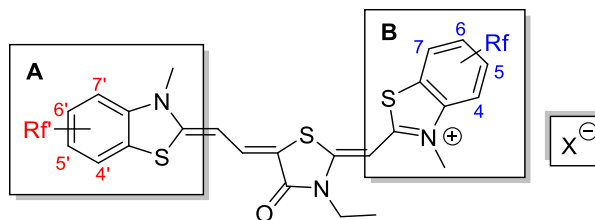
Figure 18 The proposed mechanism of the synthesis of **11c**

### 3. The biological results

The eighteen rhodacyanine analogues, which include a few that have been previously reported<sup>7</sup> (i.e. compounds **10c**, **11a**, and **11c**) and fifteen novel candidates, were firstly studied on the anti-leishmanial activity against the indigenous *Leishmania* species in Thailand, including *Leishmania martiniquensis* and *L. orientalis*. Due to the poor water solubility of these compounds, they were dissolved in dimethyl sulfoxide (DMSO) and sonicated with heating for 15 minutes to prepare the stock solution at 400  $\mu\text{M}$ . From the previous report,<sup>84</sup> the parasites can tolerate a culture medium containing 1% DMSO. Therefore, the use of DMSO in such a small concentration should not affect the biological activities. The screening test includes the study on both stages of parasites: promastigotes (a flagellated leishmanial form) and axenic amastigotes (a nonflagellated leishmanial form) (see in Section 2.2, Chapter I), and cytotoxicity toward normal cells.

First, each rhodacyanine was evaluated for its *in vitro* anti-leishmanial activity against promastigote stages of *L. martiniquensis* strain LSCM1 at the screening concentration of 0.25  $\mu\text{M}$  and the inhibiting percentages of parasitic proliferation were tabulated in **Table 12**. Most compounds can effectively kill the parasites except for compounds **11j**, **11k**, and **11q**, which contains 6-CF<sub>3</sub>, 6-OCF<sub>3</sub>, and 6'-CF<sub>3</sub>, respectively. This result is become more obvious when the concentration was decreased into 0.1  $\mu\text{M}$ . Among these analogues, eight compounds, including **10c**, **11c**, **11g**, **11i**, **11l**, **11p**, and **11a**, were selected for further evaluating the half maximal inhibitory concentration or IC<sub>50</sub> values. All selected fluorine-containing rhodacyanines possessed better inhibitory activity than **11a**, which is the unsubstituted rhodacyanine included as the reference. Their IC<sub>50</sub> values were in the range of 76-272 nM compared to the value of 658 nM for compound **11a**. Although these analogues were slightly less effective than amphotericin B (IC<sub>50</sub> = 30 nM), as discussed in Section 2.3.4 in Chapter II, amphotericin B is an intravenous drug making it inconvenient and costly due to the required hospitalization. When comparing with miltefosine, all of the analogues were significantly more active. Interestingly, **11c** (containing 5-F; also known as SJL-01) exhibited significant activity with 186-fold greater efficiency than miltefosine (IC<sub>50</sub> values: **11c** = 85 nM; miltefosine = 15.76  $\mu\text{M}$ ). It should be noted that the comparison was made at the parasite level *in vitro*, which may not necessarily reflect the true efficacy. Nevertheless, the activities comparable or better than existing drugs in use are welcoming signs. There was no significant difference between the IC<sub>50</sub> values of **11c** and **10c**; hence, this revealed that the counter anion did not cause any effect to the bioactivity.

**Table 12** The *in vitro* anti-leishmanial activities of eighteen rhodacyanine analogues against promastigotes of *L. martiniquensis* compared to the reference drugs.



Compounds	Rf'	Rf	X	Promastigotes of <i>L. martiniquensis</i>		
				%inhibition <sup>a</sup>		IC <sub>50</sub> <sup>a</sup> (μM)
				0.1 μM	0.25 μM	
10c	-	5-F	OTs	85.4 ± 0.5	89.5 ± 0.7	0.076 ± 0.008
11a	-	-	Cl	21.0 ± 1.5	70.8 ± 3.5	0.658 ± 0.028
11b	-	4-F	Cl	37.7 ± 2.6	64.1 ± 4.3	n.d. <sup>b</sup>
11c	-	5-F	Cl	82.8 ± 0.7	89.3 ± 1.1	0.085 ± 0.015
11d	-	6-F	Cl	57.1 ± 0.9	71.1 ± 1.1	n.d. <sup>b</sup>
11e	-	7-F	Cl	41.1 ± 2.6	85.2 ± 2.8	n.d. <sup>b</sup>
11f	4'-F	-	Cl	30.0 ± 2.1	73.0 ± 0.4	n.d. <sup>b</sup>
11g	5'-F	-	Cl	76.9 ± 0.5	89.2 ± 0.4	0.139 ± 0.005
11h	6'-F	-	Cl	40.3 ± 10.4	87.8 ± 0.8	n.d. <sup>b</sup>
11i	7'-F	-	Cl	56.1 ± 2.4	92.7 ± 1.0	0.272 ± 0.006
11j	-	6-CF <sub>3</sub>	Cl	10.5 ± 0.5	24.9 ± 3.3	n.d. <sup>b</sup>
11k	-	6-OCF <sub>3</sub>	Cl	8.7 ± 0.9	27.1 ± 1.8	n.d. <sup>b</sup>
11l	-	5,6-diF	Cl	80.6 ± 2.2	91.2 ± 0.5	0.106 ± 0.009
11m	5'-F	5-F	Cl	56.4 ± 4.0	79.8 ± 0.4	n.d. <sup>b</sup>
11n	6'-F	6-F	Cl	17.6 ± 1.3	62.9 ± 1.6	n.d. <sup>b</sup>
11o	5'-F	6-F	Cl	43.9 ± 8.0	75.9 ± 2.7	n.d. <sup>b</sup>
11p	6'-F	5-F	Cl	54.3 ± 8.1	93.4 ± 0.2	0.142 ± 0.022
11q	6'-CF <sub>3</sub>	5-F	Cl	5.9 ± 3.2	39.2 ± 2.9	n.d. <sup>b</sup>
<b>Miltefosine</b>				inactive <sup>b</sup>	inactive <sup>b</sup>	15.790 ± 3.564
<b>Amphotericin B</b>				94.2 ± 0.2	97.5 ± 0.4	0.031 ± 0.016

<sup>a</sup> IC<sub>50</sub> (the half maximal inhibitory concentration, μM) and %inhibition at specified concentration of compounds (%) were expressed as the mean values of three replicates ± standard deviations (SD). <sup>b</sup> inactive = no significant difference to the negative control (the absence of the test compound); n.d. = not determined.



Since there are two indigenous *Leishmania* species in Thailand, one of which has been originally discovered in Thailand is *L. orientalis* (previously called *L. siamensis*), the anti-leishmanial activities of the eighteen rhodacyanines against the two stages of *L. orientalis* were further evaluated.

According to the previous screening test, each of those compounds was investigated for its inhibition on promastigote proliferation of *L. orientalis* at the concentration of 0.25  $\mu\text{M}$ . The *in vitro* anti-leishmanial activities were expressed in percent inhibition (%) as tabulated in **Table 13**. The results show that most analogues inhibited effectively as shown by the inhibiting percentage of more than 75%. However, two compounds, including compound **11k** (compound with 6-OCF<sub>3</sub>) and **11q** (compound with 6'-CF<sub>3</sub> and 5-F), showed relatively poor activities against this parasite. When the concentration was reduced into 0.1  $\mu\text{M}$ , the activity of some compounds dramatically dropped, such as compound **11n**, where the inhibitory percentage was abruptly diminished from 76% to 2% at the concentration of 0.25 and 0.1  $\mu\text{M}$ , respectively. Eight fluorinated rhodacyanines, including compound **10c**, **11b**, **11c**, **11d**, **11g**, **11h**, **11l**, and **11m**, and the unsubstituted fluorinated compound (**11a**) were selected for further determining the IC<sub>50</sub> values. Surprisingly, the introduction of fluorine atom at the position 6 as in compound **11d** exhibited the most potency with the IC<sub>50</sub> value as low as 40 nM; meanwhile, miltefosine showed almost no efficacy for this activity. Thus, this novel fluorinated rhodacyanine can be a new candidate for further study on the anti-leishmaniasis against promastigotes of *L. orientalis*, although it is still less effective than amphotericin B.

Despite the fact that the axenic amastigote of *L. martiniquensis* could not be formed, it was possible to culture this parasite stage for *L. orientalis*; therefore, only the anti-leishmanial activity against axenic amastigote of *L. orientalis* was investigated. The screening activity of all analogues was determined at the concentration of 0.25  $\mu\text{M}$  where the result was displayed in **Table 13**. All analogues that contain fluorine or perfluoroalkyl group enhanced the proliferative inhibition against axenic amastigote of *L. orientalis* compared to the unsubstituted fluorinate one, however, only the compounds showing good inhibition (more than 75%) were selected for further determination of the IC<sub>50</sub> values. Nine fluorinated rhodacyanine analogues, including compound **10c**, **11c**, **11d**, **11g**, **11h**, **11l**, **11m**, **11o**, and **11p**, exhibited the axenic proliferation inhibition with the IC<sub>50</sub> values ranging from 77 to 223 nM, where compound **11a** showed a much poorer activity (IC<sub>50</sub> = 909 nM).

**Table 13** The *in vitro* anti-leishmanial activity against *L. orientalis* and the cytotoxicity.

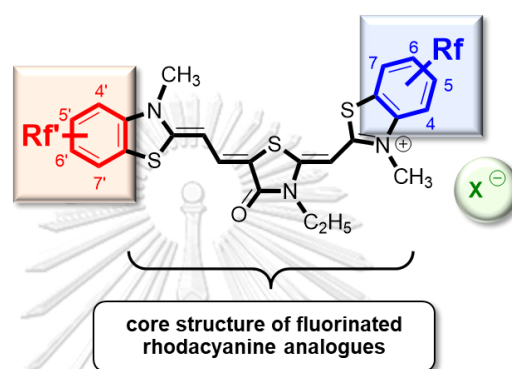
Compounds	<i>L. orientalis</i>					J774A.1 macrophage	
	Promastigotes			Axenic amastigotes		%cytotoxicity <sup>a</sup>	
	%inhibition <sup>a</sup>		IC <sub>50</sub> <sup>a</sup> (μM)	%inhibition <sup>a</sup>		0.25 μM    4.0 μM	
	0.1 μM	0.25 μM		0.25 μM	IC <sub>50</sub> <sup>a</sup> (μM)		
<b>10c</b>	78.8 ± 1.8	91.7 ± 1.2	0.098 ± 0.001	91.0 ± 0.6	0.110 ± 0.012	n.t. <sup>b</sup>	31.1 ± 5.6
<b>11a</b>	11.5 ± 3.5	81.5 ± 5.4	0.302 ± 0.030	36.8 ± 5.0	0.909 ± 0.004	n.t. <sup>b</sup>	19.2 ± 0.7
<b>11b</b>	67.5 ± 3.0	92.9 ± 1.2	0.065 ± 0.004	58.2 ± 1.5	n.d. <sup>b</sup>	n.t. <sup>b</sup>	24.9 ± 0.9
<b>11c</b>	66.2 ± 7.4	91.7 ± 0.9	0.104 ± 0.001	86.5 ± 2.9	0.080 ± 0.002	n.t. <sup>b</sup>	26.9 ± 1.5
<b>11d</b>	85.7 ± 1.3	95.4 ± 0.6	0.040 ± 0.002	78.5 ± 1.5	0.200 ± 0.007	n.t. <sup>b</sup>	41.3 ± 3.8
<b>11e</b>	13.9 ± 7.1	88.9 ± 2.1	n.d. <sup>b</sup>	42.9 ± 4.7	n.d. <sup>b</sup>	n.t. <sup>b</sup>	88.5 ± 7.5
<b>11f</b>	33.0 ± 7.4	84.2 ± 2.1	n.d. <sup>b</sup>	40.2 ± 1.6	n.d. <sup>b</sup>	n.t. <sup>b</sup>	13.4 ± 4.1
<b>11g</b>	50.1 ± 2.9	90.4 ± 0.6	0.133 ± 0.003	92.2 ± 1.3	0.134 ± 0.026	n.t. <sup>b</sup>	37.0 ± 1.1
<b>11h</b>	60.0 ± 7.8	96.0 ± 1.0	0.088 ± 0.001	91.2 ± 0.6	0.223 ± 0.014	n.t. <sup>b</sup>	61.8 ± 10.4
<b>11i</b>	inactive <sup>b</sup>	75.4 ± 4.0	n.d. <sup>b</sup>	47.9 ± 0.8	n.d. <sup>b</sup>	n.t. <sup>b</sup>	72.8 ± 8.8
<b>11j</b>	39.0 ± 8.1	87.6 ± 0.9	n.d. <sup>b</sup>	71.1 ± 5.4	n.d. <sup>b</sup>	0.5 ± 1.1	33.3 ± 0.8
<b>11k</b>	12.5 ± 9.8	60.9 ± 5.3	n.d. <sup>b</sup>	59.2 ± 2.8	n.d. <sup>b</sup>	n.t. <sup>b</sup>	48.6 ± 9.5
<b>11l</b>	61.6 ± 4.8	89.5 ± 0.8	0.114 ± 0.002	92.8 ± 0.4	0.077 ± 0.001	n.t. <sup>b</sup>	18.6 ± 3.8
<b>11m</b>	57.5 ± 6.4	81.5 ± 0.3	0.161 ± 0.008	87.9 ± 0.7	0.080 ± 0.003	n.t. <sup>b</sup>	13.8 ± 4.9
<b>11n</b>	1.9 ± 1.9	76.0 ± 1.9	n.d. <sup>b</sup>	62.1 ± 3.2	n.d. <sup>b</sup>	n.t. <sup>b</sup>	46.0 ± 4.4
<b>11o</b>	20.4 ± 4.4	79.3 ± 0.7	n.d. <sup>b</sup>	88.9 ± 0.5	0.081 ± 0.018	n.t. <sup>b</sup>	21.0 ± 1.9
<b>11p</b>	32.3 ± 7.8	93.0 ± 0.3	n.d. <sup>b</sup>	93.0 ± 0.4	0.085 ± 0.005	n.t. <sup>b</sup>	20.7 ± 3.8
<b>11q</b>	inactive <sup>b</sup>	33.3 ± 2.8	n.d. <sup>b</sup>	68.4 ± 8.0	n.d. <sup>b</sup>	13.3 ± 1.2	52.2 ± 3.6
<b>MF<sup>b</sup></b>	inactive <sup>b</sup>	4.0 ± 4.5	n.d. <sup>b</sup>	24.9 ± 3.3	n.d. <sup>b</sup>	7.3 ± 0.2	12.4 ± 4.3
<b>AM<sup>b</sup></b>	96.2 ± 0.2	96.7 ± 0.1	0.023 ± 0.003	91.1 ± 1.0	0.108 ± 0.003	n.t. <sup>b</sup>	16.7 ± 1.1

<sup>a</sup> IC<sub>50</sub> (the half maximal inhibitory concentration, μM), %inhibition at specified concentration of compounds (%), and %cytotoxicity at specified concentration of compounds (%) were expressed as the mean values of three replicates ± standard deviations (SD). <sup>b</sup> inactive = no significant difference to the negative control (the absence of the test compound); n.d. = not determined; n.t. = nontoxic to murine macrophages cell line, no significant difference to the negative control (the absence of the test compound). <sup>c</sup> MF: miltefosine; AM: amphotericin B.

It is noteworthy that the introduction of two fluorine atoms into either both terminal benzothiazole rings or just one ring of compound **11l**, **11m**, **11o**, and **11p** enhanced the activity (IC<sub>50</sub> = 77, 80, 81, and 85 nM, respectively), which are even more potent than amphotericin B (IC<sub>50</sub> = 108 nM). This indicated that, in order to enhance the anti-leishmanial activity against axenic amastigotes of *L. orientalis*, rhodacyanine containing at least one fluorine atom at the position 5 would give the best potency. Moreover, these rhodacyanine analogues were also tested the cytotoxicity toward murine macrophage cell line, J774A.1 (**Table 13**). At the highest

concentration at 4.0  $\mu\text{M}$ , only a few compounds were toxic showing in moderate to high %cytotoxicity, including compound **11e**, **11h**, and **11q** (%cytotoxicity = 88%, 62%, and 52%, respectively). Fortunately, the most potent compounds, such as **11c**, has a low toxicity toward the normal cell line.

According to this correlation, we can establish the structure-activity relationship (SAR) of the fluorine-containing rhodacyanine analogues effecting on the *in vitro* anti-leishmanial activity against *L. martiniquensis* and *L. orientalis* as follows:

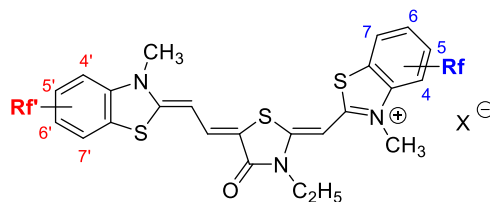


- (1) Introduction of fluorine atom(s) at position 5, 6, 5', or 6' enhances the potency.
- (2) The 5,6-diF rhodacyanine is the most effective compound for the axenic stage of *L. orientalis*.
- (3) Replacing 6'-H of compound **11c** by  $-\text{CF}_3$  group decreases the activity.
- (4) The rhodacyanine should not contain  $-\text{CF}_3$  or  $-\text{OCF}_3$  group at position 6.
- (5) There is no significant difference between the counter anions, where X is either OTs or Cl.

#### 4. The *in silico* ADMET properties

After we established the structure-activity relationship, it is crucial to understand the pharmacokinetic and pharmacodynamic properties of these analogues for further development into drug candidates. Moreover, the insight in the pharmacological properties of those agents may also lead to the clarification of their mechanism of action. As for the preliminary test, we analysed the *in silico* ADMET (absorption, distribution, metabolism, excretion, and toxicity) properties using Maestro Schrödinger's QikProp v3.9 module with the support from Associate Professor Dr. Ng Chew Hee and Miss Mak Kit-Kay from International Medical University, Malaysia.

**Table 14** The structure of fluorinated rhodacyanine analogues and the *in silico* ADMET properties analysis



Code	Rf	Rf'	X	#rtvFG	QLogPo/w	QLogS	QLogBB	CNS	QPPCaco (nm·s <sup>-1</sup> )	QLog HERG	Metab of HOA	Percentage of HOA	vLRO5
10c	5-F	-	OTs	0	7.746	-9.410	0.059	1	3901.428	-6.852	5	100	1
11a	-	-	Cl	0	7.479	-8.941	-0.050	0	4015.842	-6.925	5	100	1
11b	4-F	-	Cl	0	7.637	-9.157	0.022	1	4065.763	-6.838	5	100	1
11c	5-F	-	Cl	0	7.746	-9.410	0.059	1	3901.428	-6.852	5	100	1
11d	6-F	-	Cl	0	7.706	-9.286	0.061	1	4048.873	-6.784	5	100	1
11e	7-F	-	Cl	0	7.688	-9.262	0.042	1	4030.470	-6.810	5	100	1
11f	-	4'-F	Cl	0	7.585	-8.993	0.026	1	4041.975	-6.764	5	100	1
11g	-	5'-F	Cl	0	7.741	-9.375	0.062	1	3992.543	-6.824	5	100	1
11h	-	6'-F	Cl	0	7.748	-9.416	0.059	1	3897.276	-6.852	5	100	1
11i	-	7'-F	Cl	0	7.659	-9.152	0.049	1	4034.065	-6.767	5	100	1
11j	6-CF <sub>3</sub>	-	Cl	0	8.509	-10.498	0.224	1	3977.860	-6.865	5	100	2
11k	6-OCF <sub>3</sub>	-	Cl	0	8.643	-10.479	0.173	1	4020.452	-6.890	6	100	2
11l	5,6-diF	-	Cl	0	7.946	-9.680	0.159	1	4040.863	-6.688	5	100	2
11m	5-F	5'-F	Cl	0	7.988	-9.777	0.176	1	3972.619	-6.700	5	100	2
11n	6-F	6'-F	Cl	0	7.993	-9.786	0.179	1	4000.565	-6.707	5	100	2
11o	6-F	5'-F	Cl	0	7.987	-9.775	0.176	1	3989.158	-6.704	5	100	2
11p	5-F	6'-F	Cl	0	7.994	-9.794	0.175	1	3941.058	-6.702	5	100	2
11q	5-F	6'-CF <sub>3</sub>	Cl	0	8.710	-10.766	0.332	1	4037.635	-6.681	5	100	2

<sup>a</sup> #rtvFG means number of reactive functional groups; QLogPo/w is a predicted octanol/water partition coefficient; QLogS is prediction of aqueous solubility level; QLogBB is a predicted brain/blood partition coefficient; CNS stands for central nervous system activity; QPPCaco is a predicted apparent gut-blood barrier permeability; QLogHERG is a predicted IC<sub>50</sub> value for blockage of HERG K<sup>+</sup> channels; #Metab means number of likely metabolic reactions (1 - 8); Percentage of HOA means percentage of human oral absorption level; vLRO5, violations to Lipinski's rule of five.

The properties are tabulated in **Table 14**, where #rtvFG indicates number of reactive functional groups: 0 = no reactive functional groups, 1 = mild presence of reactive functional groups, 2 = high presence of reactive functional groups, all rhodacyanines have no reactive functional group, such as -OH and -NH<sub>2</sub> group, so the values are 0. QLogPo/w is the predicted octanol/water partition coefficient, where the recommended range is between -2.0 to 6.5. However, the rhodacyanine analogues express the values out of the recommended range due to

their high hydrophobicity. This is in line with the prediction of aqueous solubility level (QPlogS), which the recommended range is between -6.5 to 0.5. All the numbers are also out of the range.

Interestingly, all values of QPlogBB, which is the predicted brain/blood partition coefficient, are in the middle of the recommended range (-3.0 to 1.2). In addition, for the CNS (a central nervous system activity), where -2 means completely inactive, -1 means very low activity, 0 means low activity, 1 means medium activity, and 2 means completely active; all compounds are considered to have medium activity to CNS except for compound **11a**. This suggests that the fluorinated rhodacyanine analogues (**11b-11q**) have potential to be further studied on cerebral leishmaniasis or other diseases related to the nervous system. The predicted apparent gut-blood barrier permeability (QPPCaco) of these analogues is relatively high as all numbers are greater than 500 which can be accounted for by their high lipophilicity.

As for the toxicity, the predicted  $IC_{50}$  value for the blockage of HERG  $K^+$  channels (QPlogHERG) was calculated, where the value below than -5 is to be concerned. From the table, it is shown that these analogues have relatively low values, hence they may result in Q-T syndrome. The violations to Lipinski's rule of five (vLRO5)<sup>85</sup> is a useful criteria for evaluating the drug-likeness of biological active molecules for orally bioavailable drug. The rule states that an orally active drug should not violate more than of the following criteria: molecular weight less than 500 Da, log P less than 5 (high lipophilicity), less than five H-bond donors (expressed as sum of OH and NH groups) and less than ten H-bond acceptors (expressed as sum of O and N atoms). All of the rhodacyanine analogues violate at least one criterion, since the log P values are greater than 5. In addition, the molecular weight of compound **11j-11q** are also greater than 500 Da. Although Ro5 is one of the most widely used factor to predict compounds that could be orally active, exception to the rules are more than common. As an example, atorvastatin (Lipitor®), a major drug for cardiovascular diseases, probably would not have a chance to get to clinical trials if it were pre-evaluated by the Ro5, where the compound did not pass two criteria.<sup>86</sup> Therefore, Ro5 sometimes needs to be carefully used. However, all compounds exhibit exceptional predicted human oral absorption (%HOA) at 100%; thus, these analogues could be potentially be developed into novel oral anti-leishmanial drugs. Due to this indication, the metabolic stability for taking an oral administration needs to be determined; therefore, the number of metabolism (#Metab) of fluorinated rhodacyanine analogues was predicted as shown in **Table 14**. Five metabolic processes can occur with these analogues, where compound **11k** (compound containing 6-OCF<sub>3</sub>) can be metabolised through six pathways, thereby these may affect the drug pharmacokinetics: the bioavailability, the elimination half-life, and drug clearance.

## 5. Metabolic stability

According to the previous study on a related rhodacyanine based-antimalarial drug,<sup>53</sup> compound MKT-077 is rapidly metabolised by P450 enzyme where the  $t_{1/2}$  is around 5 minutes (see Section 2.5.1, Chapter I). Furthermore, the *in silico* ADMET properties prediction (**Table 14**) revealed that a few functional groups of these analogues (i.e., aromatic ring) can be metabolised through several enzymatic processes. Therefore, it is crucial to experimentally study the metabolic stability of the compounds. Since, the installation of fluorine substituent at a suitable position on drug molecules can improve the metabolic stability (as described in Section 2.6, Chapter I), the two rhodacyanine analogues (**11a** and **11c**) were selected for this study to clarify that the introduction of fluorine atom at position 5 can improve the metabolic stability or not. In this study, verapamil, a drug which is generally known to be rapidly metabolised by liver microsomes, was used as a positive control.

With the purpose of using fluorinated rhodacyanine as an oral drug for anti-leishmaniasis; therefore, there is a need to perform *in vitro* metabolic stability testing to identify its pharmacokinetics properties. By performing *in vitro* study, it allows us to predict *in vivo* pharmacokinetics parameters such as bioavailability and half-life. The rationale to carry metabolic stability testing is to design a safer way with desirable bioavailability and half-life, thereby reducing frequent dosing and improve patient compliance.

### 5.1 Metabolic stability of verapamil

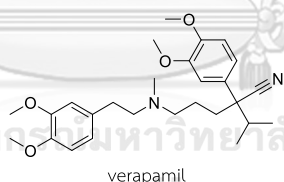


**Table 15** The area ratio, percentage of remaining, and metabolised verapamil in the presence of human liver microsomes at 0, 5, 15 and 30 minutes comparing to the control (verapamil without microsomes)

Verapamil	Analyte area <sup>a</sup>	IS area <sup>b</sup>	Area ratio (analyte/IS area)	%Metabolised	%Remaining (R)	lnR
Control	11829	857	13.803	-	-	-
0 min	13659	781	17.489	0.00	100.0	4.61
5 min	12426	812	15.303	12.5	87.50	4.47
15 min	11837	782	15.137	13.5	86.55	4.46
30 min	4620	724	6.381	63.5	36.49	3.60

<sup>a</sup> Analyte area is an integrated peak area of verapamil obtained from HPLC chromatogram.

<sup>b</sup> IS area means an integrated peak area of internal standard, metronidazole, obtained from HPLC chromatogram.

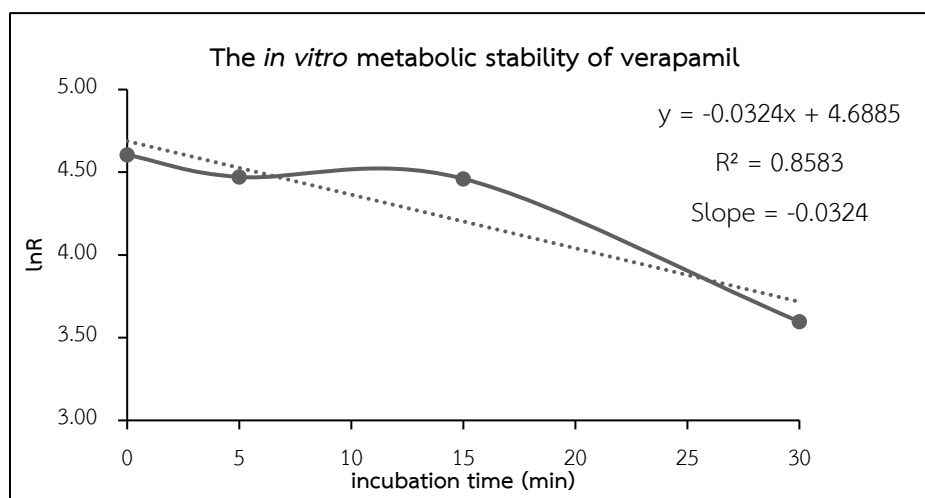


**Figure 19** Metabolic stability of verapamil in human liver microsomes expressed in graph of percentage remaining (%) against time (minute).

**Calculation:** with the information provided by the slope, both half-life ( $t_{1/2}$ ), the elimination rate constant ( $K_e$ ), and microsomal intrinsic clearance ( $mCL_{int}$ ) can be calculated by using the following equation:

$$\text{Half-life: } t_{1/2} = -\frac{\ln 2}{\text{slope}} = \frac{-0.693}{-0.0324} = 21.39 \text{ minutes}$$

$$\text{The elimination rate constant: } K_e = \frac{\ln 2}{t_{1/2}} = \frac{0.693}{21.39} = 0.032 \text{ min}^{-1}$$

$$\begin{aligned} \text{Microsomal intrinsic clearance: } mCL_{int} &= \frac{\ln 2 \times 1000}{t_{1/2}(\text{min}) \times \text{protein concentration (mg/mL)}} \\ &= \frac{\ln 2 \times 1000}{21.39 \text{ min} \times 0.5 \text{ (mg/mL)}} \\ &= 64.78 \text{ } \mu\text{L/min/mg} \end{aligned}$$

**Table 16** The microsomal intrinsic clearance of verapamil of human liver microsomes calculated based on the available data.

Source of liver microsome	Slope (0-30min)	$t_{1/2}$ (min)	Protein Concentration <sup>a</sup> (mg/mL)	$K_e$ ( $\text{min}^{-1}$ )	$mCL_{int}$ ( $\mu\text{L/min/mg}$ )
Human	-0.0324	21.39	0.5	0.032	64.8

<sup>a</sup> This indicates the amount of microsomal protein concentration that can bind to substance. If there is a large amount, the  $mCL_{int}$  value will decrease.

## 5.2 Metabolic stability of 11a

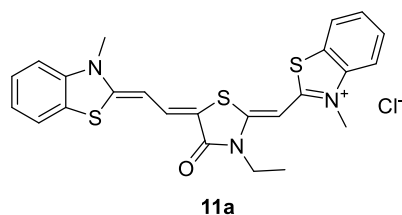


**Table 17** The area ratio, percentage of remaining, and metabolised **11a** in the presence of human liver microsomes at 0, 5, 15 and 30 minutes comparing to the control (**11a** without microsomes)

<b>11a</b>	Analyte area <sup>a</sup>	IS area <sup>b</sup>	Area ratio (analyte/IS area)	%Metabolised	%Remaining (R)	lnR
Control	1305	1669	0.782	-	-	-
0 min	1217	1549	0.786	0.00	100.0	4.61
5 min	652	1632	0.400	49.2	50.85	3.93
15 min	669	1653	0.405	48.5	51.51	3.94
30 min	460	1710	0.269	65.8	34.24	3.53

<sup>a</sup> Analyte area is an integrated peak area of compound **11a** obtained from HPLC chromatogram.

<sup>b</sup> IS area means an integrated peak area of internal standard, metronidazole, obtained from HPLC chromatogram.

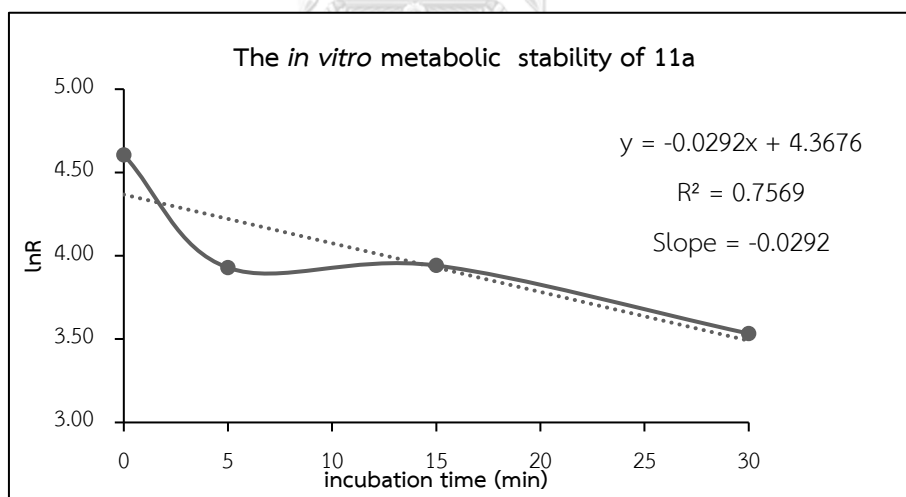


**Figure 20** Metabolic stability of 11a in human liver microsomes expressed in graph of percentage remaining (%) against time (minute).

**Calculation:** with the information provided by the slope, both half-life ( $t_{1/2}$ ), the elimination rate constant ( $K_e$ ), and microsomal intrinsic clearance ( $mCL_{int}$ ) can be calculated by using the following equation:

$$\text{Half-life: } t_{1/2} = -\frac{\ln 2}{\text{slope}} = \frac{-0.693}{-0.0292} = 23.73 \text{ minutes}$$



$$\begin{aligned} \text{The elimination rate constant: } K_e &= \frac{\ln 2}{t_{1/2}} = \frac{0.693}{23.73} = 0.029 \text{ min}^{-1} \\ \text{Microsomal intrinsic clearance: } mCL_{int} &= \frac{\ln 2 \times 1000}{t_{1/2}(\text{min}) \times \text{protein concentration (mg/mL)}} \\ &= \frac{\ln 2 \times 1000}{23.73 \text{ min} \times 0.5 \text{ (mg/mL)}} \\ &= 58.45 \mu\text{L/min/mg} \end{aligned}$$

**Table 18** The microsomal intrinsic clearance of verapamil of human liver microsomes calculated based on the available data.

Source of liver microsome	Slope (0-30min)	$t_{1/2}$ (min)	Protein Concentration <sup>a</sup> (mg/mL)	$K_e$ ( $\text{min}^{-1}$ )	$mCL_{int}$ ( $\mu\text{L/min/mg}$ )
Human	-0.0292	23.73	0.5	0.029	58.45

<sup>a</sup>This indicates the amount of microsomal protein concentration that can bind to substance. If there is a large amount, the  $mCL_{int}$  value will decrease.

### 5.3 Metabolic stability of 11c

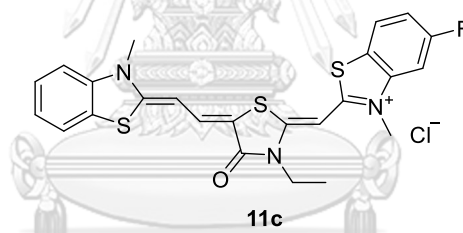


**Table 19** The area ratio, percentage of remaining, and metabolised **11c** in the present of human liver microsomes at 0, 5, 15 and 30 minutes comparing to the control (**11c** without microsomes)

<b>11c</b>	Analyte area <sup>a</sup>	IS area <sup>b</sup>	Area ratio (analyte/IS area)	%Metabolised	%Remaining (R)	lnR
Control	1207	1577	0.765	-	-	-
0 min	1217	1659	0.734	0.00	100.0	4.61
5 min	1003	1608	0.624	15.0	85.03	4.44
15 min	752	1632	0.461	37.2	62.81	4.14
30 min	491	1697	0.289	60.6	39.44	3.67

<sup>a</sup> Analyte area is an integrated peak area of compound **11c** obtained from HPLC chromatogram.

<sup>b</sup> IS area means an integrated peak area of internal standard, metronidazole, obtained from HPLC chromatogram.

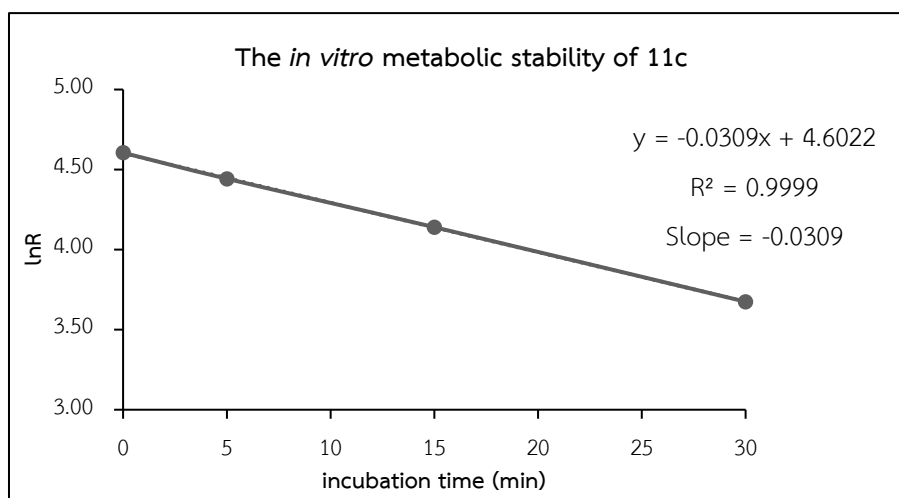


**Figure 21** Metabolic stability of **11c** in human liver microsomes expressed in graph of percentage remaining (%) against time (minute).

**Calculation:** with the information provided by the slope, both half-life ( $t_{1/2}$ ), the elimination rate constant ( $K_e$ ), and microsomal intrinsic clearance ( $mCL_{int}$ ) can be calculated by using the following equation:

$$\text{Half-life: } t_{1/2} = -\frac{\ln 2}{\text{slope}} = \frac{-0.693}{-0.0309} = 22.43 \text{ minutes}$$

$$\text{The elimination rate constant: } K_e = \frac{\ln 2}{t_{1/2}} = \frac{0.693}{22.43} = 0.031 \text{ min}^{-1}$$

$$\begin{aligned} \text{Microsomal intrinsic clearance: } mCL_{int} &= \frac{\ln 2 \times 1000}{t_{1/2}(\text{min}) \times \text{protein concentration (mg/ml)}} \\ &= \frac{\ln 2 \times 1000}{22.43 \text{ min} \times 0.5 \text{ (mg/ml)}} \\ &= 61.82 \text{ } \mu\text{L/min/mg} \end{aligned}$$

**Table 20** The microsomal intrinsic clearance of verapamil of human liver microsomes calculated based on the available data.

Source of liver microsome	Slope (0-30min)	$t_{1/2}$ (min)	Protein Concentration <sup>a</sup> (mg/mL)	$K_e$ ( $\text{min}^{-1}$ )	$mCL_{int}$ ( $\mu\text{L/min/mg}$ )
Human	-0.0309	22.43	0.5	0.031	61.82

<sup>a</sup> This indicates the amount of microsomal protein concentration that can bind to substance. If there is a large amount, the  $mCL_{int}$  value will decrease.

#### 5.4 A comparison of the metabolic stabilities between three compounds

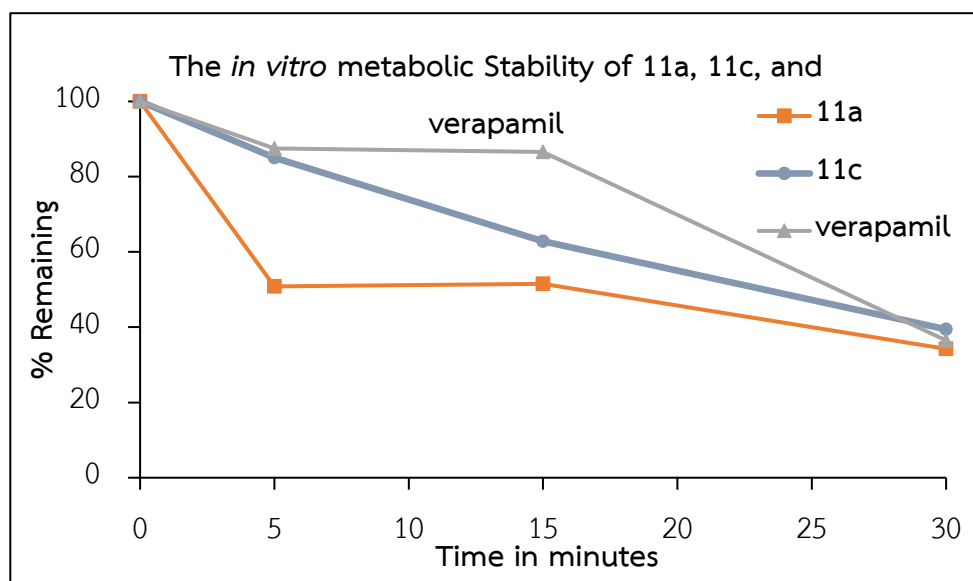


**Figure 22** The percentage remaining of each compounds against the incubation times in the presence of human liver microsomes

**Table 21** Comparison the in vitro metabolic stability of compound **11a**, **11c**, and verapamil by human liver microsomes

Compounds	$t_{1/2}$ (minutes)	$mCL_{int}$ ( $\mu\text{L}/\text{min}/\text{mg}$ )
<b>11a</b>	23.73	58.45
<b>11c</b>	22.43	61.82
verapamil	21.39	64.80

As for the results in **Table 21**, the half-life ( $t_{1/2}$ ) of **11a** and **11c** is 24 and 22 minutes, respectively. This indicates that the two selected compounds are rapidly metabolised by human liver microsomes, which contain a pool of CYP-enzymes. The key reaction mainly involves phase I oxidation reaction.<sup>87</sup> As a result, the calculated drug clearance is quite rapid ( $\sim 58\text{-}62 \mu\text{L}/\text{min}/\text{mg}$ ), and the presence of fluorine does not improve this metabolic stability. Nevertheless, these stability values are in the same range as verapamil, which is a currently used drug. This suggests that this class of compound can still be useful, although further structural optimization should be performed to improve their metabolic stability.

## 6. Electrochemistry

Recently, the fluorescent rhodacyanines previously reported in 2016<sup>46</sup> was shown to interact with *Plasmodium falciparum* mitochondria. Thus, the uptake of the rhodacyanines in

mitochondria plays an important role in its anti-malarial activity (as described in Section 2.5.2, Chapter I). However, the mechanism of action of these fluorinated rhodacyanine analogues for anti-leishmaniasis has not yet been clarified. In a search for the mechanism of action, one of the most relevant mechanism involves to the generation of reactive oxygen species (ROS) or reactive nitrogen species (RNS), where the imbalance between ROS and the cellular defence system is called oxidative stress leading to parasite death by apoptosis. Therefore, numerous molecules have been synthesised by introducing what relates to the functional group or structure that can produce ROS.

For example, nitro-containing semicarbazone derivatives were reported to show anti-leishmanial activities against *L. infantum* in 2015.<sup>88</sup> Since the introduction of nitro group can induce the ROS generation, the authors determined the reduction potential using cyclic voltammetry to clearly explain the correlation between the anti-leishmanial activities and the reduction potentials of the semicarbazone derivatives. Interestingly, the most potent compound exhibits the lowest reductive potential. This suggests us to suspect that the fluorinated rhodacyanine analogues may also induce ROS generation. Although each of these analogues does not contain a nitro group, the corresponding cationic benzothiazoles were redox active, and their oxidative and reductive potentials had been elucidated using cyclic voltammetry.<sup>89</sup> Besides, we propose that the introduction of fluorine atom could affect the reductive potentials due to its high electronegativity (see Section 2.6, Chapter I) through the inductive effect.

The protocol for the cyclic voltammetry measurements of the selected rhodacyanines: **11a**, **11c**, and **11g** in this work was modified from the previous report mentioned above (with the support from Dr. Parichatr Vanalabhapatana and Miss Kantima Chitchak), using a glassy carbon electrode containing tetrabutylammonium perchlorate-dimethylformamide (TBAP-DMF) electrolyte at a scan rate of  $100 \text{ mV}\cdot\text{s}^{-1}$ . The cyclic voltammograms are displayed in **Figure 23** with the potential scans ranging from -1.80 to +0.90 V, where the electrolyte solution was collected as a background showing in **Figure 23a** (dashed line). The peak potential was negatively screened from -0.70 to -1.80 V, and meanwhile the reduction peak of **11a** keep rising to a single irreversible combined wave with a broad shoulder starting at -1.53 V and a peak potential of approximately -1.35 V. As for the oxidation screened from -0.7 to +0.9 V, the oxidation of this compound indicates the three consecutive irreversible anodic waves with the peak potentials of +0.30, +0.49, and +0.72 V, while a small cathodic peak at -0.34 V was obtained through the reverse scan (+0.9 to -0.7 V). Furthermore, the peak potential of two selected fluorinated rhodacyanines (**11c** and **11g**) were negatively and positively scanned with the same condition ranging from -1.8 to +0.9 V. Their cyclic voltammograms are illustrated in **Figure 23b**. Since the only difference between these two compounds (**11c** and **11g**) and **11a** is the introduction of

fluorine substituent at position 5-F and 5'-F, the electrochemical behaviors are comparable to **11a** (non-fluorine substituent analogue). Furthermore, the scan rate studies (*i.e.*, plots of cathodic peak currents *versus* square root of scan rates) of **11a**, **11c**, and **11g** as exhibited in **Figure 24** demonstrate linear behavior which indicates the diffusion-controlled reduction processes of these analogues.

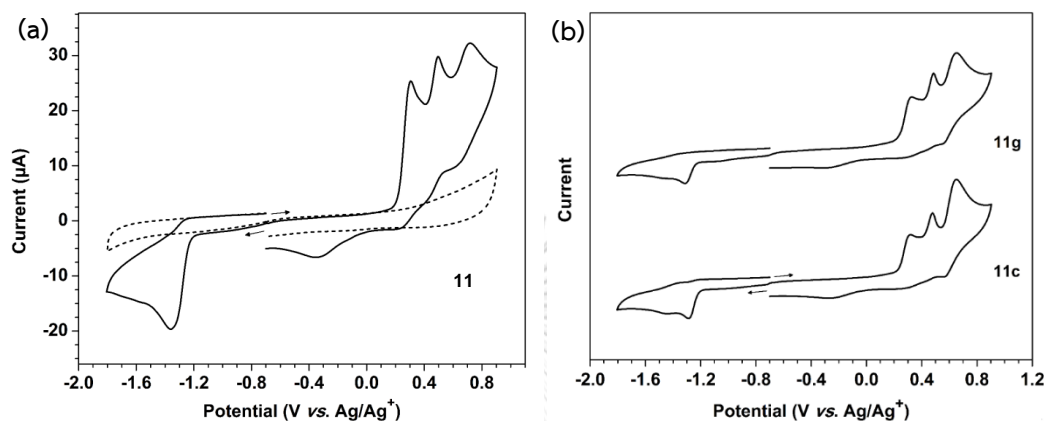
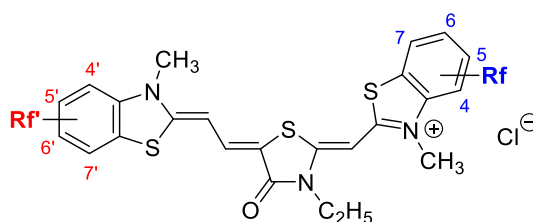


**Figure 23** Cyclic voltammograms recorded with a glassy carbon electrode (area = 0.071 cm<sup>2</sup>) at 100 mV·s<sup>-1</sup> for DMF containing 0.10 M TBAP in the presence of 1.0 mM (a) **11a** (solid lines) and DMF containing only 0.10 M TBAP (dashed lines); (b) **11c** and **11g**. Potential scans go from -0.70 to -1.80 to -0.70 V and -0.70 to +0.90 to -0.70 V.

All electrochemical information obtained from the cyclic voltammograms of these three rhodacyanine analogues were tabulated in **Table 22**. Interestingly, we found the similar correlation to a previous report<sup>88</sup> that the most potent rhodacyanine **11c** expressed the lowest reductive potential. Thus, the introduction of fluorine at position 5 on the benzothiazolium ring could slightly enhance the ROS generation compared to the unsubstituted benzothiolium analogue. Due to the electron acceptor of the benzothiazolium ring, the introduction of a fluorine atom at the *meta*-position (5-F) of the benzothiazolium cation could enhance its ability to accept an electron by the electron withdrawing effect of the fluorine. Furthermore, it is noteworthy to highlight that the introduction of fluorine atom to the rhodacyanine induces a slight positive shift of the cathodic peak potential (~40-60 mV). Although the results might not pinpoint the exact mechanism of action of these rhodacyanine analogues against *Leishmania* parasites proliferation, it serves as a preliminary results for further investigation on the *in vitro* or *in vivo* intracellular ROS generation.

**Table 22** Peak potential values for cyclic voltammograms of **11a**, **11c**, and **11g**.



Compound	Rf'	Rf	Reduction	Oxidation			
			(forward)	(forward)		(reverse)	
			$E_{pc1}$ (V)	$E_{pa1}$ (V)	$E_{pa2}$ (V)	$E_{pa3}$ (V)	$E_{pc1'}$ (V)
<b>11a</b>	-	-	-1.35	+0.30	+0.49	+0.72	-0.34
<b>11c</b>	-	5-F	-1.29	+0.32	+0.48	+0.65	-0.25
<b>11g</b>	5'-F	-	-1.31	+0.33	+0.49	+0.65	-0.27

$E_{pc}$  = cathodic peak potential; and  $E_{pa}$  = anodic peak potential.

The potential is quoted with respect to Ag/Ag<sup>+</sup> reference electrode having a potential of 0.542 V versus standard hydrogen electrode (SHE).<sup>28</sup>

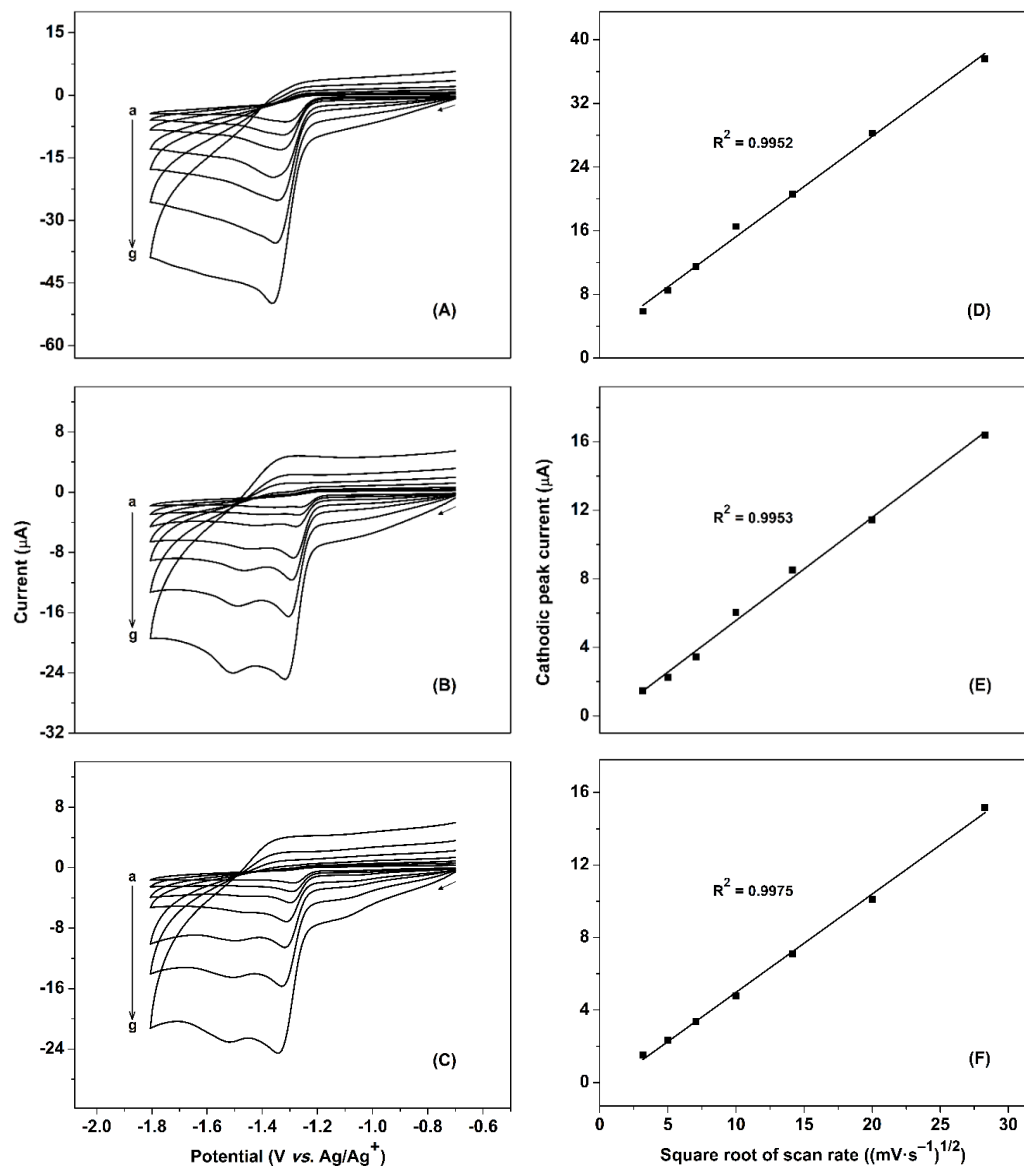


**Figure 24** Cyclic voltammograms recorded with a glassy carbon electrode (area = 0.071 cm<sup>2</sup>) from -0.70 to -1.80 to -0.70 V at 10-800 mV·s<sup>-1</sup> in DMF containing 0.10 M TBAP and 1.0 mM (A) **11a**, (B) **11c**, and (C) **11g**. (D) to (F) depict the corresponding plots of cathodic peak current obtained from the cyclic voltammograms of **11a**, **11c**, and **11g**, respectively, versus square root of scan rate.

## CHAPTER IV

### CONCLUSION

In conclusion, fifteen novel and three known fluorinated rhodacyanine analogues were successfully synthesised over four steps with overall yields ranging from 10% to 27%. The anti-leishmanial activities were investigated against promastigote and axenic amastigote stages of *Leishmania martiniquensis* and *L. orientalis*, the indigenous *Leishmania* species in Thailand. Comparing with the unsubstituted rhodacyanine (**11a**) as a reference compound, most of the fluorinated analogues exhibited greater inhibitions towards *Leishmania* parasite proliferation. It should be noted that some analogues such as **11c**, **11l**, **11m**, **11o**, and **11p** are more potent than the currently available antileishmanial drugs, such as miltefosine and amphotericin B. The structure-activity relationship (SAR) illustrated that the different positions of fluorine atom significantly affect the anti-leishmanial activity, whereas the presence of  $-CF_3$  and the  $-OCF_3$  substituents substantially decreased the anti-leishmanial activity. This trend could be explained by the decrease in aqueous solubility predicted by the *in silico* ADMET properties analysis of these analogues. Although they are rapidly metabolised by human liver microsomes, further metabolic enzymes (i.e., P450 enzymes) as well as *in vivo* test should be investigated to obtain more understanding about metabolic stability of these compounds. Other predicted ADMET properties also suggested that this rhodacyanine class might be developed into oral anti-leishmanial drugs and their suitability for treating cerebral leishmaniasis or other disease related to the nervous system. The apparent correlation of the less negative reduction potentials of the two fluorinated rhodacyanine analogues (**11c** and **11g**) compared to **11a** (non-fluorinated one) in the electrochemical study with their enhanced anti-leishmanial activities encourages further investigation related to the free radical mechanism of action, such as the intracellular ROS generation leading to parasite apoptosis. This development of fluorinated rhodacyanine analogues for anti-leishmaniasis not only identified some potent analogues that warrant further *in vivo* studies, but also provide highly important information for the development of even more effective rhodacyanine-based anti-leishmanial drugs in the future.



## REFERENCES

1. Das, A.; ALI, N., Vaccine Development Against *Leishmania donovani*. **2012**, *3* (99), 1-19.
2. Croft, S. L.; Coombs, G. H., Leishmaniasis—Current Chemotherapy and Recent Advances in the Search for Novel Drugs. *Trends in Parasitology* **2003**, *19* (11), 502-508.
3. Croft, S. L.; Sundar, S.; Fairlamb, A. H., Drug Resistance in Leishmaniasis. *Clinical Microbiology Reviews* **2006**, *19* (1), 111-126.
4. Ouellette, M.; Drummelsmith, J.; Papadopoulou, B., Leishmaniasis: Drugs in the Clinic, Resistance and New Developments. *Drug Resistance Updates* **2004**, *7* (4), 257-266.
5. Croft, S. L.; Olliaro, P., Leishmaniasis chemotherapy—challenges and opportunities. *Clinical Microbiology and Infection* **2011**, *17* (10), 1478-1483.
6. Takasu, K.; Terauchi, H.; Inoue, H., Antileishmanial Activities of Rhodacyanine Dyes. *Heterocycles* **2004**, *64*, 215-221.
7. Yang, M.; Arai, C.; Bakar Md, A.; Lu, J.; Ge, J.-F.; Pudhom, K.; Takasu, K.; Kasai, K.; Kaiser, M.; Brun, R.; Yardley, V.; Itoh, I.; Ihara, M., Fluorinated Rhodacyanine (SJL-01) Possessing High Efficacy for Visceral Leishmaniasis (VL). *Journal of Medicinal Chemistry* **2010**, *53* (1), 368-373.
8. Gillis, E. P.; Eastman, K. J.; Hill, M. D.; Donnelly, D. J.; Meanwell, N. A., Applications of Fluorine in Medicinal Chemistry. *Journal of Medicinal Chemistry* **2015**, *58* (21), 8315-8359.
9. Torres-Guerrero, E.; Quintanilla-Cedillo, M. R.; Ruiz-Esmenjaud, J.; Arenas, R., Leishmaniasis: a Review. *F1000Res* **2017**, *6*, 750-750.
10. Sangshetti, J. N.; Kalam Khan, F. A.; Kulkarni, A. A.; Arote, R.; Patil, R. H., Antileishmanial Drug Discovery: Comprehensive Review of the Last 10 Years. *RSC Advances* **2015**, *5* (41), 32376-32415.
11. Alvar, J.; Vélez, I. D.; Bern, C.; Herrero, M.; Desjeux, P.; Cano, J.; Jannin, J.; Boer, M. d.; the, W. H. O. L. C. T., Leishmaniasis Worldwide and Global Estimates of Its

- Incidence. *PLOS ONE* **2012**, 7 (5), e35671.
12. Killick-Kendrick, R., The Life-Cycle of *Leishmania* in the Sandfly with Special Reference to the Form Infective to the Vertebrate Host. *Annales de Parasitologie Humaine et Comparee* **1990**, 65, 37-42.
  13. Esch, K. J.; Petersen, C. A., Transmission and Epidemiology of Zoonotic Protozoal Diseases of Companion Animals. *Clinical Microbiology Reviews* **2013**, 26 (1), 58-85.
  14. McGwire, B. S.; Satoskar, A. R., Leishmaniasis: Clinical Syndromes and Treatment. *QJM: An International Journal of Medicine* **2013**, 107 (1), 7-14.
  15. de Vries, H. J. C.; Reedijk, S. H.; Schallig, H. D. F. H., Cutaneous Leishmaniasis: Recent Developments in Diagnosis and Management. *American Journal of Clinical Dermatology* **2015**, 16 (2), 99-109.
  16. Ahluwalia, S.; Lawn, S. D.; Kanagalingam, J.; Grant, H.; Lockwood, D. N. J., Mucocutaneous Leishmaniasis: an Imported Infection Among Travellers to Central and South America. *BMJ* **2004**, 329 (7470), 842-844.
  17. Chappuis, F.; Sundar, S.; Hailu, A.; Ghalib, H.; Rijal, S.; Peeling, R. W.; Alvar, J.; Boelaert, M., Visceral Leishmaniasis: What Are the Needs for Diagnosis, Treatment and Control? *Nature Reviews Microbiology* **2007**, 5 (11), S7-S16.
  18. Olivier, M.; Badaró, R.; Medrano, F. J.; Moreno, J., The Pathogenesis of Leishmania/HIV Co-Infection: Cellular and Immunological Mechanisms. *Annals of Tropical Medicine & Parasitology* **2003**, 97 (sup1), 79-98.
  19. Thakur, C. P.; Kumar, K., Post kala-azar Dermal Leishmaniasis: a Neglected Aspect of Kala-Azar Control Programmes. *Annals of Tropical Medicine & Parasitology* **1992**, 86 (4), 355-359.
  20. Alvar, J.; Cañavate, C.; Gutiérrez-Solar, B.; Jiménez, M.; Laguna, F.; López-Vélez, R.; Molina, R.; Moreno, J., Leishmania and Human Immunodeficiency Virus Coinfection: the First 10 Years. *Clinical Microbiology Reviews* **1997**, 10 (2), 298-319.
  21. World Health Organization *Clinical forms of the leishmaniasis*. [https://www.who.int/leishmaniasis/disease/clinical\\_forms\\_leishmaniasis/en/](https://www.who.int/leishmaniasis/disease/clinical_forms_leishmaniasis/en/) (accessed 7<sup>th</sup> November 2019).
  22. Tiunan, T. S.; Santos, A. O.; Ueda-Nakamura, T.; Filho, B. P. D.; Nakamura, C. V., Recent Advances in Leishmaniasis Treatment. *International Journal of Infectious*

- Diseases* **2011**, *15* (8), e525-e532.
23. Nagle, A. S.; Khare, S.; Kumar, A. B.; Supek, F.; Buchynskyy, A.; Mathison, C. J. N.; Chennamaneni, N. K.; Pendem, N.; Buckner, F. S.; Gelb, M. H.; Molteni, V., Recent Developments in Drug Discovery for Leishmaniasis and Human African Trypanosomiasis. *Chemical Reviews* **2014**, *114* (22), 11305-11347.
  24. Zulfiqar, B.; Shelper, T. B.; Avery, V. M., Leishmaniasis Drug Discovery: Recent Progress and Challenges in Assay Development. *Drug Discovery Today* **2017**, *22* (10), 1516-1531.
  25. Frézard, F.; Demicheli, C.; Ribeiro, R. R., Pentavalent Antimonials: New Perspectives for Old Drugs. *Molecules* **2009**, *14* (7), 2317-2336.
  26. Wise, E. S.; Armstrong, M. S.; Watson, J.; Lockwood, D. N., Monitoring Toxicity Associated with Parenteral Sodium Stibogluconate in the Day-Case Management of Returned Travellers with New World Cutaneous Leishmaniasis. *PLOS Neglected Tropical Diseases* **2012**, *6* (6), e1688.
  27. Patel, T. A.; Lockwood, D. N., Pentamidine as Secondary Prophylaxis for Visceral Leishmaniasis in the Immunocompromised Host: Report of Four Cases. *Tropical Medicine & International Health* **2009**, *14* (9), 1064-1070.
  28. Sands, M.; Kron, M. A.; Brown, R. B., Pentamidine: A Review. *Reviews of Infectious Diseases* **1985**, *7* (5), 625-634.
  29. Sundar, S.; Chakravarty, J., Leishmaniasis: an Update of Current Pharmacotherapy. *Expert Opinion on Pharmacotherapy* **2013**, *14* (1), 53-63.
  30. Sundar, S., Drug Resistance in Indian Visceral Leishmaniasis. *Tropical Medicine & International Health* **2001**, *6* (11), 849-854.
  31. Alves, F.; Bilbe, G.; Blesson, S.; Goyal, V.; Monnerat, S.; Mowbray, C.; Muthoni Ouattara, G.; Pécou, B.; Rijal, S.; Rode, J.; Solomos, A.; Strub-Wourgaft, N.; Wasunna, M.; Wells, S.; Zijlstra, E. E.; Arana, B.; Alvar, J., Recent Development of Visceral Leishmaniasis Treatments: Successes, Pitfalls, and Perspectives. *Clinical Microbiology Reviews* **2018**, *31* (4), e00048-18.
  32. Sundar, S.; Chakravarty, J., Paromomycin in the Treatment of Leishmaniasis. *Expert Opinion on Investigational Drugs* **2008**, *17* (5), 787-794.
  33. Sykes, J. E.; Papich, M. G., Chapter 10 - Antiprotozoal Drugs. In *Canine and Feline*

- Infectious Diseases*, Sykes, J. E., Ed. W.B. Saunders: Saint Louis, 2014; pp 97-104.
34. Sundar, S.; Chakravarty, J., Liposomal Amphotericin B and Leishmaniasis: Dose and Response. *J Glob Infect Dis* **2010**, *2* (2), 159-166.
  35. Dupont, B., Overview of the Lipid Formulations of Amphotericin B. *Journal of Antimicrobial Chemotherapy* **2002**, *49* (suppl\_1), 31-36.
  36. Lemke, A.; Kiderlen, A. F.; Kayser, O., Amphotericin B. *Applied Microbiology and Biotechnology* **2005**, *68* (2), 151-162.
  37. Khan, N.; Rawlings, B.; Caffrey, P., A Labile Point in Mutant Amphotericin Polyketide Synthases. *Biotechnology Letters* **2011**, *33* (6), 1121-1126.
  38. Olliaro, P.; Darley, S.; Laxminarayan, R.; Sundar, S., Cost-Effectiveness Projections of Single and Combination Therapies for Visceral Leishmaniasis in Bihar, India. *Tropical Medicine & International Health* **2009**, *14* (8), 918-925.
  39. Paris, C.; Loiseau, P. M.; Bories, C.; Bréard, J., Miltefosine Induces Apoptosis-Like Death in *Leishmania donovani* Promastigotes. *Antimicrobial Agents and Chemotherapy* **2004**, *48* (3), 852-859.
  40. Sunyoto, T.; Potet, J.; Boelaert, M., Why Miltefosine—a Life-Saving Drug for Leishmaniasis—Is Unavailable to People Who Need it the Most. *BMJ Global Health* **2018**, *3* (3), e000709.
  41. Thisyakorn, U.; Jongwutiwes, S.; Vanichsetakul, P.; Lertsapcharoen, P., Visceral Leishmaniasis: the First Indigenous Case Report in Thailand. *Transactions of The Royal Society of Tropical Medicine and Hygiene* **1999**, *93* (1), 23-24.
  42. Sarasombath, P. T., Leishmaniasis: An Evolving Public Health Concern in Thailand. *Sriraj Medical Journal* **2018**, *70*, 363-376.
  43. Leelayoova, S.; Siripattanapipong, S.; Hitakarun, A.; Kato, H.; Tan-ariya, P.; Siriyasatien, P.; Osatakul, S.; Mungthin, M., Multilocus Characterization and Phylogenetic Analysis of *Leishmania Siamensis* Isolated from Autochthonous Visceral Leishmaniasis Cases, Southern Thailand. *BMC Microbiology* **2013**, *13* (60), 1-7.
  44. Leelayoova, S.; Siripattanapipong, S.; Manomat, J.; Piyaraj, P.; Tan-Ariya, P.; Bualert, L.; Mungthin, M., Leishmaniasis in Thailand: A Review of Causative Agents and Situations. *The American Society of Tropical Medicine and Hygiene* **2017**, *96*

- (3), 534-542.
45. Zhu, Z., Thirty-Five Years of Studies on the Chemistry of Polymethine Cyanine Dyes. *Dyes and Pigments* **1995**, *27* (2), 77-111.
46. Takasu, K.,  $\pi$ -Delocalized Lipophilic Cations as New Candidates for Antimalarial, Antitrypanosomal and Antileishmanial Agents: Synthesis, Evaluation of Antiprotozoal Potency, and Insight into Their Action Mechanisms. *Chemical and Pharmaceutical Bulletin* **2016**, *64* (7), 656-667.
47. Shindy, H. A., Fundamentals in the Chemistry of Cyanine Dyes: A Review. *Dyes and Pigments* **2017**, *145*, 505-513.
48. Koya, K.; Li, Y.; Wang, H.; Ukai, T.; Tatsuta, N.; Kawakami, M.; Shishido, T.; Chen, L. B., MKT-077, a Novel Rhodacyanine Dye in Clinical Trials, Exhibits Anticarcinoma Activity in Preclinical Studies Based on Selective Mitochondrial Accumulation. *Cancer Research* **1996**, *56* (3), 538-543.
49. Modica-Napolitano, J. S.; Koya, K.; Weisberg, E.; Brunelli, B. T.; Li, Y.; Chen, L. B., Selective Damage to Carcinoma Mitochondria by the Rhodacyanine MKT-077. *Cancer Research* **1996**, *56* (3), 544-550.
50. Propper, D. J.; Braybrooke, J. P.; Taylor, D. J.; Lodi, R.; Styles, P.; Cramer, J. A.; Collins, W. C. J.; Levitt, N. C.; Talbot, D. C.; Ganesan, T. S.; Harris, A. L., Phase I trial of the Selective Mitochondrial Toxin MKT 077 in Chemo-Resistant Solid tumours. *Annals of Oncology* **1999**, *10* (8), 923-927.
51. Wadhwa, R.; Sugihara, T.; Yoshida, A.; Nomura, H.; Reddel, R. R.; Simpson, R.; Maruta, H.; Kaul, S. C., Selective Toxicity of MKT-077 to Cancer Cells Is Mediated by Its Binding to the hsp70 Family Protein mot-2 and Reactivation of p53 Function. *Cancer Research* **2000**, *60* (24), 6818-6821.
52. Li, X.; Srinivasan, S. R.; Connarn, J.; Ahmad, A.; Young, Z. T.; Kabza, A. M.; Zuideweg, E. R. P.; Sun, D.; Gestwicki, J. E., Analogues of the Allosteric Heat Shock Protein 70 (Hsp70) Inhibitor, MKT-077, As Anti-Cancer Agents. *ACS Medicinal Chemistry Letters* **2013**, *4* (11), 1042-1047.
53. Srinivasan, S. R.; Shao, H.; Li, X.; Gestwicki, J. E., Allosteric Inhibitors of Hsp70: Drugging the Second Chaperone of Tumorigenesis. In *Heat Shock Protein Inhibitors:*

- Success Stories*, McAlpine, S. R.; Edkins, A. L., Eds. Springer International Publishing: Cham, 2016; pp 131-162.
54. Takasu, K.; Inoue, H.; Kim, H.-S.; Suzuki, M.; Shishido, T.; Wataya, Y.; Ihara, M., Rhodacyanine Dyes as Antimalarials. 1. Preliminary Evaluation of Their Activity and Toxicity. *Journal of Medicinal Chemistry* **2002**, *45* (5), 995-998.
55. Pudhom, K.; Kasai, K.; Terauchi, H.; Inoue, H.; Kaiser, M.; Brun, R.; Ihara, M.; Takasu, K., Synthesis of Three Classes of Rhodacyanine Dyes and Evaluation of Their *In Vitro* and *In Vivo* Antimalarial Activity. *Bioorganic & Medicinal Chemistry* **2006**, *14* (24), 8550-8563.
56. Ge, J.-F.; Arai, C.; Yang, M.; Bakar Md, A.; Lu, J.; Ismail, N. S. M.; Wittlin, S.; Kaiser, M.; Brun, R.; Charman, S. A.; Nguyen, T.; Morizzi, J.; Itoh, I.; Ihara, M., Discovery of Novel Benzo[a]phenoxazine SSJ-183 as a Drug Candidate for Malaria. *ACS Medicinal Chemistry Letters* **2010**, *1* (7), 360-364.
57. Ihara, M.; Takasu, K.; Terauchi, H.; Inoue, H.; Takahashi, M.; Sekita, S., Antileishmanial Activities of Rhodacyanine Dyes. *Heterocycles* **2004**, *64*, 215-221.
58. Purser, S.; Moore, P. R.; Swallow, S.; Gouverneur, V., Fluorine in Medicinal Chemistry. *Chemical Society Reviews* **2008**, *37* (2), 320-330.
59. Zhou, Y.; Wang, J.; Gu, Z.; Wang, S.; Zhu, W.; Aceña, J. L.; Soloshonok, V. A.; Izawa, K.; Liu, H., Next Generation of Fluorine-Containing Pharmaceuticals, Compounds Currently in Phase II-III Clinical Trials of Major Pharmaceutical Companies: New Structural Trends and Therapeutic Areas. *Chemical Reviews* **2016**, *116* (2), 422-518.
60. Pitzer, K. S., The Nature of the Chemical Bond and the Structure of Molecules and Crystals: An Introduction to Modern Structural Chemistry. *Journal of the American Chemical Society* **1960**, *82* (15), 4121-4121.
61. Dalton, J., Pharmacokinetics and Metabolism in Drug Design. Methods and Principles in Medicinal Chemistry. Volume 31. Second Revised Edition By Dennis A. Smith, Han van de Waterbeemd, and Don K. Walker. *Journal of Medicinal Chemistry* **2006**, *49*, 7556-7557.
62. Bondi, A., van der Waals Volumes and Radii. *The Journal of Physical Chemistry* **1964**, *68* (3), 441-451.

63. *Fluorine in Pharmaceutical and Medicinal Chemistry*. IMPERIAL COLLEGE PRESS: 2011; Vol. Volume 6, p 572.
64. Masimirembwa, C. M.; Bredberg, U.; Andersson, T. B., Metabolic Stability for Drug Discovery and Development. *Clinical Pharmacokinetics* **2003**, *42* (6), 515-528.
65. Guengerich, F. P., Cytochrome P450 and Chemical Toxicology. *Chemical Research in Toxicology* **2008**, *21* (1), 70-83.
66. Rosenblum, S. B.; Huynh, T.; Afonso, A.; Davis, H. R.; Yumibe, N.; Clader, J. W.; Burnett, D. A., Discovery of 1-(4-Fluorophenyl)-(3*R*)-[3-(4-fluorophenyl)-(3*S*)-hydroxypropyl]-(4*S*)-(4-hydroxyphenyl)-2-azetidinone (SCH 58235): A Designed, Potent, Orally Active Inhibitor of Cholesterol Absorption. *Journal of Medicinal Chemistry* **1998**, *41* (6), 973-980.
67. Griffin, J. P., *The Textbook of Pharmaceutical Medicine: 6th Edition*. 2009; p 1-758.
68. Swallow, S., Chapter Two - Fluorine in Medicinal Chemistry. In *Progress in Medicinal Chemistry*, Lawton, G.; Witty, D. R., Eds. Elsevier: 2015; Vol. 54, pp 65-133.
69. Müller, K.; Faeh, C.; Diederich, F., Fluorine in Pharmaceuticals: Looking Beyond Intuition. *Science* **2007**, *317* (5846), 1881-1886.
70. Smart, B. E., Fluorine Substituent Effects (on Bioactivity). *Journal of Fluorine Chemistry* **2001**, *109* (1), 3-11.
71. Kim, D.; Wang, L.; Beconi, M.; Eiermann, G. J.; Fisher, M. H.; He, H.; Hickey, G. J.; Kowalchick, J. E.; Leiting, B.; Lyons, K.; Marsilio, F.; McCann, M. E.; Patel, R. A.; Petrov, A.; Scapin, G.; Patel, S. B.; Roy, R. S.; Wu, J. K.; Wyratt, M. J.; Zhang, B. B.; Zhu, L.; Thornberry, N. A.; Weber, A. E., (2*R*)-4-Oxo-4-[3-(Trifluoromethyl)-5,6-dihydro[1,2,4]triazolo[4,3-*a*]pyrazin-7(8*H*)-yl]-1-(2,4,5-trifluorophenyl)butan-2-amine: A Potent, Orally Active Dipeptidyl Peptidase IV Inhibitor for the Treatment of Type 2 Diabetes. *Journal of Medicinal Chemistry* **2005**, *48* (1), 141-151.
72. Benedí, C.; Bravo, F.; Uriz, P.; Fernández, E.; Claver, C.; Castellón, S., Synthesis of 2-Substituted-Benzothiazoles by Palladium-Catalyzed Intramolecular Cyclization of *O*-Bromophenylthioureas and *O*-Bromophenylthioamides. *Tetrahedron Letters* **2003**, *44* (32), 6073-6077.
73. Sanz Sharley, D. D.; Williams, J. M. J., Acetic Acid as a Catalyst for the *N*-acylation of

- Amines Using Esters as the Acyl Source. *Chemical Communications* **2017**, 53 (12), 2020-2023.
74. Shi, D.-F.; Bradshaw, T. D.; Wrigley, S.; McCall, C. J.; Lelieveld, P.; Fichtner, I.; Stevens, M. F. G., Antitumor Benzothiazoles. 3. Synthesis of 2-(4-Aminophenyl)benzothiazoles and Evaluation of Their Activities against Breast Cancer Cell Lines *in Vitro* and *in Vivo*. *Journal of Medicinal Chemistry* **1996**, 39 (17), 3375-3384.
75. Klochko, O. P.; Fedyunyayeva, I. A.; Khabuseva, S. U.; Semenova, O. M.; Terpetschnig, E. A.; Patsenker, L. D., Benzodipyrrolenine-Based Biscyanine Dyes: Synthesis, Molecular Structure and Spectroscopic Characterization. *Dyes and Pigments* **2010**, 85 (1), 7-15.
76. El-Mahdy, A., An Efficient One-Pot Synthesis of Benzo[1,4]Thiazines, Benzo[1,3]Thiazoles and Benzo[1,5]Thiazepines. *Current Organic Synthesis* **2016**, 13, 604-611.
77. Gao, D.; Li, A.; Guan, L.; Zhang, X.; Wang, L. Y., Solvent-Dependent Ratiometric Fluorescent Merocyanine Dyes: Spectral Properties, Interaction with BSA as well as Biological Applications. *Dyes and Pigments* **2016**, 129, 163-173.
78. Pirmohamed, M., Williams, D., Madden, S., Templeton, E., Park, B. K., Metabolism and Bioactivation of Clozapine by Human Liver *In Vitro*. *Journal of Pharmacology and Experimental Therapeutics* **1995**, 272 (3), 984-990.
79. Pavlishchuk, V. V.; Addison, A. W., Conversion Constants for Redox Potentials Measured *versus* Different Reference Electrodes in Acetonitrile Solutions at 25 °C. *Inorganica Chimica Acta* **2000**, 298 (1), 97-102.
80. Ozturk, T.; Ertas, E.; Mert, O., Use of Lawesson's Reagent in Organic Syntheses. *Chemical Reviews* **2007**, 107 (11), 5210-5278.
81. Amatore, C.; Azzabi, M.; Jutand, A., Role and Effects of Halide Ions on the Rates And Mechanisms of Oxidative Addition of Iodobenzene to Low-Ligated Zerovalent Palladium Complexes Pd(PPh<sub>3</sub>)<sub>2</sub>. *Journal of the American Chemical Society* **1991**, 113 (22), 8375-8384.
82. Downer, N. K.; Jackson, Y. A., Synthesis of Benzothiazoles Via ipso Substitution of *Ortho*-Methoxythiobenzamides. *Organic & Biomolecular Chemistry* **2004**, 2 (20),



3039-3043.

83. F. M. El-Mahdy, A.; S. Mohamed, O.; A.H. El-Sherif, H.; A. Hozien, Z., An Efficient One-Pot Synthesis of Benzo[1,4]Thiazines, Benzo[1,3]Thiazoles and Benzo[1,5]Thiazepines. *Current Organic Synthesis* **2017**, *14* (4), 604-611.
84. De Muylder, G.; Ang, K. K. H.; Chen, S.; Arkin, M. R.; Engel, J. C.; McKerrow, J. H., A Screen Against Leishmania Intracellular Amastigotes: Comparison to a Promastigote Screen and Identification of a Host Cell-Specific Hit. *PLoS neglected tropical diseases* **2011**, *5* (7), e1253-e1253.
85. Zhang, M.-Q.; Wilkinson, B., Drug Discovery Beyond the 'Rule-of-Five'. *Current Opinion in Biotechnology* **2007**, *18* (6), 478-488.
86. Giménez, B. G.; Santos, M. S.; Ferrarini, M.; Fernandes, J. P. S.; Fernandes, J. P. S., Evaluation of Blockbuster Drugs Under the Rule-of-five. *Die Pharmazie - An International Journal of Pharmaceutical Sciences* **2010**, *65* (2), 148-152.
87. McDonnell, A.; Dang, C., Basic Review of the Cytochrome P450 System. *Journal of the advanced practitioner in oncology* **2013**, *4*, 263-268.
88. Mendoza-Martínez, C.; Galindo-Sevilla, N.; Correa-Basurto, J.; Ugalde-Saldivar, V. M.; Rodríguez-Delgado, R. G.; Hernández-Pineda, J.; Padierna-Mota, C.; Flores-Alamo, M.; Hernández-Luis, F., Antileishmanial Activity of Quinazoline Derivatives: Synthesis, Docking Screens, Molecular Dynamic Simulations and Electrochemical Studies. *European Journal of Medicinal Chemistry* **2015**, *92*, 314-331.
89. Lenhard, J. R.; Cameron, A. D., Electrochemistry and Electronic Spectra of Cyanine Dye Radicals in Acetonitrile. *The Journal of Physical Chemistry* **1993**, *97* (19), 4916-4925.



APPENDICES

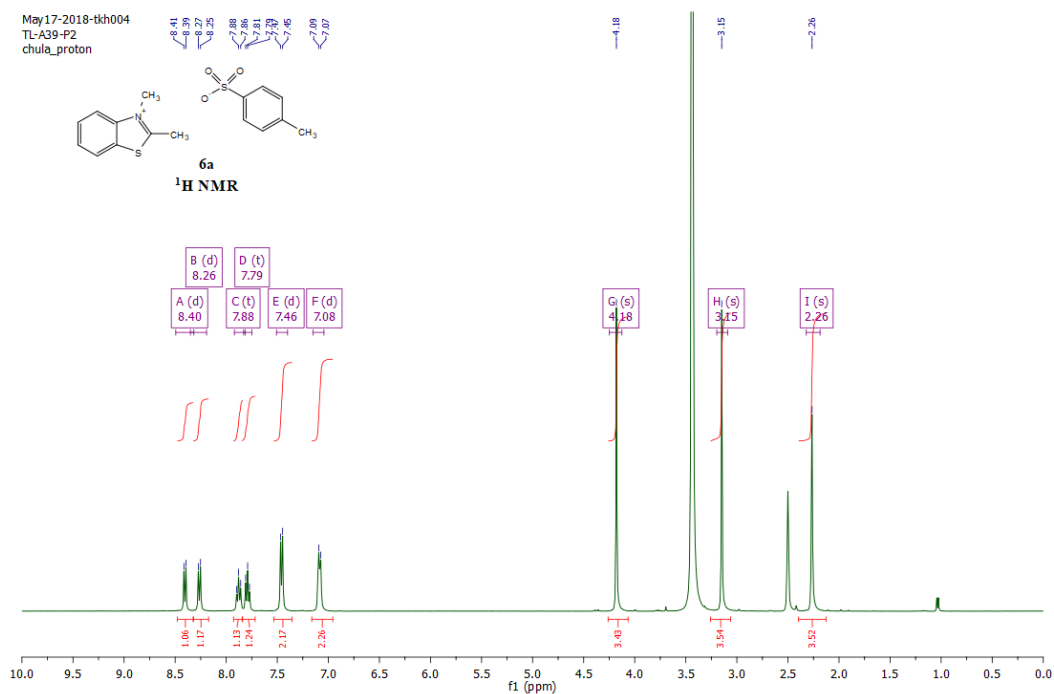
จุฬาลงกรณ์มหาวิทยาลัย  
**CHULALONGKORN UNIVERSITY**



## 2,3-Dimethylbenzo[d]thiazol-3-ium 4-methylbenzenesulfonate (6a)

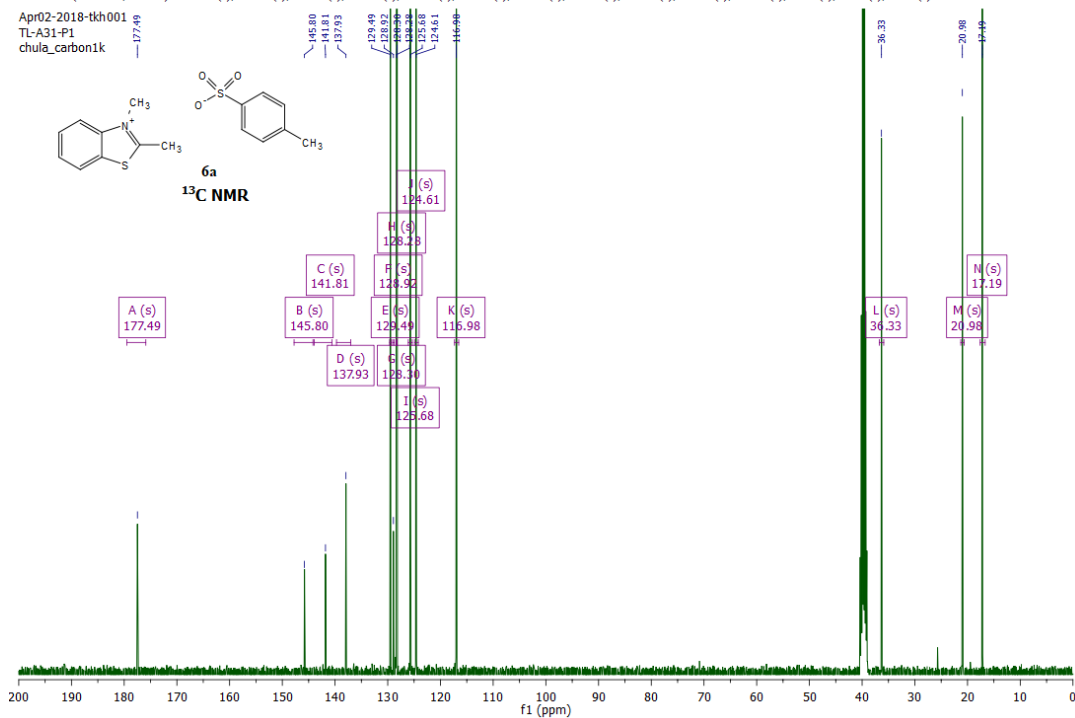
$^1\text{H NMR}$  (400 MHz, DMSO)  $\delta$  8.40 (d,  $J=8.1$  Hz, 1H), 8.26 (d,  $J=8.4$  Hz, 1H), 7.88 (t,  $J=7.8$  Hz, 1H), 7.79 (t,  $J=7.7$  Hz, 1H), 7.46 (d,  $J=7.8$  Hz, 2H), 7.08 (d,  $J=7.6$  Hz, 2H), 4.18 (s, 3H), 3.15 (s, 3H), 2.26 (s, 3H).

May17-2018-tkh004  
TL-A39-P2  
chula\_proton

Figure 25  $^1\text{H NMR}$  spectrum of 6a

$^{13}\text{C NMR}$  (101 MHz, DMSO)  $\delta$  177.49 (s), 145.80 (s), 141.81 (s), 137.93 (s), 129.49 (s), 128.92 (s), 128.30 (s), 128.28 (s), 125.68 (s), 124.61 (s), 116.98 (s), 36.33 (s), 20.98 (s), 17.19 (s).

Apr02-2018-tkh001  
TL-A31-P1  
chula\_carbon1k

Figure 26  $^{13}\text{C NMR}$  spectrum of 6a

## Mass Spectrum List Report

**Analysis Info**  
Analysis Name D:\Data\Data Service\190318\TL-A39-P1\_RB4\_01\_2321.d  
Method nv\_pos\_5min\_profile\_190214.m  
Sample Name TL-A39-P1  
Comment  
Acquisition Date 3/18/2019 7:24:09 PM  
Operator CU.  
Instrument / Ser# micrOTOF-Q II 10335

**Acquisition Parameter**

Source Type	ESI	Ion Polarity	Positive	Set Nebulizer	3.0 Bar
Focus	Not active	Set Capillary	4000 V	Set Dry Heater	200 °C
Scan Begin	100 m/z	Set End Plate Offset	-500 V	Set Dry Gas	8.0 l/min
Scan End	1500 m/z	Set Collision Cell RF	250.0 Vpp	Set Divert Valve	Waste

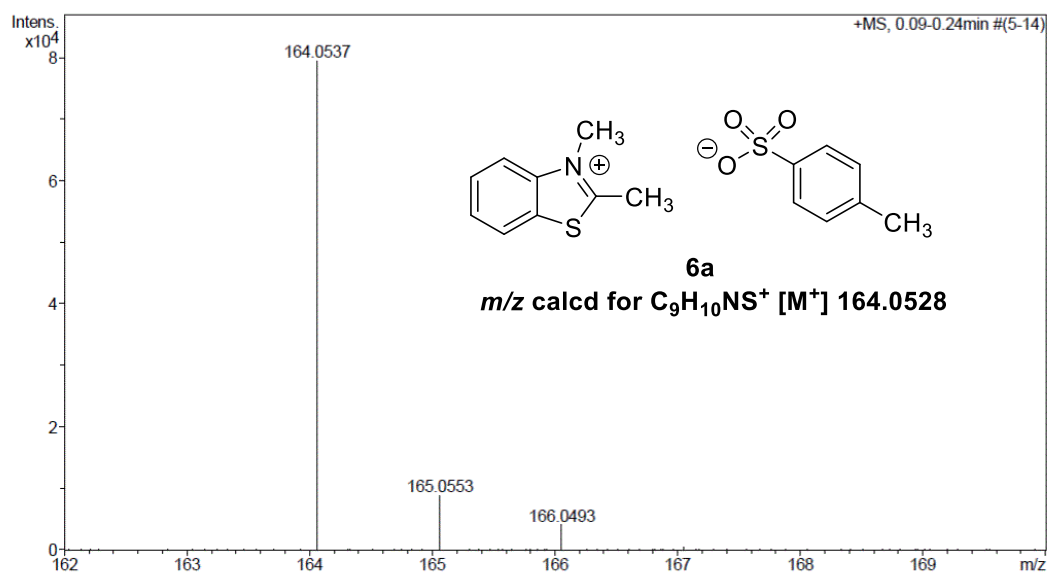
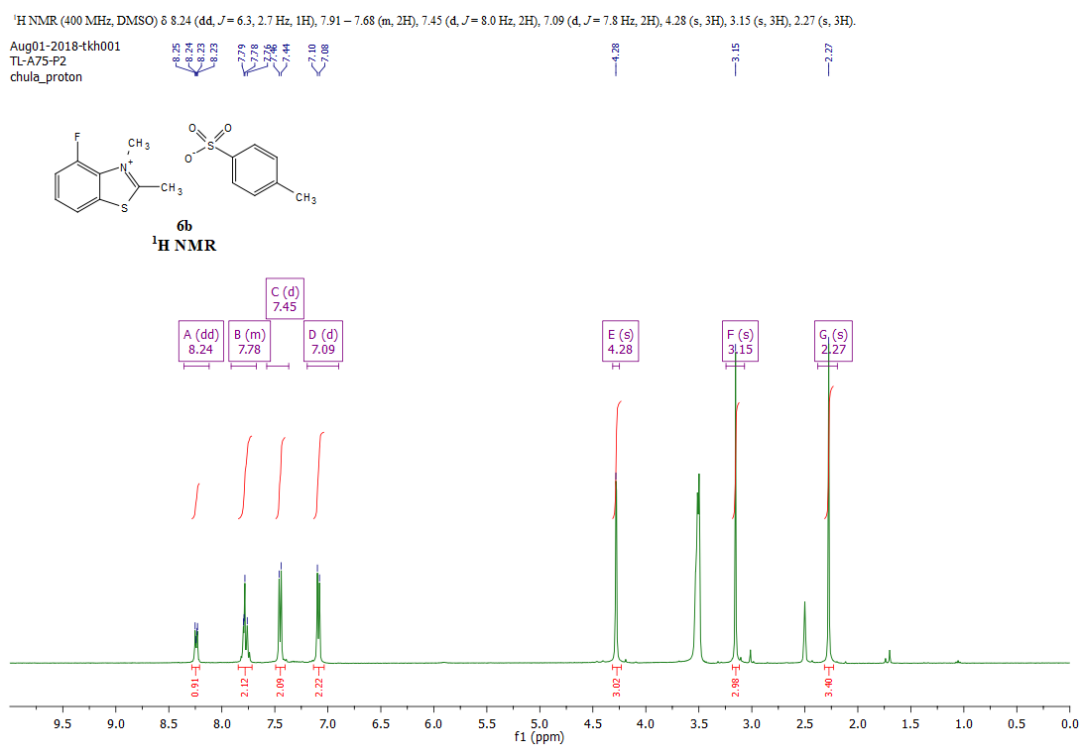
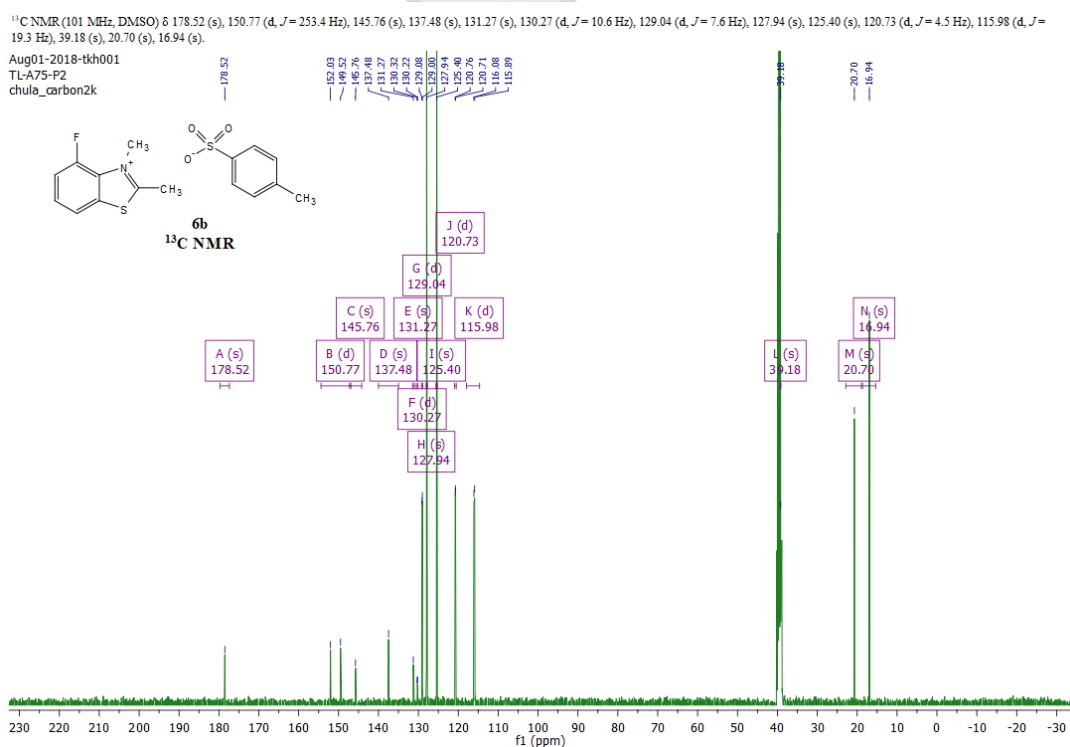
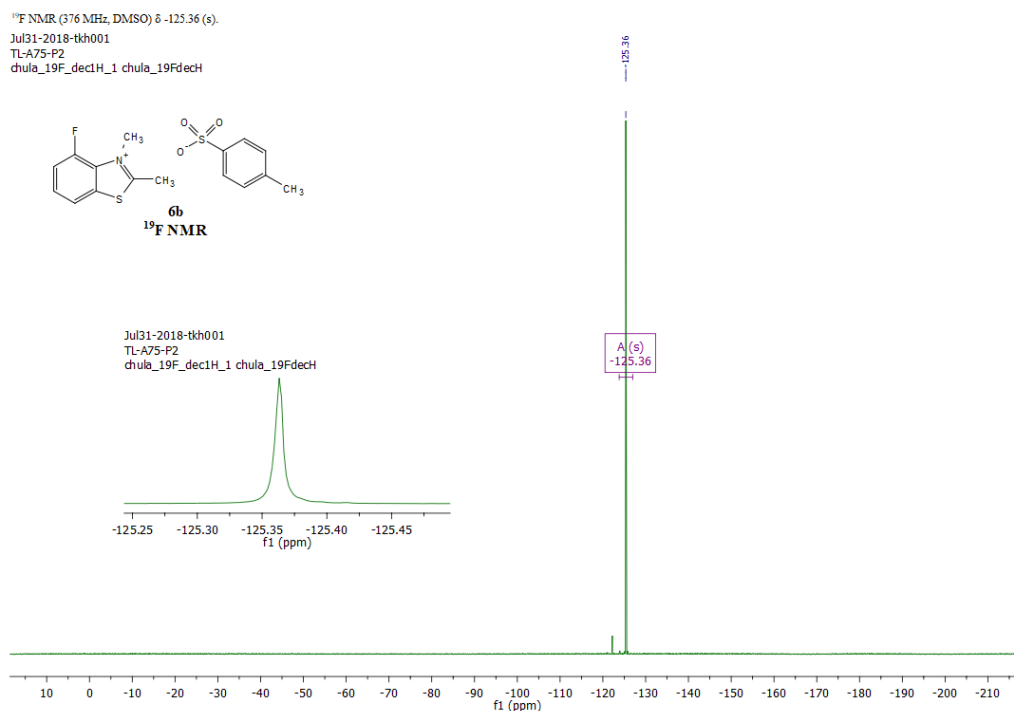


Figure 27 HRMS spectrum of 6a

## 4-Fluoro-2,3-dimethylbenzo[d]thiazol-3-ium 4-methylbenzenesulfonate (6b)

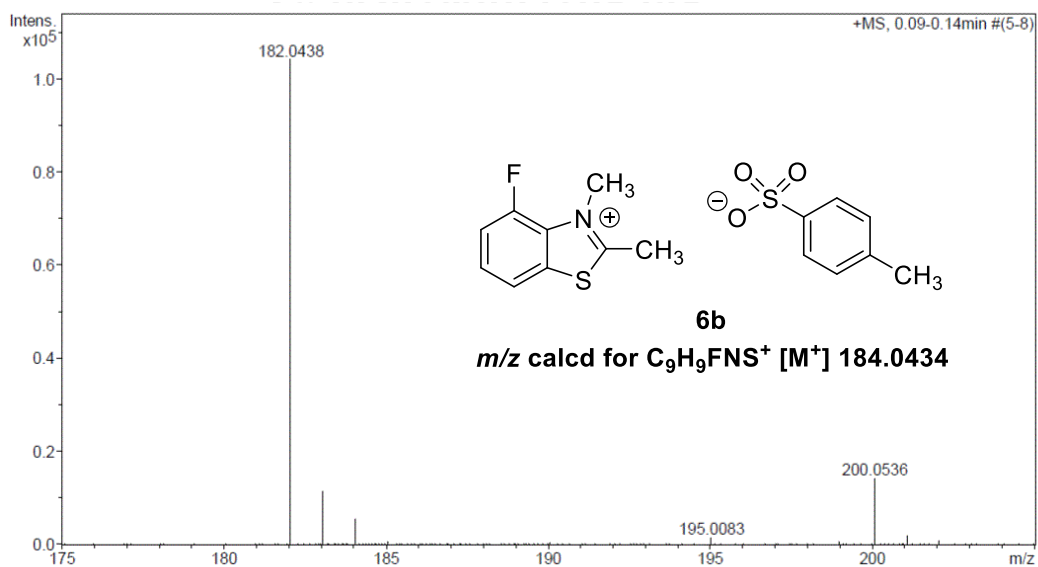
Figure 28 <sup>1</sup>H NMR spectrum of 6bFigure 29 <sup>13</sup>C NMR spectrum of 6b

Figure 30 <sup>19</sup>F NMR spectrum of **6b**

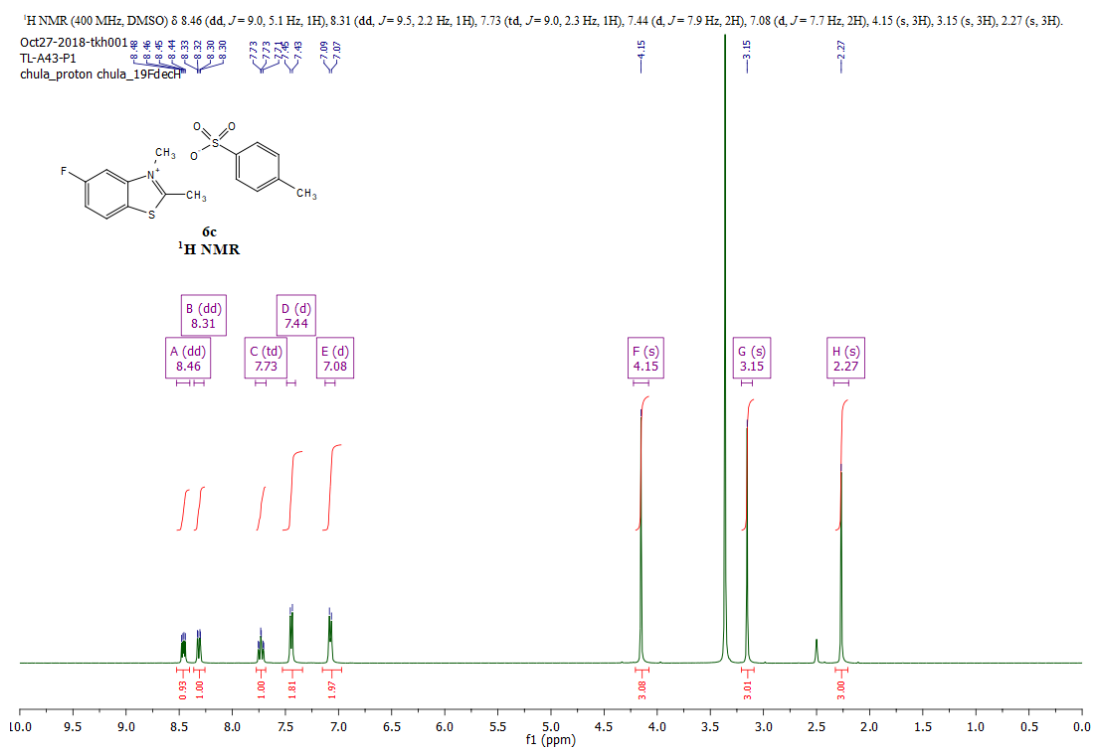
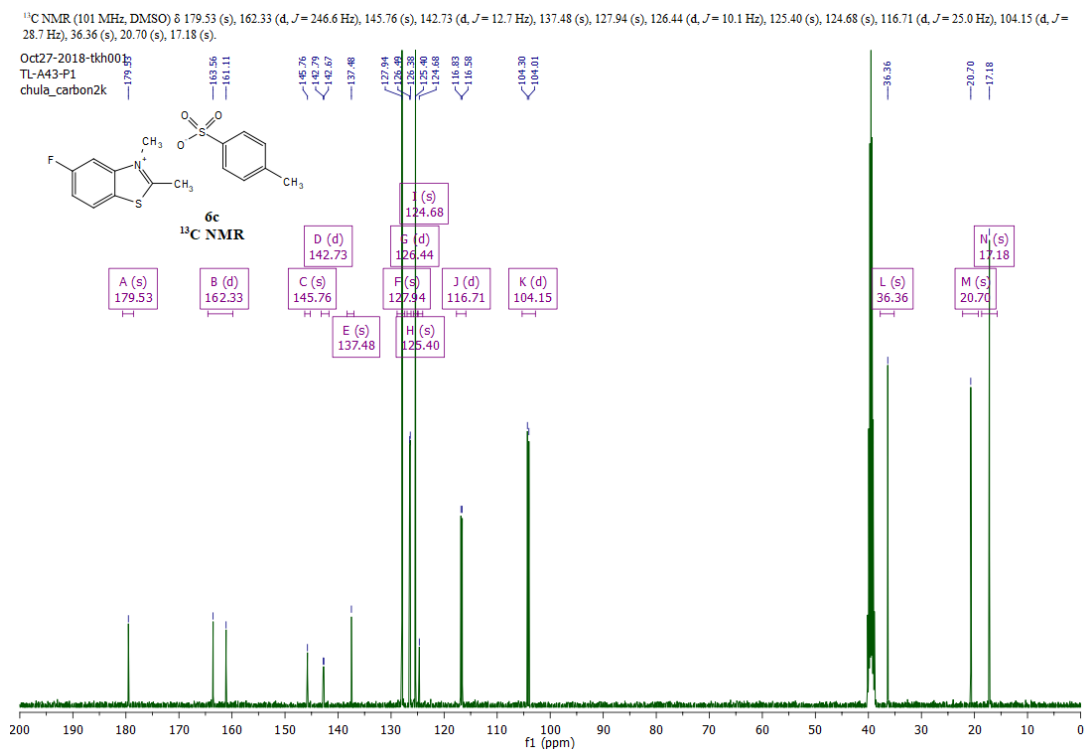
## Mass Spectrum List Report

Analysis Info		Acquisition Date	3/18/2019 7:36:57 PM
Analysis Name	D:\Data\Data Service\190318\TL-A75-P1_RB6_01_2323.d	Operator	CU.
Method	nv_pos_5min_profile_190214.m	Instrument / Ser#	microTOF-Q II 10335
Sample Name	TL-A75-P1		
Comment			

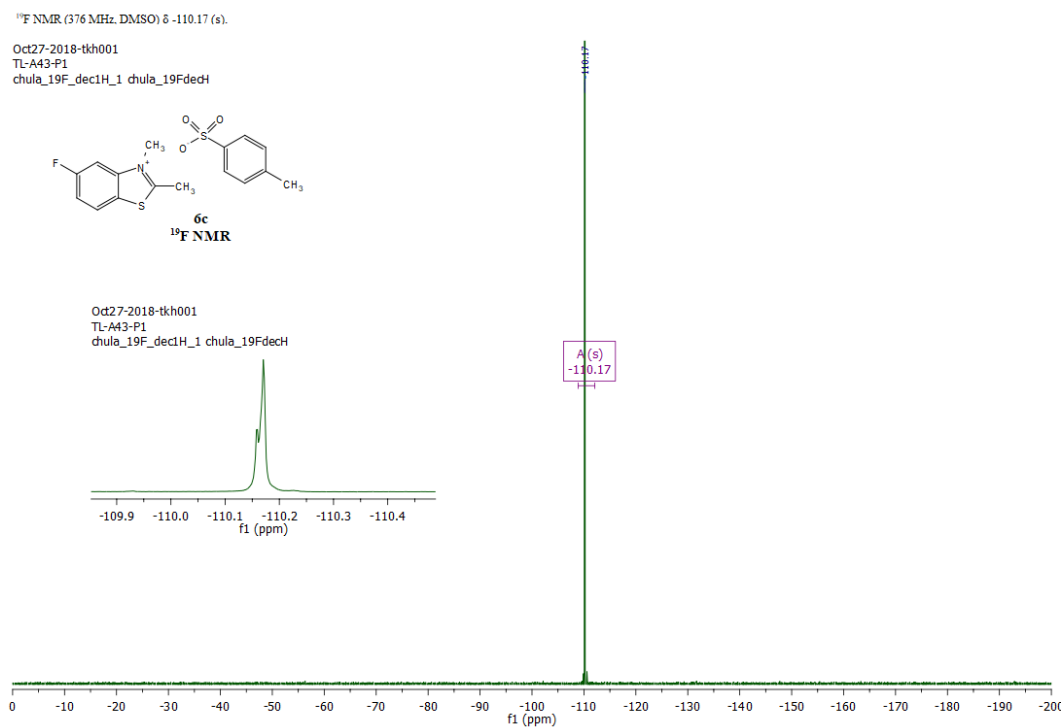
Acquisition Parameter			
Source Type	ESI	Ion Polarity	Positive
Focus	Not active	Set Capillary	4000 V
Scan Begin	100 m/z	Set End Plate Offset	-500 V
Scan End	1500 m/z	Set Collision Cell RF	250.0 Vpp
		Set Nebulizer	3.0 Bar
		Set Dry Heater	200 °C
		Set Dry Gas	8.0 l/min
		Set Divert Valve	Waste

Figure 31 HRMS spectrum of **6b**

## 5-Fluoro-2,3-dimethylbenzo[d]thiazol-3-ium 4-methylbenzenesulfonate (6c)

Figure 32 <sup>1</sup>H NMR spectrum of 6cFigure 33 <sup>13</sup>C NMR spectrum of 6c



Figure 34 <sup>19</sup>F NMR spectrum of **6c**

## Mass Spectrum List Report

### Analysis Info

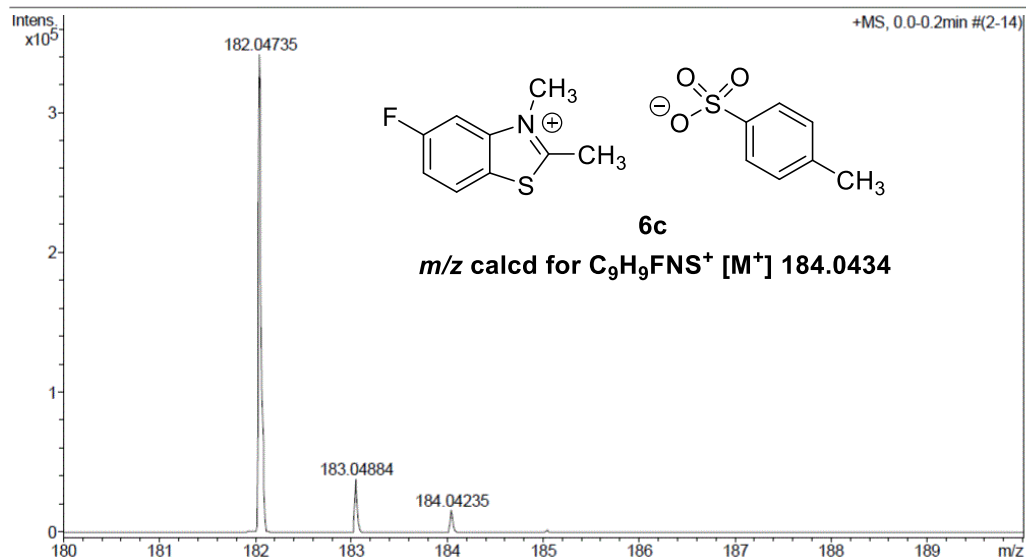
Analysis Name D:\Data\Data Service\180910\_pos\_TL-A43-P1.d  
Method NV\_pos\_0.3min\_profile\_1segment\_lowNubulizerDrygas.m  
Sample Name 180910\_pos\_TL-A43-P1  
Comment

Acquisition Date 9/10/2018 4:49:03 PM

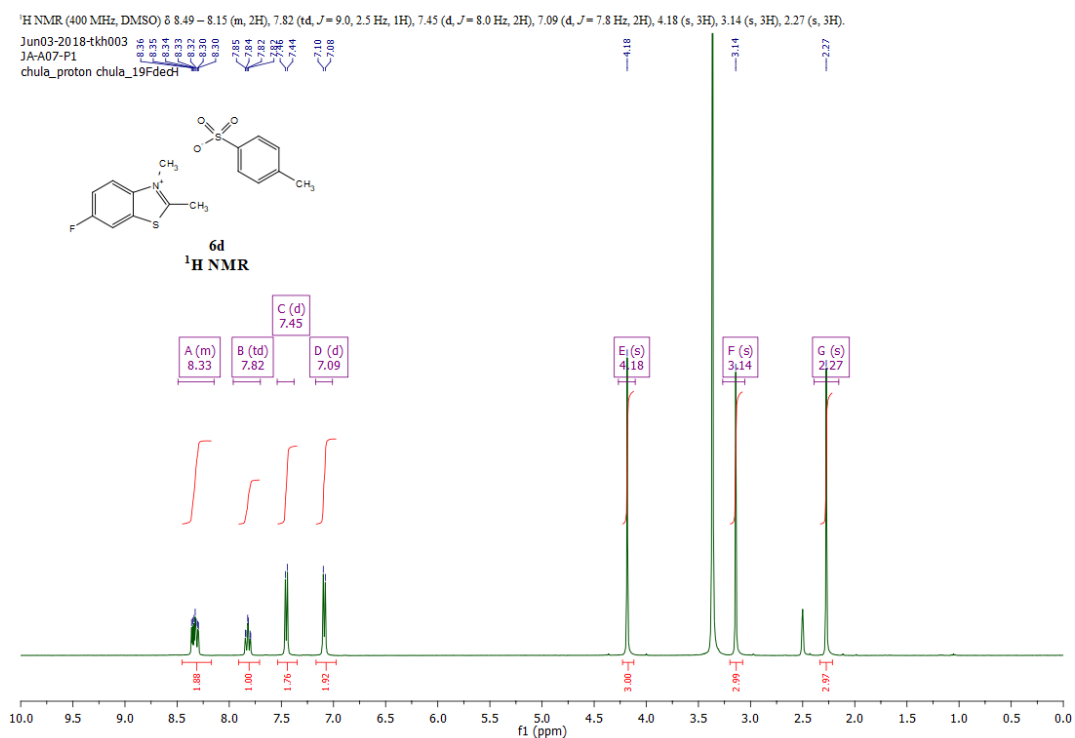
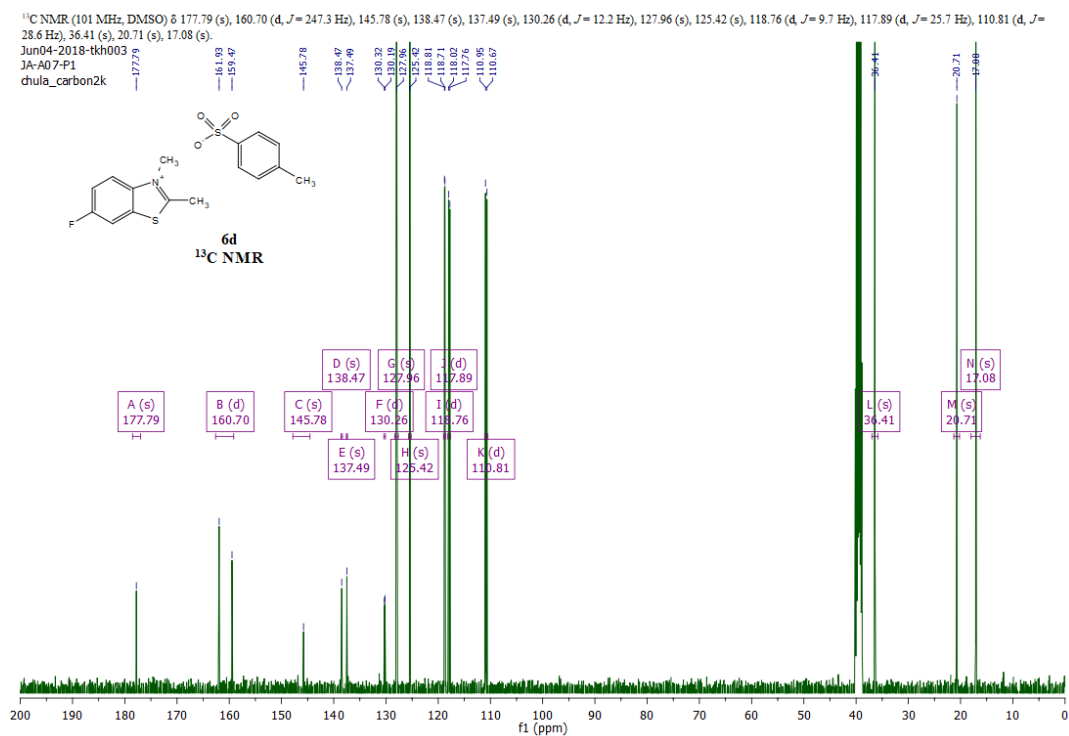
Operator CU.  
Instrument / Ser# micrOTOF-Q II 10335

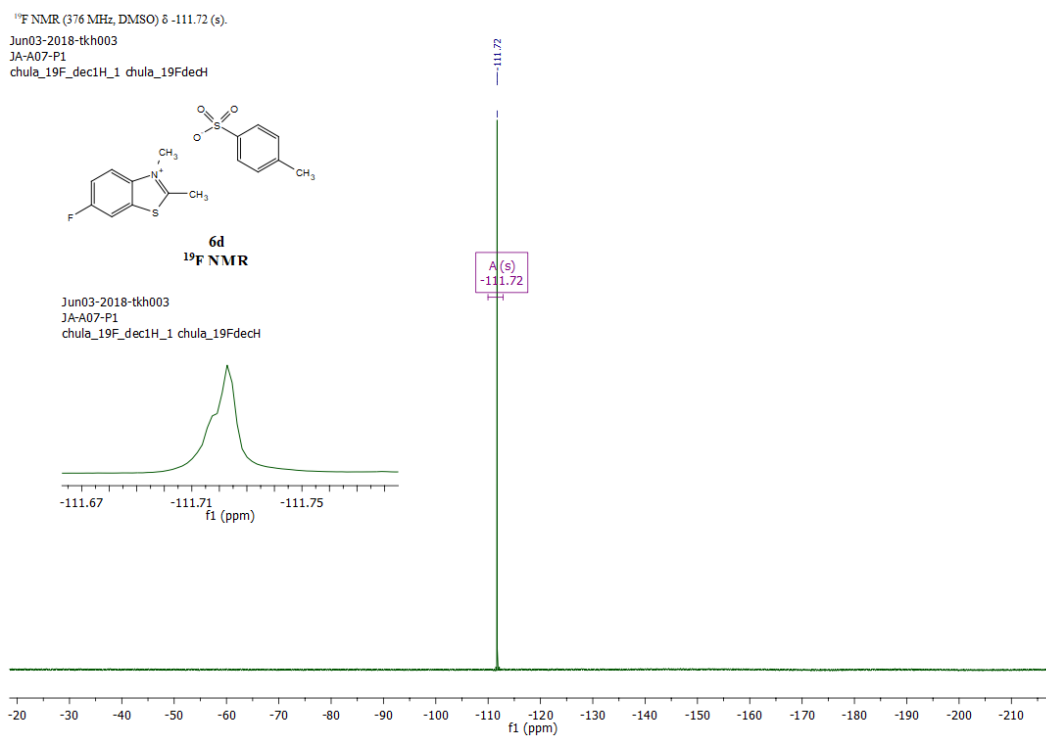
### Acquisition Parameter

Source Type	ESI	Ion Polarity	Positive	Set Nebulizer	0.4 Bar
Focus	Not active	Set Capillary	4000 V	Set Dry Heater	200 °C
Scan Begin	50 m/z	Set End Plate Offset	-500 V	Set Dry Gas	4.0 l/min
Scan End	1500 m/z	Set Collision Cell RF	150.0 Vpp	Set Divert Valve	Waste

Figure 35 HRMS spectrum of **6c**

## 6-Fluoro-2,3-dimethylbenzo[d]thiazol-3-ium 4-methylbenzenesulfonate (6d)

Figure 36 <sup>1</sup>H NMR spectrum of 6dFigure 37 <sup>13</sup>C NMR spectrum of 6d

Figure 39 <sup>19</sup>F NMR spectrum of 6d

## Mass Spectrum List Report

<b>Analysis Info</b>		Acquisition Date	3/18/2019 7:48:08 PM
Analysis Name	D:\Data\Data Service\190318\JA-A07-P1_RB8_01_2325.d	Operator	CU.
Method	nv_pos_5min_profile_190214.m	Instrument / Ser#	microTOF-Q II 10335
Sample Name	JA-A07-P1		
Comment			

## Acquisition Parameter

Source Type	ESI	Ion Polarity	Positive	Set Nebulizer	3.0 Bar
Focus	Not active	Set Capillary	4000 V	Set Dry Heater	200 °C
Scan Begin	100 m/z	Set End Plate Offset	-500 V	Set Dry Gas	8.0 l/min
Scan End	1500 m/z	Set Collision Cell RF	250.0 Vpp	Set Divert Valve	Waste

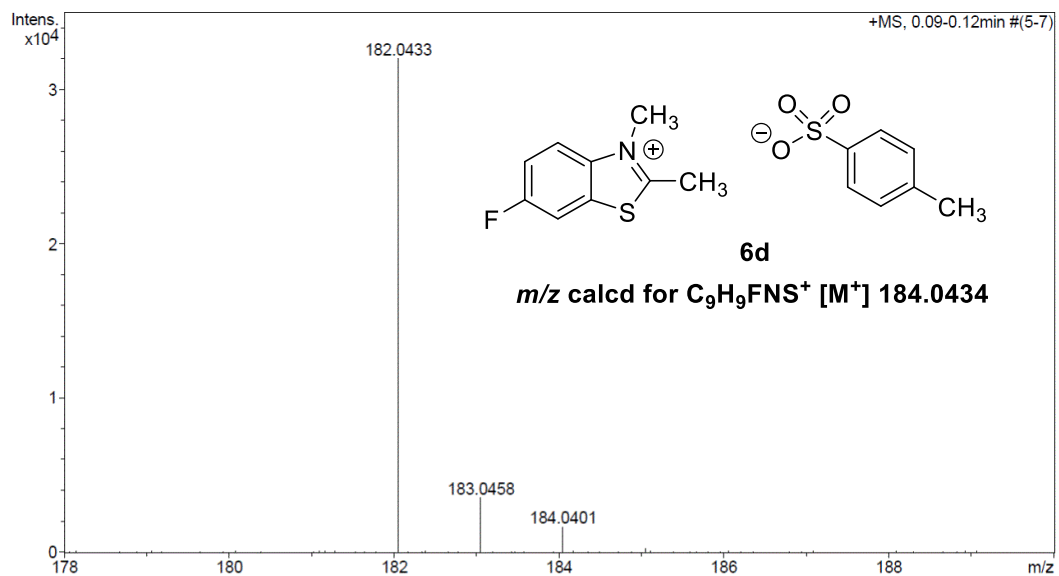


Figure 38 HRMS spectrum of 6d

## 7-Fluoro-2,3-dimethylbenzo[d]thiazol-3-ium 4-methylbenzenesulfonate (6e)

<sup>1</sup>H NMR (400 MHz, DMSO)  $\delta$  8.19 (d,  $J = 8.5$  Hz, 1H), 7.95 (td,  $J = 8.3, 5.4$  Hz, 1H), 7.76 (t,  $J = 8.9$  Hz, 1H), 7.44 (d,  $J = 8.0$  Hz, 2H), 7.08 (d,  $J = 7.8$  Hz, 2H), 4.23 (s, 3H), 3.22 (s, 3H), 2.27 (s, 3H).

Jan21-2019-tkh001

TL-B47-P2

chula\_proton chula\_19FdeH

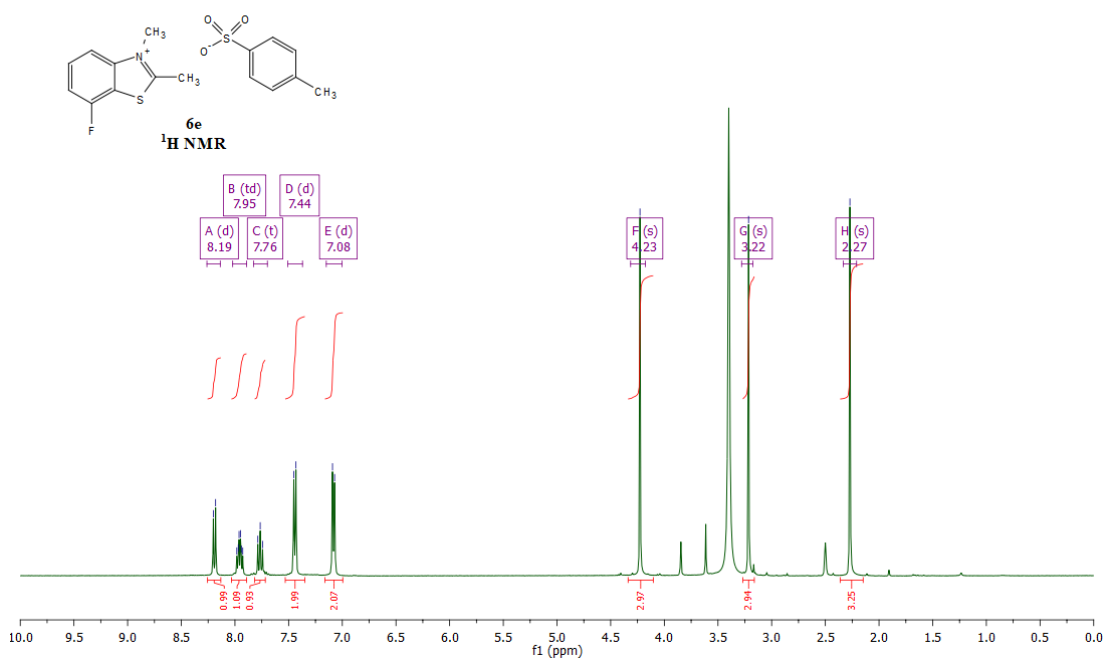


Figure 40 <sup>1</sup>H NMR spectrum of 6e

<sup>13</sup>C NMR (101 MHz, DMSO)  $\delta$  178.41 (s), 155.80 (d,  $J = 250.2$  Hz), 145.75 (s), 143.84 (d,  $J = 5.3$  Hz), 137.51 (s), 131.44 (d,  $J = 7.6$  Hz), 127.97 (s), 125.41 (s), 116.40 (d,  $J = 23.0$  Hz), 114.04 (d,  $J = 17.5$  Hz), 113.59 (d,  $J = 3.9$  Hz), 36.97 (s), 20.72 (s), 17.37 (s).

Jan21-2019-tkh001

TL-B47-P2

chula\_carbon1k

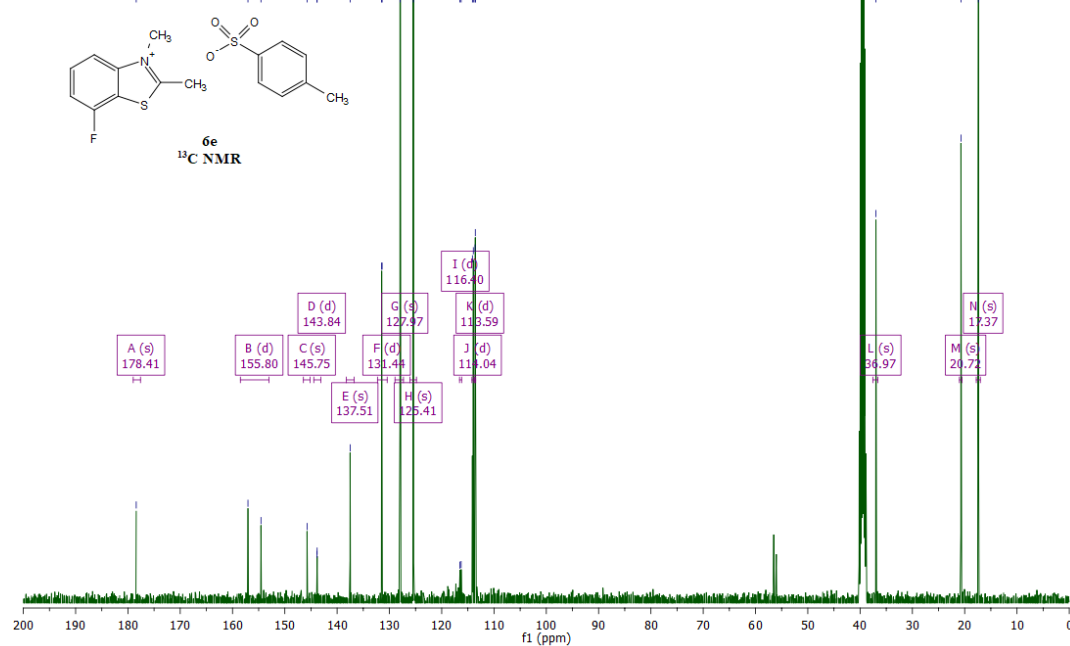
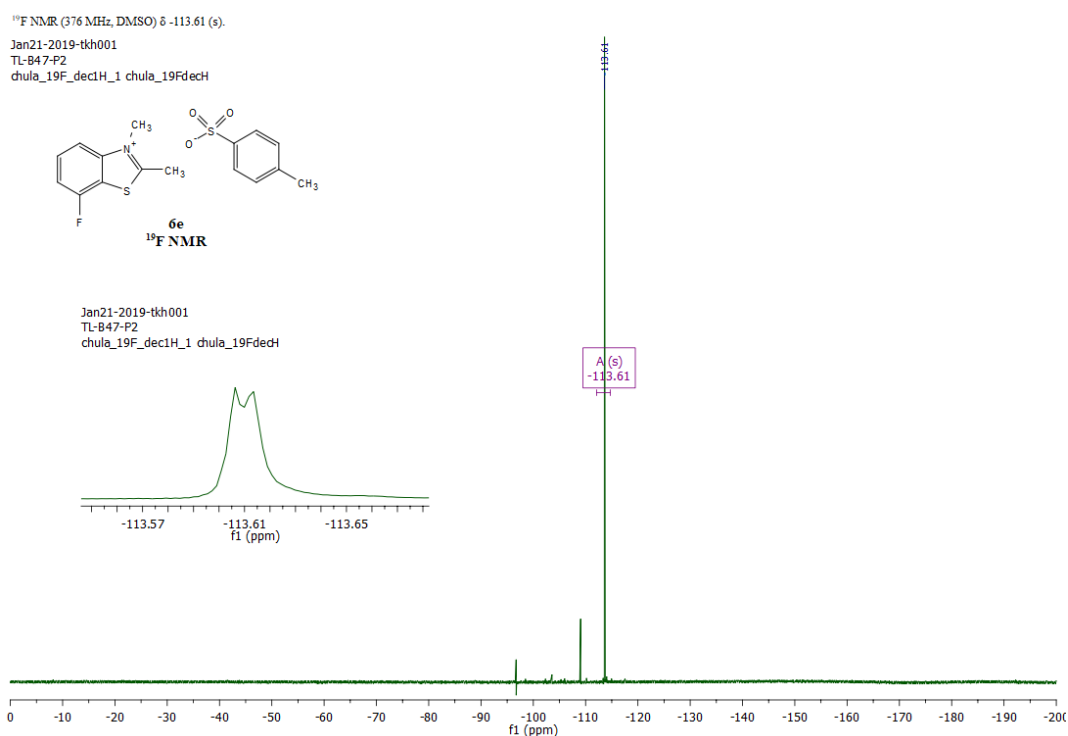


Figure 41 <sup>13</sup>C NMR spectrum of 6e

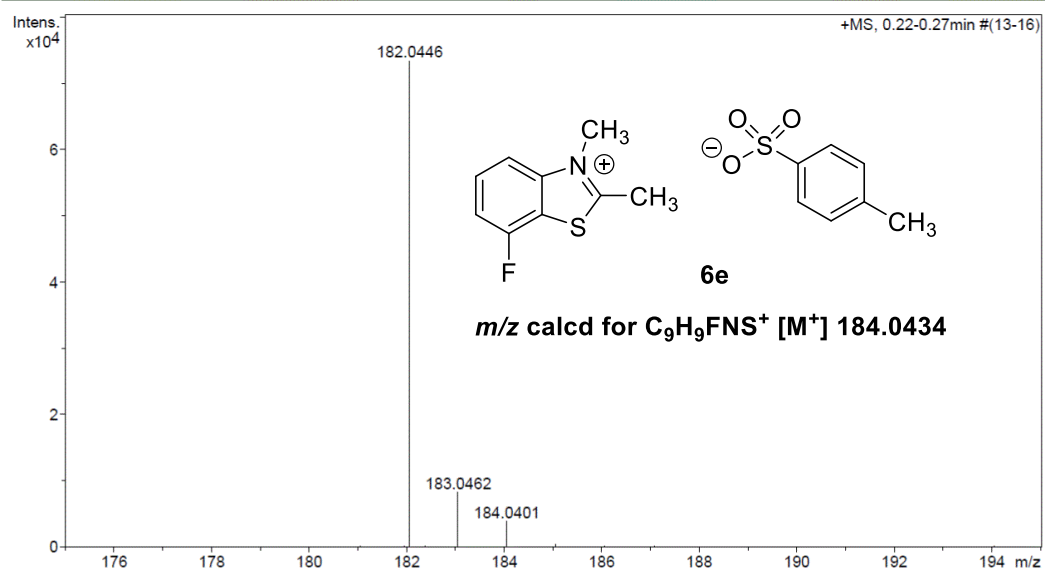
Figure 43 <sup>19</sup>F NMR spectrum of **6e**

## Mass Spectrum List Report

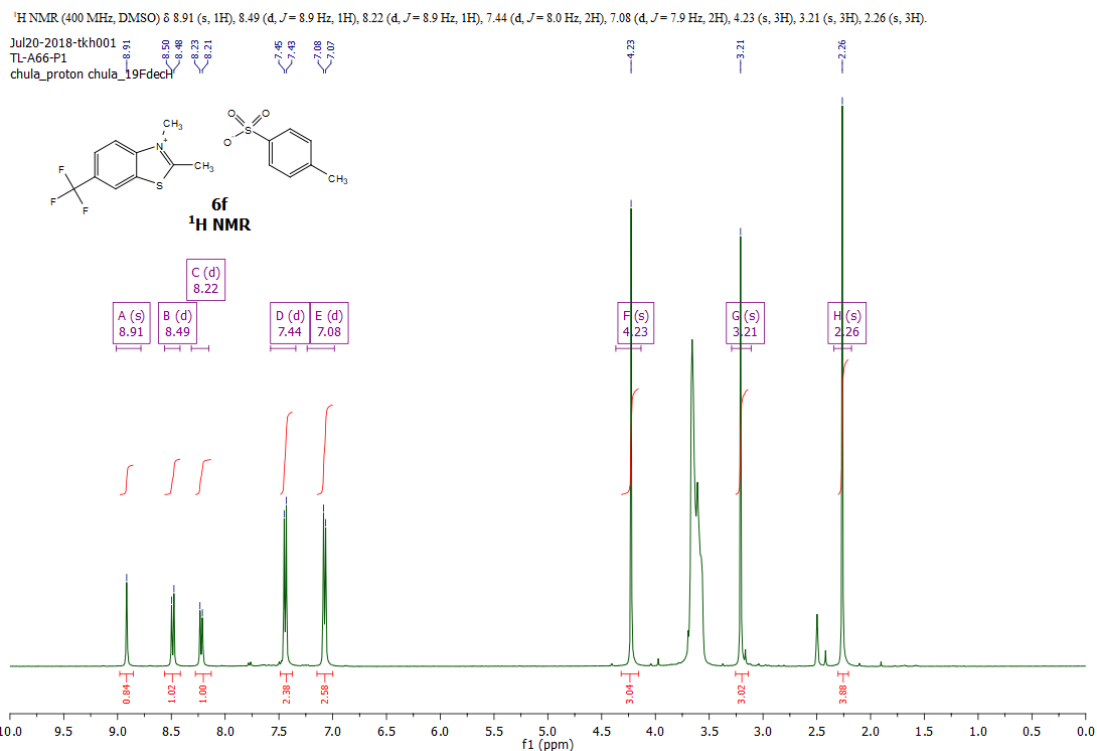
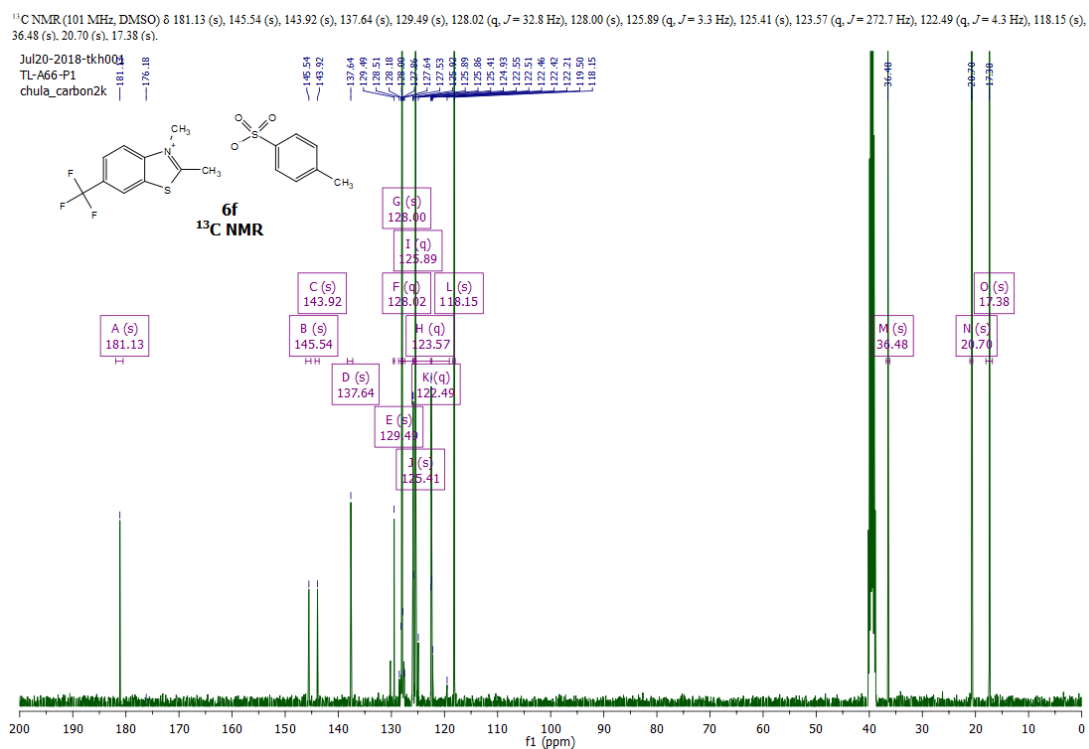
Analysis Info		Acquisition Date	
Analysis Name	D:\Data\Data Service\190401\TL-B47-P2_RC5_01_2446.d	4/1/2019 8:08:30 PM	
Method	nv_pos_5min_profile_190214.m	Operator	CU.
Sample Name	TL-B47-P2	Instrument / Ser#	micrOTOF-Q II 10335
Comment			

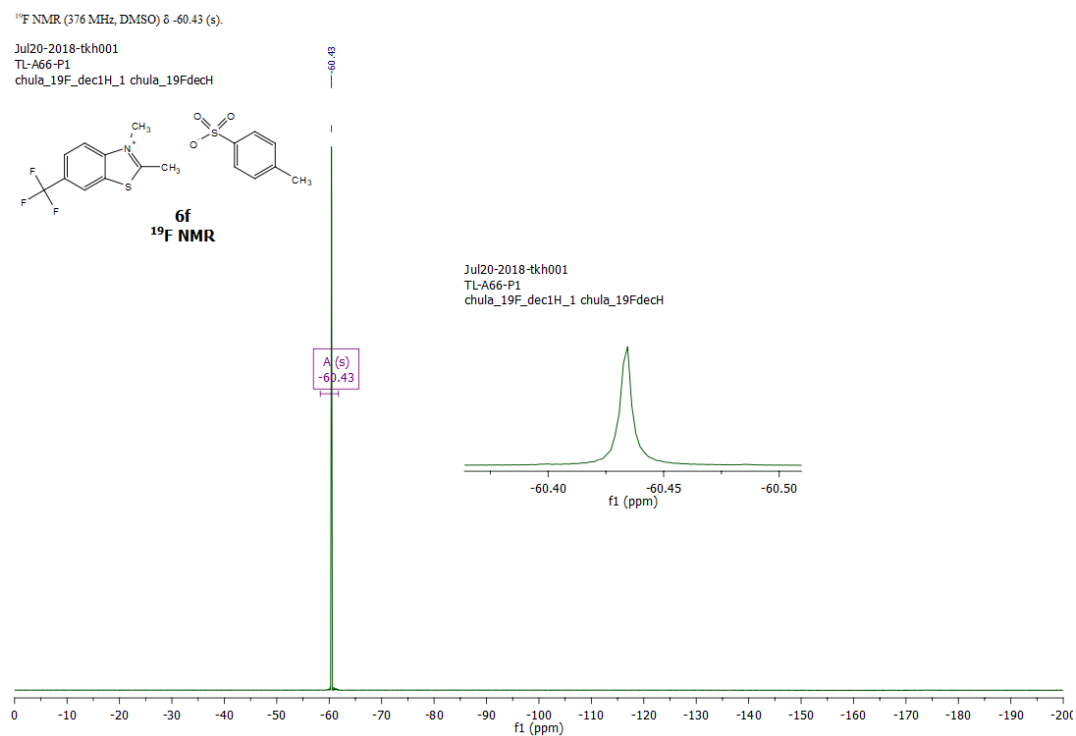
## Acquisition Parameter

Source Type	ESI	Ion Polarity	Positive	Set Nebulizer	3.0 Bar
Focus	Not active	Set Capillary	4000 V	Set Dry Heater	200 °C
Scan Begin	100 m/z	Set End Plate Offset	-500 V	Set Dry Gas	8.0 l/min
Scan End	1500 m/z	Set Collision Cell RF	250.0 Vpp	Set Divert Valve	Waste

Figure 42 HRMS spectrum of **6e**

## 2,3-Dimethyl-6-(trifluoromethyl)benzo[d]thiazol-3-ium 4-methylbenzenesulfonate (6f)

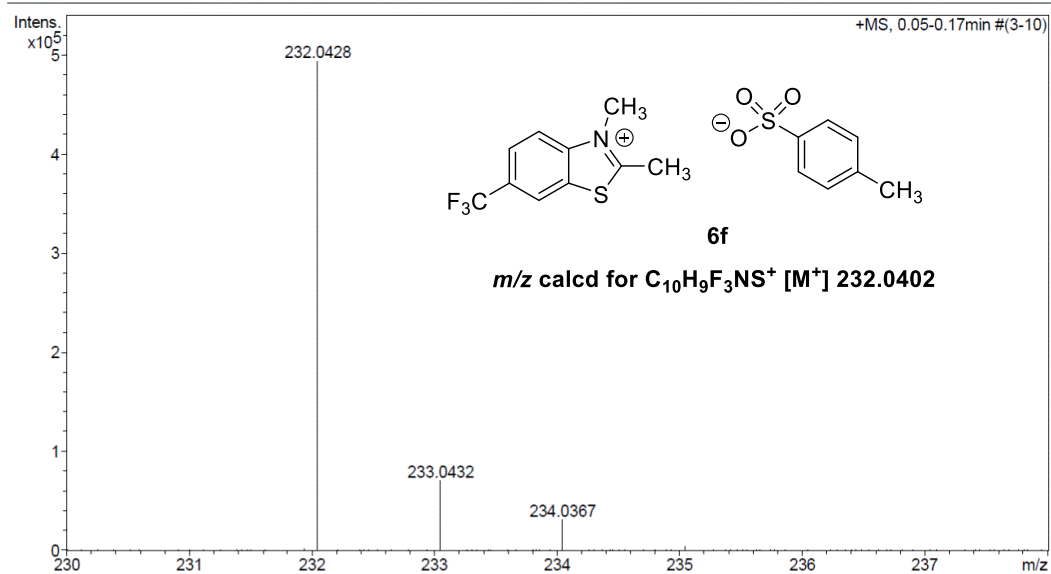
Figure 44 <sup>1</sup>H NMR spectrum of 6fFigure 45 <sup>13</sup>C NMR spectrum of 6f

Figure 47 <sup>19</sup>F NMR spectrum of **6f**

## Mass Spectrum List Report

Analysis Info		Acquisition Date
Analysis Name	D:\Data\Data Service\190318\TL-A66-P1_RB5_01_2322.d	3/18/2019 7:30:31 PM
Method	nv_pos_5min_profile_190214.m	Operator CU.
Sample Name	TL-A66-P1	Instrument / Ser# micrOTOF-Q II 10335
Comment		

Acquisition Parameter			
Source Type	ESI	Ion Polarity	Positive
Focus	Not active	Set Capillary	4000 V
Scan Begin	100 m/z	Set End Plate Offset	-500 V
Scan End	1500 m/z	Set Collision Cell RF	250.0 Vpp
		Set Nebulizer	3.0 Bar
		Set Dry Heater	200 °C
		Set Dry Gas	8.0 l/min
		Set Divert Valve	Waste

Figure 46 HRMS spectrum of **6f**

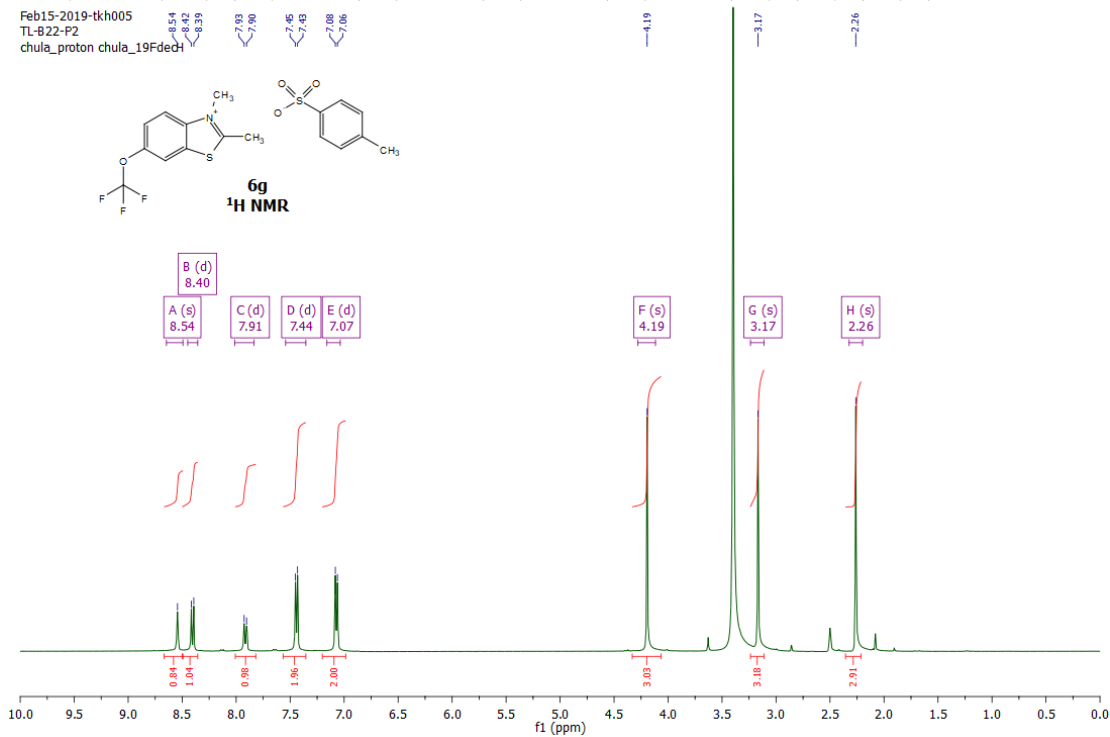
## 2,3-Dimethyl-6-(trifluoromethoxy)benzo[d]thiazol-3-ium 4-methylbenzenesulfonate (6g)

<sup>1</sup>H NMR (400 MHz, DMSO)  $\delta$  8.54 (s, 1H), 8.40 (d,  $J=9.2$  Hz, 1H), 7.91 (d,  $J=9.0$  Hz, 1H), 7.44 (d,  $J=7.7$  Hz, 2H), 7.07 (d,  $J=7.8$  Hz, 2H), 4.19 (s, 3H), 3.17 (s, 3H), 2.26 (s, 3H).

Feb15-2019-tkh005

TL-B22-F2

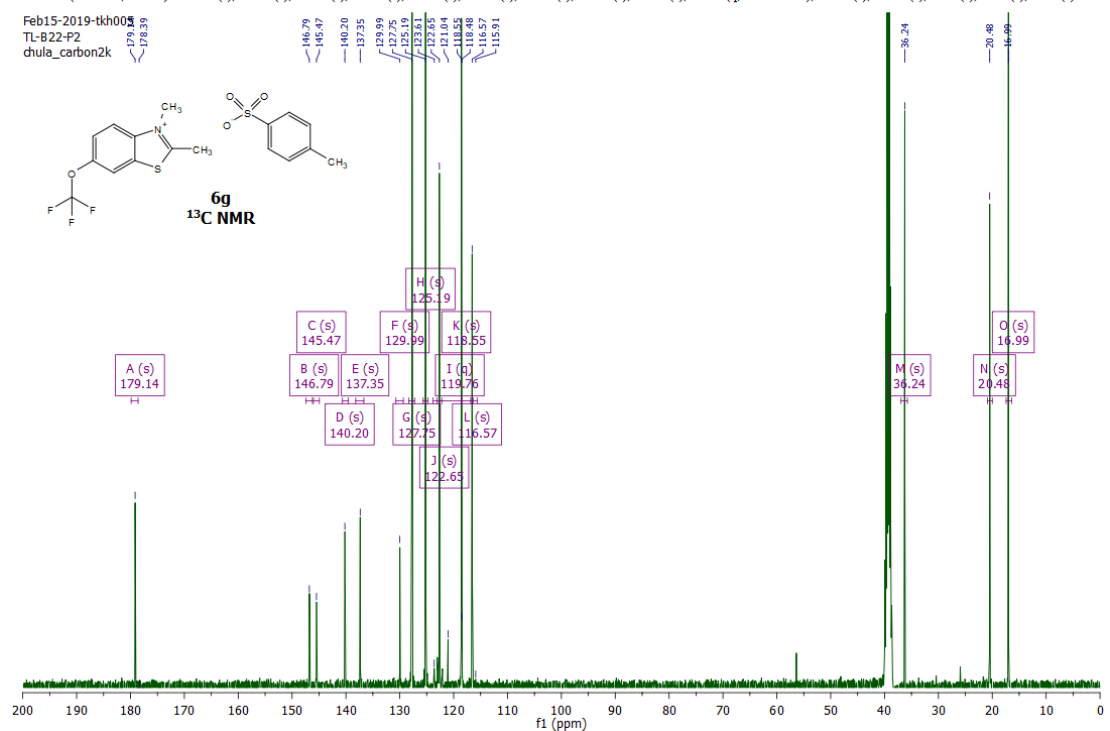
chula\_proton chula\_19Fdeh

Figure 48 <sup>1</sup>H NMR spectrum of 6g<sup>13</sup>C NMR (101 MHz, DMSO)  $\delta$  179.14 (s), 146.79 (s), 145.47 (s), 140.20 (s), 137.35 (s), 129.99 (s), 127.75 (s), 125.19 (s), 122.65 (s), 119.76 (q,  $J=258.2$  Hz), 118.55 (s), 116.57 (s), 36.24 (s), 20.48 (s), 16.99 (s).

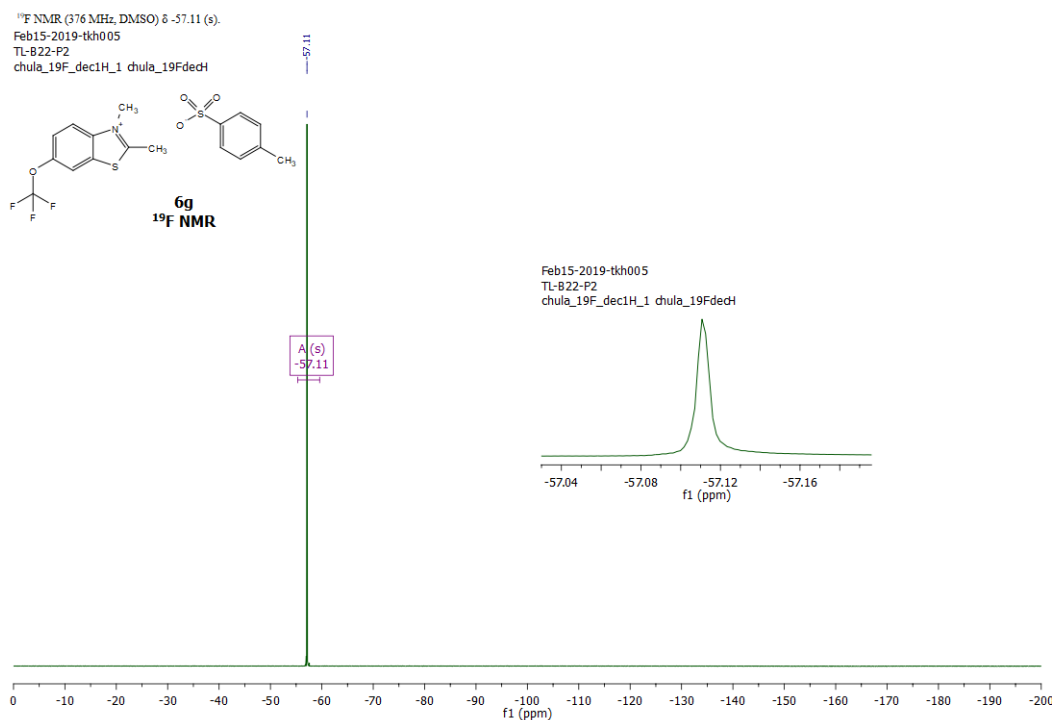
Feb15-2019-tkh005

TL-B22-F2

chula\_carbon2k

Figure 49 <sup>13</sup>C NMR spectrum of 6g



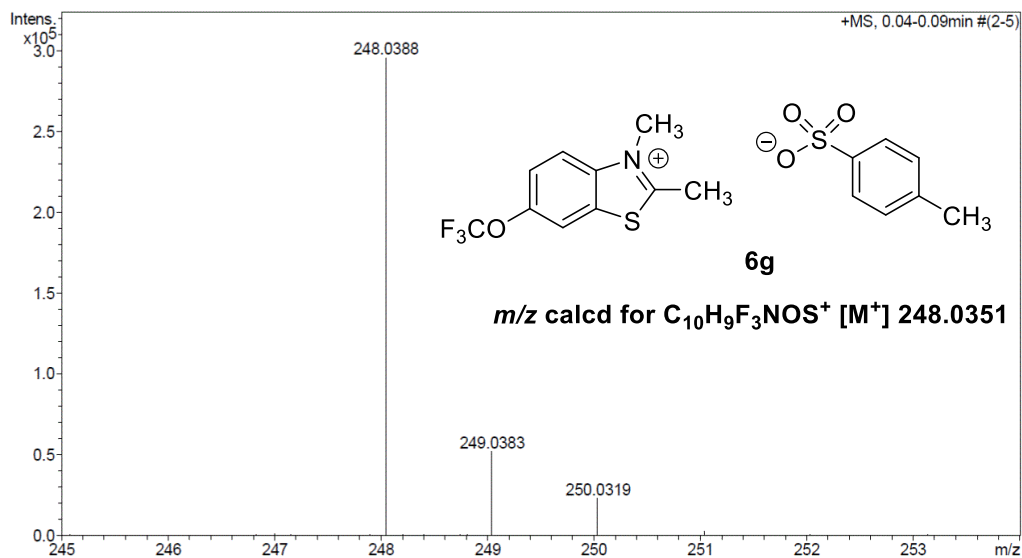
Figure 50 <sup>19</sup>F NMR spectrum of **6g**

## Mass Spectrum List Report

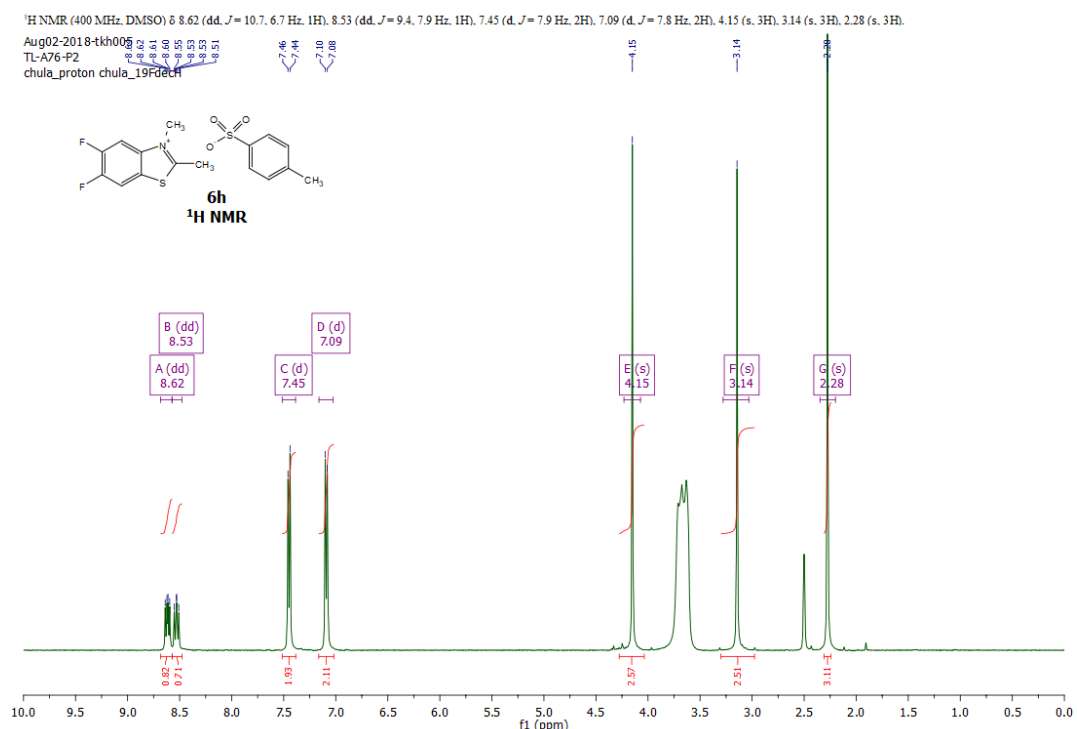
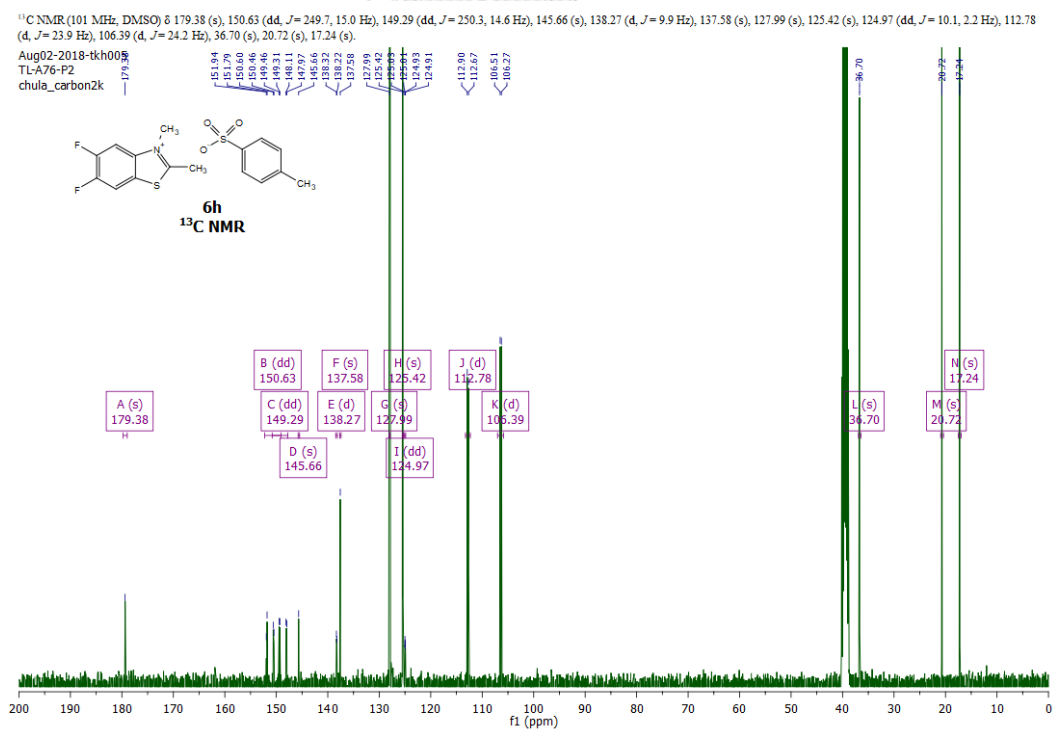
Analysis Info		Acquisition Date	3/18/2019 7:54:34 PM
Analysis Name	D:\Data\Data Service\190318\TL-B22-P1_RC1_01_2326.d	Operator	CU.
Method	nv_pos_5min_profile_190214.m	Instrument / Ser#	micrOTOF-Q II 10335
Sample Name	TL-B22-P1		
Comment			

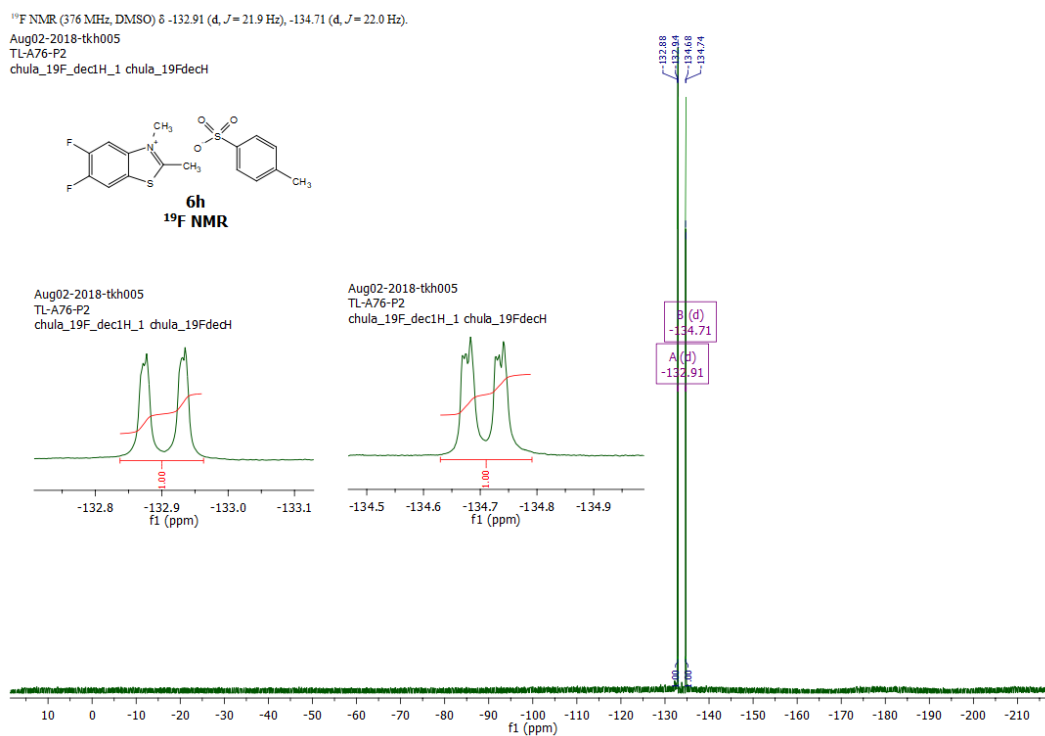
## Acquisition Parameter

Source Type	ESI	Ion Polarity	Positive	Set Nebulizer	3.0 Bar
Focus	Not active	Set Capillary	4000 V	Set Dry Heater	200 °C
Scan Begin	100 m/z	Set End Plate Offset	-500 V	Set Dry Gas	8.0 l/min
Scan End	1500 m/z	Set Collision Cell RF	250.0 Vpp	Set Divert Valve	Waste

Figure 51 HRMS spectrum of **6g**

## 5,6-Difluoro-2,3-dimethylbenzo[d]thiazol-3-ium 4-methylbenzenesulfonate (6h)

Figure 52 <sup>1</sup>H NMR spectrum of 6hFigure 53 <sup>13</sup>C NMR spectrum of 6h

Figure 54 <sup>19</sup>F NMR spectrum of 6h

## Mass Spectrum List Report

<b>Analysis Info</b>	Acquisition Date 3/18/2019 7:43:23 PM
Analysis Name D:\Data\Data Service\190318\TL-A76-P2_RB7_01_2324.d	Operator CU.
Method nv_pos_5min_profile_190214.m	Instrument / Ser# micrOTOF-Q II 10335
Sample Name TL-A76-P2	
Comment	

**Acquisition Parameter**

Source Type ESI	Ion Polarity Positive	Set Nebulizer 3.0 Bar
Focus Not active	Set Capillary 4000 V	Set Dry Heater 200 °C
Scan Begin 100 m/z	Set End Plate Offset -500 V	Set Dry Gas 8.0 l/min
Scan End 1500 m/z	Set Collision Cell RF 250.0 Vpp	Set Divert Valve Waste

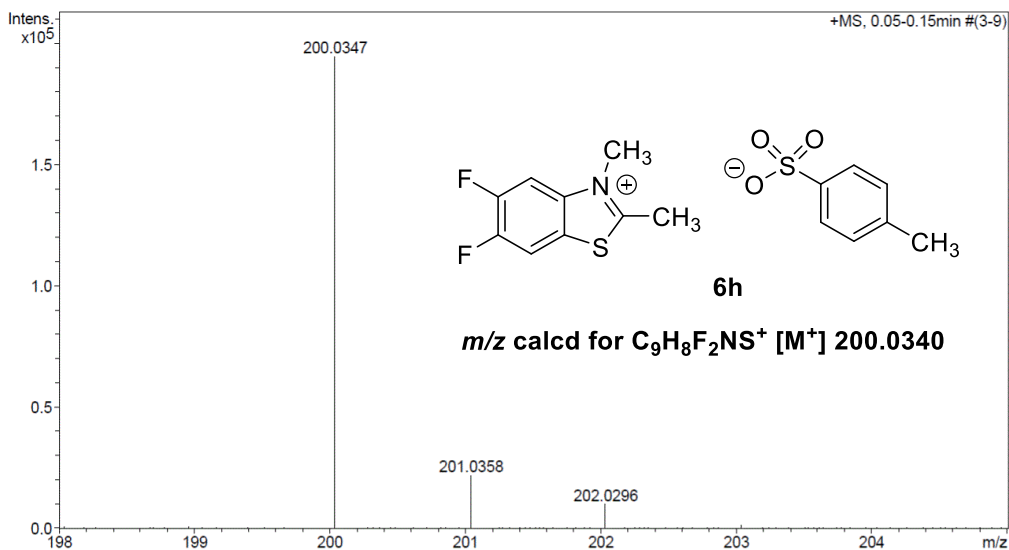


Figure 55 HRMS spectrum of 6h



*N*-((3-Ethyl-4-oxo-2-thioxothiazolidin-5-ylidene)methyl)-*N*-phenylpropionamide (7)

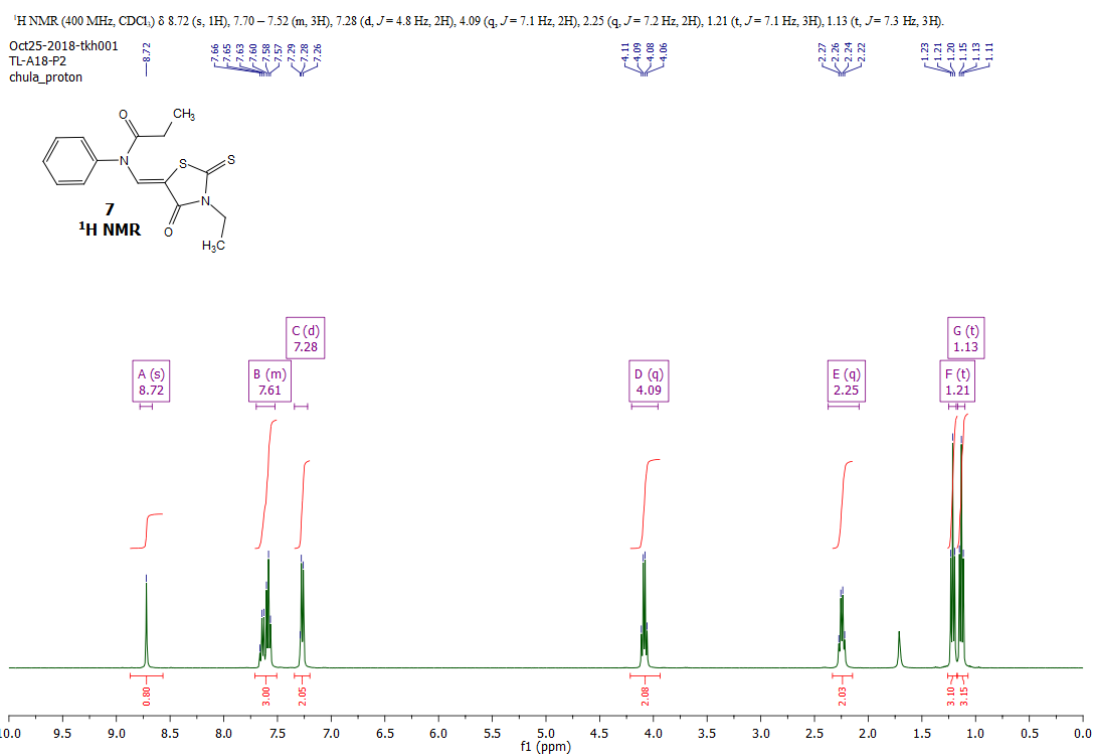


Figure 56 <sup>1</sup>H NMR spectrum of 7

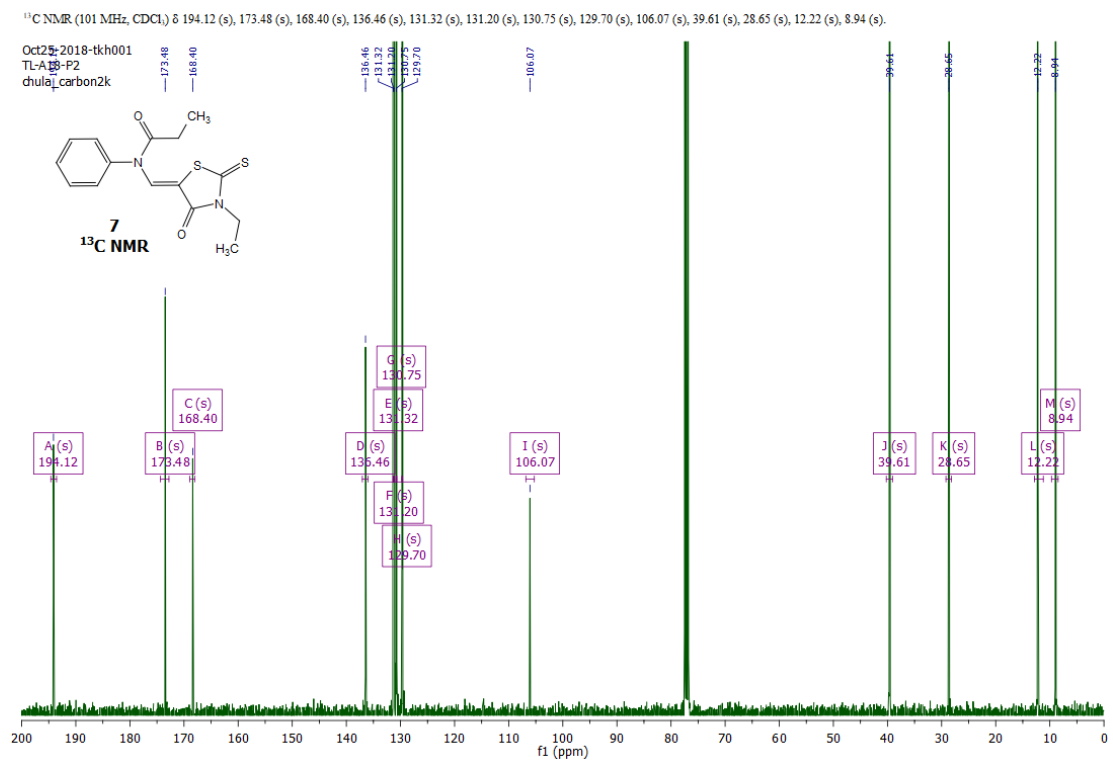


Figure 57 <sup>13</sup>C NMR spectrum of 7

2-(3-Ethyl-5-(2-(3-methylbenzo[d]thiazol-2(3H)-ylidene)ethylidene)ethylidene)-4-oxothiazolidin-2-ylidene)methyl)-3-methylbenzo[d]thiazol-3-ium chloride (11a)

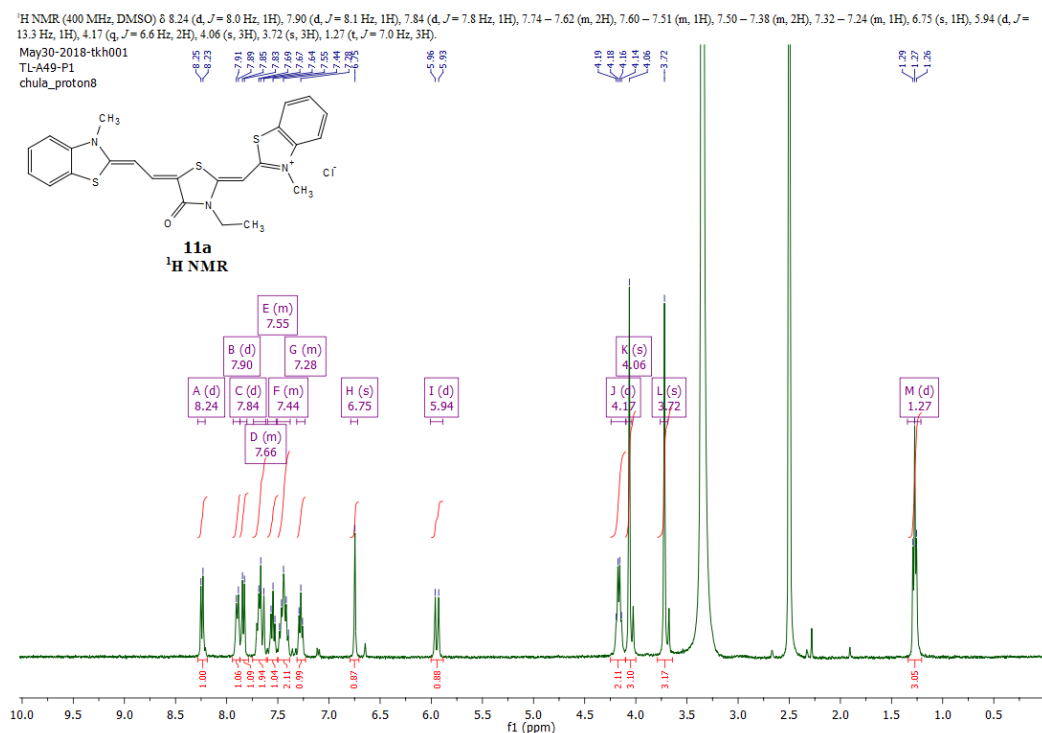


Figure 58 <sup>1</sup>H NMR spectrum of 11a

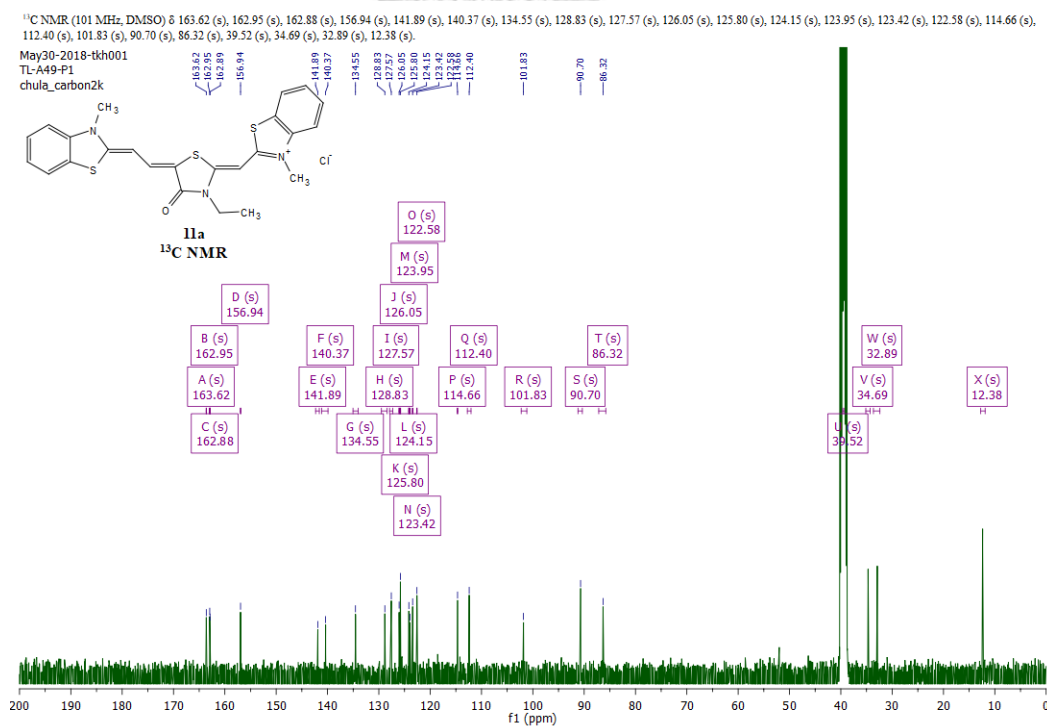


Figure 59 <sup>13</sup>C NMR spectrum of 11a

## Mass Spectrum List Report

**Analysis Info**  
Analysis Name D:\Data\Data Service\190318\TL-A49-P1\_RC2\_01\_2328.d  
Method nv\_pos\_5min\_profile\_190214.m  
Sample Name TL-A49-P1  
Comment  
Acquisition Date 3/18/2019 8:07:26 PM  
Operator CU.  
Instrument / Ser# micrOTOF-Q II 10335

### Acquisition Parameter

Source Type	ESI	Ion Polarity	Positive	Set Nebulizer	3.0 Bar
Focus	Not active	Set Capillary	4000 V	Set Dry Heater	200 °C
Scan Begin	100 m/z	Set End Plate Offset	-500 V	Set Dry Gas	8.0 l/min
Scan End	1500 m/z	Set Collision Cell RF	250.0 Vpp	Set Divert Valve	Waste

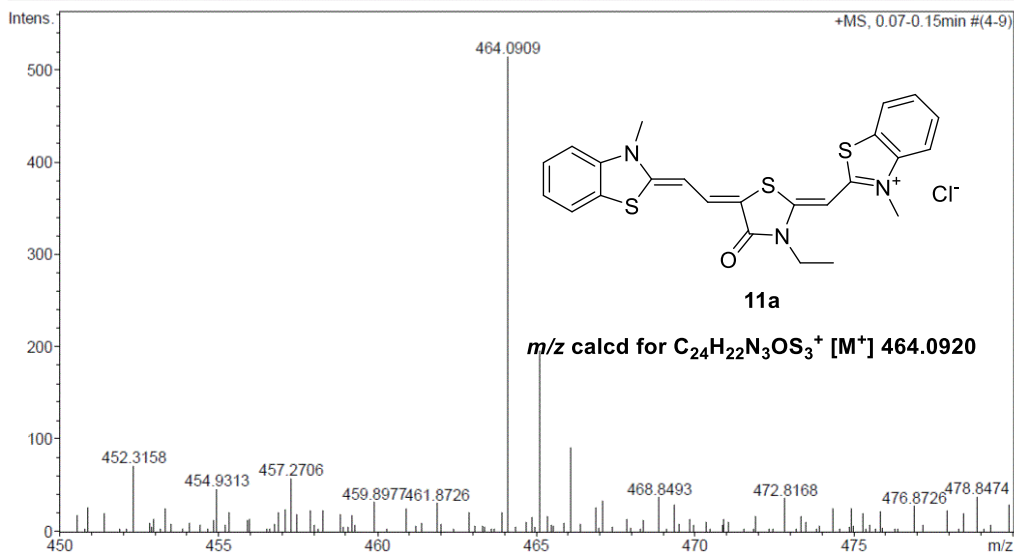


Figure 60 HRMS spectrum of 11a



2-(3-Ethyl-5-(2-(3-methylbenzo[d]thiazol-2(3H)-ylidene)ethylidene)ethylidene)-4-oxothiazolidin-2-ylidene)methyl)-4-fluoro-3-methylbenzo[d]thiazol-3-ium chloride (11b)

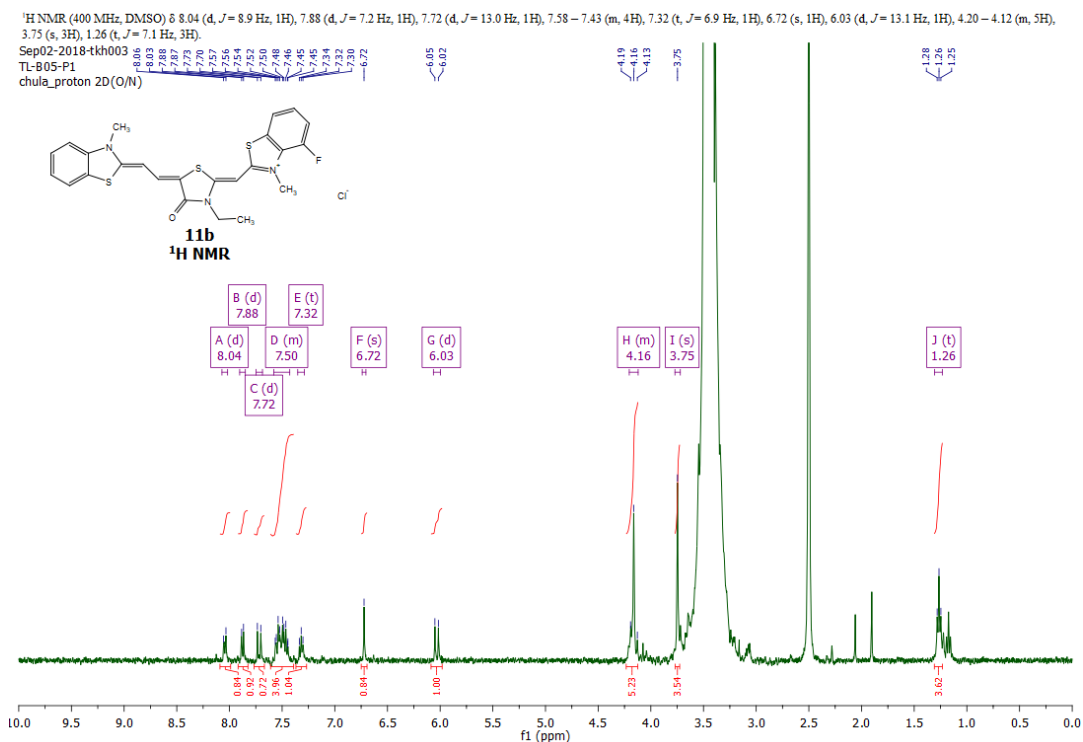


Figure 61 <sup>1</sup>H NMR spectrum of 11b

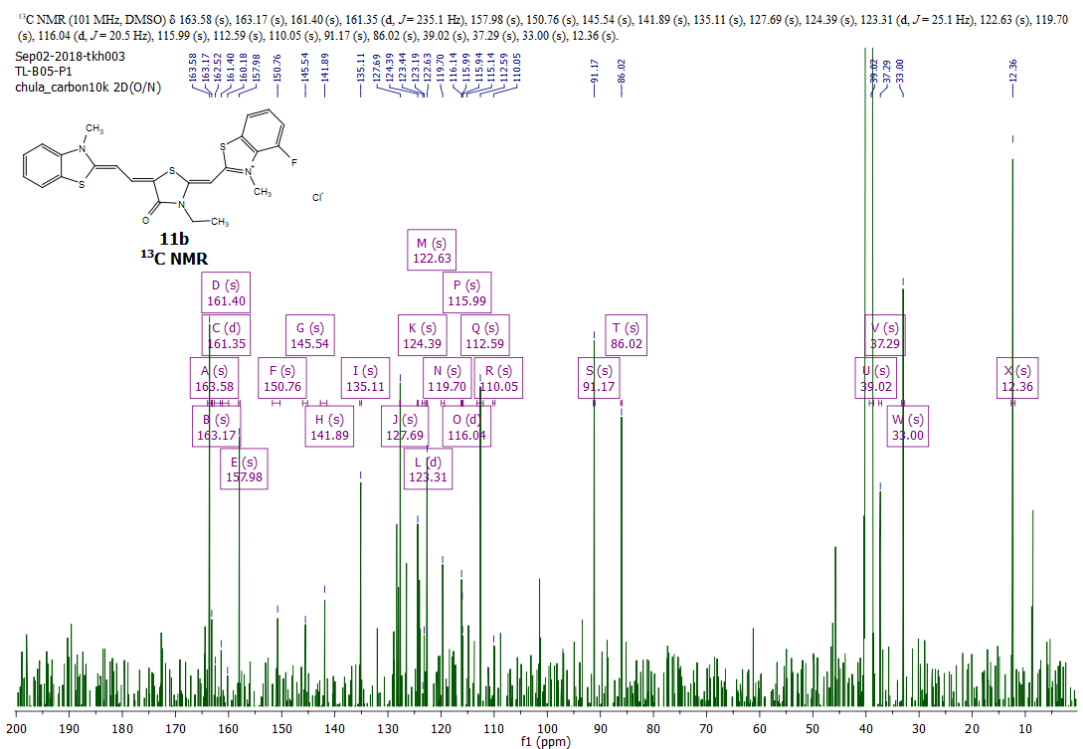
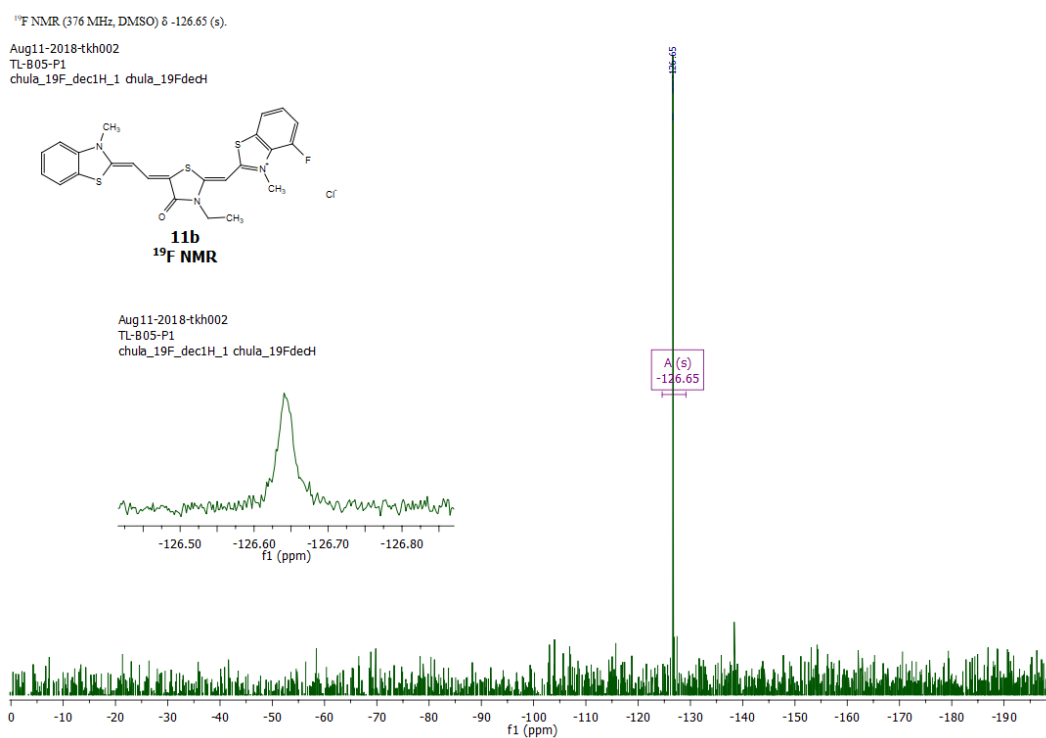
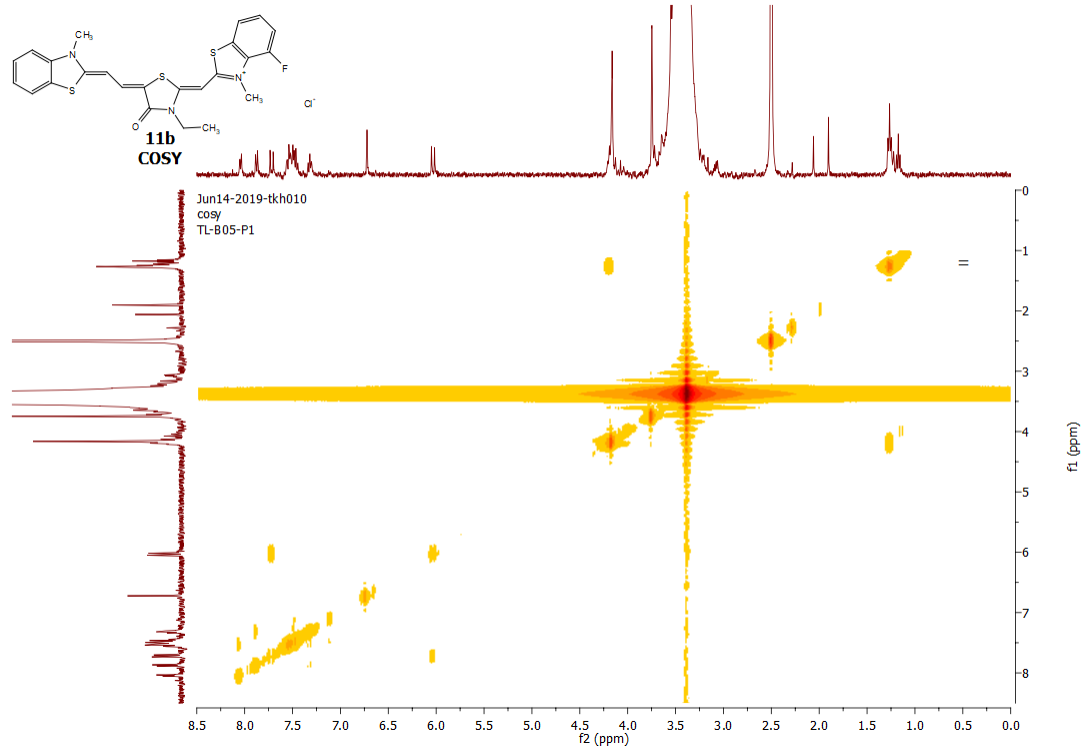


Figure 62 <sup>13</sup>C NMR spectrum of 11b

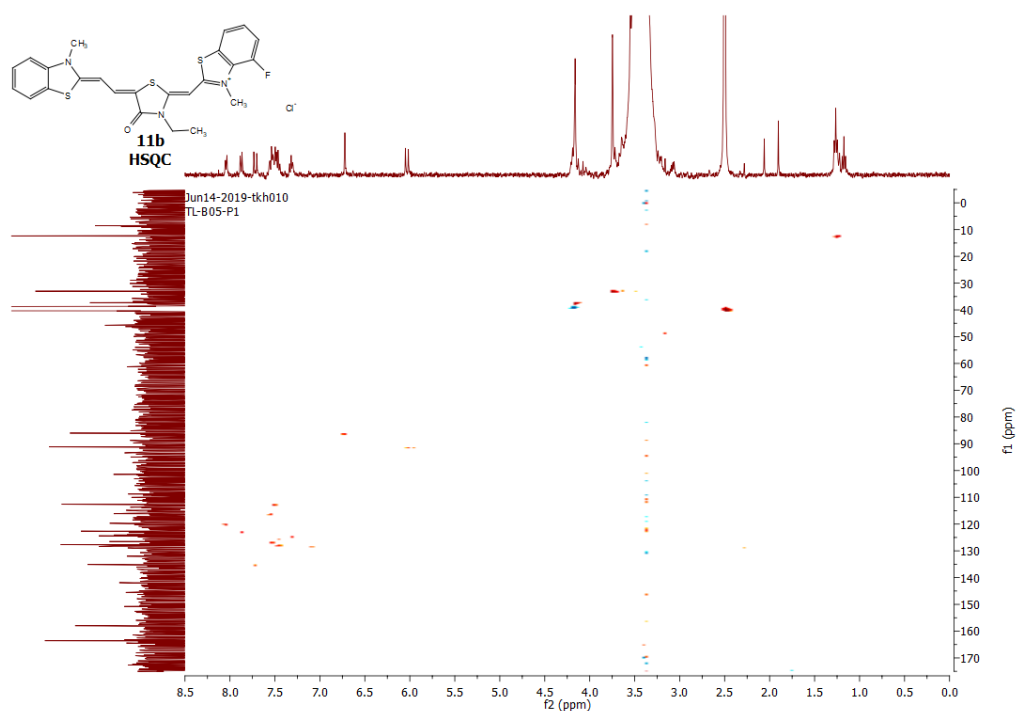




(a)



(b)

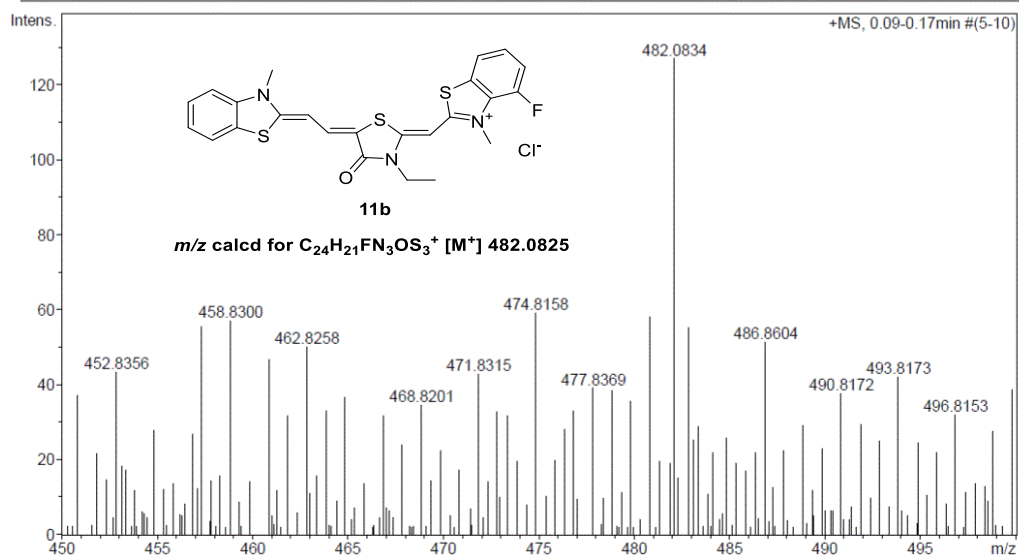
Figure 64 2D NMR spectra of **11b** (a) COSY; and (b) HSQC spectrum

### Mass Spectrum List Report

<b>Analysis Info</b>		<b>Acquisition Date</b>	3/18/2019 9:52:50 PM
Analysis Name	D:\Data\Data Service\190318\TL-B05-P1_RC8_01_2342.d	Operator	CU.
Method	nv_pos_5min_profile_190214.m	Instrument / Ser#	microTOF-Q II 10335
Sample Name	TL-B05-P1		
Comment			

#### Acquisition Parameter

Source Type	ESI	Ion Polarity	Positive	Set Nebulizer	3.0 Bar
Focus	Not active	Set Capillary	4000 V	Set Dry Heater	200 °C
Scan Begin	100 m/z	Set End Plate Offset	-500 V	Set Dry Gas	8.0 l/min
Scan End	1500 m/z	Set Collision Cell RF	250.0 Vpp	Set Divert Valve	Waste

Figure 65 HRMS spectrum of **11b**

2-(3-Ethyl-5-(2-(3-methylbenzo[d]thiazol-2(3H)-ylidene)ethylidene)ethylidene)-4-oxothiazolidin-2-ylidene)methyl)-5-fluoro-3-methylbenzo[d]thiazol-3-ium 4-methylbenzenesulfonate (10c)

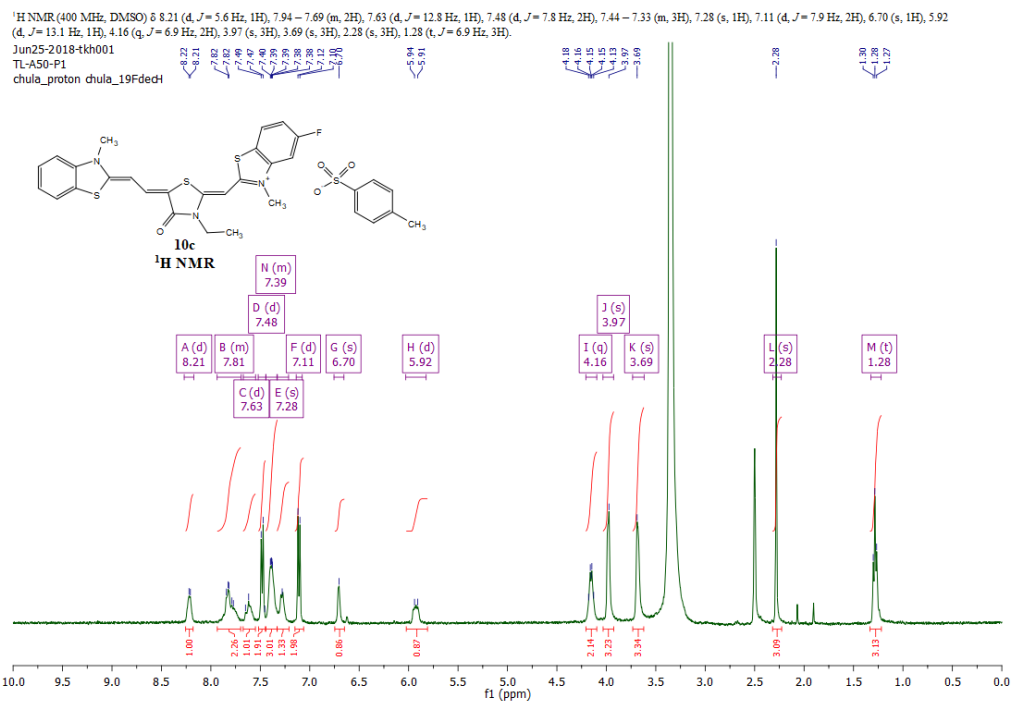


Figure 66 <sup>1</sup>H NMR spectrum of 10c

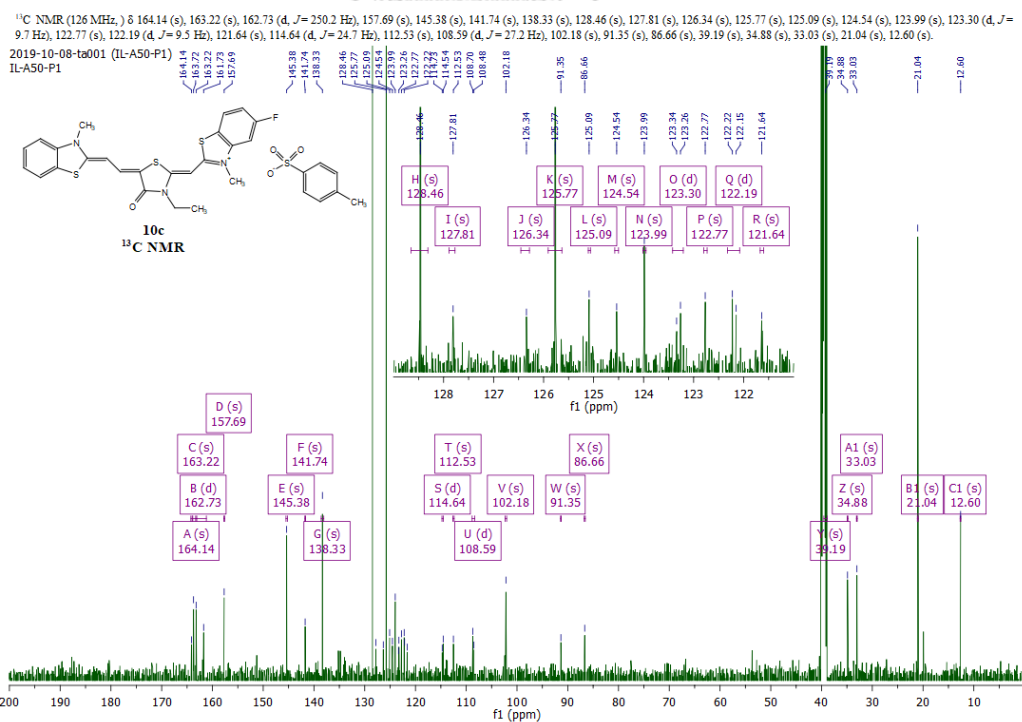
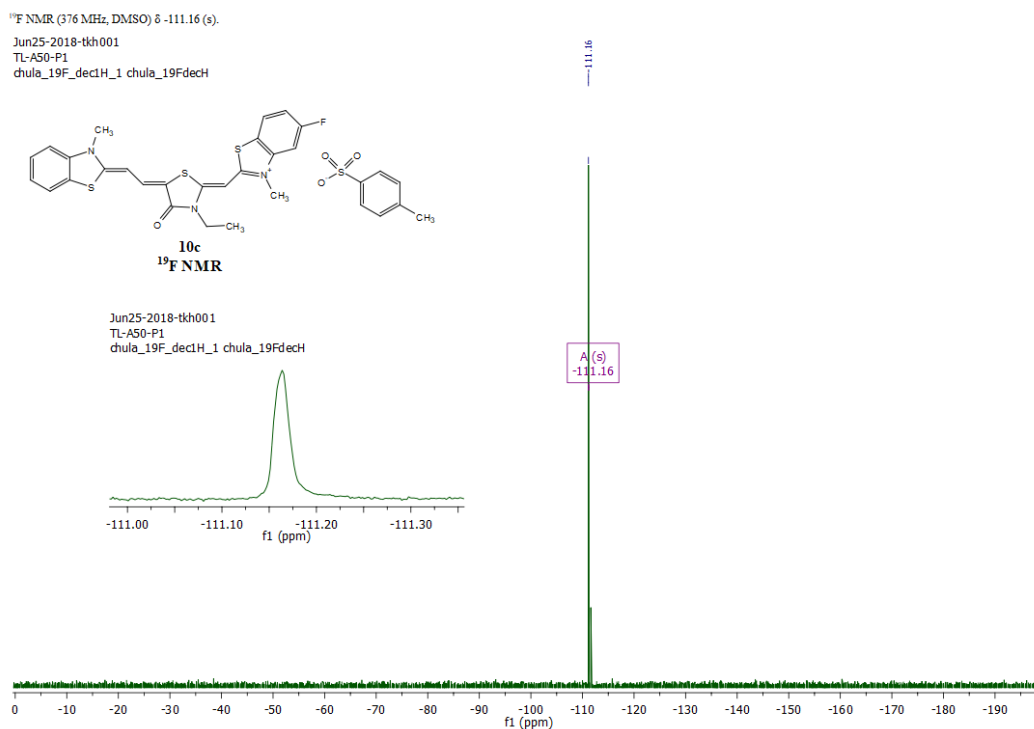


Figure 67 <sup>13</sup>C NMR spectrum of 10c

Figure 68 <sup>19</sup>F NMR spectrum of 10c

## Mass Spectrum List Report

<b>Analysis Info</b>	Acquisition Date 3/18/2019 9:10:56 PM
Analysis Name D:\Data\Data Service\190318\TL-A50-P1_RC3_01_2337.d	Operator CU.
Method nv_pos_5min_profile_190214.m	Instrument / Ser# microTOF-Q II 10335
Sample Name TL-A50-P1	
Comment	

## Acquisition Parameter

Source Type ESI	Ion Polarity Positive	Set Nebulizer 3.0 Bar
Focus Not active	Set Capillary 4000 V	Set Dry Heater 200 °C
Scan Begin 100 m/z	Set End Plate Offset -500 V	Set Dry Gas 8.0 l/min
Scan End 1500 m/z	Set Collision Cell RF 250.0 Vpp	Set Divert Valve Waste

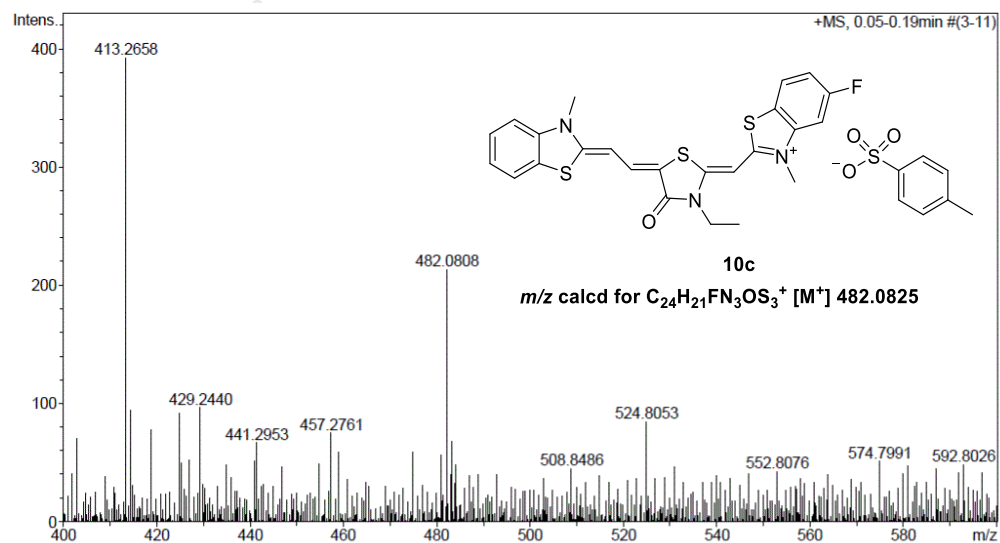


Figure 69 HRMS spectrum of 10c

2-(3-Ethyl-5-(2-(3-methylbenzo[d]thiazol-2(3H)-ylidene)ethylidene)ethylidene)-4-oxothiazolidin-2-ylidene)methyl)-5-fluoro-3-methylbenzo[d]thiazol-3-ium chloride (11c)

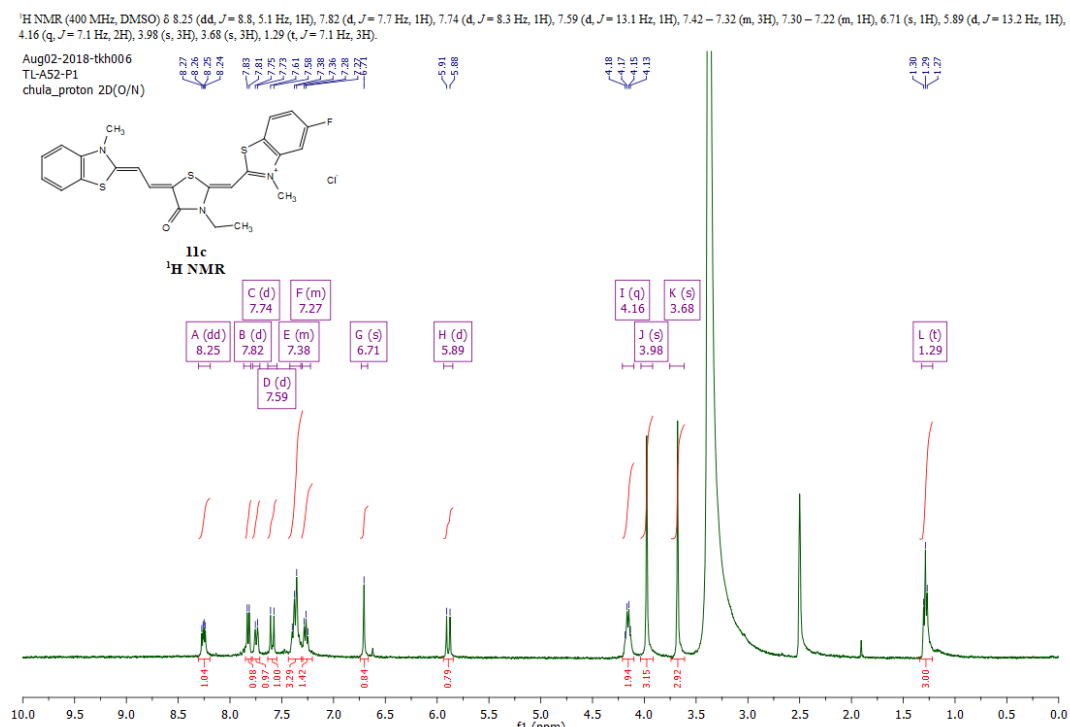


Figure 70 <sup>1</sup>H NMR spectrum of 11c

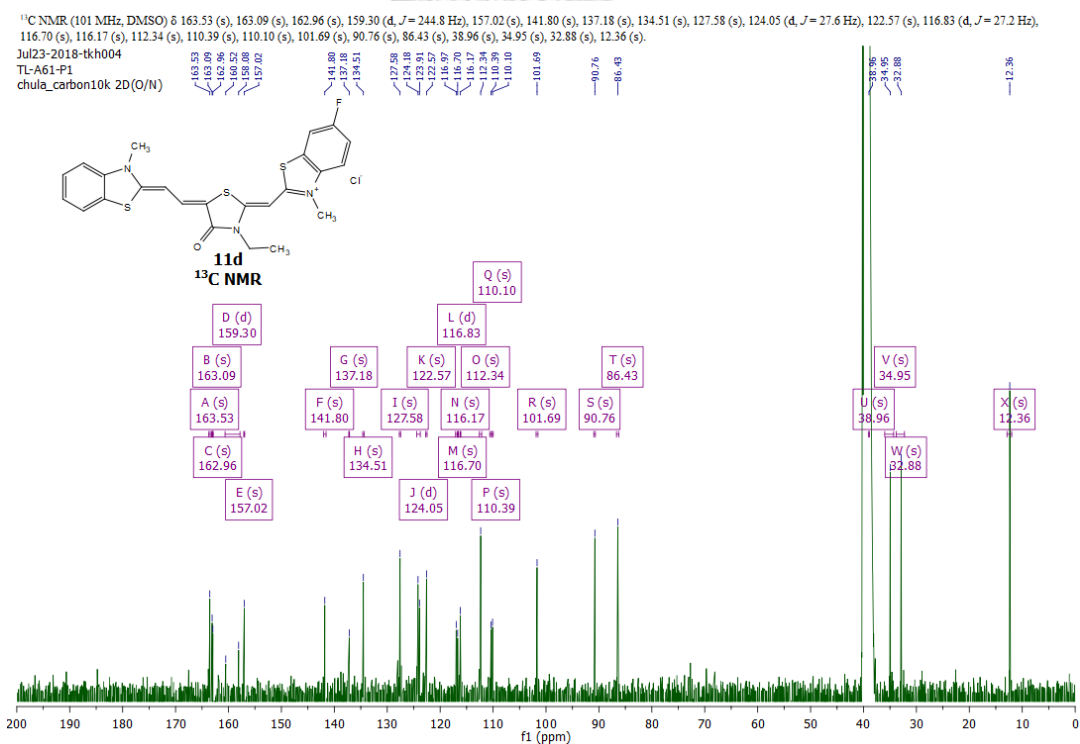
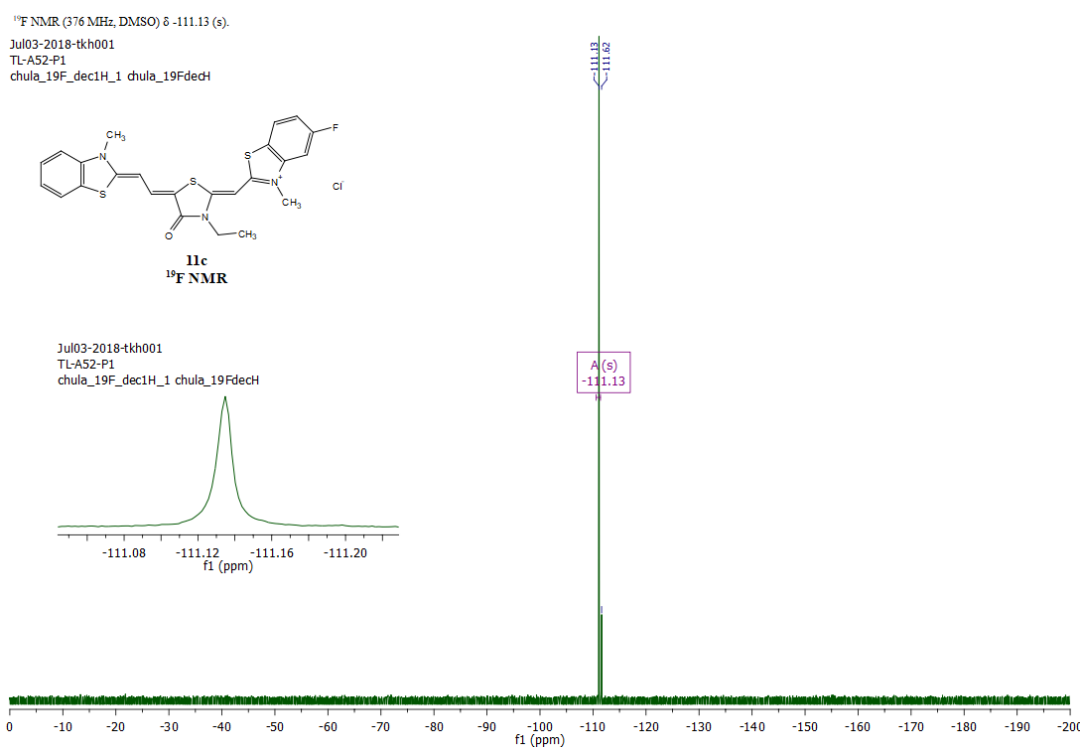
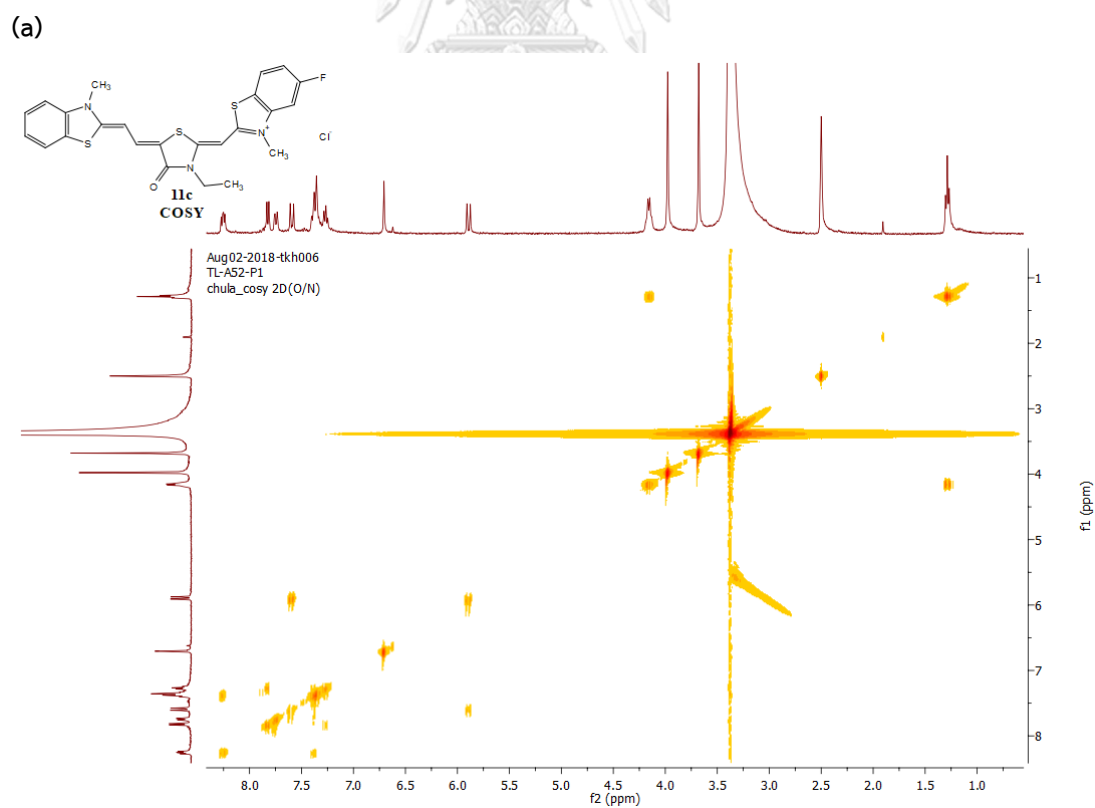
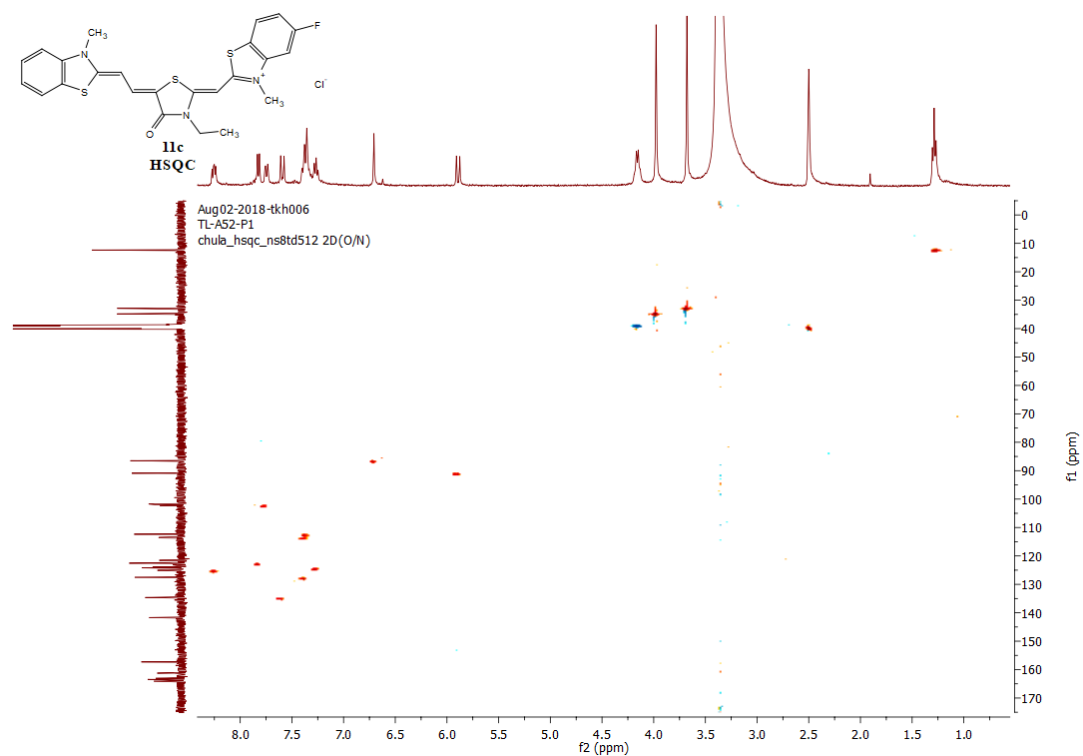


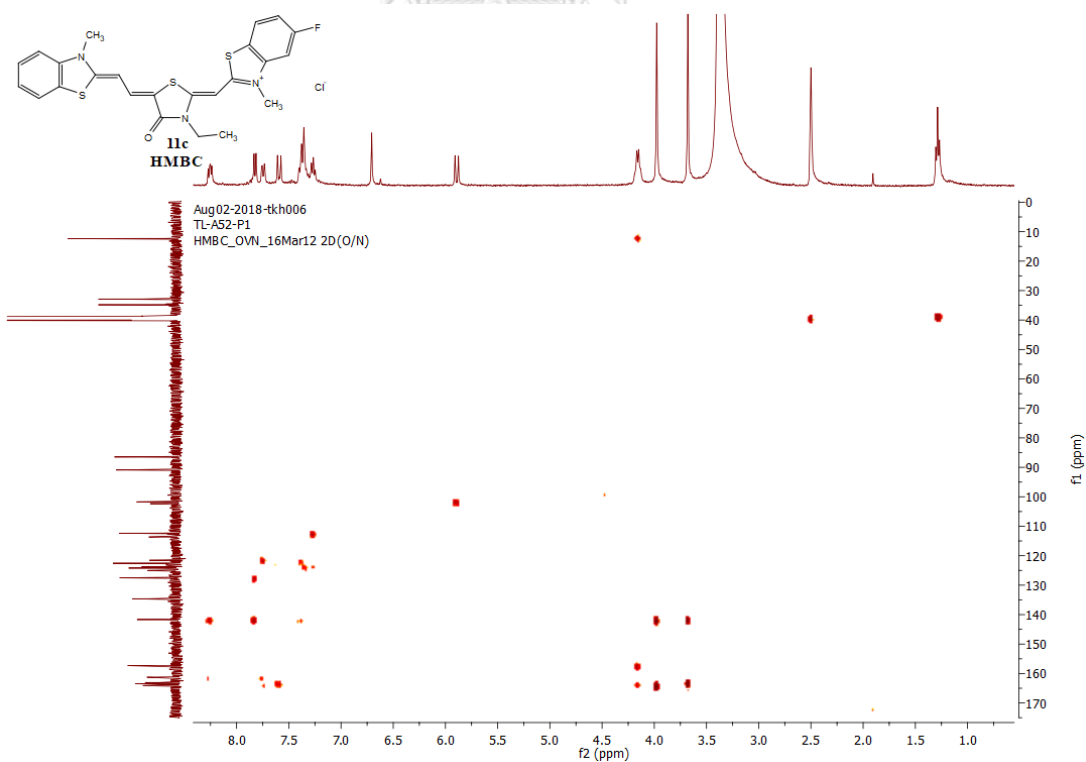
Figure 71 <sup>13</sup>C NMR spectrum of 11c

Figure 72  $^{19}\text{F}$  NMR spectrum of 11c

(b)



(c)

Figure 73 2D NMR spectra of **11c** (a) COSY; (b) HSQC; and (c) HMBC spectrum

## Mass Spectrum List Report

**Analysis Info**  
Analysis Name D:\Data\Data Service\180910\_pos\_TL-A52-PI.d  
Method NV\_pos\_0.3min\_profile\_1segment\_lowNubulizerDrygas.m  
Sample Name 180910\_pos\_TL-A52-PI  
Comment  
Acquisition Date 9/10/2018 4:36:59 PM  
Operator CU.  
Instrument / Ser# micrOTOF-Q II 10335

**Acquisition Parameter**  
Source Type ESI Ion Polarity Positive Set Nebulizer 0.4 Bar  
Focus Not active Set Capillary 4000 V Set Dry Heater 200 °C  
Scan Begin 50 m/z Set End Plate Offset -500 V Set Dry Gas 4.0 l/min  
Scan End 1500 m/z Set Collision Cell RF 150.0 Vpp Set Divert Valve Waste

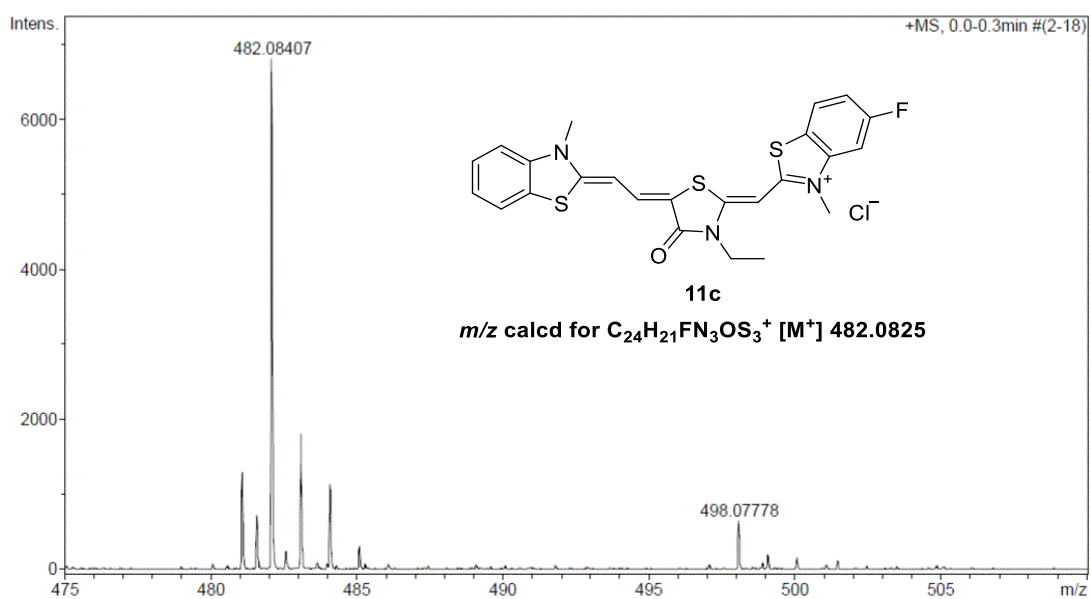


Figure 74 HRMS spectrum of 11c



2-(3-Ethyl-5-(2-(3-methylbenzo[d]thiazol-2(3H)-ylidene)ethylidene)ethylidene)-4-oxothiazolidin-2-ylidene)methyl)-6-fluoro-3-methylbenzo[d]thiazol-3-ium chloride (11d)

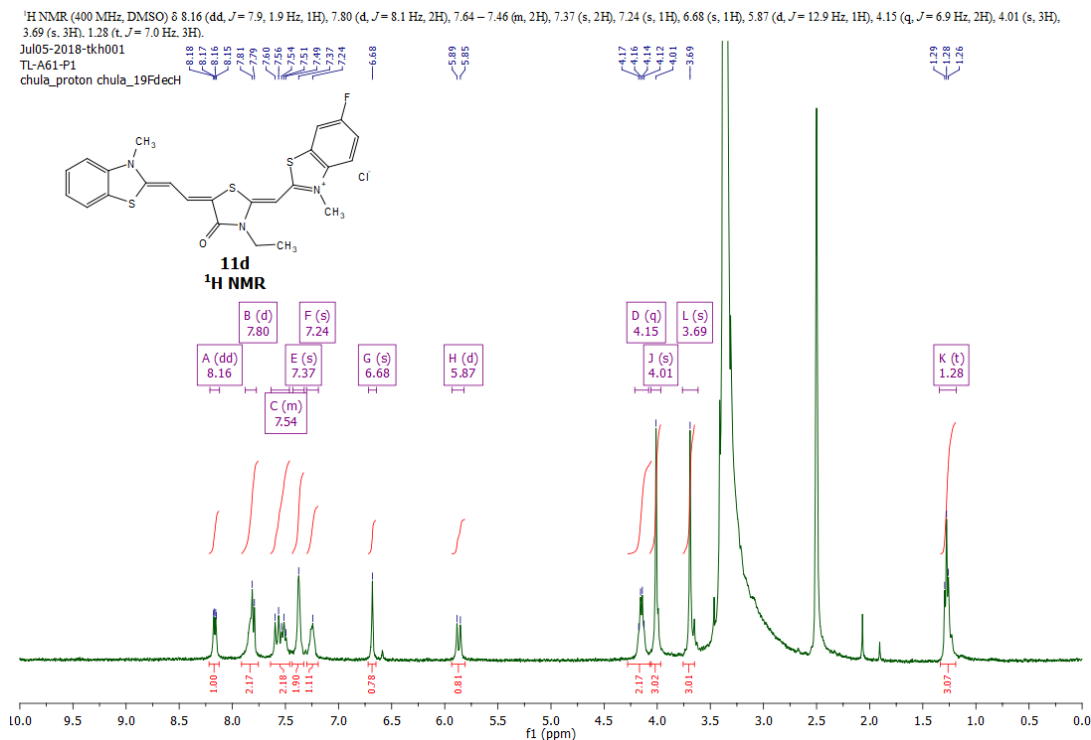


Figure 75 <sup>1</sup>H NMR spectrum of 11d

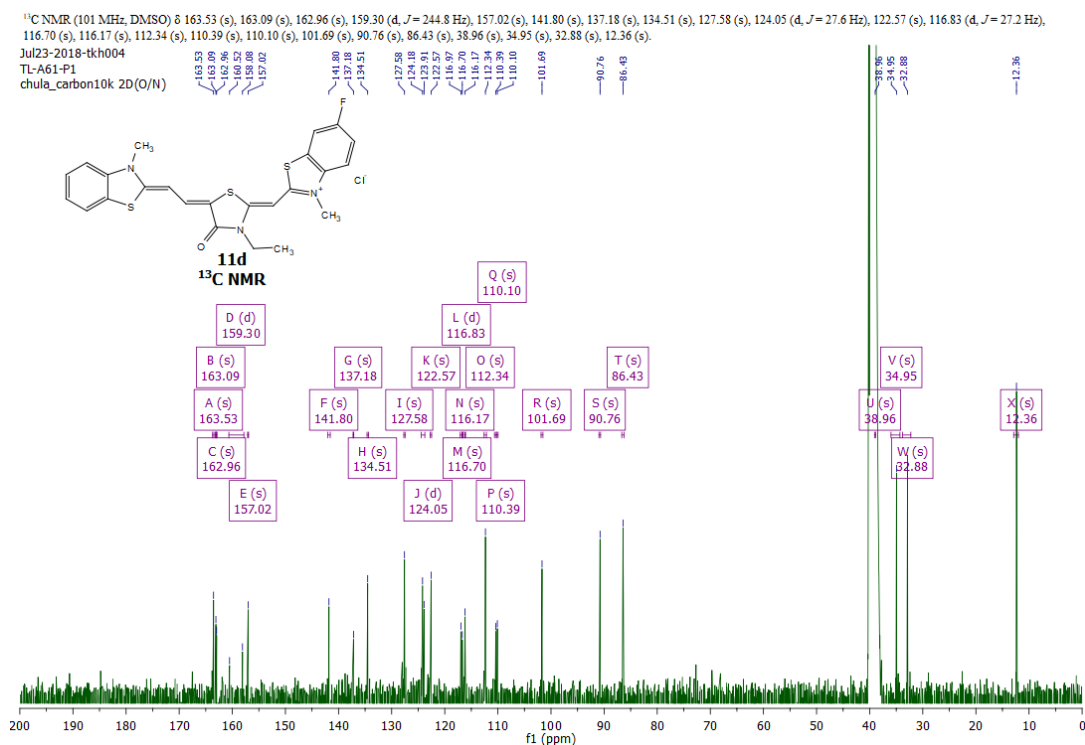
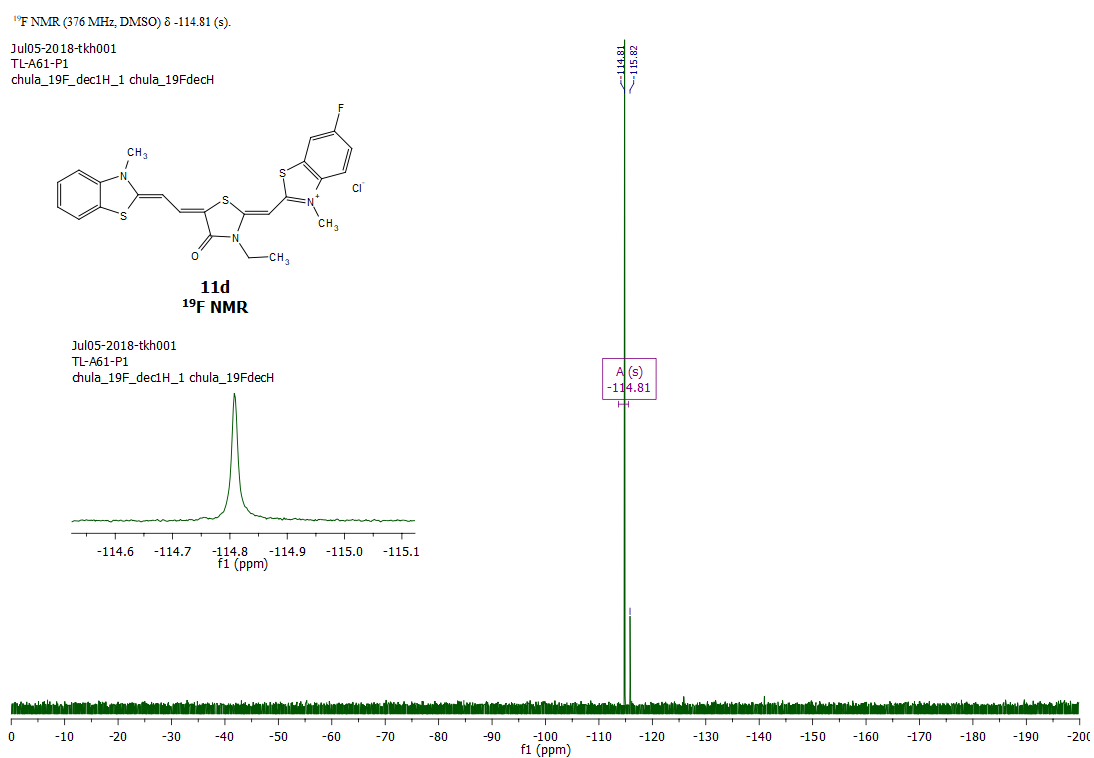
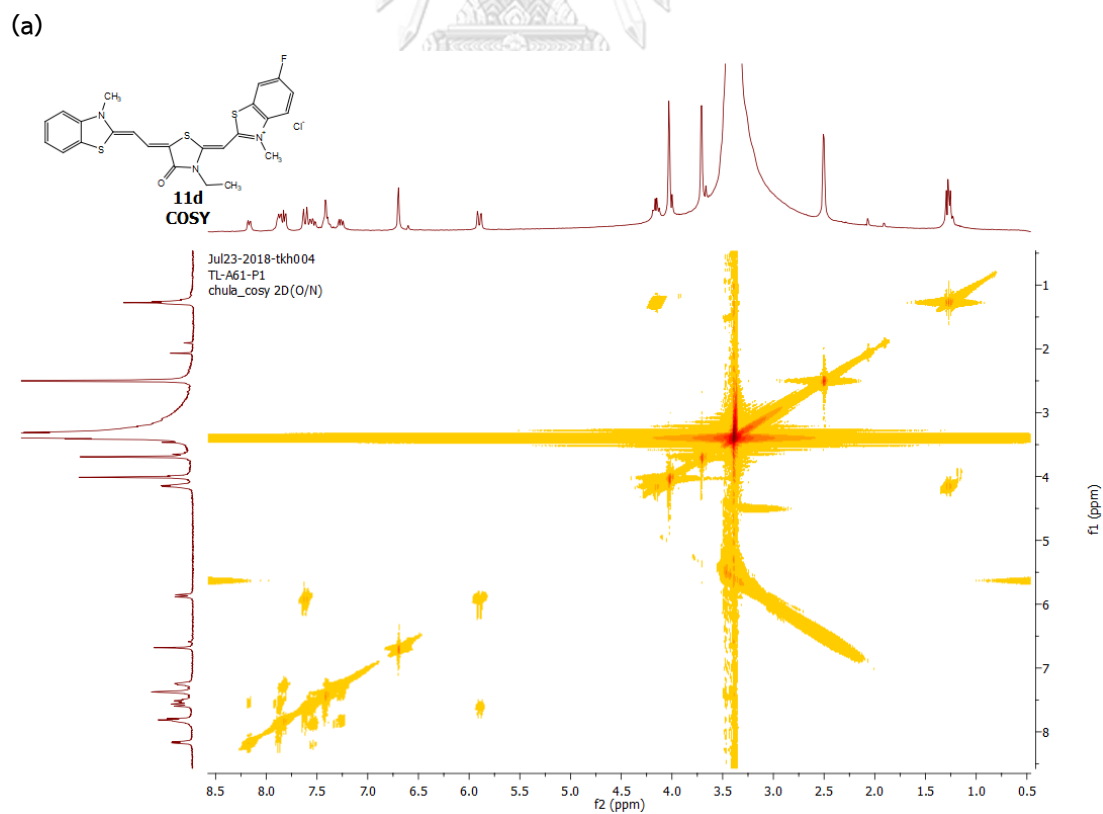
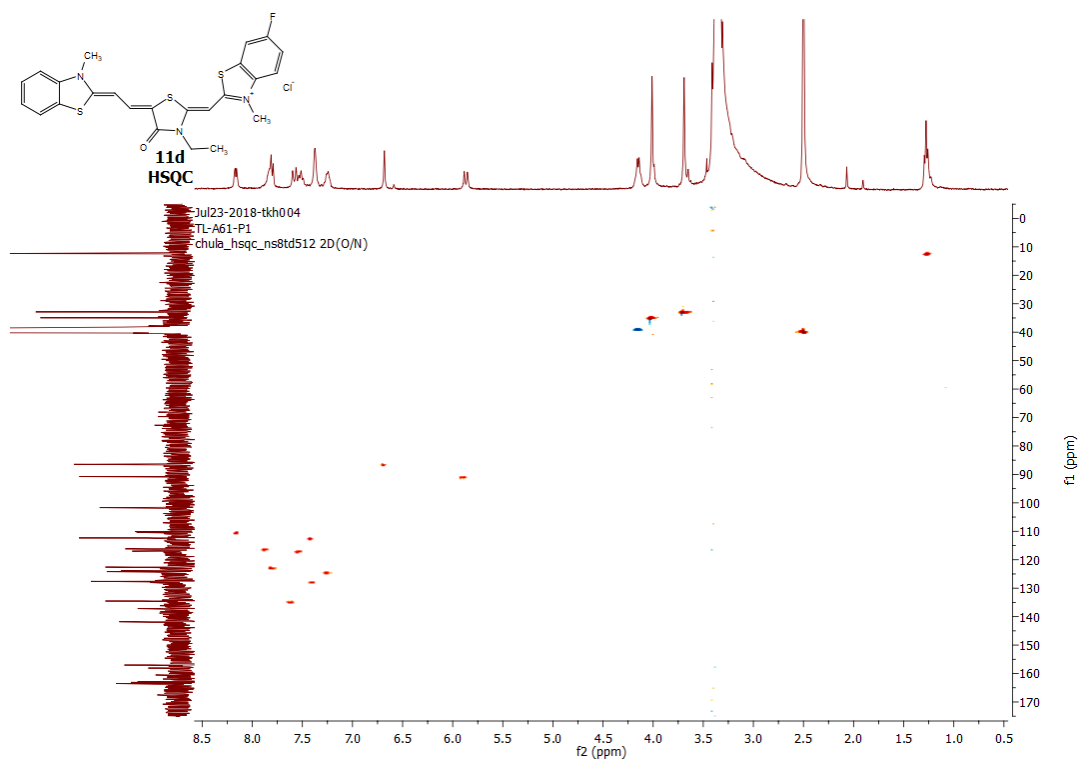


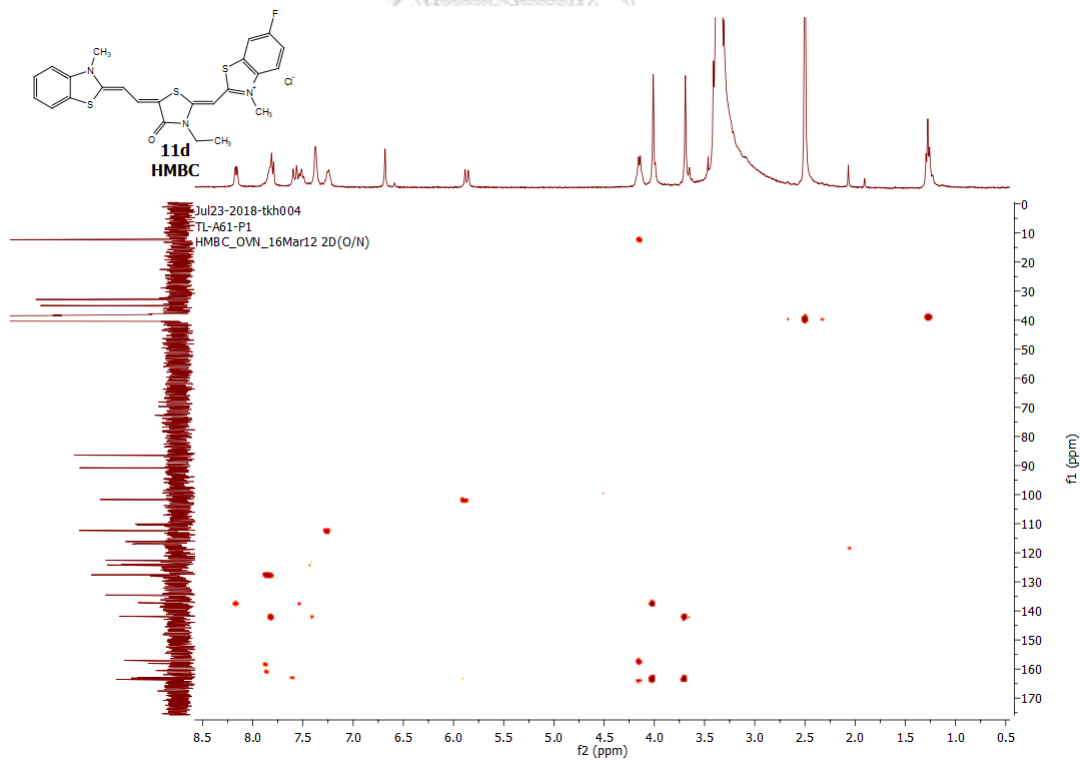
Figure 76 <sup>13</sup>C NMR spectrum of 11d

Figure 77  $^{19}\text{F}$  NMR spectrum of **11d**

(b)



(c)

Figure 78 2D NMR spectra of **11d** (a) COSY; (b) HSQC; and (c) HMBC spectrum

## Mass Spectrum List Report

**Analysis Info**  
Analysis Name D:\Data\Data Service\190318\TL-A61-P1\_RC5\_01\_2339.d  
Method nv\_pos\_5min\_profile\_190214.m  
Sample Name TL-A61-P1  
Comment  
Acquisition Date 3/18/2019 9:34:43 PM  
Operator CU.  
Instrument / Ser# micrOTOF-Q II 10335

**Acquisition Parameter**

Source Type	ESI	Ion Polarity	Positive	Set Nebulizer	3.0 Bar
Focus	Not active	Set Capillary	4000 V	Set Dry Heater	200 °C
Scan Begin	100 m/z	Set End Plate Offset	-500 V	Set Dry Gas	8.0 l/min
Scan End	1500 m/z	Set Collision Cell RF	250.0 Vpp	Set Divert Valve	Waste

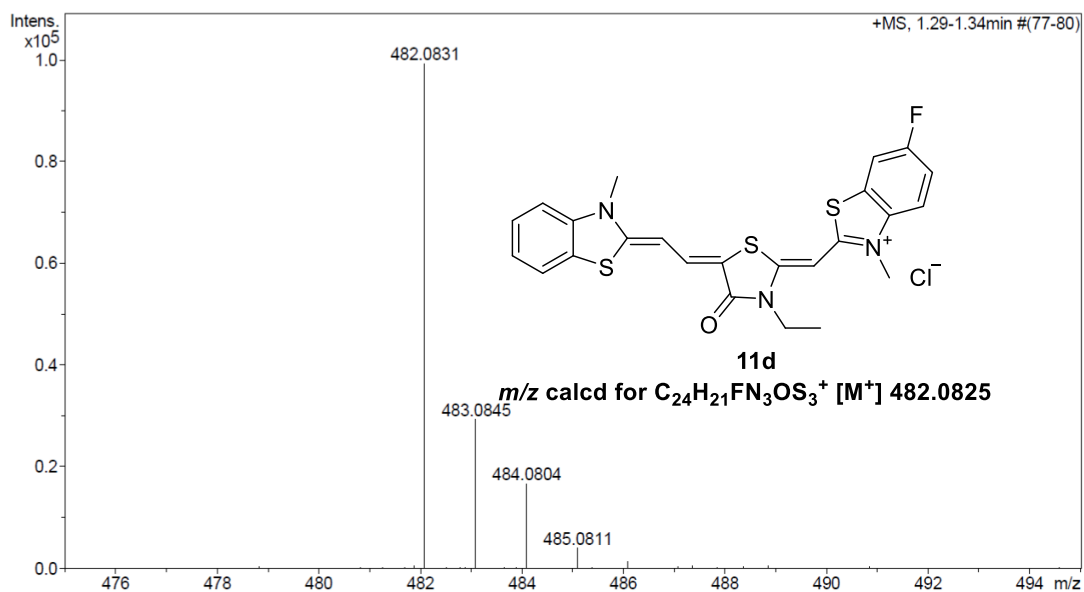


Figure 79 HRMS spectrum of 11d

2-(3-Ethyl-5-(2-(3-methylbenzo[d]thiazol-2(3H)-ylidene)ethylidene)ethylidene)-4-oxothiazolidin-2-ylidene)methyl)-7-fluoro-3-methylbenzo[d]thiazol-3-ium chloride (11e)

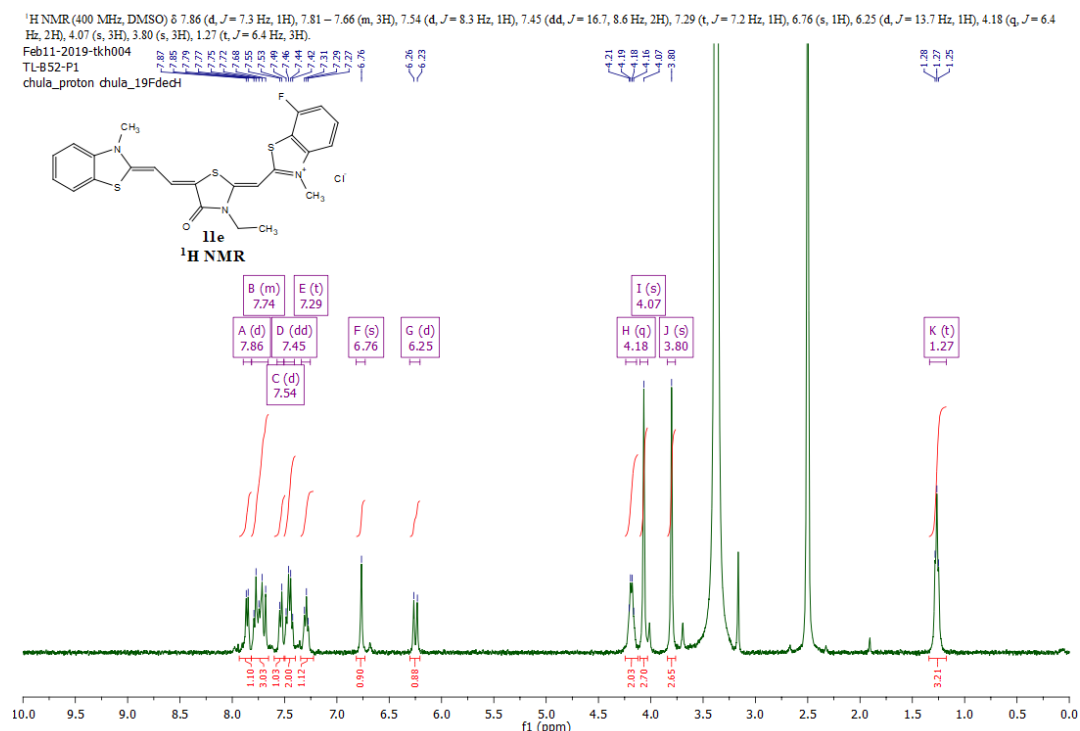


Figure 80 <sup>1</sup>H NMR spectrum of 11e

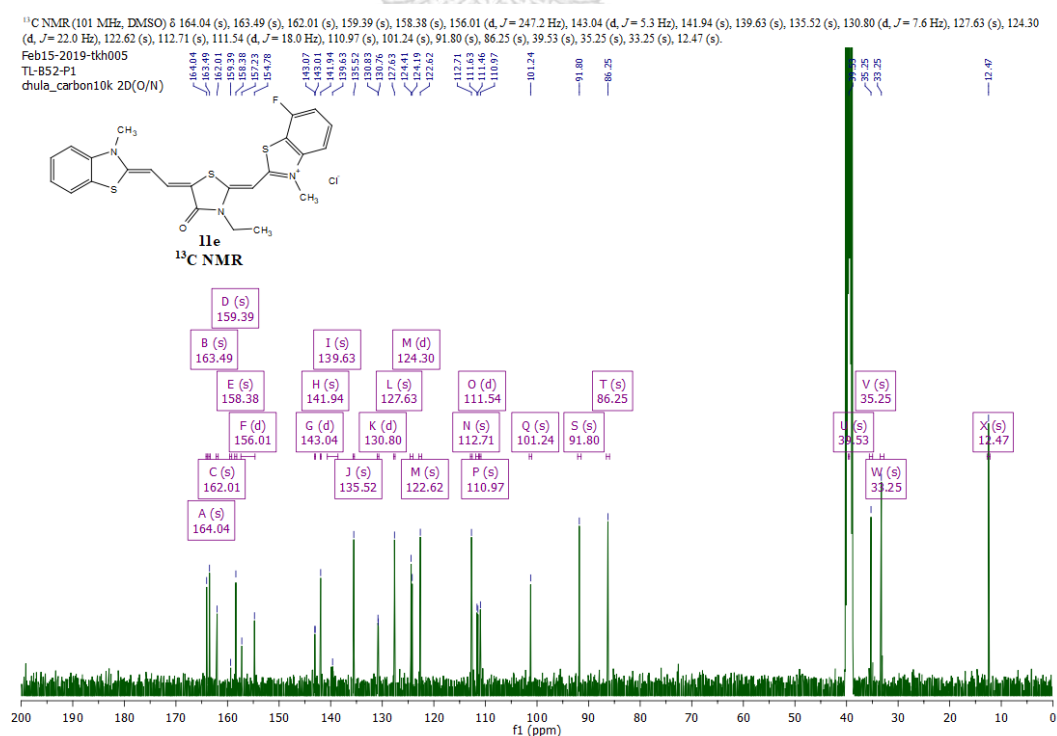


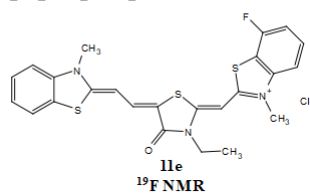
Figure 81 <sup>13</sup>C NMR spectrum of 11e

$^{19}\text{F}$  NMR (376 MHz, DMSO)  $\delta$  -114.99 (s).

Feb11-2019-tkh004

TL-B52-P1

chula\_19F\_dec1H\_1 chula\_19FdecH



Feb11-2019-tkh004

TL-B52-P1

chula\_19F\_dec1H\_1 chula\_19FdecH

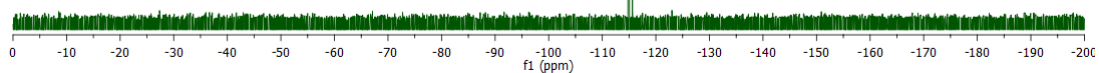
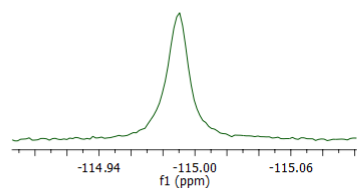
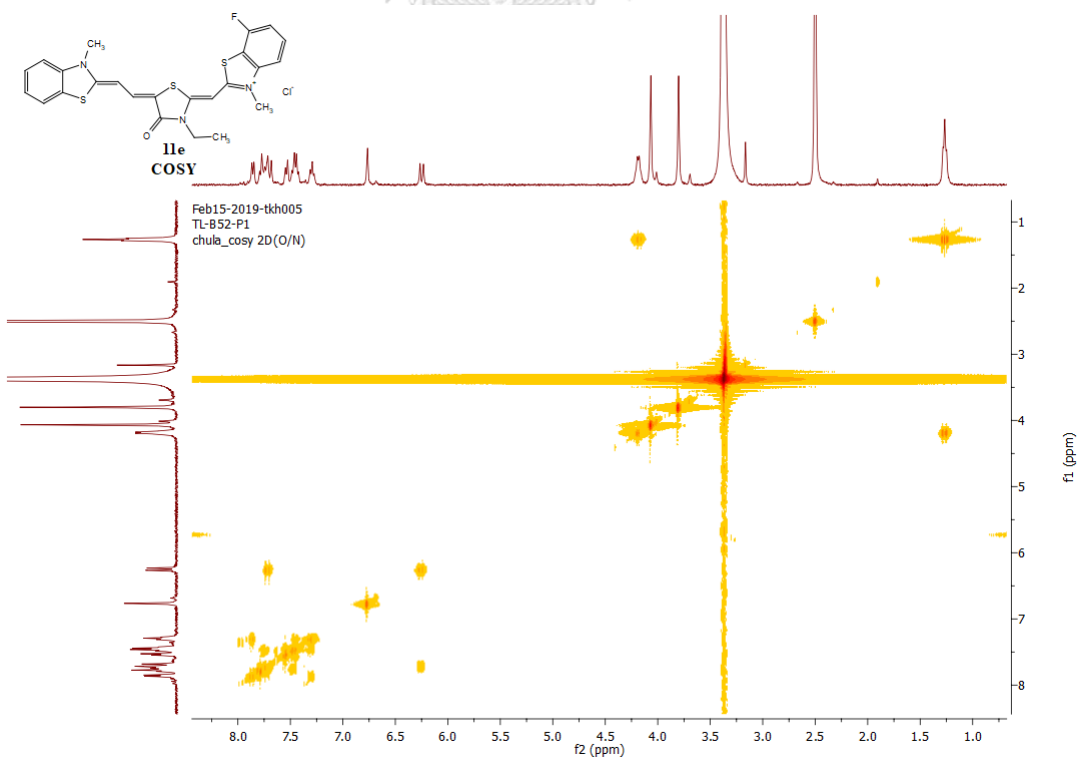
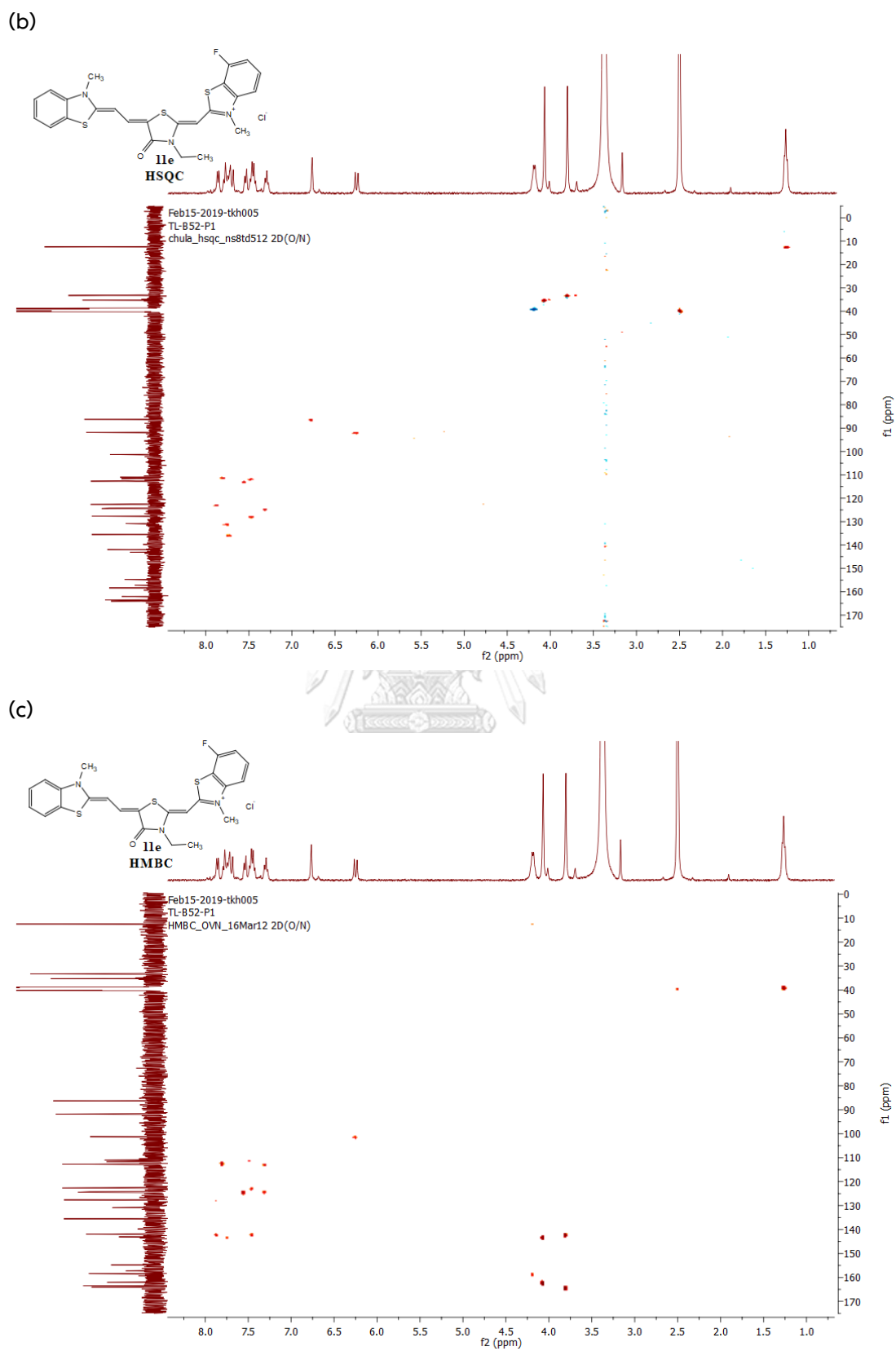


Figure 82  $^{19}\text{F}$  NMR spectrum of 11e

(a)



Figure 83 2D NMR spectra of **11e** (a) COSY; (b) HSQC; and (c) HMBC spectrum

## Mass Spectrum List Report

**Analysis Info**  
Analysis Name D:\Data\Data Service\190401\TL-B52-P1\_RD4\_01\_2455.d  
Method nv\_pos\_5min\_profile\_190214.m  
Sample Name TL-B52-P1  
Comment  
Acquisition Date 4/1/2019 9:12:40 PM  
Operator CU.  
Instrument / Ser# microTOF-Q II 10335

**Acquisition Parameter**

Source Type	ESI	Ion Polarity	Positive	Set Nebulizer	3.0 Bar
Focus	Not active	Set Capillary	4000 V	Set Dry Heater	200 °C
Scan Begin	100 m/z	Set End Plate Offset	-500 V	Set Dry Gas	8.0 l/min
Scan End	1500 m/z	Set Collision Cell RF	250.0 Vpp	Set Divert Valve	Waste

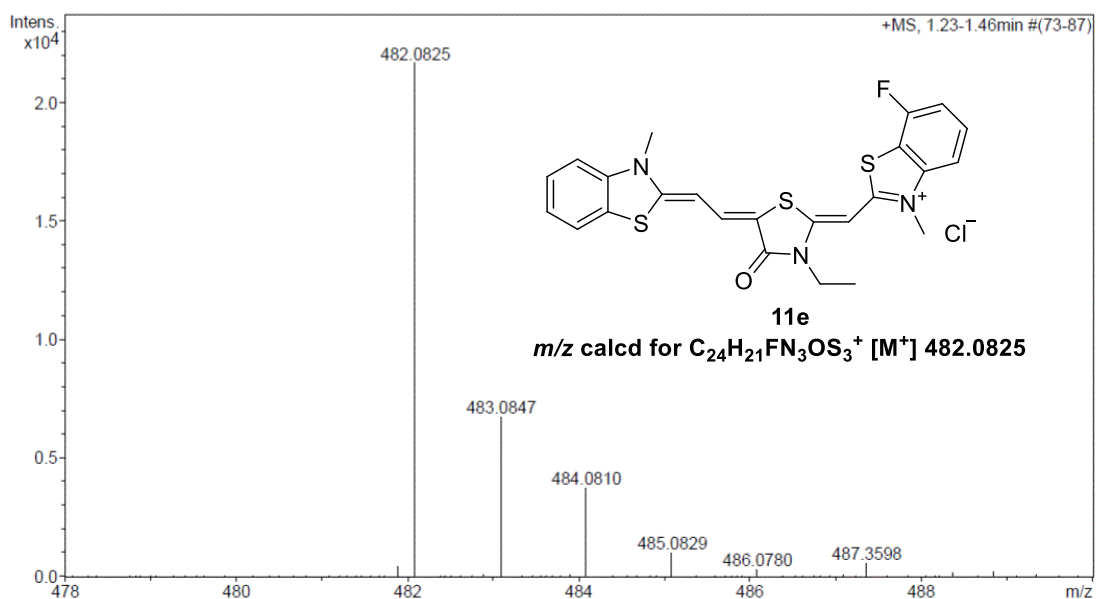


Figure 84 HRMS spectrum of 11e



2-(3-Ethyl-5-(2-(4-fluoro-3-methylbenzo[d]thiazol-2(3H)-ylidene)ethylidene)-4-oxothiazolidin-2-ylidene)methyl)-3-methylbenzo[d]thiazol-3-ium chloride (11f)

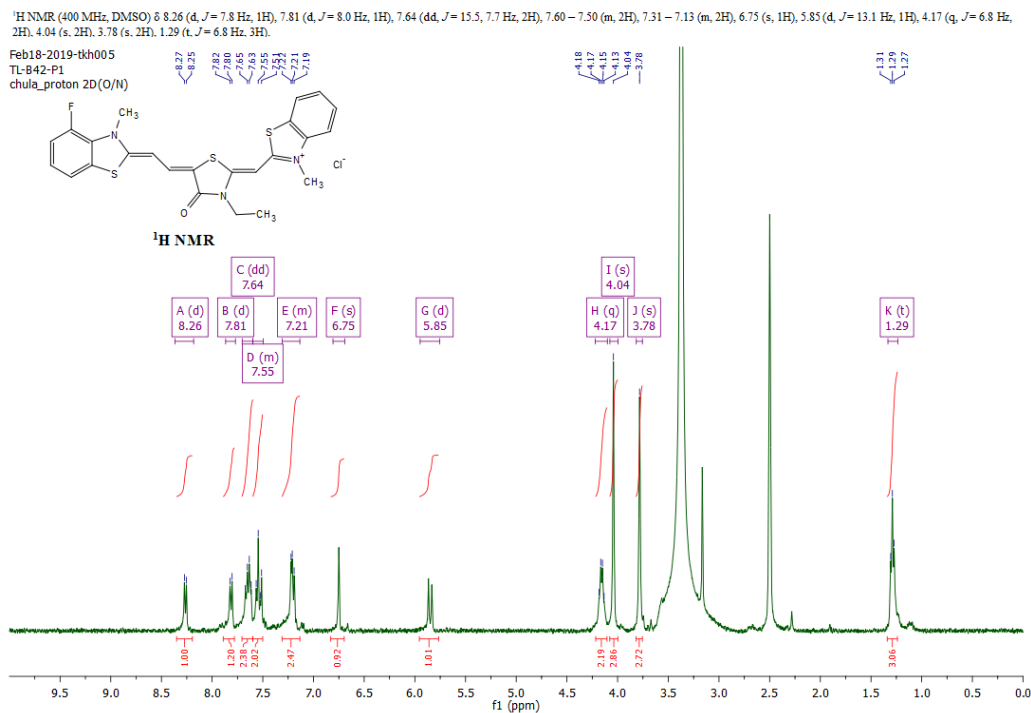


Figure 85 <sup>1</sup>H NMR spectrum of 11f

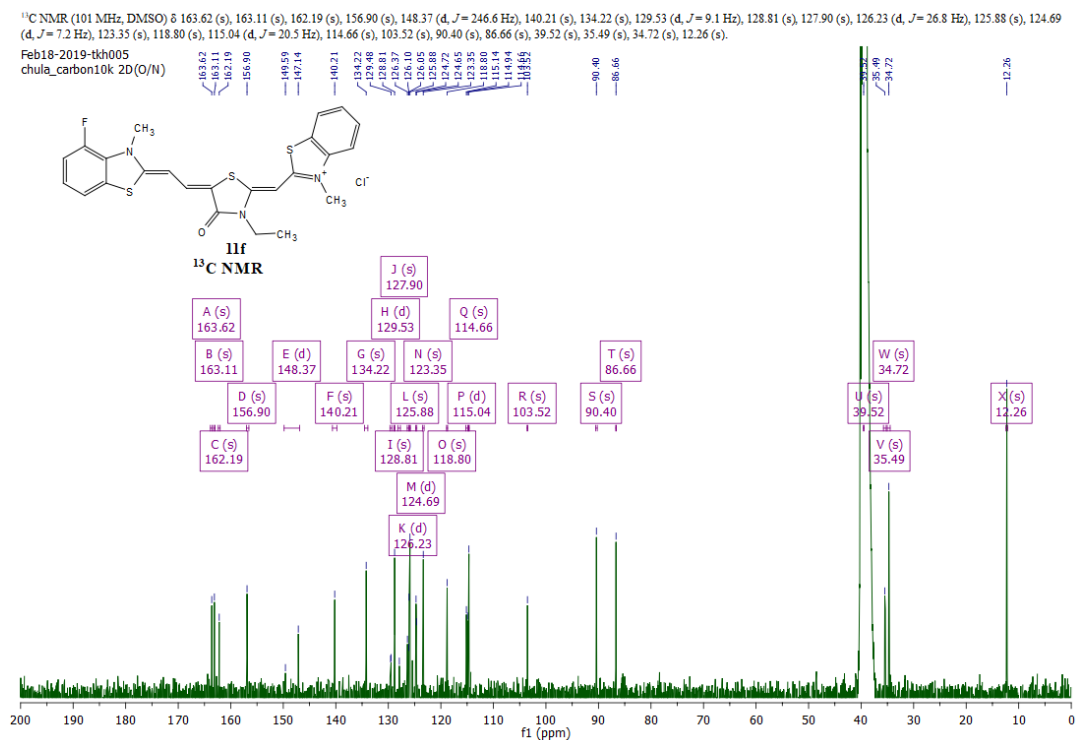
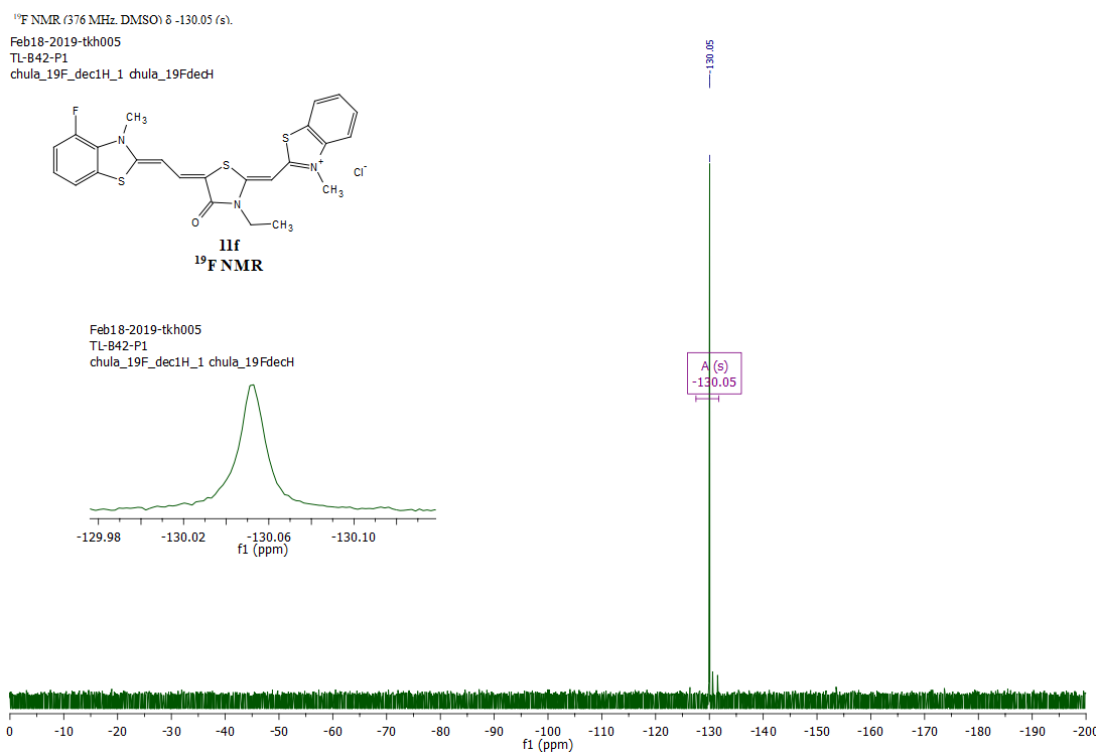
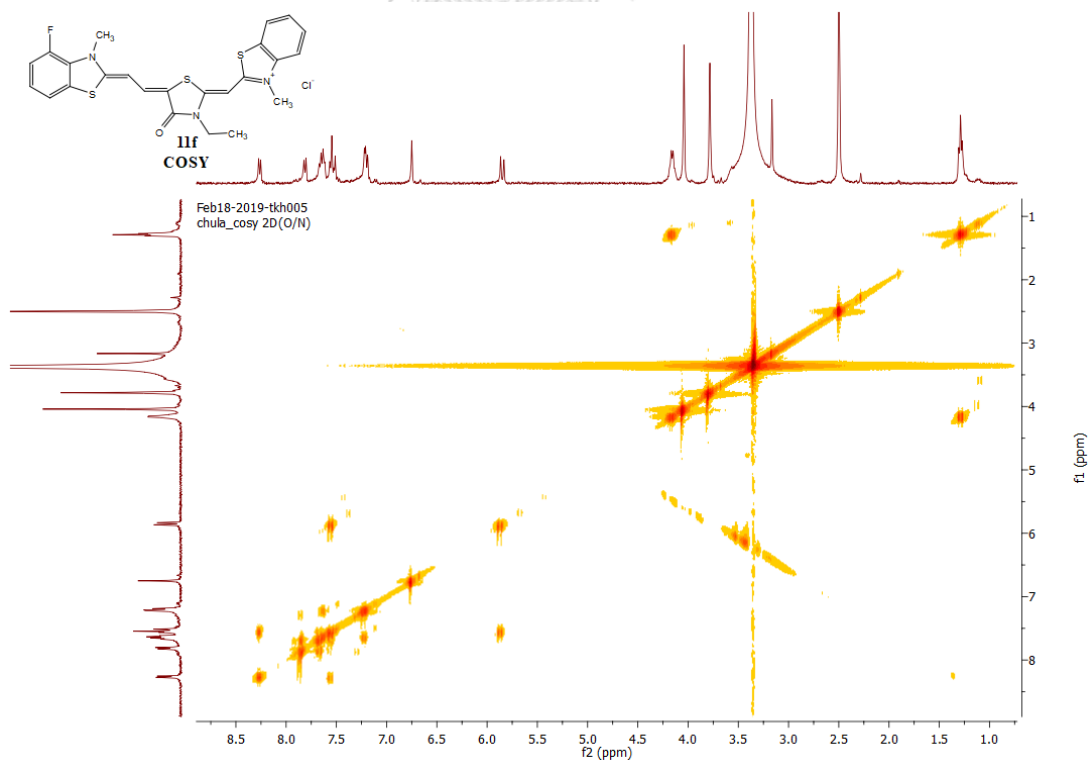


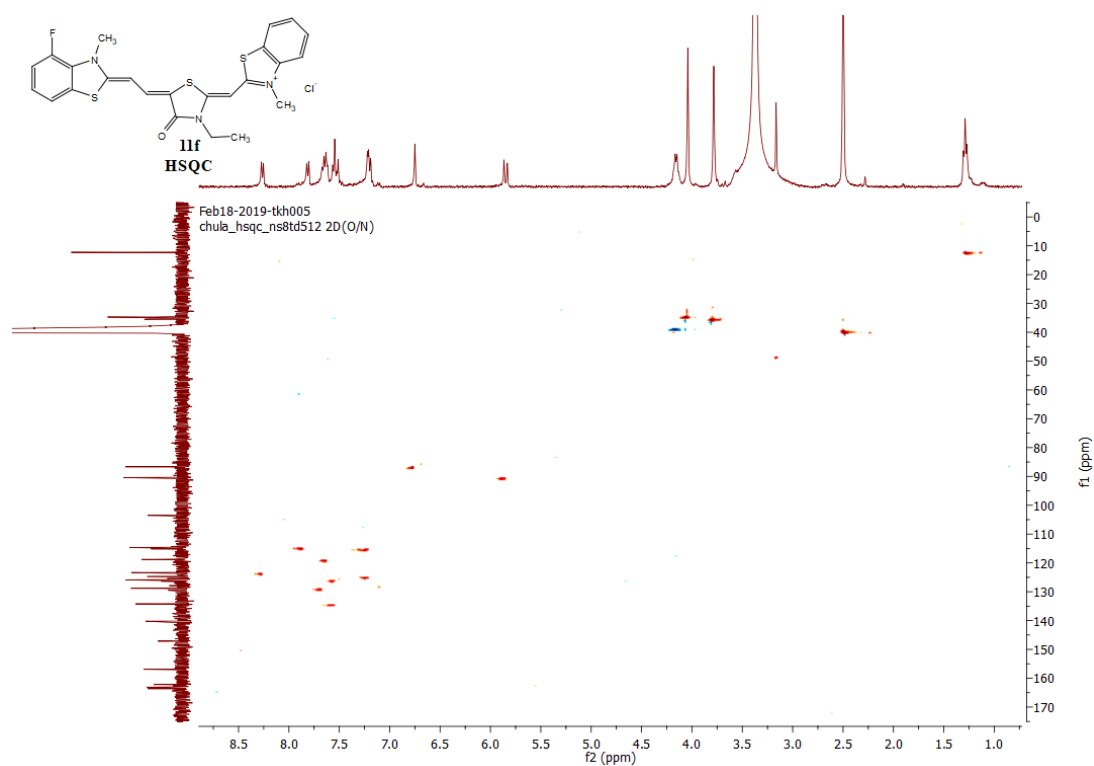
Figure 86 <sup>13</sup>C NMR spectrum of 11f

Figure 87 <sup>19</sup>F NMR spectrum of 11f

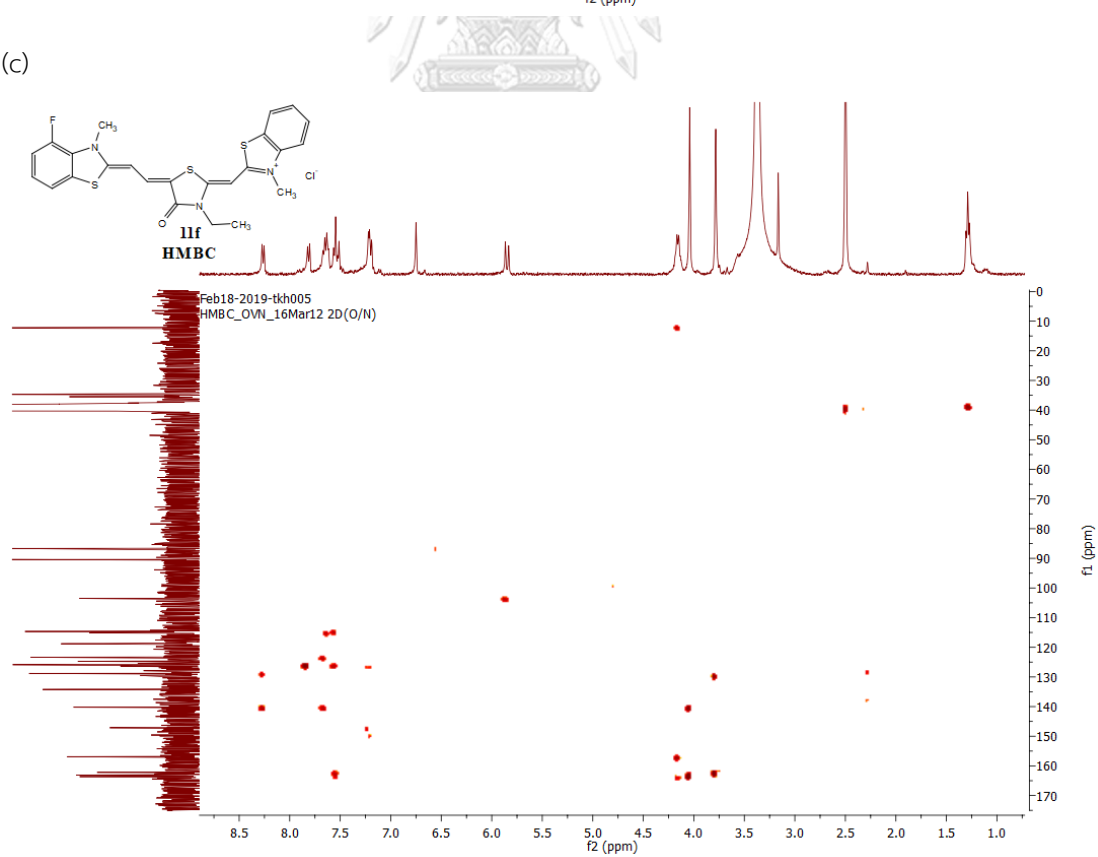
(a)



(b)



(c)

Figure 88 2D NMR spectra of **11f** (a) COSY; (b) HSQC; and (c) HMBC spectrum

## Mass Spectrum List Report

**Analysis Info**  
Analysis Name D:\Data\Data Service\190318\TL-B42-P1\_RD8\_01\_2351.d  
Method nv\_pos\_5min\_profile\_190214.m  
Sample Name TL-B42-P1  
Comment  
Acquisition Date 3/18/2019 10:50:32 PM  
Operator CU.  
Instrument / Ser# micrOTOF-Q II 10335

**Acquisition Parameter**

Source Type	ESI	Ion Polarity	Positive	Set Nebulizer	3.0 Bar
Focus	Not active	Set Capillary	4000 V	Set Dry Heater	200 °C
Scan Begin	100 m/z	Set End Plate Offset	-500 V	Set Dry Gas	8.0 l/min
Scan End	1500 m/z	Set Collision Cell RF	250.0 Vpp	Set Divert Valve	Waste

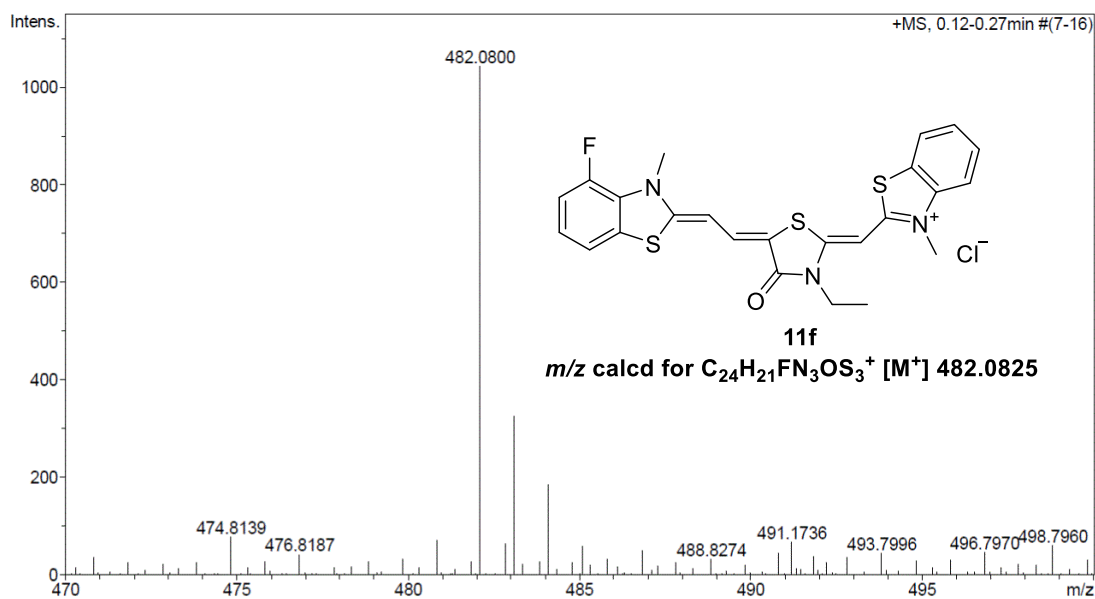


Figure 89 HRMS spectrum of 11f

2-(3-Ethyl-5-(2-(5-fluoro-3-methylbenzo[d]thiazol-2(3H)-ylidene)ethylidene)ethylidene)-4-oxothiazolidin-2-ylidene)methyl-3-methylbenzo[d]thiazol-3-ium chloride (11g)

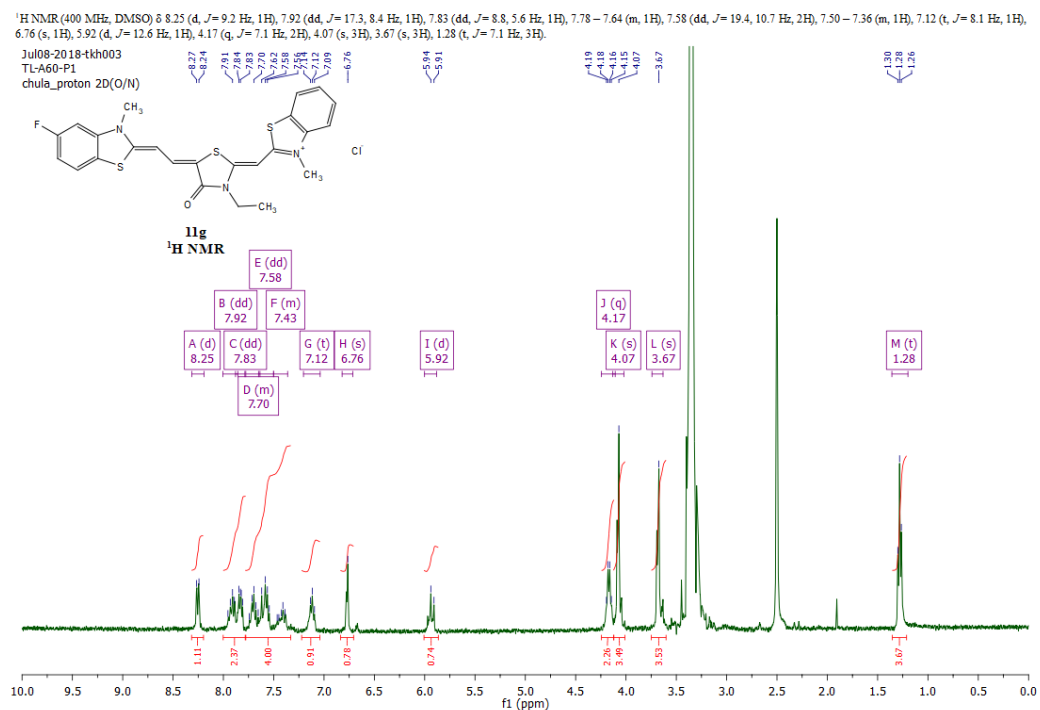


Figure 90 <sup>1</sup>H NMR spectrum of 11g

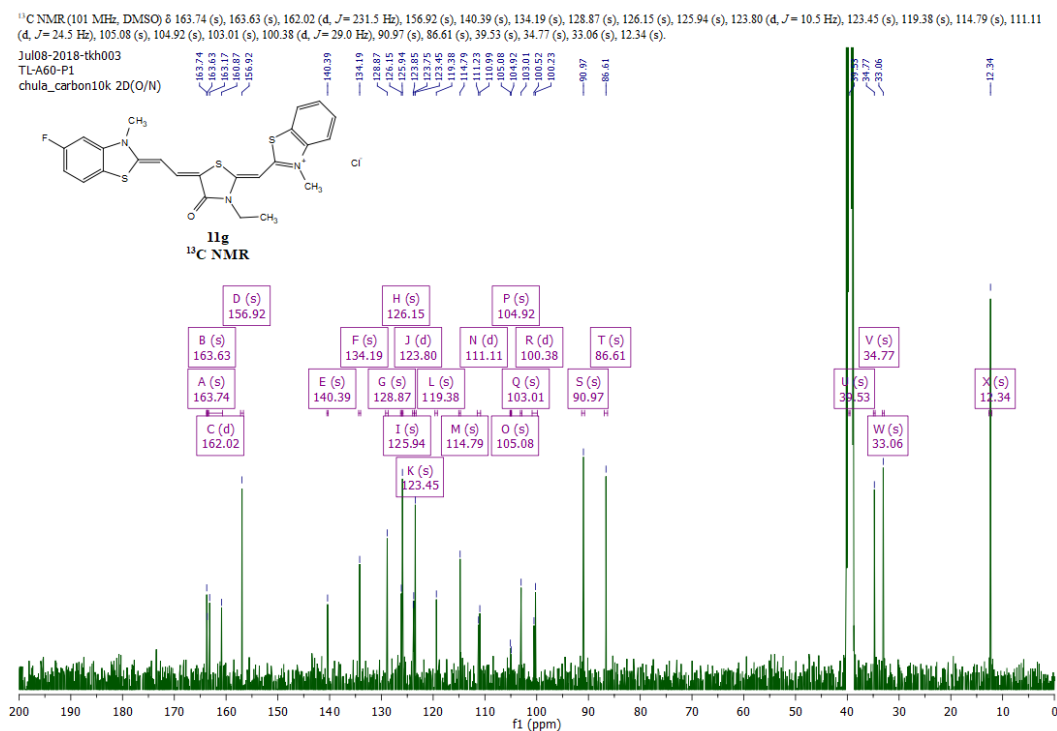
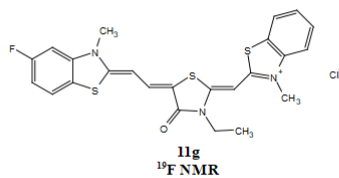


Figure 91 <sup>13</sup>C NMR spectrum of 11g

$^{19}\text{F}$  NMR (376 MHz, DMSO)  $\delta$  -113.59 (s).  
Jul05-2018-tkh002  
TL-A60-P1  
chula\_19F\_dec1H\_1 chula\_19FdecH



Jul05-2018-tkh002  
TL-A60-P1  
chula\_19F\_dec1H\_1 chula\_19FdecH

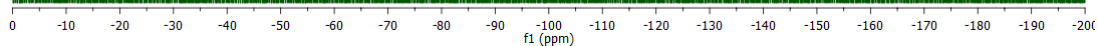
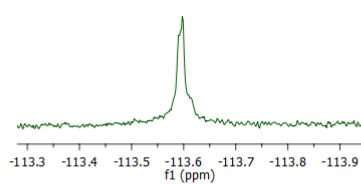
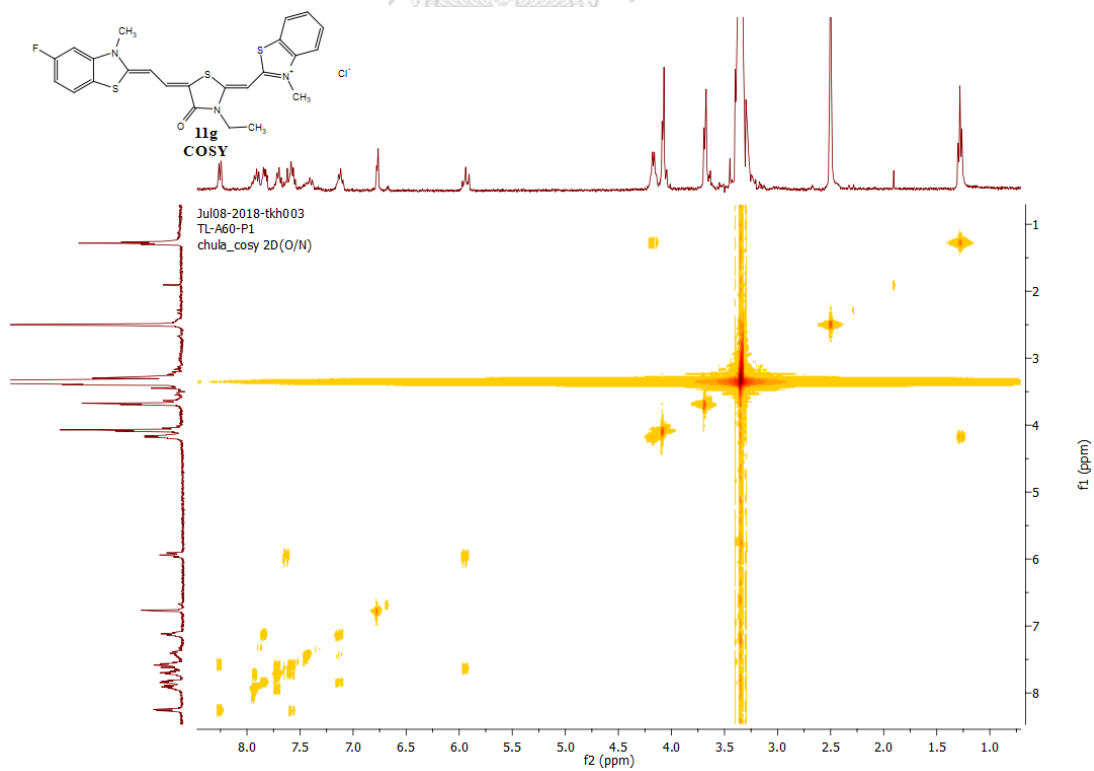


Figure 92  $^{19}\text{F}$  NMR spectrum of **11g**

(a)



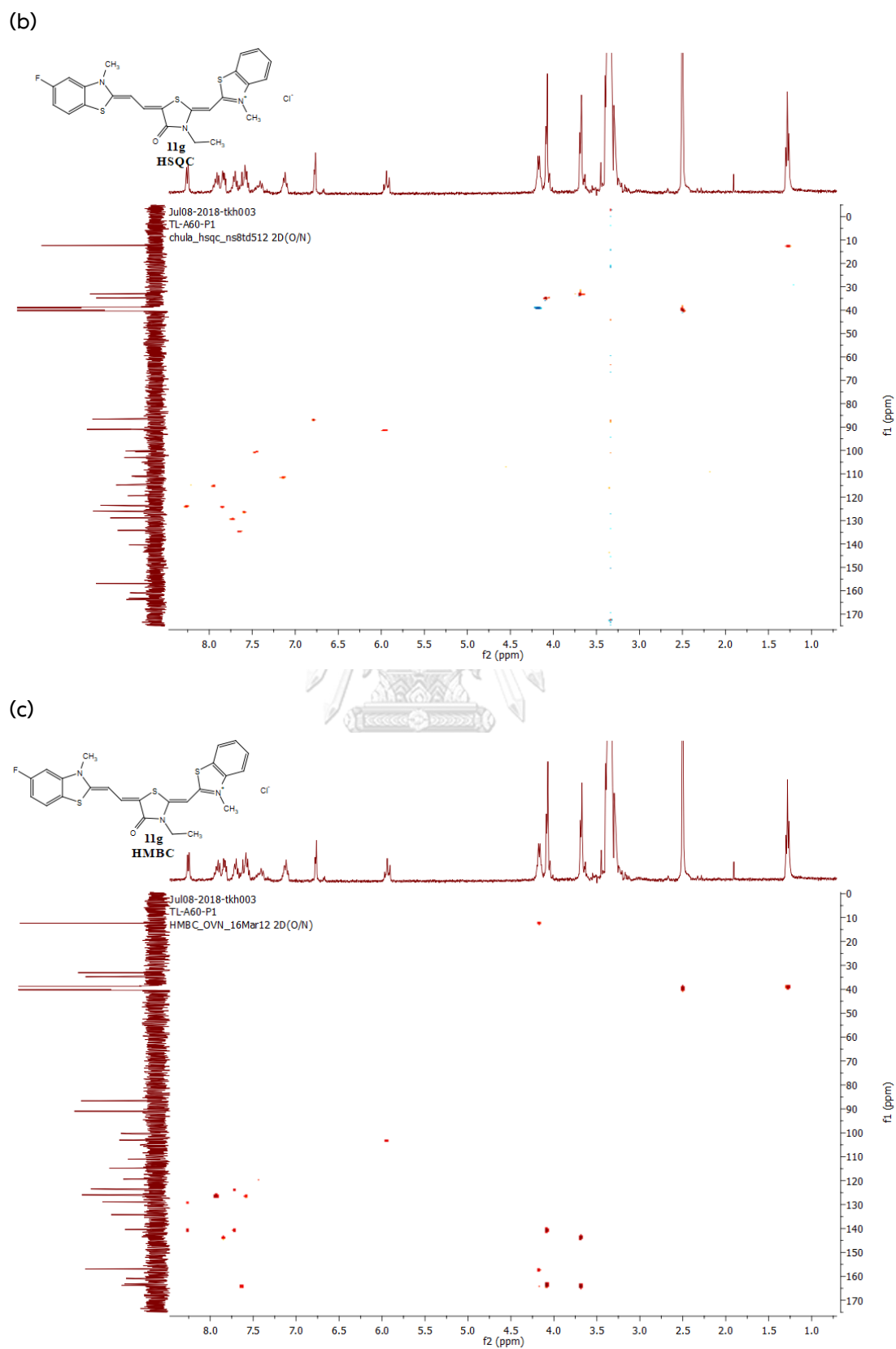


Figure 93 2D NMR spectra of **11g** (a) COSY; (b) HSQC; and (c) HMBC spectrum

## Mass Spectrum List Report

### Analysis Info

Analysis Name D:\Data\Data Service\190318\TL-A60-P1\_RC4\_01\_2338.d  
Method nv\_pos\_5min\_profile\_190214.m  
Sample Name TL-A60-P1  
Comment

Acquisition Date 3/18/2019 9:28:17 PM

Operator CU.  
Instrument / Ser# micrOTOF-Q II 10335

### Acquisition Parameter

Source Type	ESI	Ion Polarity	Positive	Set Nebulizer	3.0 Bar
Focus	Not active	Set Capillary	4000 V	Set Dry Heater	200 °C
Scan Begin	100 m/z	Set End Plate Offset	-500 V	Set Dry Gas	8.0 l/min
Scan End	1500 m/z	Set Collision Cell RF	250.0 Vpp	Set Divert Valve	Waste

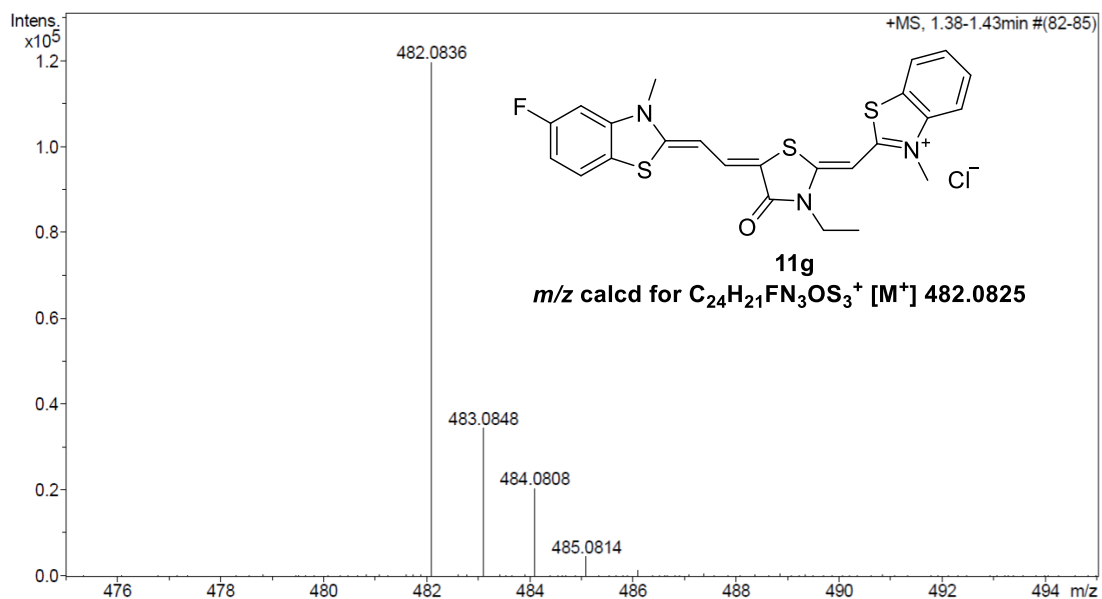


Figure 94 HRMS spectrum of **11g**



2-(3-Ethyl-5-(2-(6-fluoro-3-methylbenzo[d]thiazol-2(3H)-ylidene)ethylidene)-4-oxothiazolidin-2-ylidene)methyl)-3-methylbenzo[d]thiazol-3-ium chloride (11h)

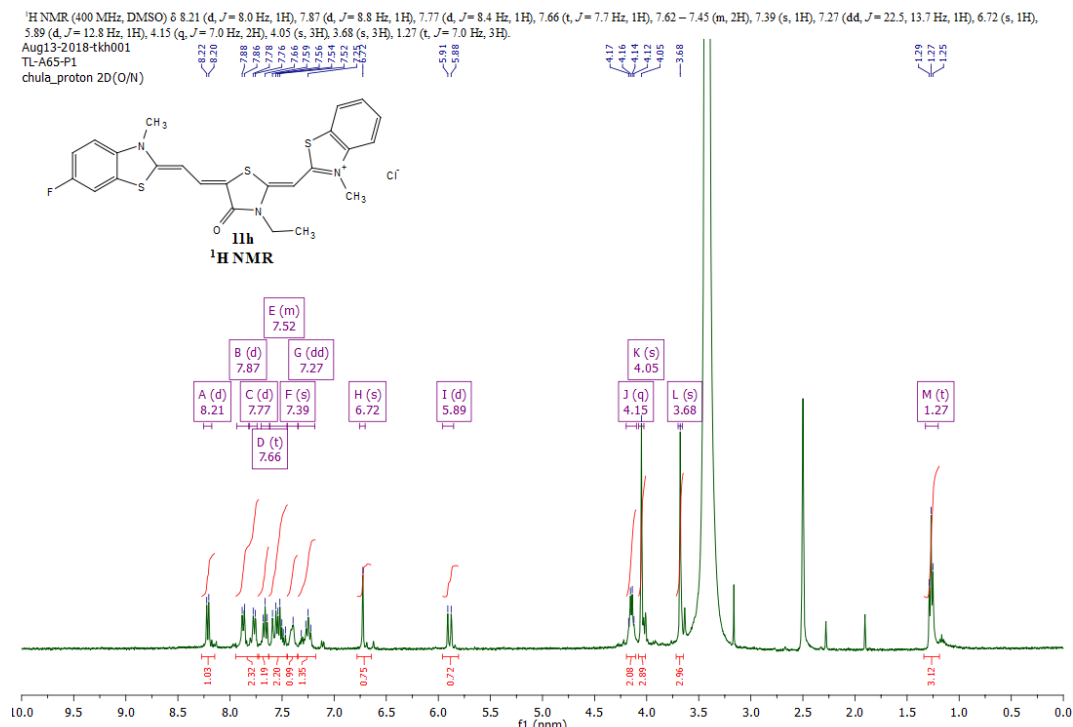


Figure 95 <sup>1</sup>H NMR spectrum of 11h

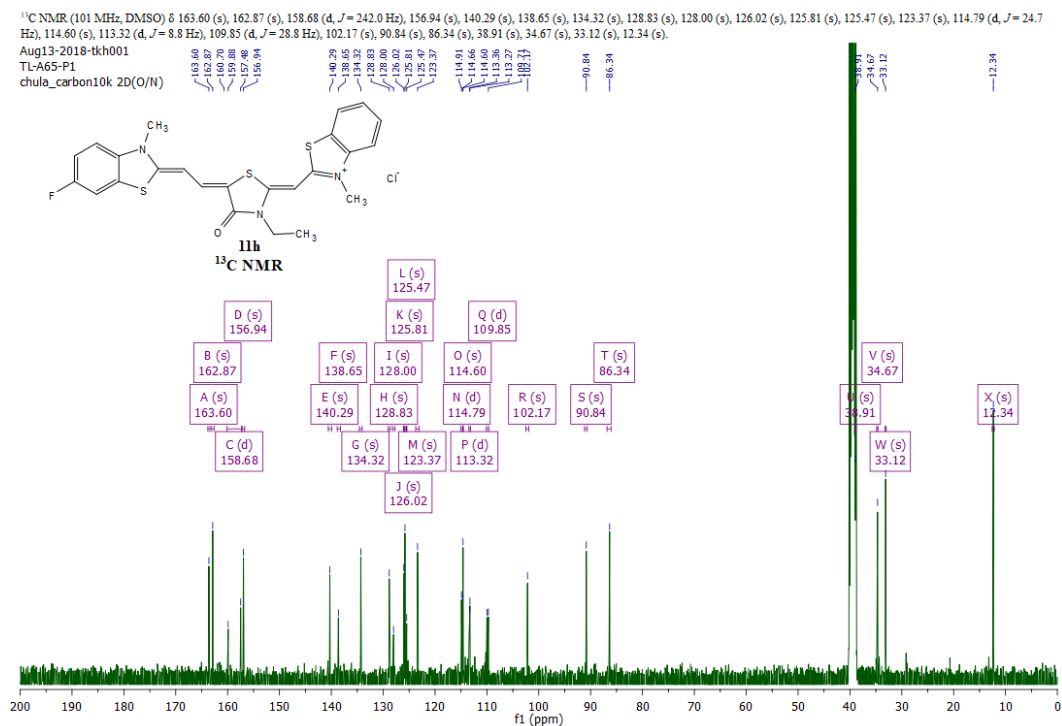
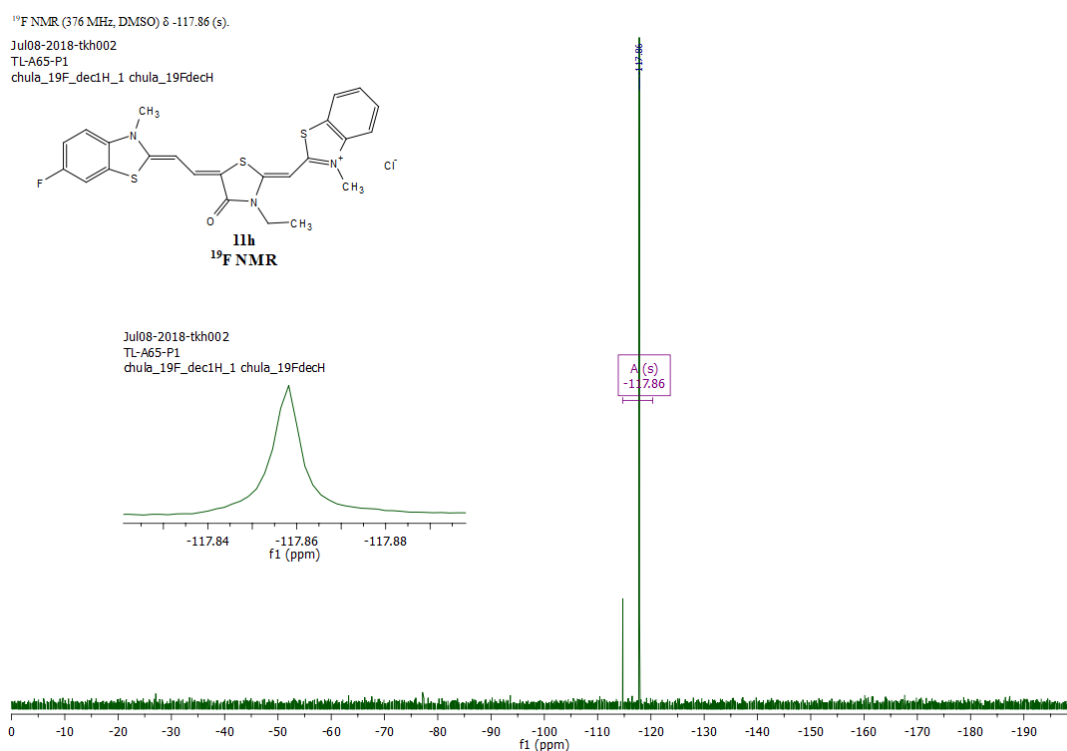
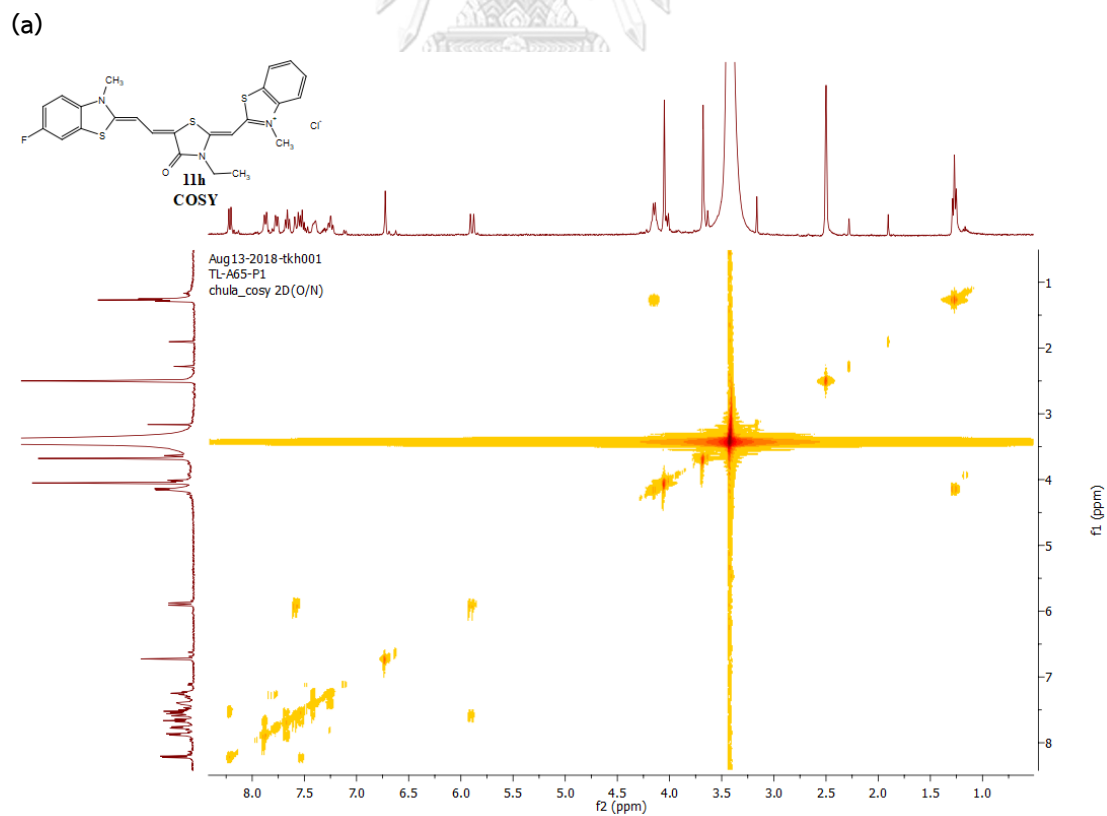
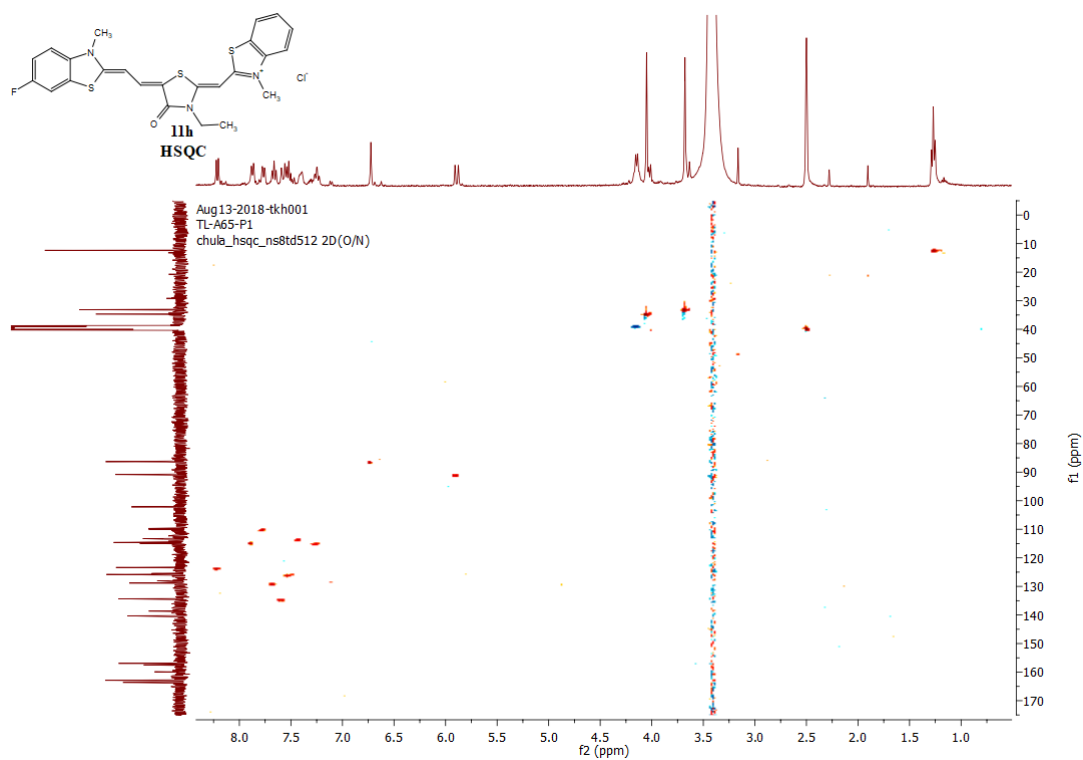


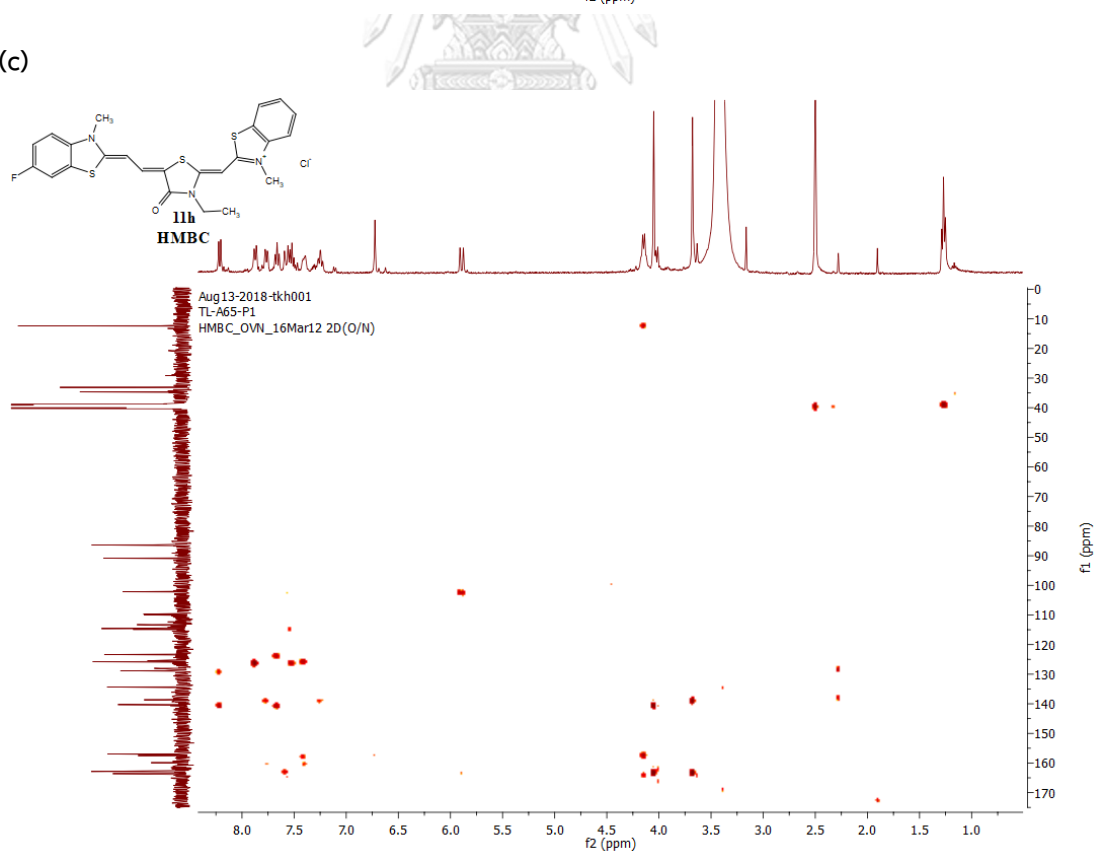
Figure 96 <sup>13</sup>C NMR spectrum of 11h

Figure 97  $^{19}\text{F}$  NMR spectrum of 11h

(b)



(c)

Figure 98 2D NMR spectra of **11h** (a) COSY; (b) HSQC; and (c) HMBC spectrum

## Mass Spectrum List Report

## Analysis Info

Analysis Name D:\Data\Data Service\190813\TL-A65-P1\_RA6\_01\_2873.d  
Method nv\_pos\_6min\_profile\_wguardcol\_190624.m  
Sample Name TL-A65-P1  
Comment

Acquisition Date 8/13/2019 4:13:49 PM

Operator CU.  
Instrument / Ser# micrOTOF-Q II 10335

## Acquisition Parameter

Source Type	ESI	Ion Polarity	Positive	Set Nebulizer	3.0 Bar
Focus	Not active	Set Capillary	4000 V	Set Dry Heater	200 °C
Scan Begin	100 m/z	Set End Plate Offset	-500 V	Set Dry Gas	8.0 l/min
Scan End	1500 m/z	Set Collision Cell RF	250.0 Vpp	Set Divert Valve	Waste

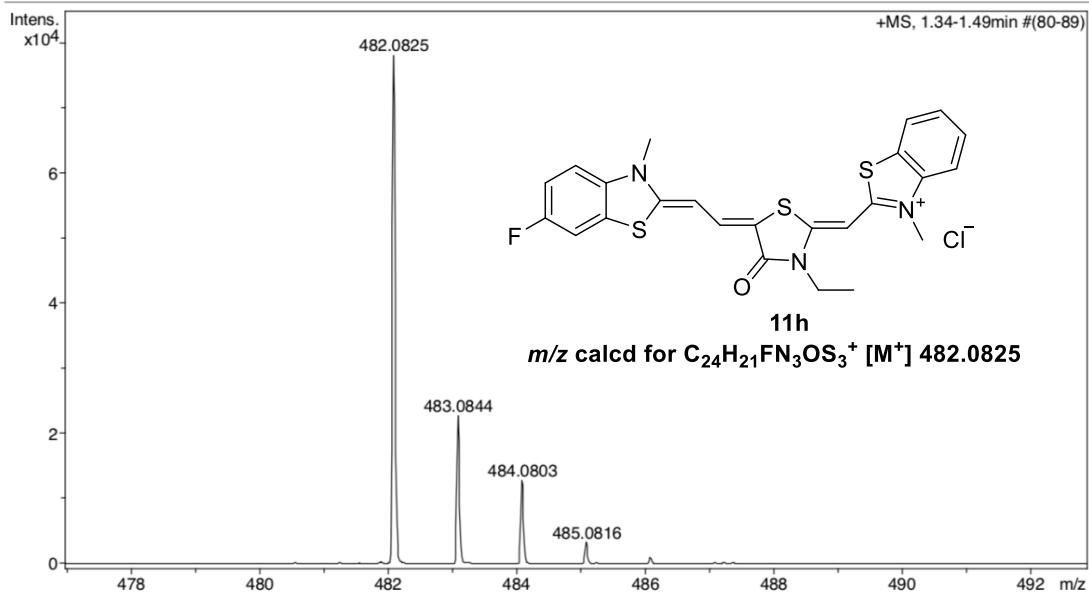


Figure 99 HRMS spectrum of 11h

2-(3-Ethyl-5-(2-(7-fluoro-3-methylbenzo[d]thiazol-2(3H)-ylidene)ethylidene)-4-oxothiazolidin-2-ylidene)methyl)-3-methylbenzo[d]thiazol-3-ium chloride (11i)

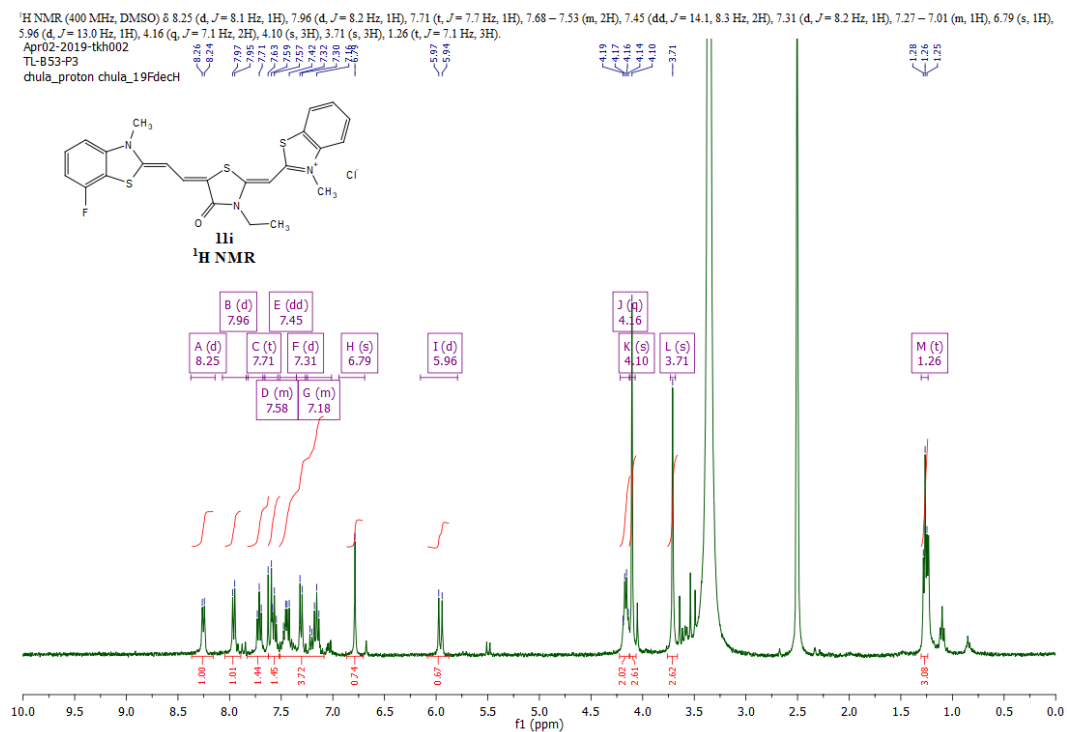


Figure 100 <sup>1</sup>H NMR spectrum of 11i

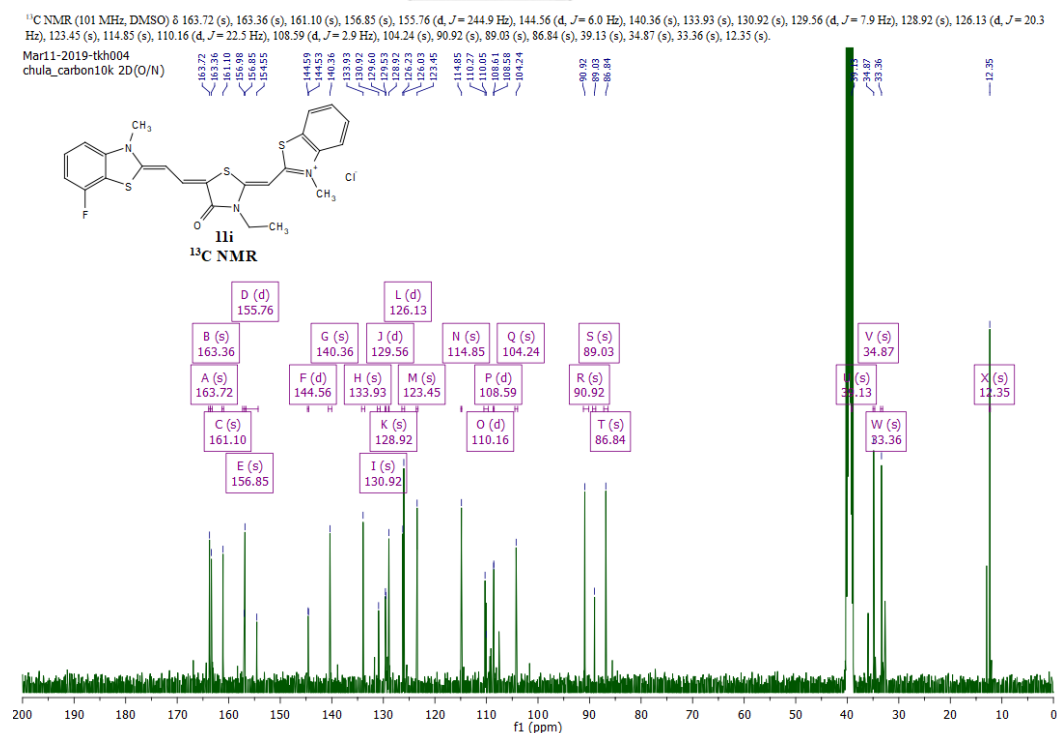
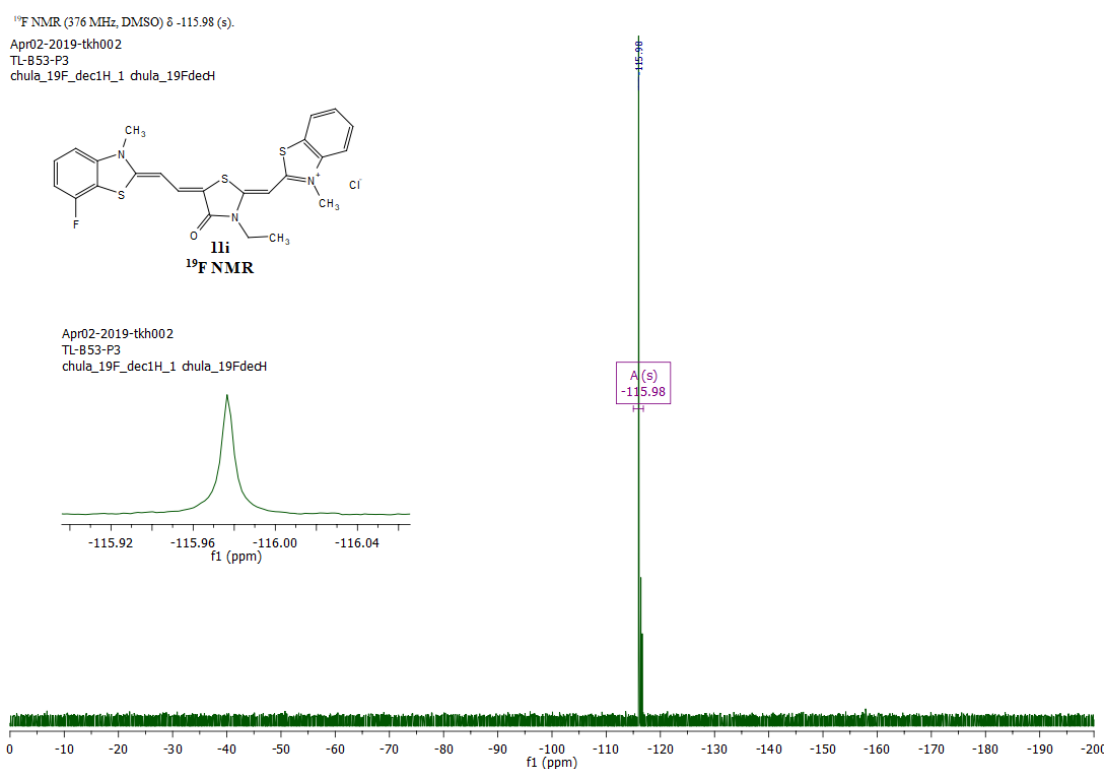
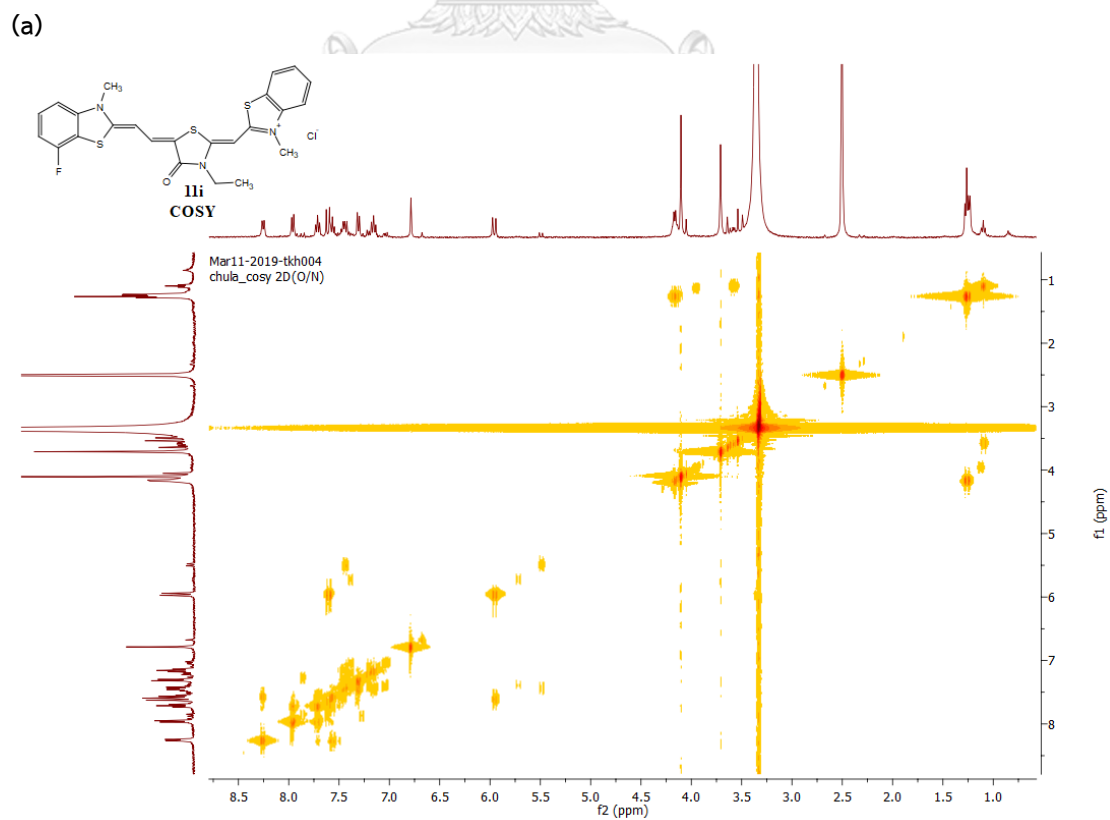
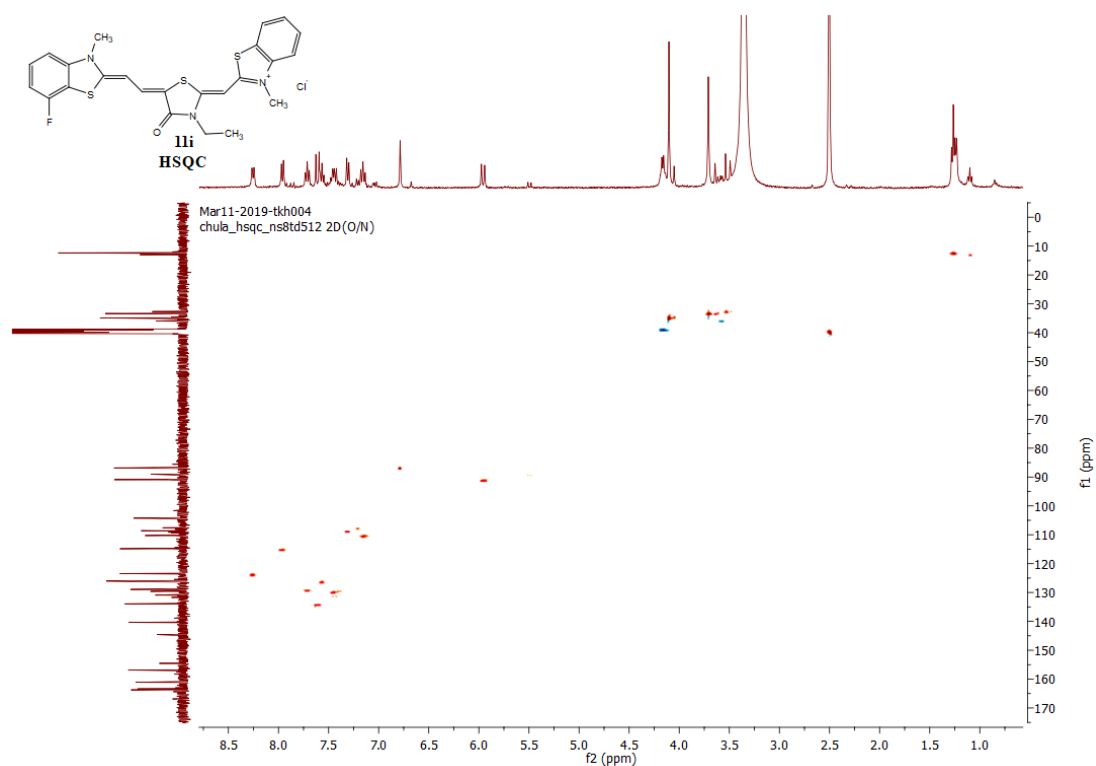


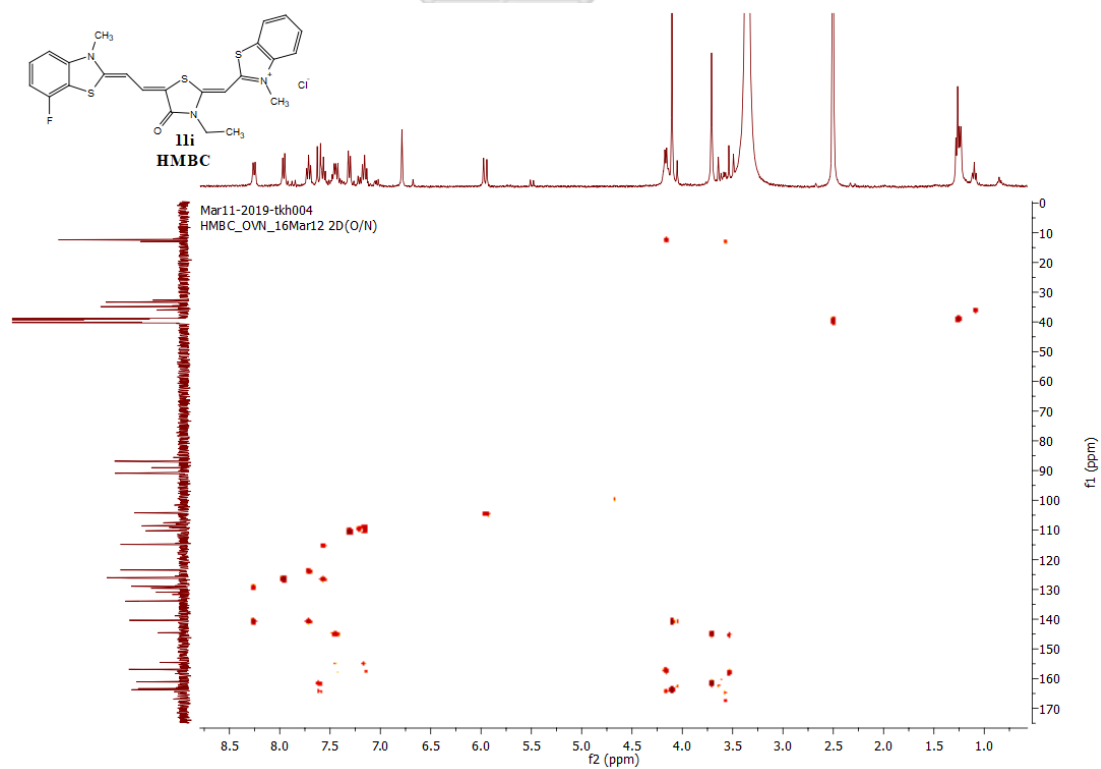
Figure 101 <sup>13</sup>C NMR spectrum of 11i

Figure 102  $^{19}\text{F}$  NMR spectrum of 11i

(b)



(c)

Figure 103 2D NMR spectra of **11i** (a) COSY; (b) HSQC; and (c) HMBC spectrum

## Mass Spectrum List Report

**Analysis Info**  
Analysis Name D:\Data\Data Service\190401\TL-B53-P1\_RC6\_01\_2448.d  
Method nv\_pos\_5min\_profile\_190214.m  
Sample Name TL-B53-P1  
Comment  
Acquisition Date 4/1/2019 8:27:30 PM  
Operator CU.  
Instrument / Ser# micrOTOF-Q II 10335

**Acquisition Parameter**

Source Type	ESI	Ion Polarity	Positive	Set Nebulizer	3.0 Bar
Focus	Not active	Set Capillary	4000 V	Set Dry Heater	200 °C
Scan Begin	100 m/z	Set End Plate Offset	-500 V	Set Dry Gas	8.0 l/min
Scan End	1500 m/z	Set Collision Cell RF	250.0 Vpp	Set Divert Valve	Waste

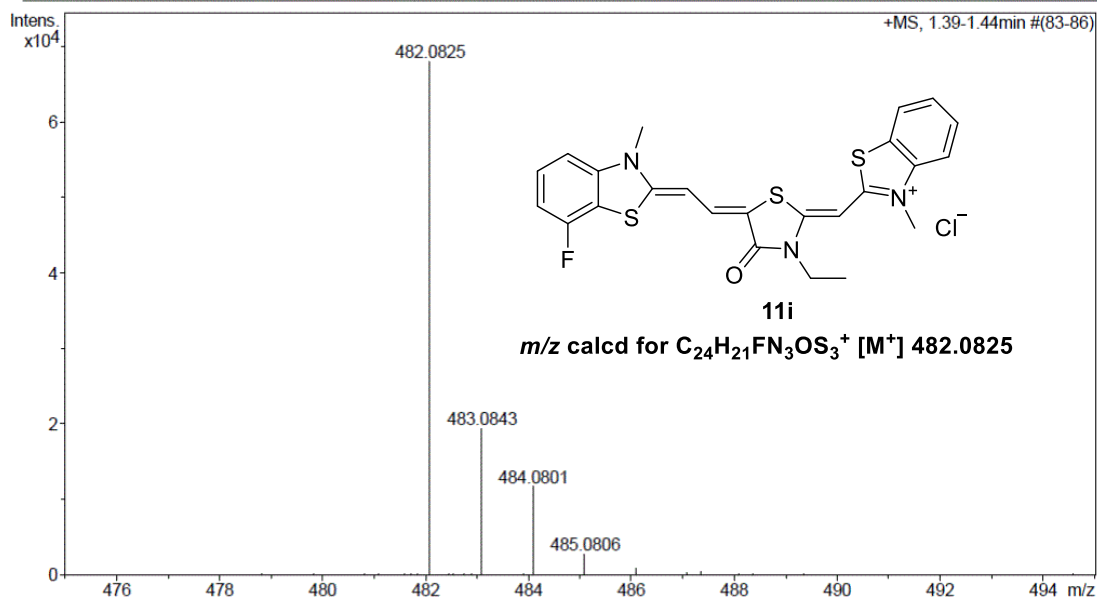


Figure 104 HRMS spectrum of 11i



2-(3-Ethyl-5-(2-(3-methylbenzo[d]thiazol-2(3H)-ylidene)ethylidene)ethylidene)-4-oxothiazolidin-2-ylidene)methyl)-3-methyl-6-(trifluoromethyl)benzo[d]thiazol-3-ium chloride (11j)

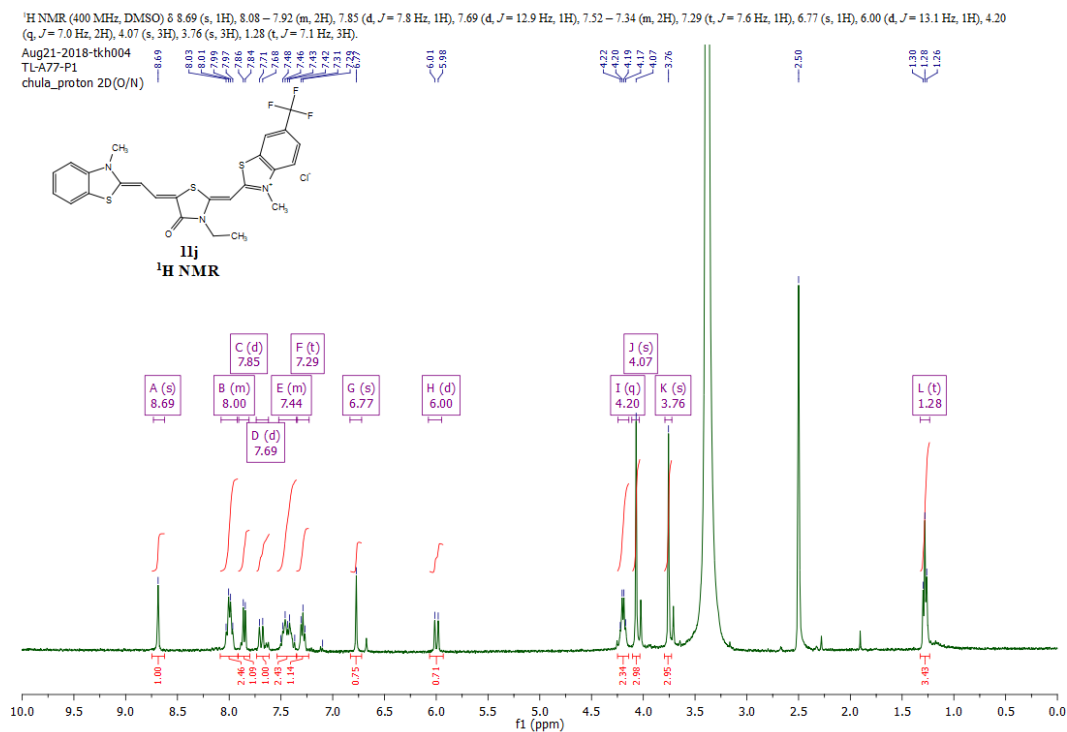


Figure 105 <sup>1</sup>H NMR spectrum of 11j

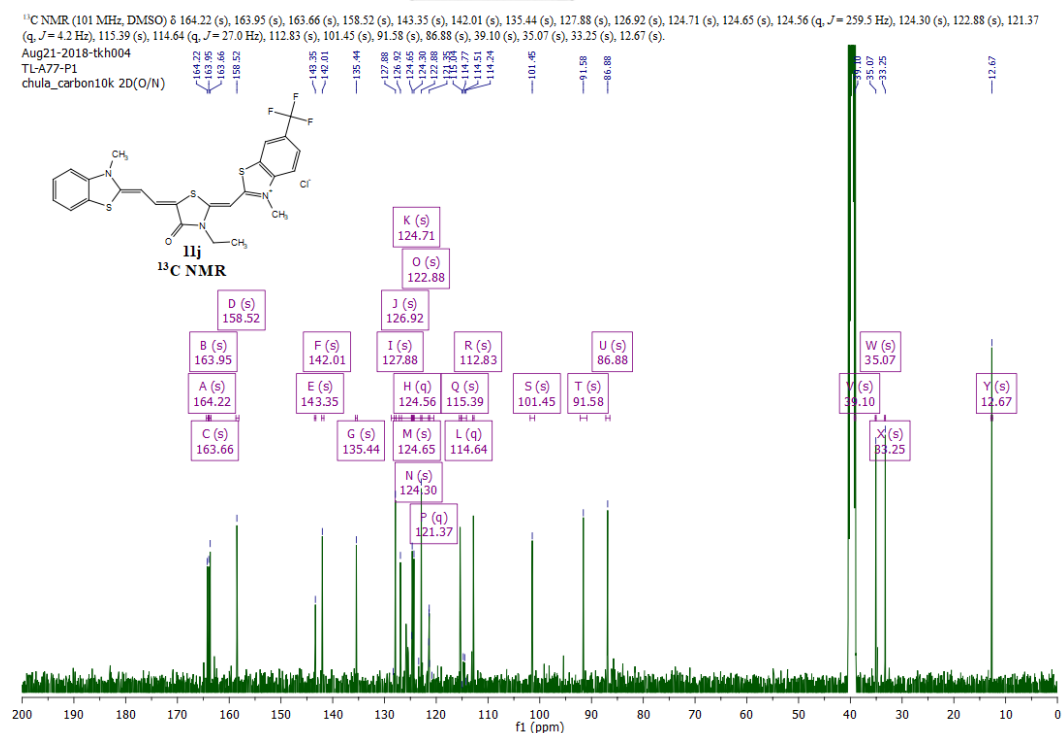
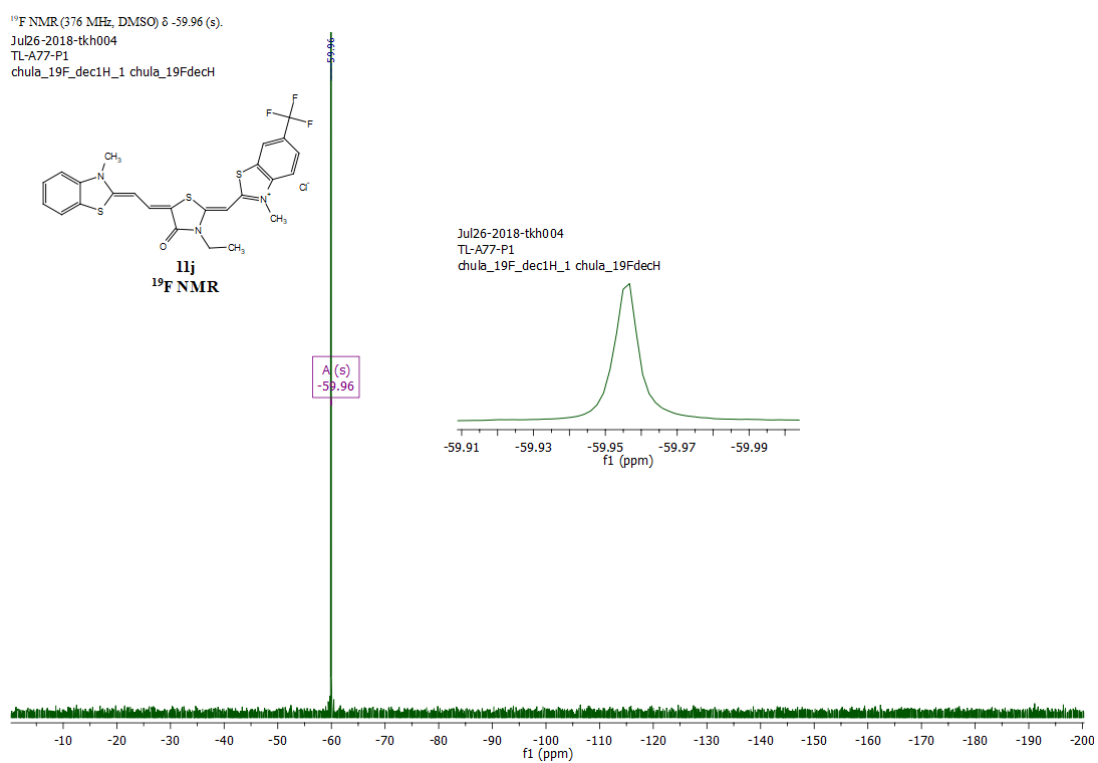
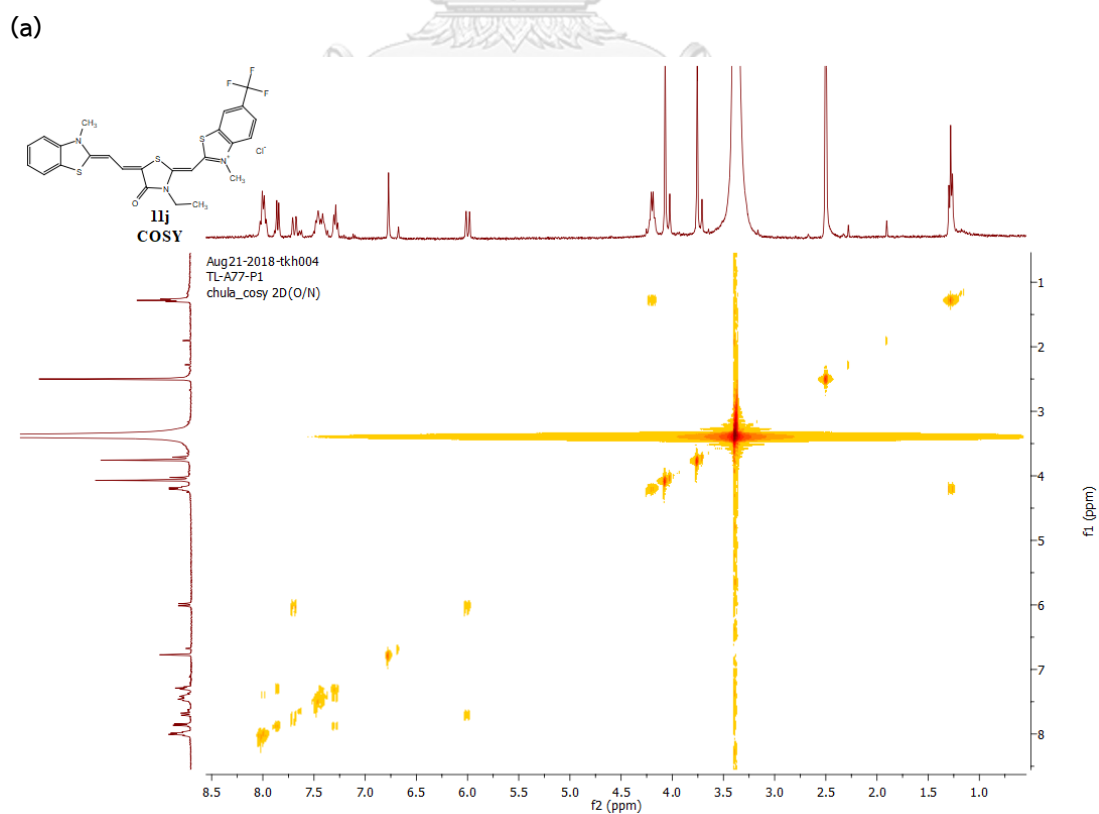
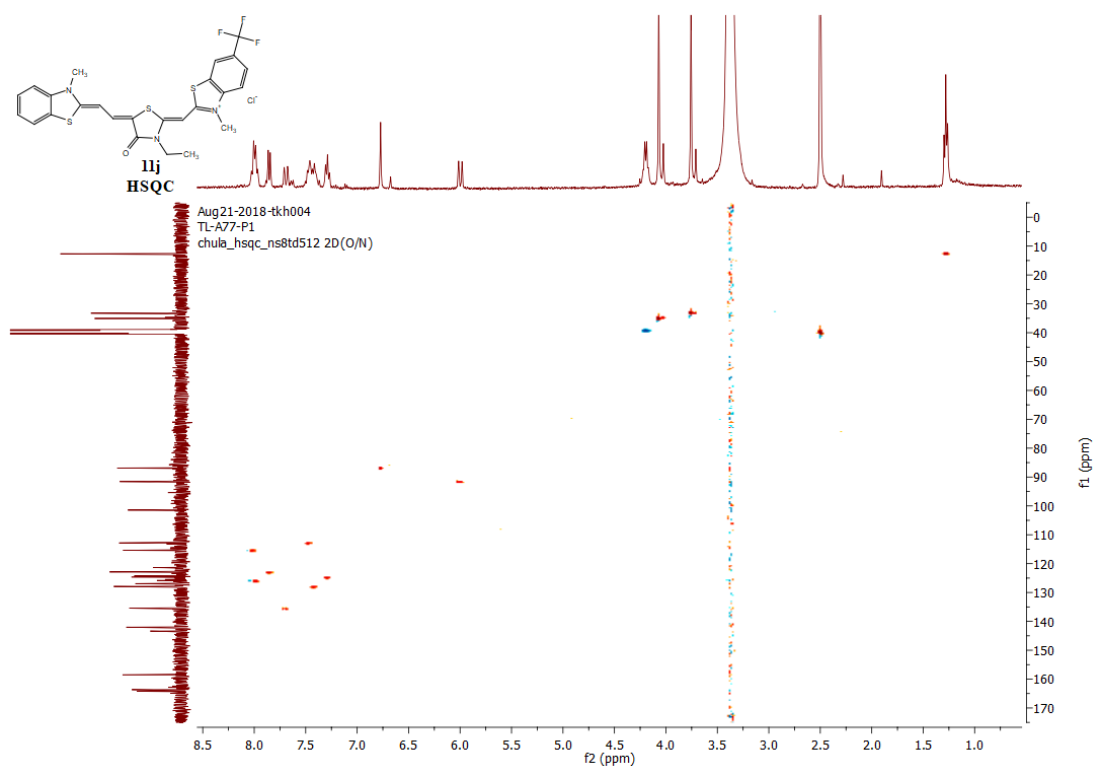


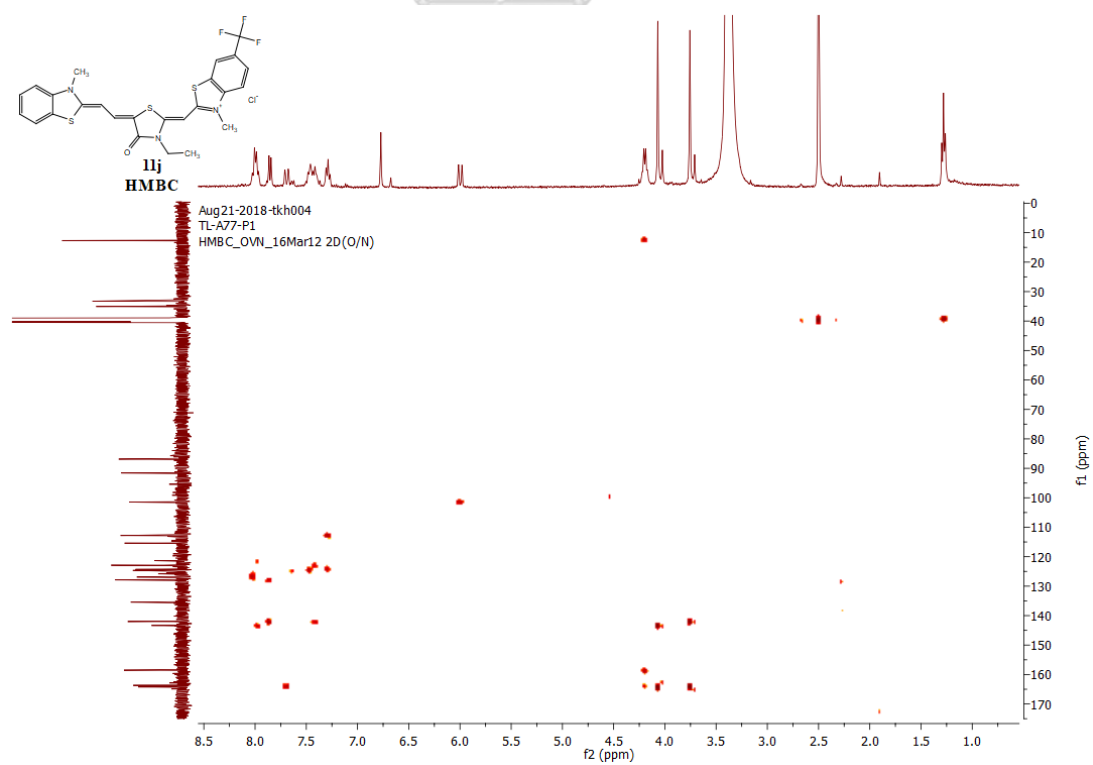
Figure 106 <sup>13</sup>C NMR spectrum of 11j

Figure 107 <sup>19</sup>F NMR spectrum of **11j**

(b)



(c)

Figure 108 2D NMR spectra of **11j** (a) COSY; (b) HSQC; and (c) HMBC spectrum

## Mass Spectrum List Report

## Analysis Info

Analysis Name D:\Data\Data Service\190401\TL-A77-P1\_RD2\_01\_2452.d  
Method nv\_pos\_5min\_profile\_190214.m  
Sample Name TL-A77-P1  
Comment

Acquisition Date 4/1/2019 8:51:13 PM

Operator CU.  
Instrument / Ser# microTOF-Q II 10335

## Acquisition Parameter

Source Type	ESI	Ion Polarity	Positive	Set Nebulizer	3.0 Bar
Focus	Not active	Set Capillary	4000 V	Set Dry Heater	200 °C
Scan Begin	100 m/z	Set End Plate Offset	-500 V	Set Dry Gas	8.0 l/min
Scan End	1500 m/z	Set Collision Cell RF	250.0 Vpp	Set Divert Valve	Waste

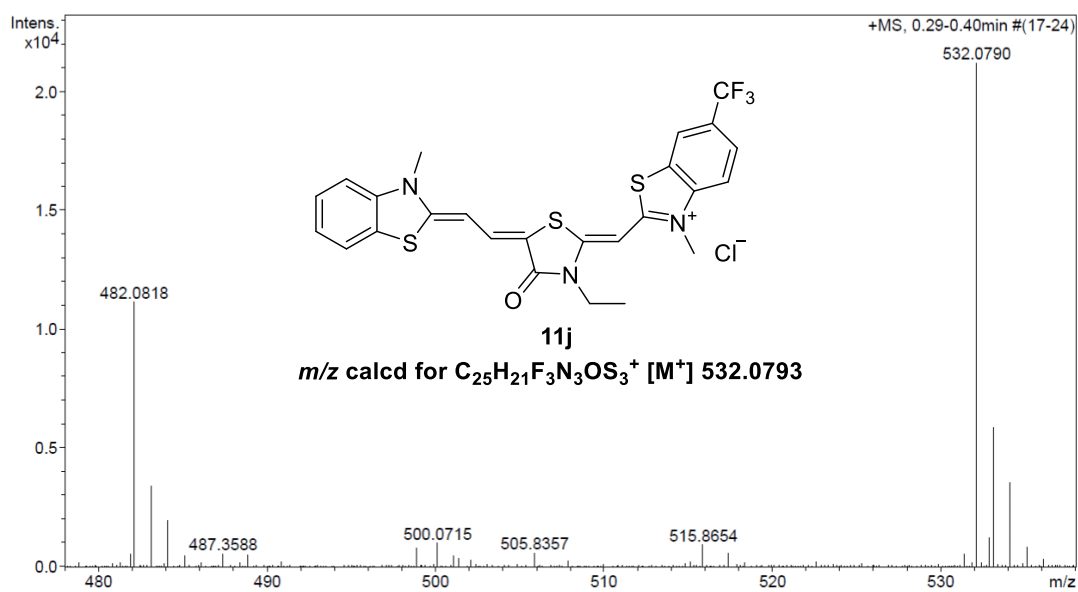


Figure 109 HRMS spectrum of 11j

2-(3-Ethyl-5-(2-(3-methylbenzo[d]thiazol-2(3H)-ylidene)ethylidene)ethylidene)-4-oxothiazolidin-2-ylidene)methyl)-3-methyl-6-(trifluoromethoxy)benzo[d]thiazol-3-ium chloride (11k)

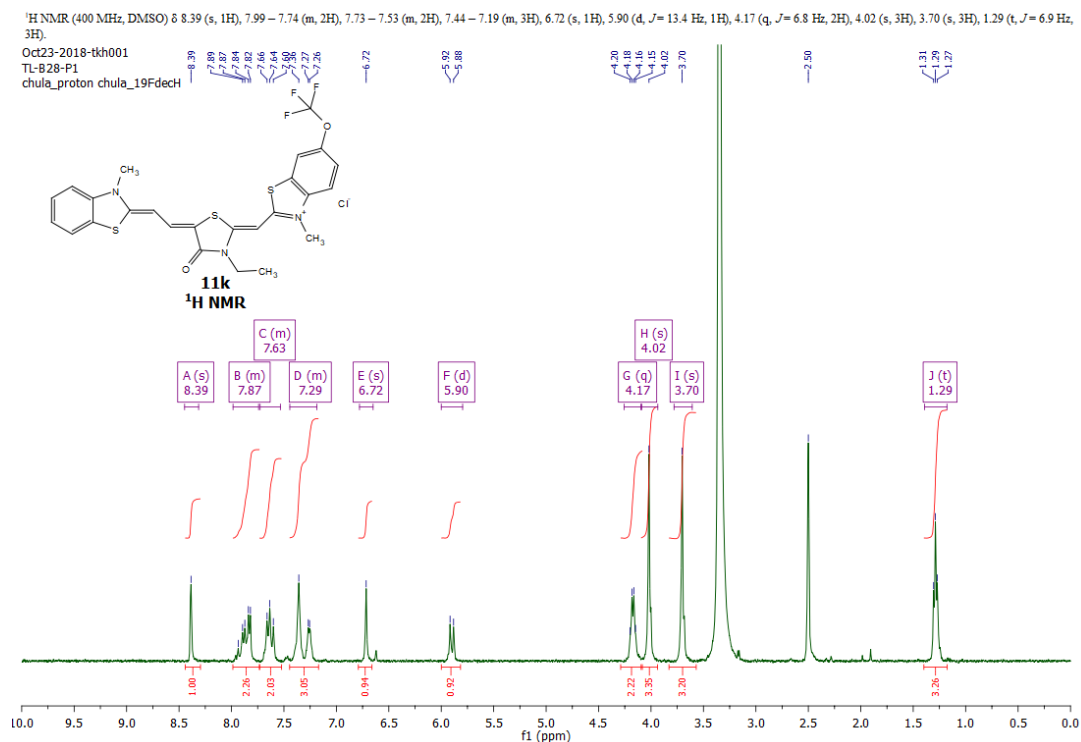


Figure 110 <sup>1</sup>H NMR spectrum of 11k

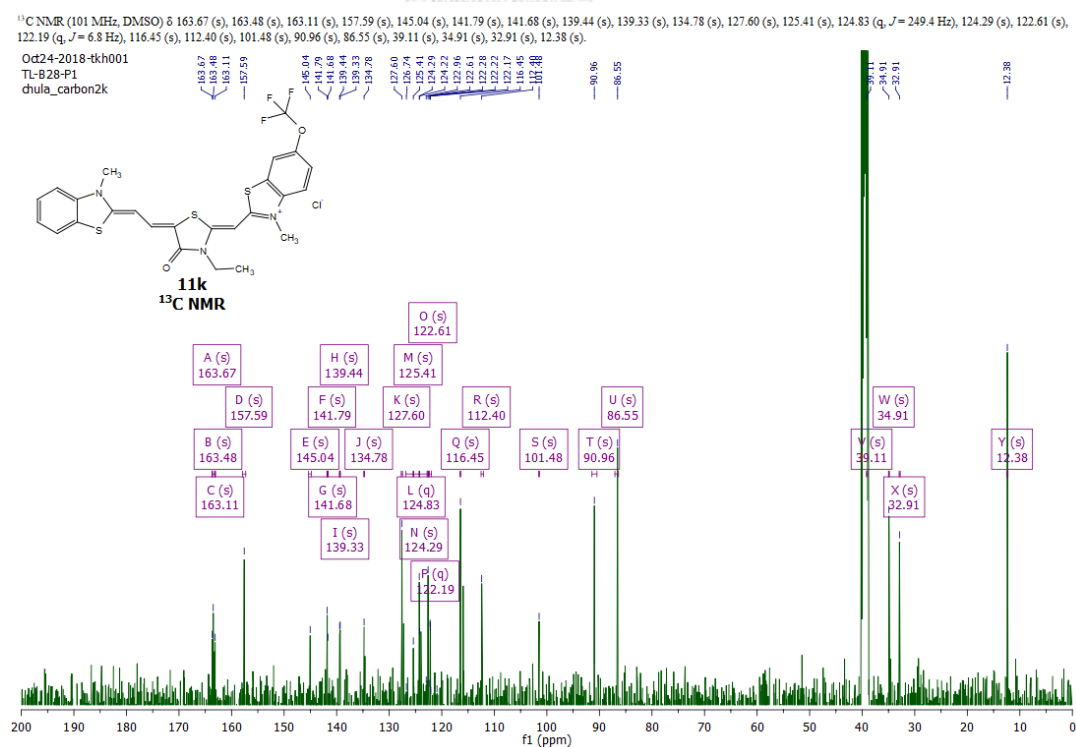
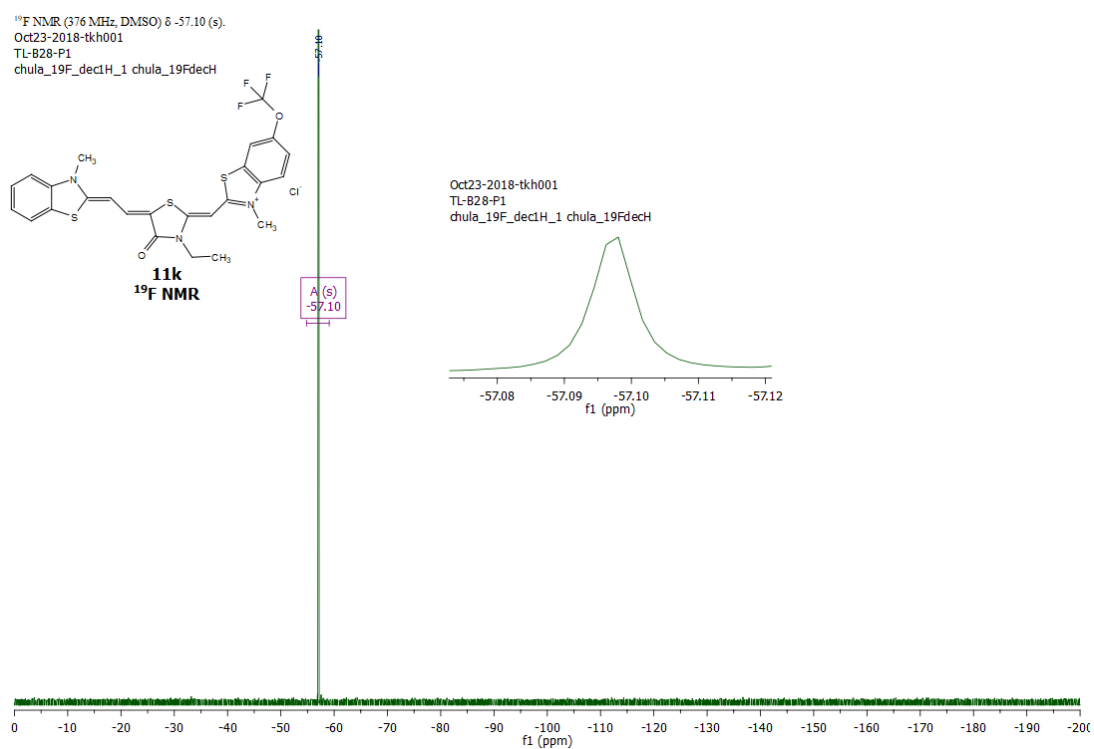
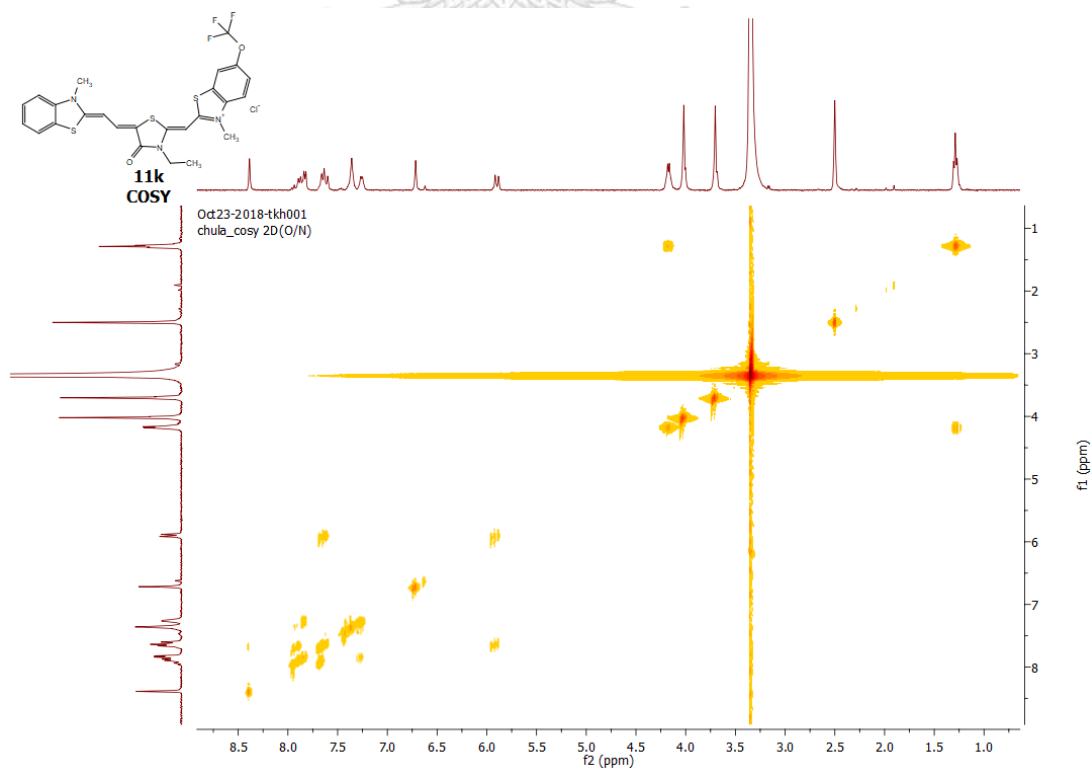


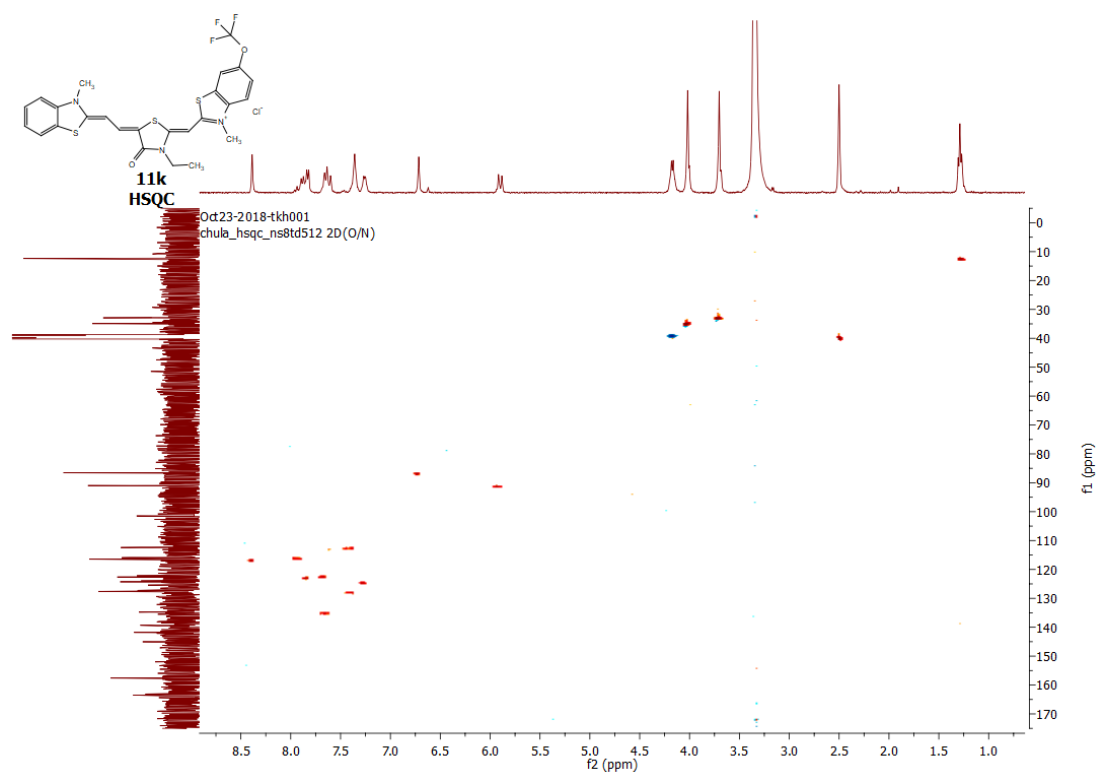
Figure 111 <sup>13</sup>C NMR spectrum of 11k

Figure 112 <sup>19</sup>F NMR spectrum of 11k

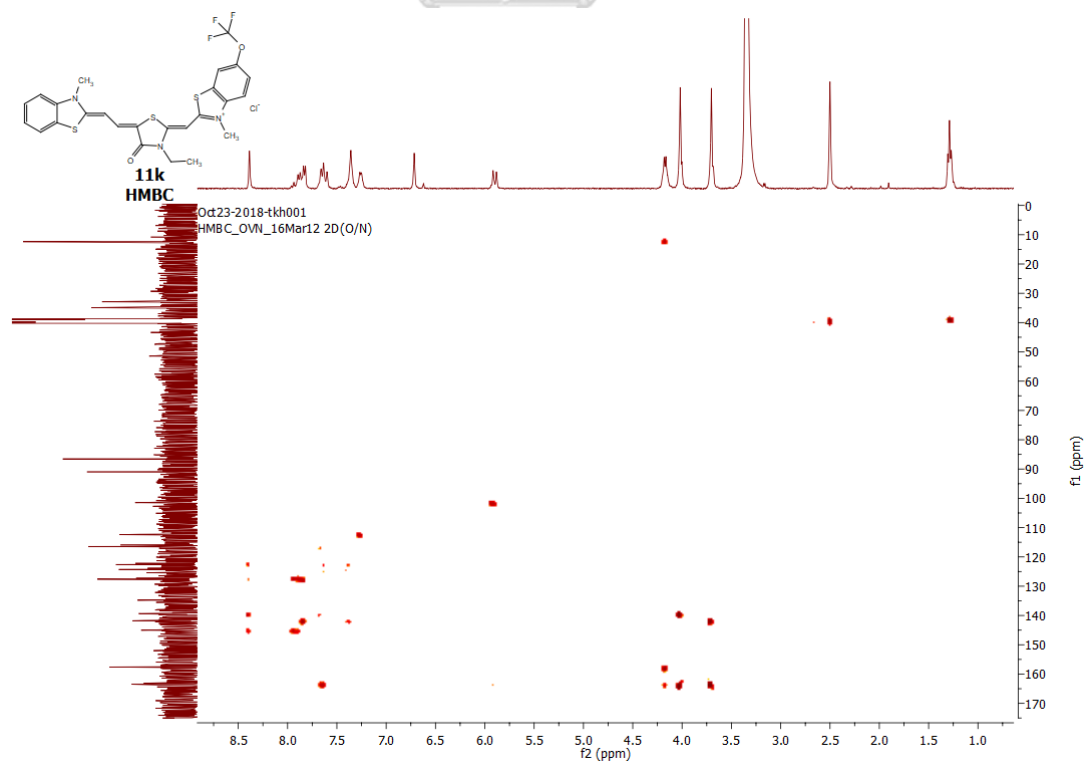
(a)



(b)



(c)

Figure 113 2D NMR spectra of **11k** (a) COSY; (b) HSQC; and (c) HMBC spectrum

## Mass Spectrum List Report

**Analysis Info**  
Analysis Name D:\Data\Data Service\190318\TL-B28-P1\_RD3\_01\_2346.d  
Method nv\_pos\_5min\_profile\_190214.m  
Sample Name TL-B28-P1  
Comment  
Acquisition Date 3/18/2019 10:18:35 PM  
Operator CU.  
Instrument / Ser# micrOTOF-Q II 10335

**Acquisition Parameter**

Source Type	ESI	Ion Polarity	Positive	Set Nebulizer	3.0 Bar
Focus	Not active	Set Capillary	4000 V	Set Dry Heater	200 °C
Scan Begin	100 m/z	Set End Plate Offset	-500 V	Set Dry Gas	8.0 l/min
Scan End	1500 m/z	Set Collision Cell RF	250.0 Vpp	Set Divert Valve	Waste

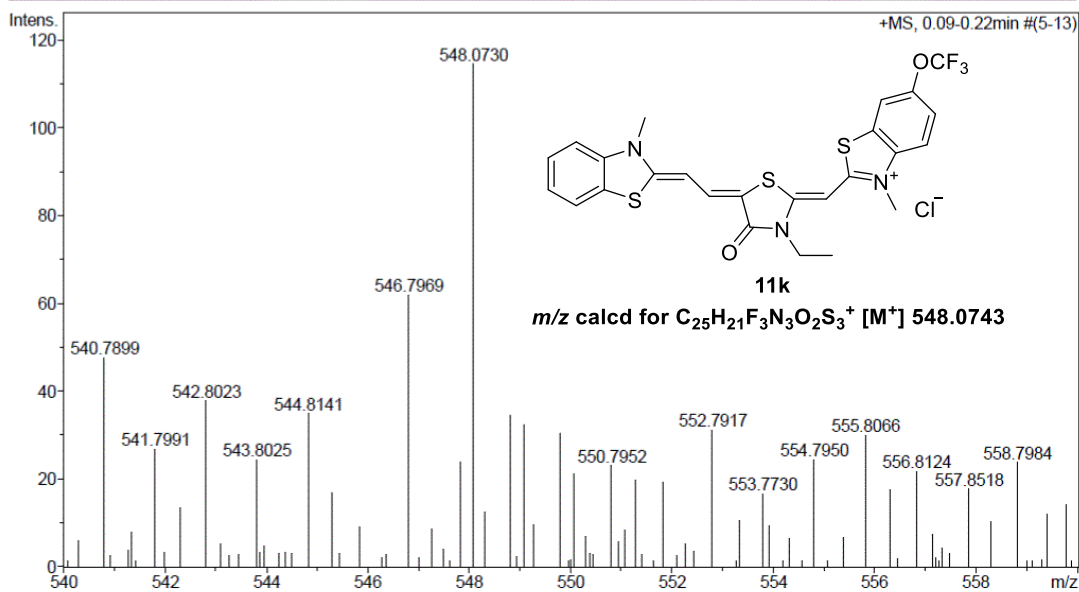


Figure 114 HRMS spectrum of 11k



2-(3-Ethyl-5-(2-(3-methylbenzo[d]thiazol-2(3H)-ylidene)ethylidene)ethylidene)-4-oxothiazolidin-2-ylidene)methyl)-5,6-difluoro-3-methylbenzo[d]thiazol-3-ium chloride (11l)

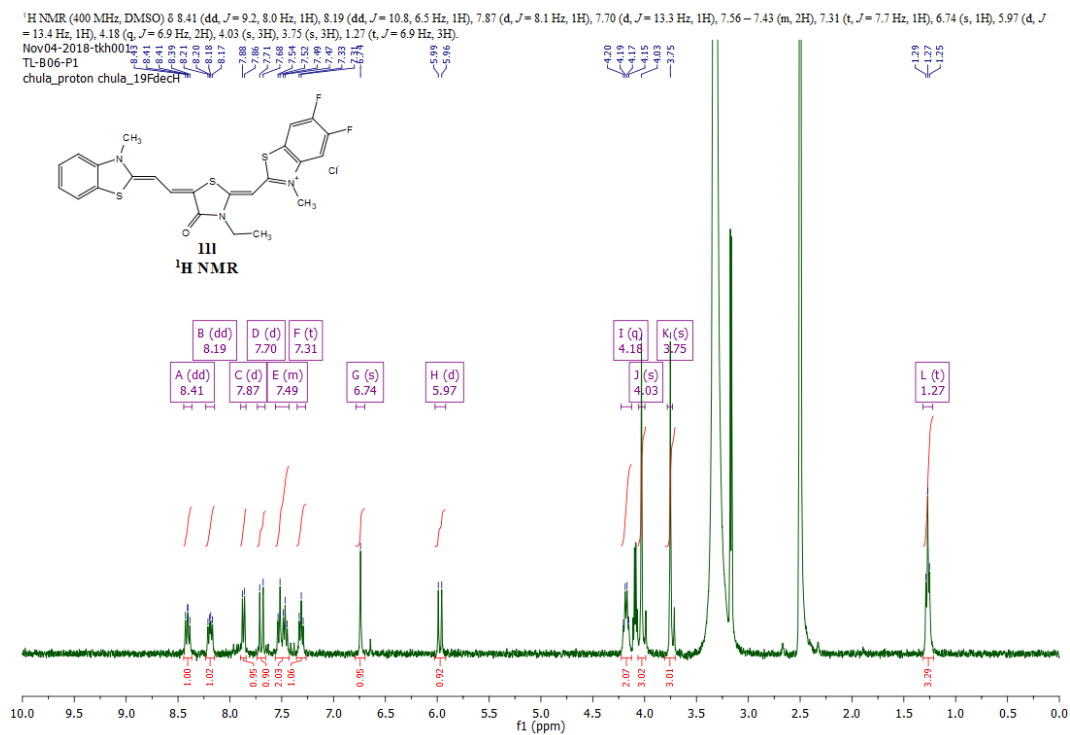


Figure 115 <sup>1</sup>H NMR spectrum of 11l

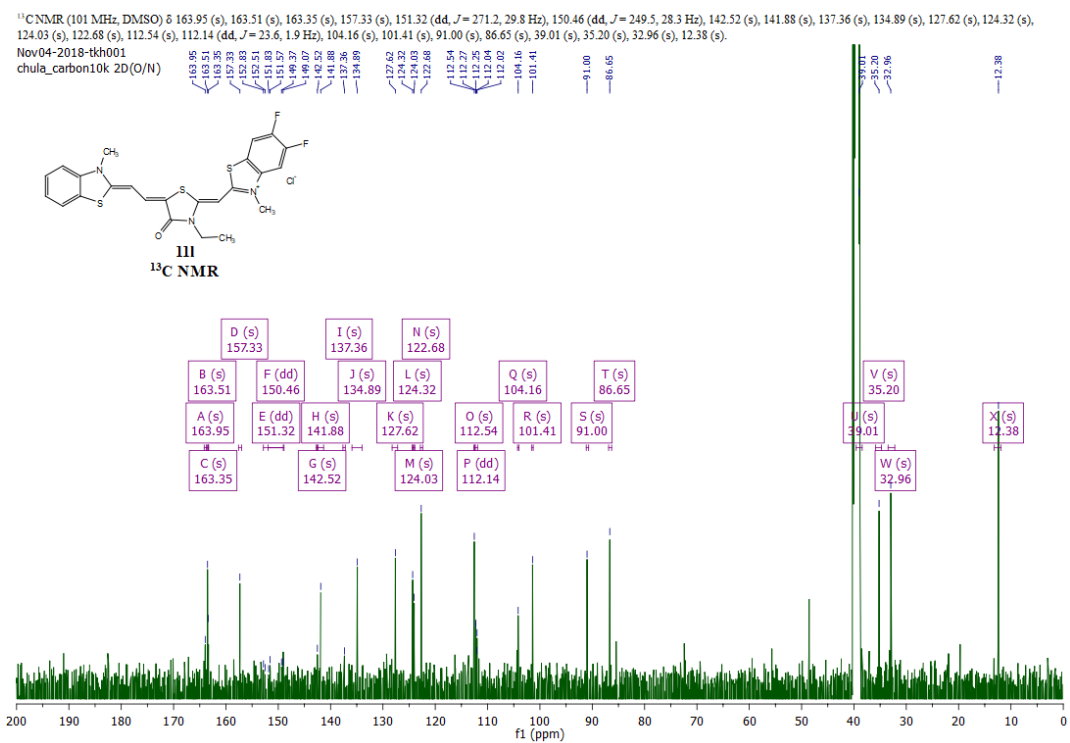


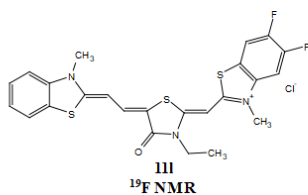
Figure 116 <sup>13</sup>C NMR spectrum of 11l

$^{19}\text{F}$  NMR (376 MHz, DMSO)  $\delta$  -134.60 (d,  $J = 22.2$  Hz), -138.72 (d,  $J = 22.1$  Hz).

Nov04-2018-tkh001

TL-B06-P1

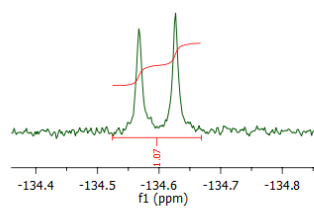
chula\_19F\_dec1H\_1 chula\_19FdecH



Nov04-2018-tkh001

TL-B06-P1

chula\_19F\_dec1H\_1 chula\_19FdecH



Nov04-2018-tkh001

TL-B06-P1

chula\_19F\_dec1H\_1 chula\_19FdecH

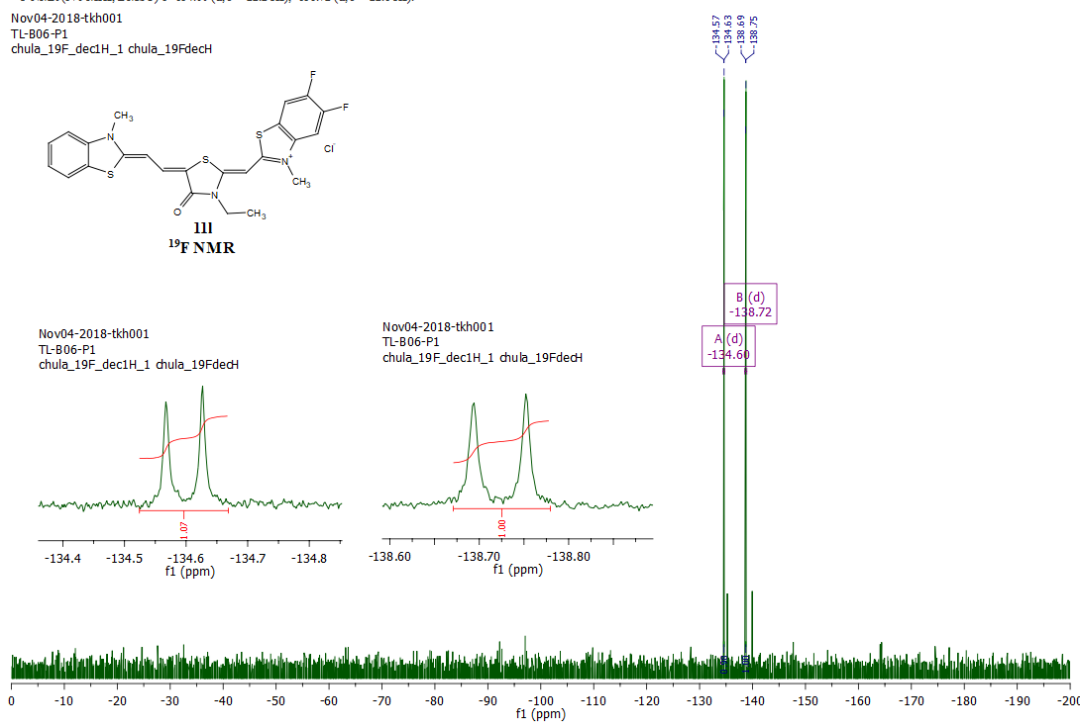
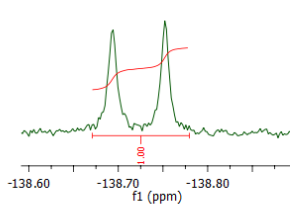
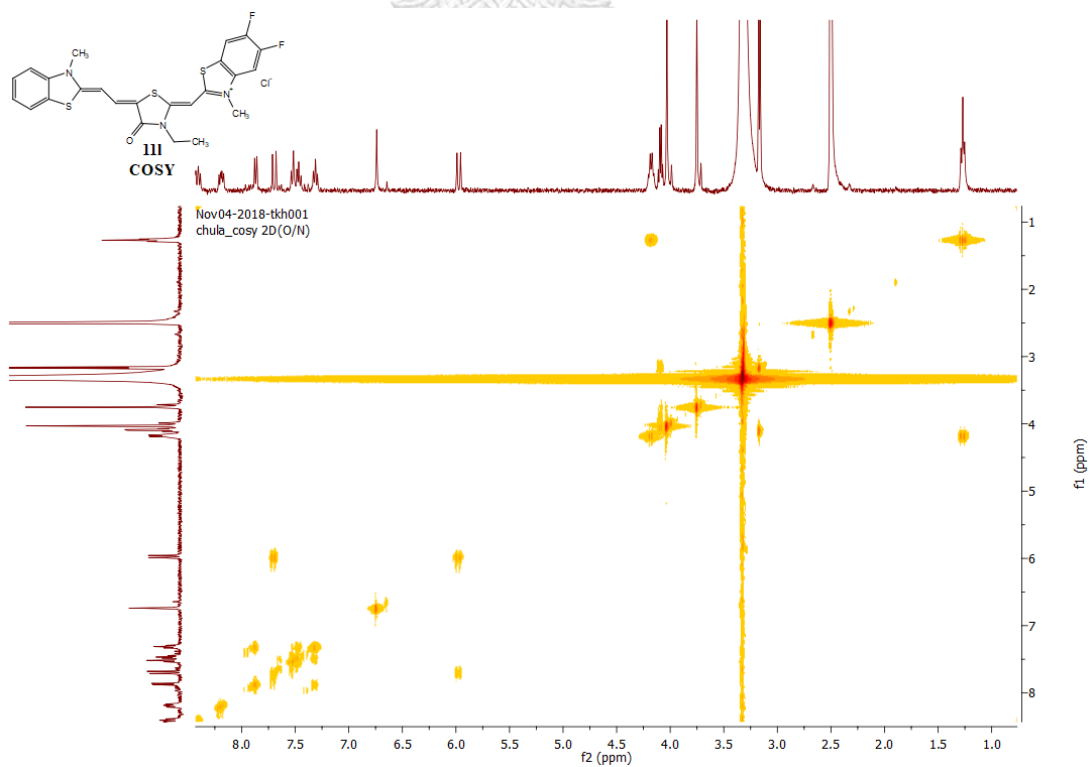
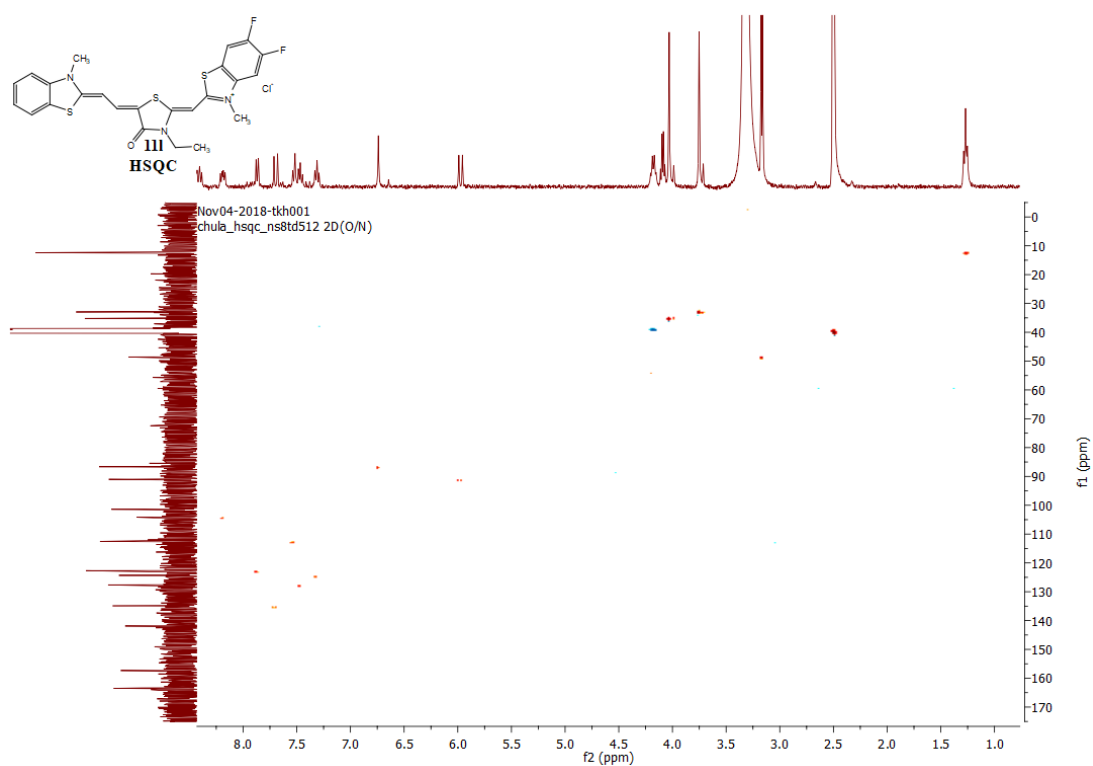


Figure 117  $^{19}\text{F}$  NMR spectrum of 11L

(a)



(b)



(c)

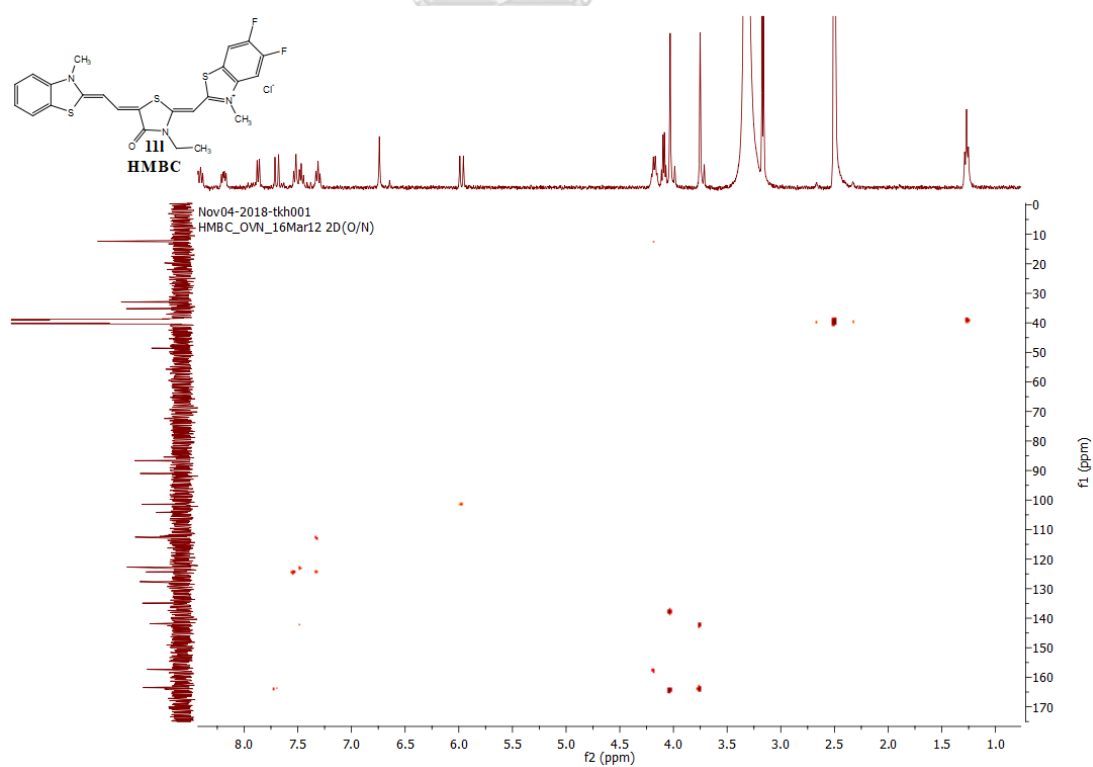


Figure 118 2D NMR spectra of 11l (a) COSY; (b) HSQC; and (c) HMBC spectrum

## Mass Spectrum List Report

## Analysis Info

Analysis Name D:\Data\Data Service\190318\TL-B06-P1\_RD1\_01\_2343.d  
Method nv\_pos\_5min\_profile\_190214.m  
Sample Name TL-B06-P1  
Comment

Acquisition Date 3/18/2019 9:59:17 PM

Operator CU.  
Instrument / Ser# microTOF-Q II 10335

## Acquisition Parameter

Source Type	ESI	Ion Polarity	Positive	Set Nebulizer	3.0 Bar
Focus	Not active	Set Capillary	4000 V	Set Dry Heater	200 °C
Scan Begin	100 m/z	Set End Plate Offset	-500 V	Set Dry Gas	8.0 l/min
Scan End	1500 m/z	Set Collision Cell RF	250.0 Vpp	Set Divert Valve	Waste

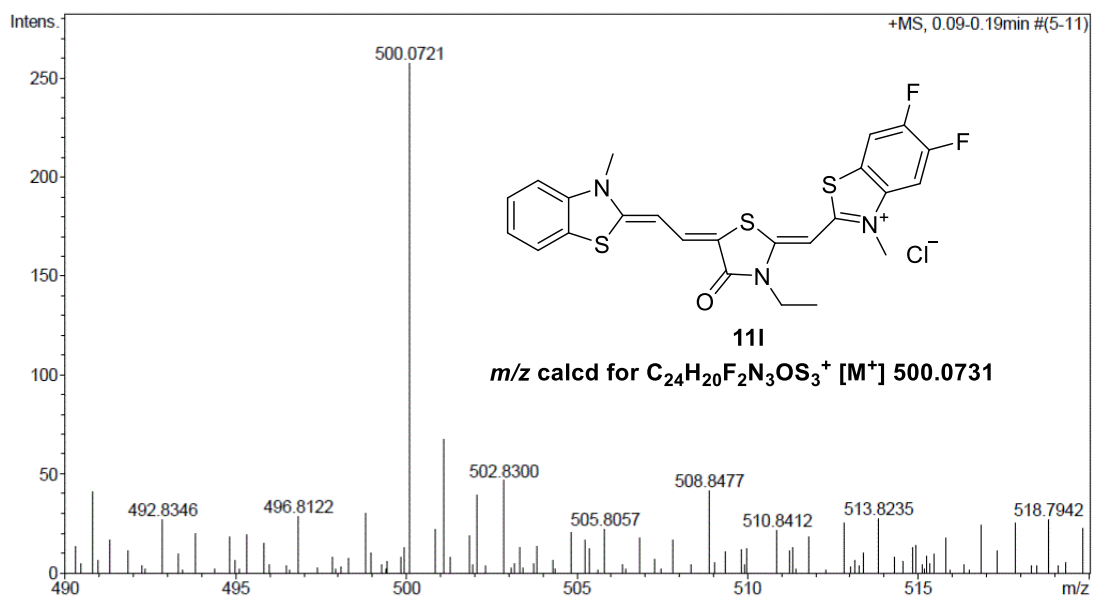


Figure 119 HRMS spectrum of 11l

2-(3-Ethyl-5-(2-(5-fluoro-3-methylbenzo[d]thiazol-2(3H)-ylidene)ethylidene)-4-oxothiazolidin-2-ylidene)methyl)-5-fluoro-3-methylbenzo[d]thiazol-3-ium chloride (11m)

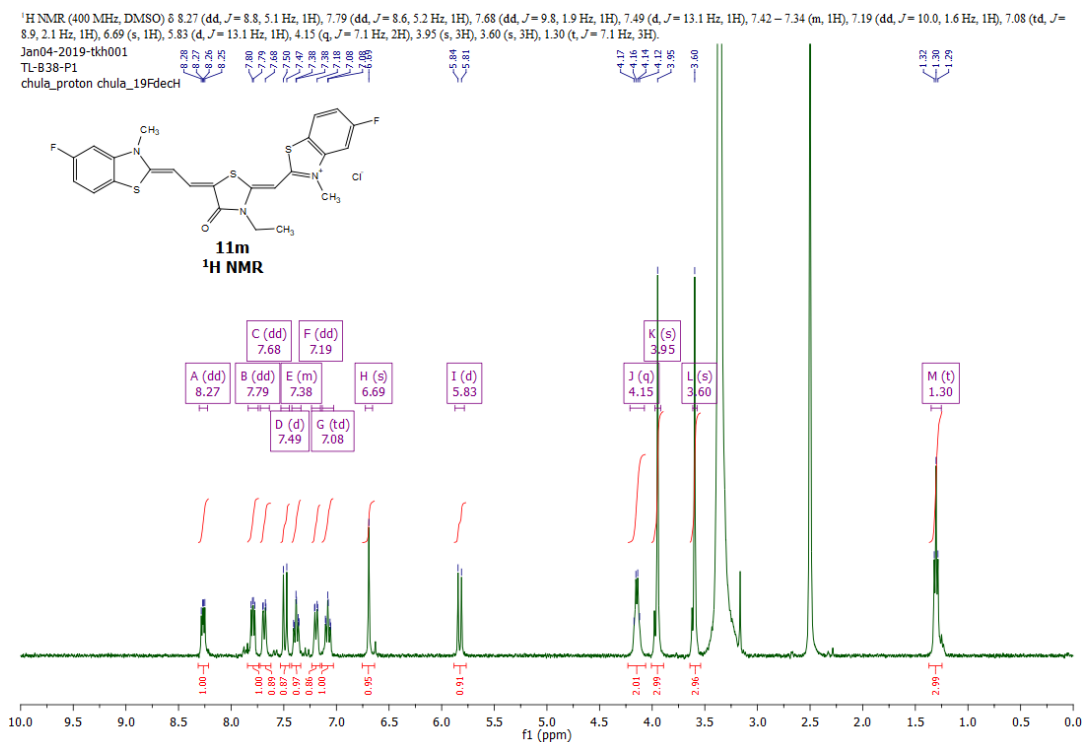


Figure 120 <sup>1</sup>H NMR spectrum of 11m

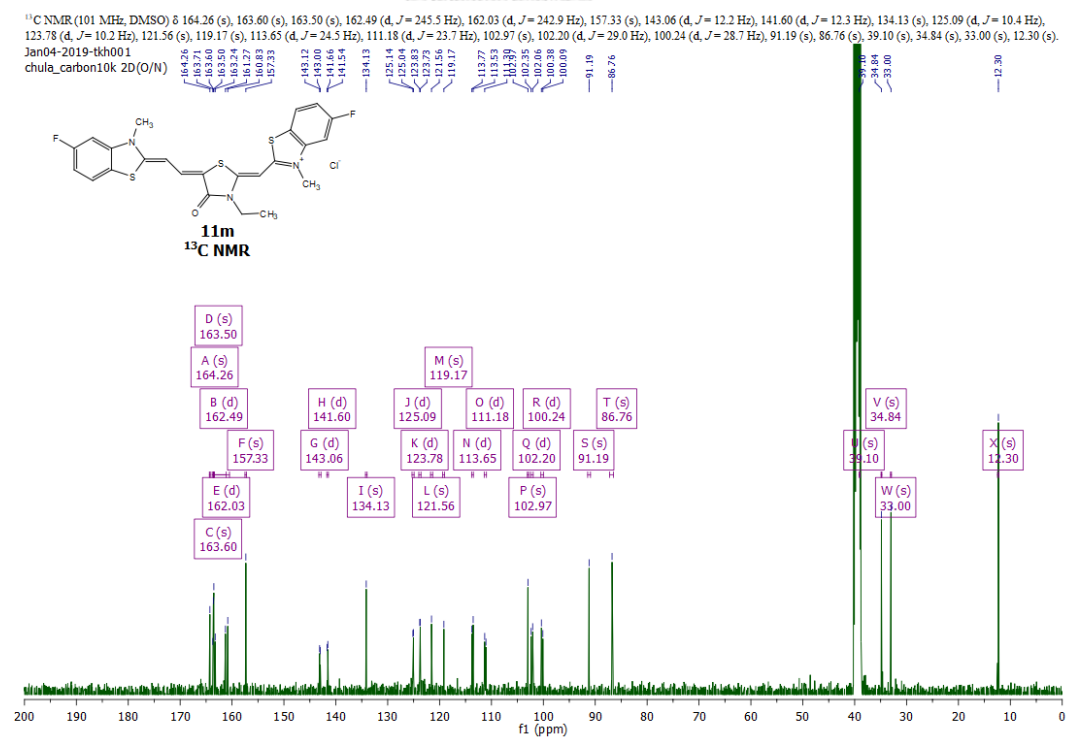
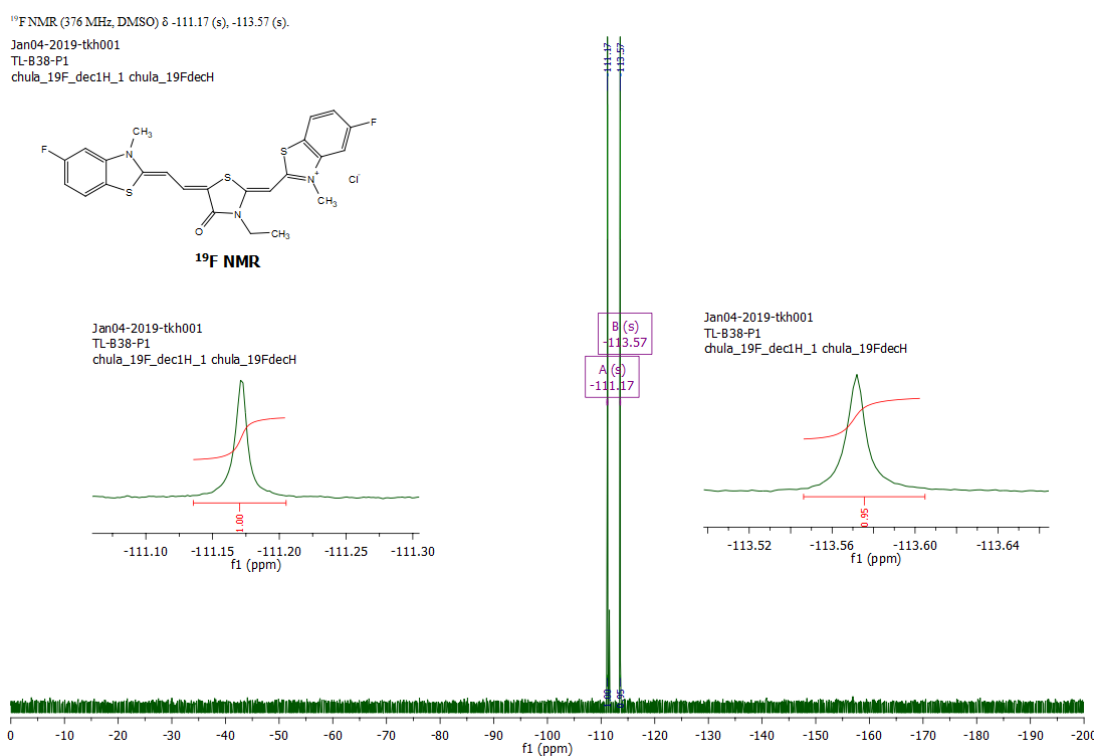
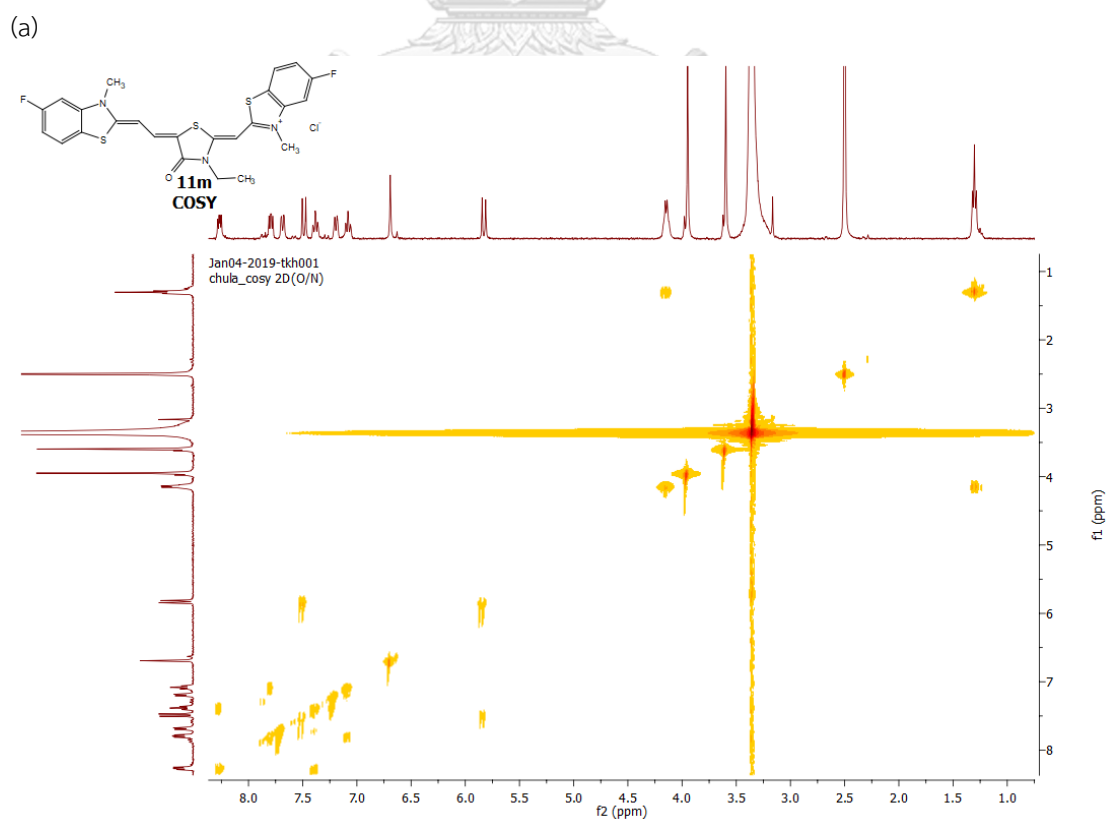
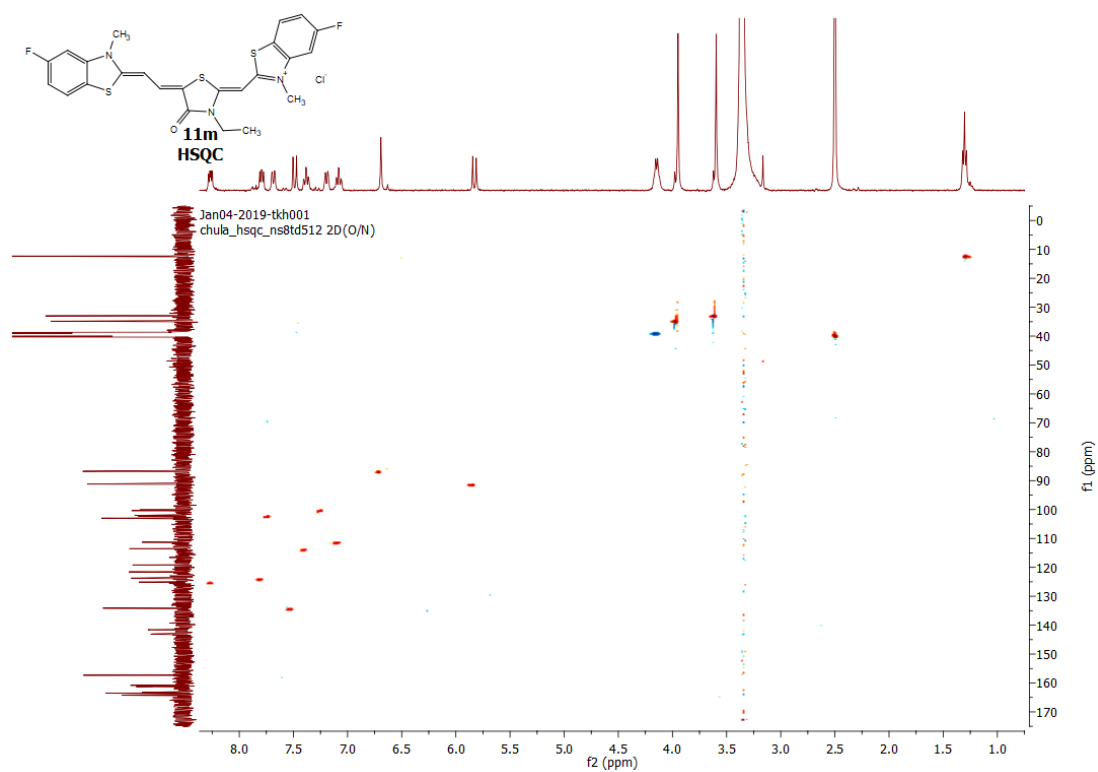


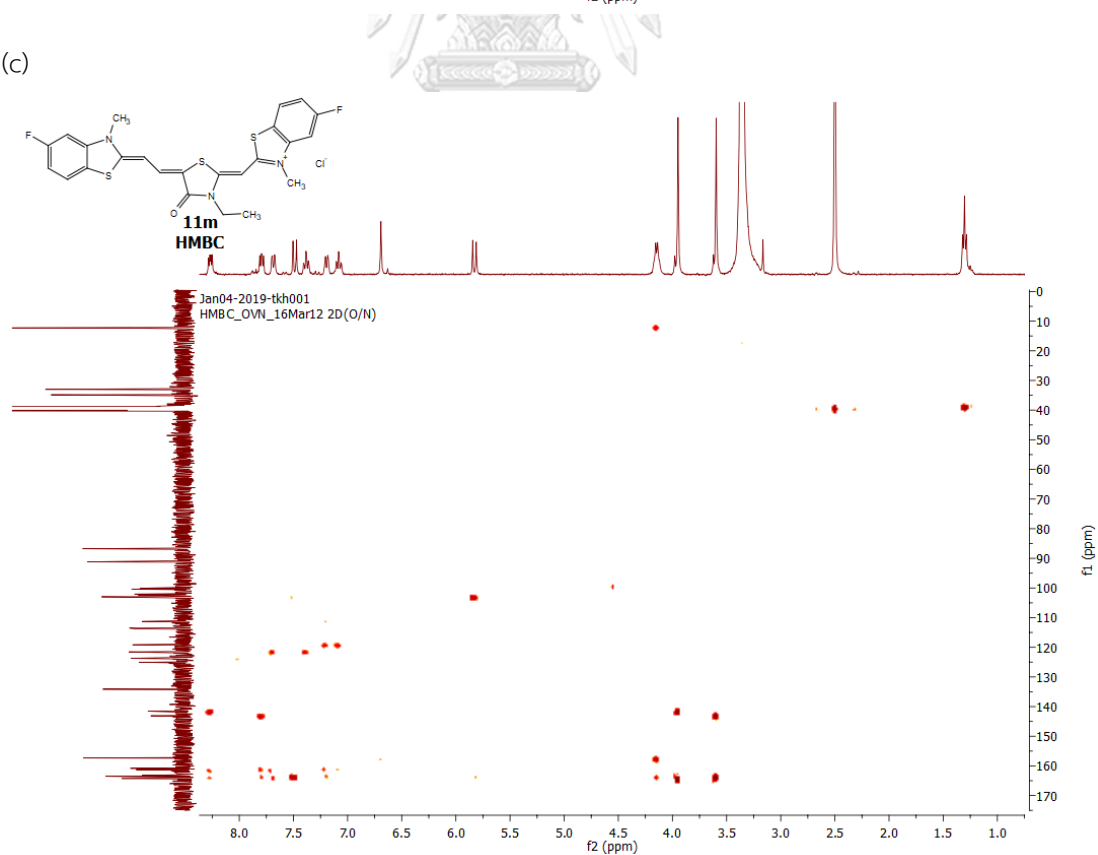
Figure 121 <sup>13</sup>C NMR spectrum of 11m

Figure 122 <sup>19</sup>F NMR spectrum of 11m

(b)



(c)

Figure 123 2D NMR spectra of **11m** (a) COSY; (b) HSQC; and (c) HMBC spectrum

## Mass Spectrum List Report

**Analysis Info**  
Analysis Name D:\Data\Data Service\190318\TL-B38-P1\_RD4\_01\_2347.d  
Method nv\_pos\_5min\_profile\_190214.m  
Sample Name TL-B38-P1  
Comment  
Acquisition Date 3/18/2019 10:25:02 PM  
Operator CU.  
Instrument / Ser# microTOF-Q II 10335

**Acquisition Parameter**

Source Type	ESI	Ion Polarity	Positive	Set Nebulizer	3.0 Bar
Focus	Not active	Set Capillary	4000 V	Set Dry Heater	200 °C
Scan Begin	100 m/z	Set End Plate Offset	-500 V	Set Dry Gas	8.0 l/min
Scan End	1500 m/z	Set Collision Cell RF	250.0 Vpp	Set Divert Valve	Waste

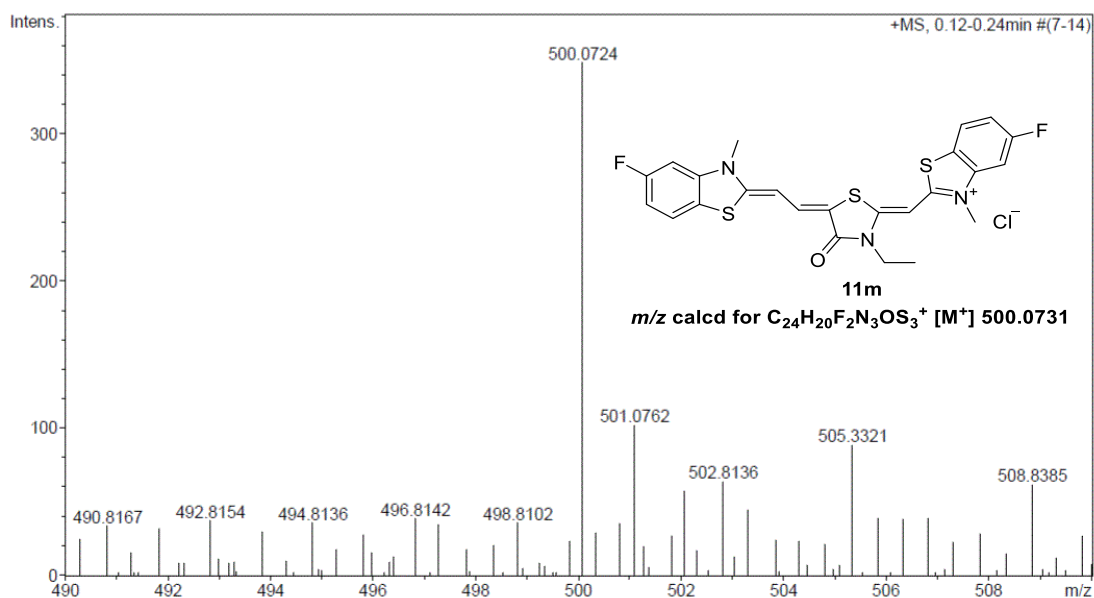


Figure 124 HRMS spectrum of 11m



2-(3-Ethyl-5-(2-(6-fluoro-3-methylbenzo[d]thiazol-2(3H)-ylidene)ethylidene)-4-oxothiazolidin-2-ylidene)methyl)-6-fluoro-3-methylbenzo[d]thiazol-3-ium chloride (11n)

<sup>1</sup>H NMR (400 MHz, DMSO) δ 8.21 (d, *J* = 7.6 Hz, 1H), 7.89 (dd, *J* = 8.2, 4.3 Hz, 1H), 7.68 – 7.51 (m, 3H), 7.37 – 7.11 (m, 2H), 6.74 (s, 1H), 5.86 (d, *J* = 13.1 Hz, 1H), 4.16 (q, *J* = 6.4 Hz, 2H), 4.05 (s, 3H), 3.82 (s, 3H), 1.28 (t, *J* = 6.4 Hz, 3H).

Feb04-2019-tkh003  
TL-B41-P1  
chula\_proton 2D(O/N)

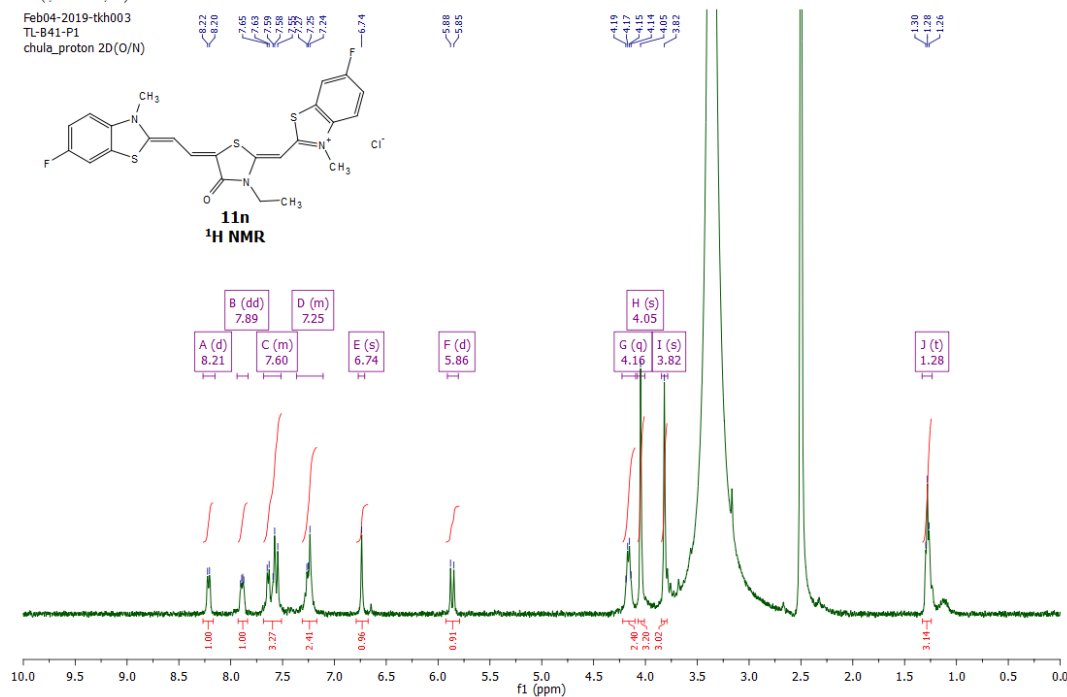


Figure 125 <sup>1</sup>H NMR spectrum of 11n

<sup>13</sup>C NMR (101 MHz, DMSO) δ 163.58 (s), 162.28 (s), 159.36 (d, *J* = 245.3 Hz), 156.98 (s), 148.39 (d, *J* = 246.9 Hz), 137.11 (s), 134.27 (s), 129.56 (s), 127.38 (s), 126.39 (d, *J* = 2.4 Hz), 124.78 (d, *J* = 7.5 Hz), 118.88 (s), 117.31 (d, *J* = 20.7 Hz), 116.89 (d, *J* = 24.8 Hz), 116.24 (d, *J* = 10.0 Hz), 115.09 (d, *J* = 20.3 Hz), 110.22 (d, *J* = 28.6 Hz), 103.34 (s), 90.48 (s), 86.81 (s), 38.96 (s), 35.53 (s), 35.04 (s), 12.29 (s).

Feb04-2019-tkh003  
TL-B41-P1  
chula\_carbon10k 2D(O/N)

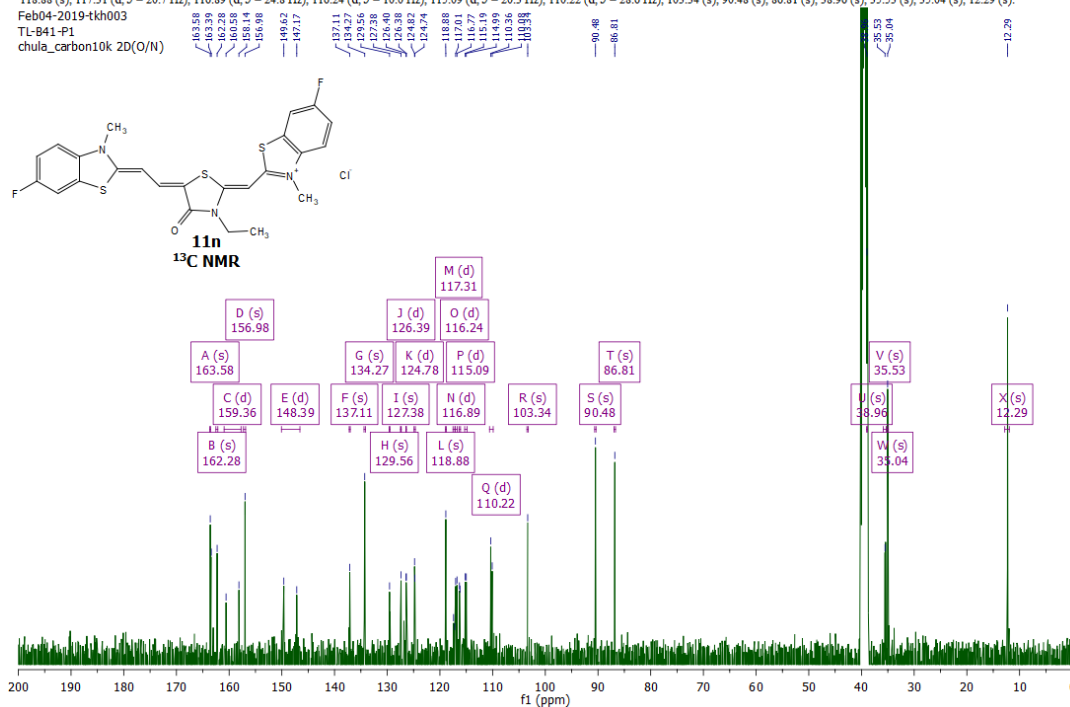
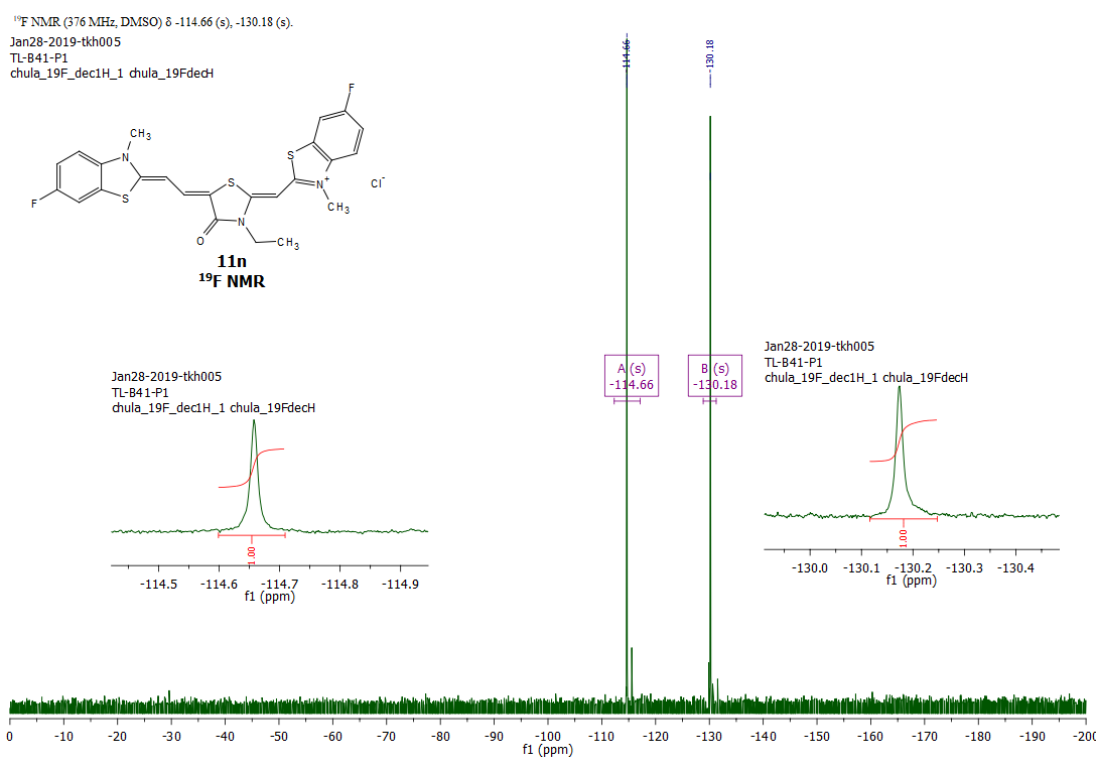
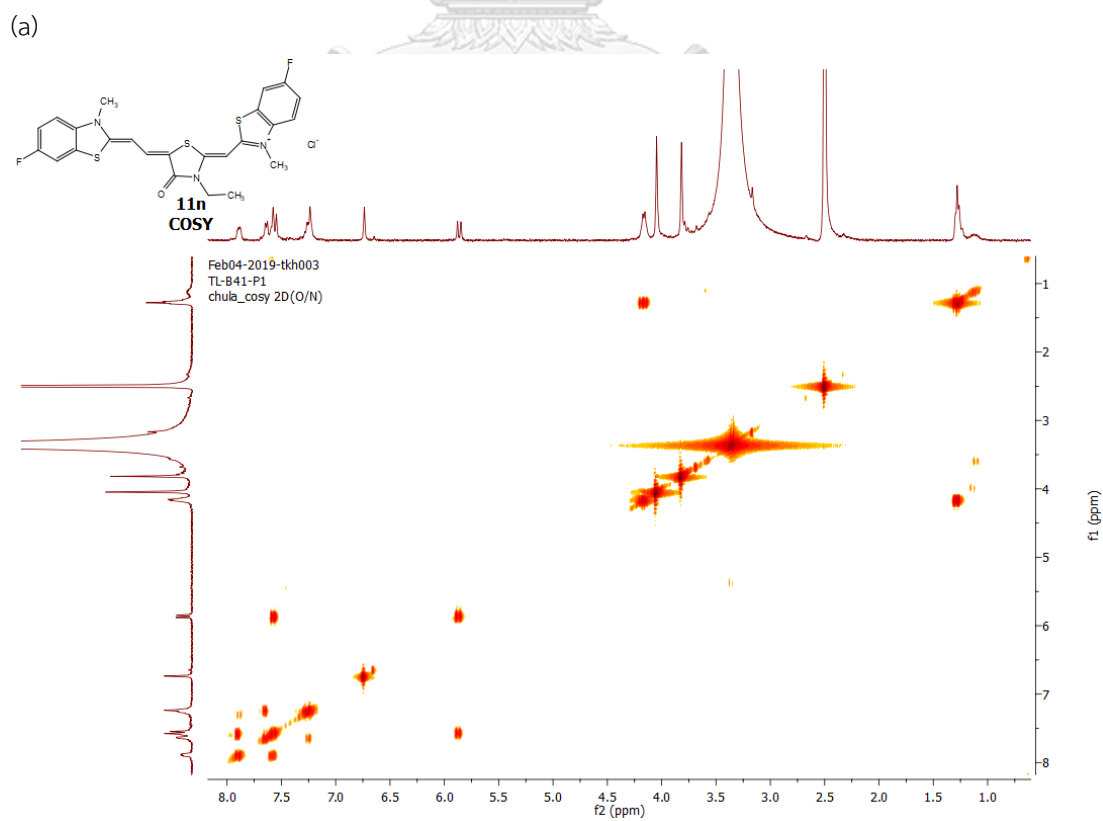
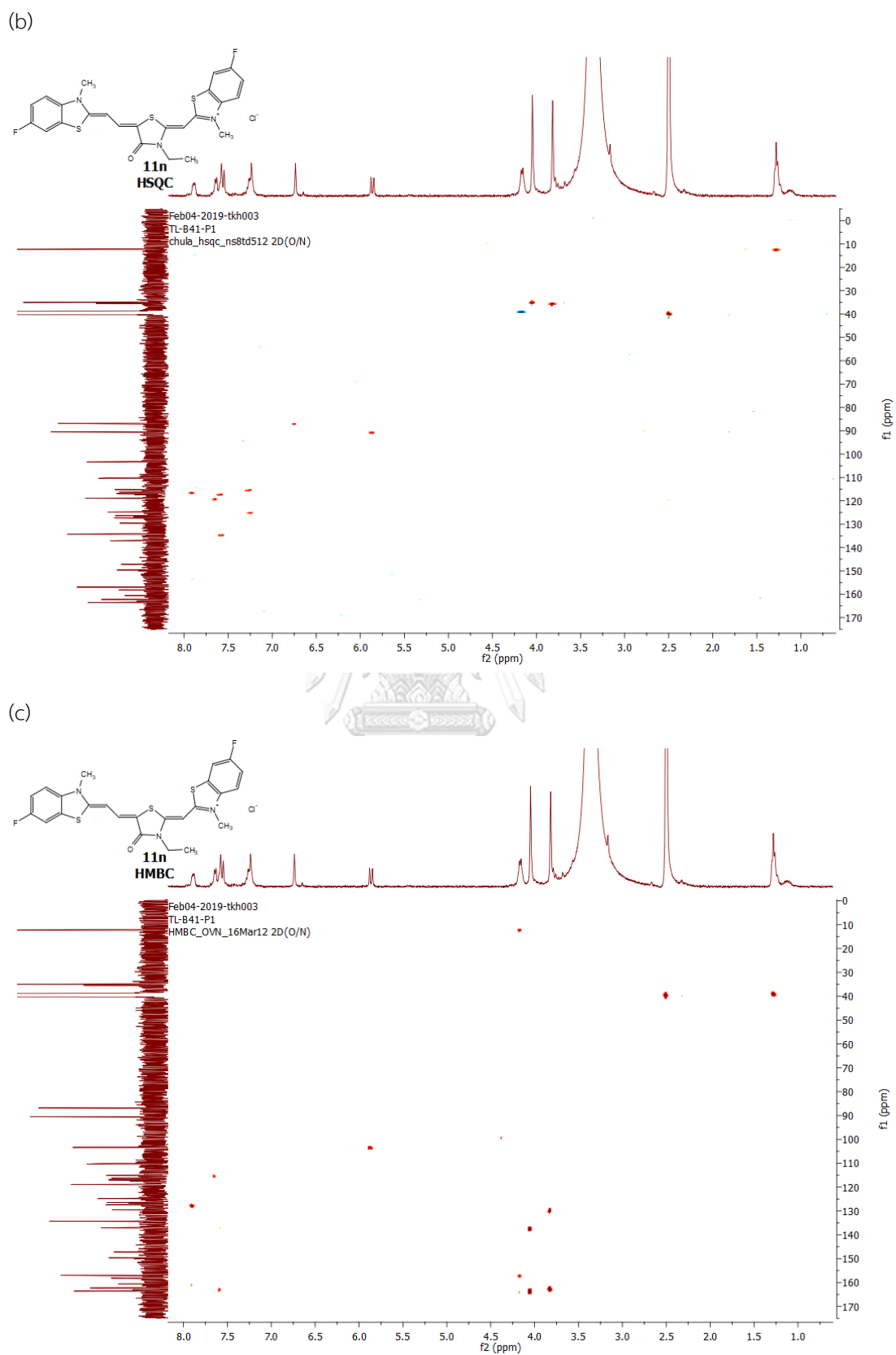


Figure 126 <sup>13</sup>C NMR spectrum of 11n

Figure 127 <sup>19</sup>F NMR spectrum of **11n**

Figure 128 2D NMR spectra of **11n** (a) COSY; (b) HSQC; and (c) HMBC spectrum

## Mass Spectrum List Report

<b>Analysis Info</b>		Acquisition Date	3/18/2019 10:44:05 PM
Analysis Name	D:\Data\Data Service\190318\TL-B41-P1_RD7_01_2350.d	Operator	CU.
Method	nv_pos_5min_profile_190214.m	Instrument / Ser#	microTOF-Q II 10335
Sample Name	TL-B41-P1		
Comment			

### Acquisition Parameter

Source Type	ESI	Ion Polarity	Positive	Set Nebulizer	3.0 Bar
Focus	Not active	Set Capillary	4000 V	Set Dry Heater	200 °C
Scan Begin	100 m/z	Set End Plate Offset	-500 V	Set Dry Gas	8.0 l/min
Scan End	1500 m/z	Set Collision Cell RF	250.0 Vpp	Set Divert Valve	Waste

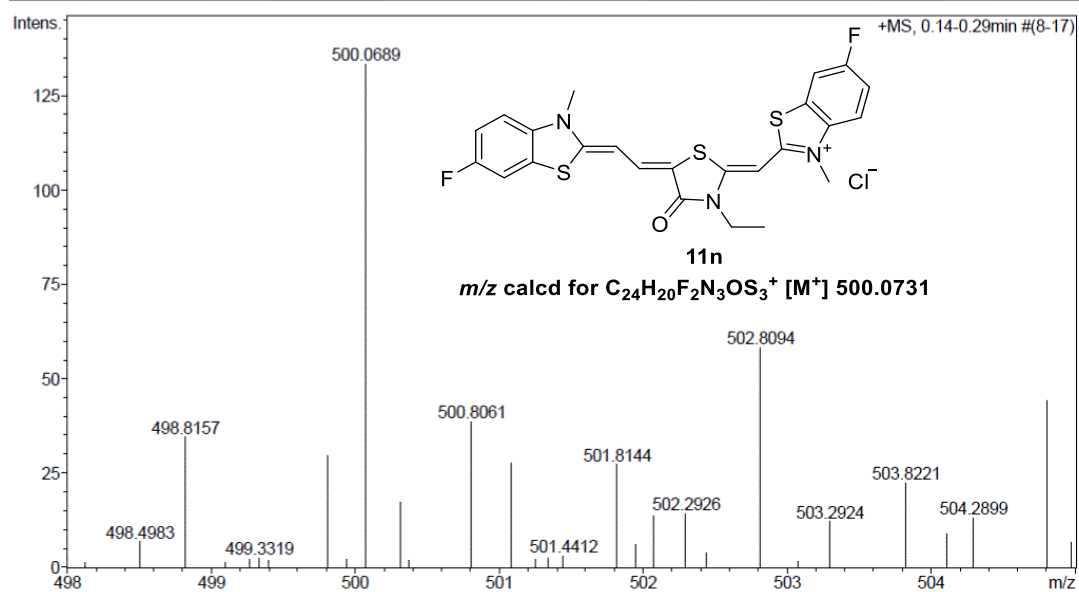


Figure 129 HRMS spectrum of 11n

2-(3-Ethyl-5-(2-(5-fluoro-3-methylbenzo[d]thiazol-2(3H)-ylidene)ethylidene)-4-oxothiazolidin-2-ylidene)methyl)-6-fluoro-3-methylbenzo[d]thiazol-3-ium chloride (11o)

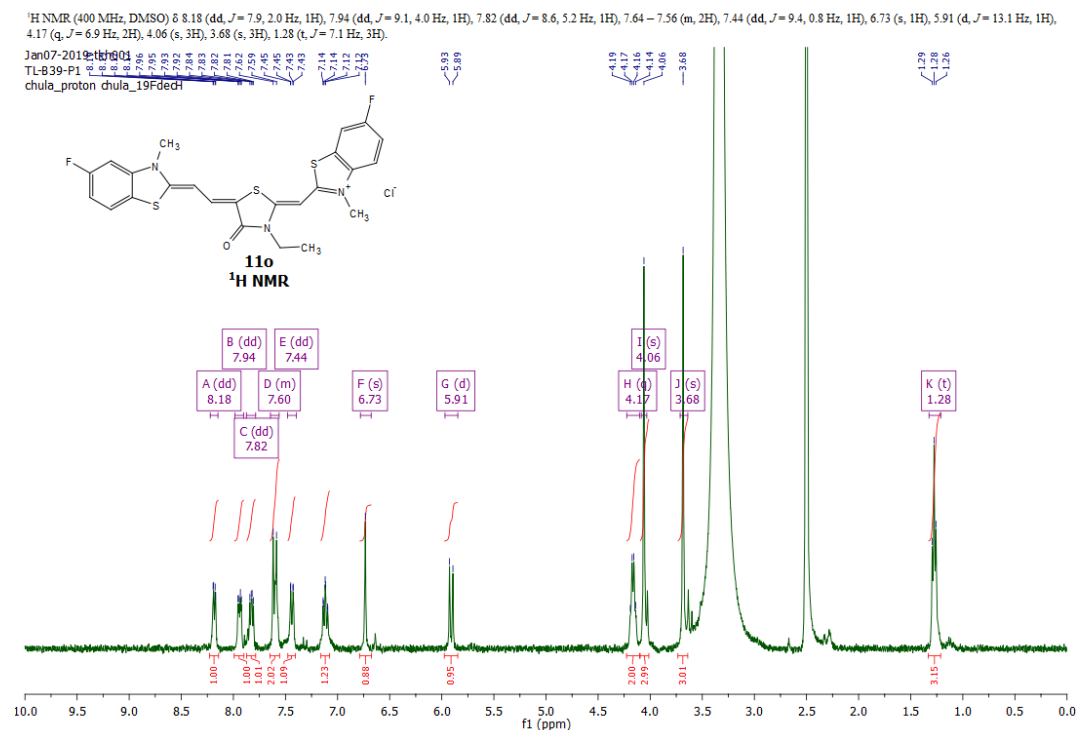


Figure 130 <sup>1</sup>H NMR spectrum of 11o

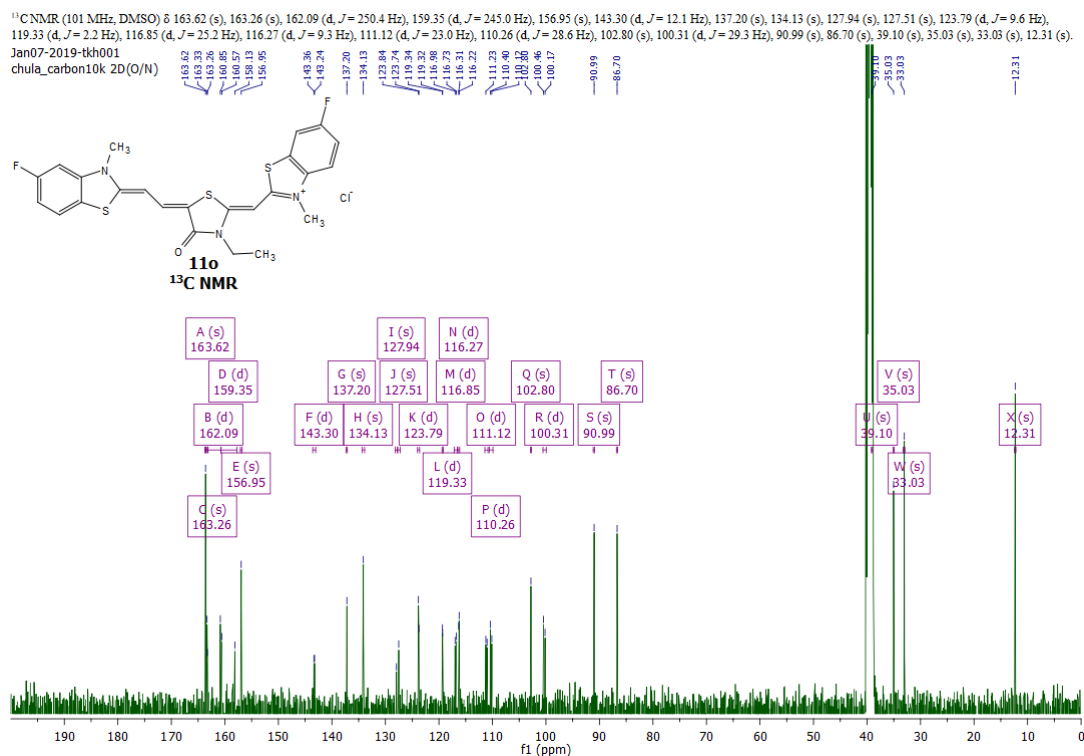
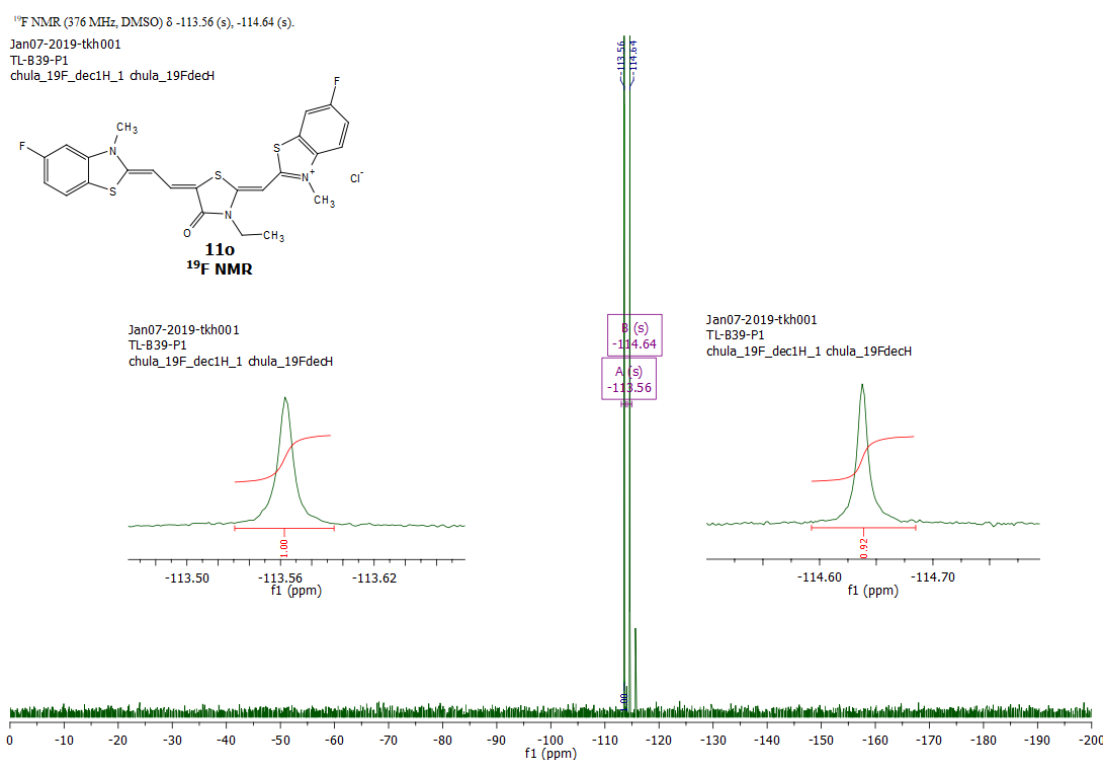
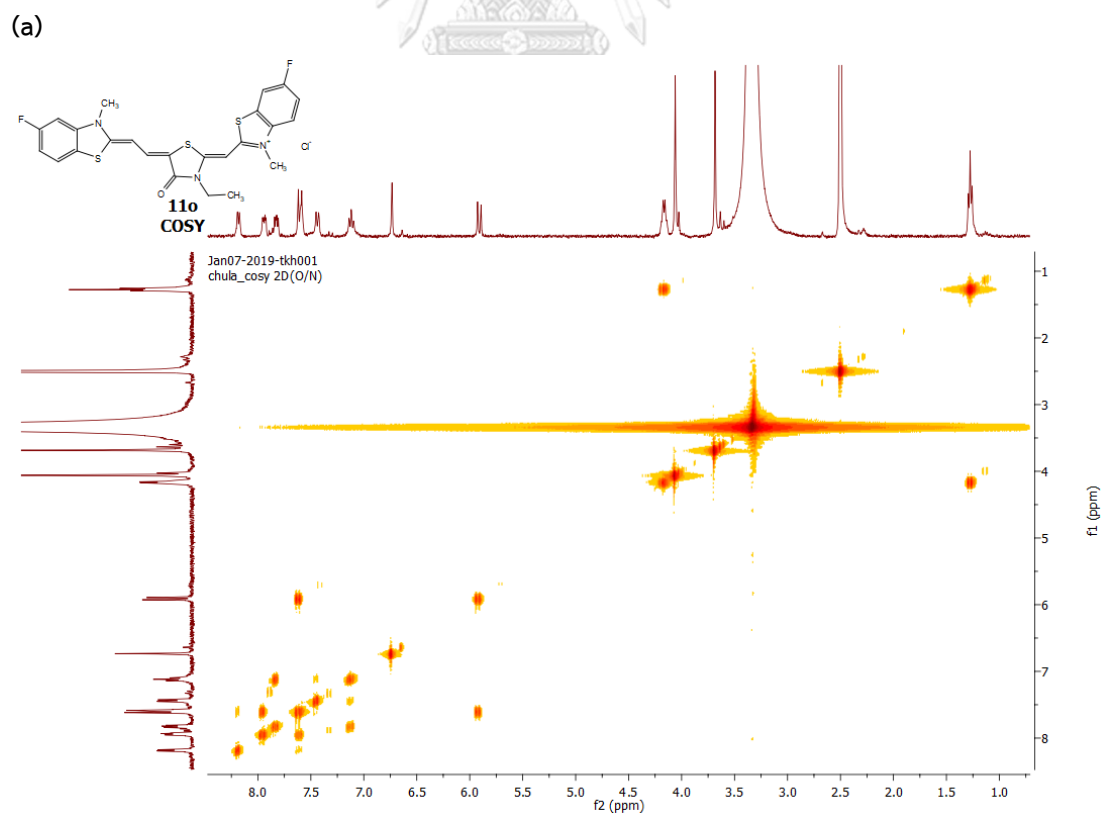
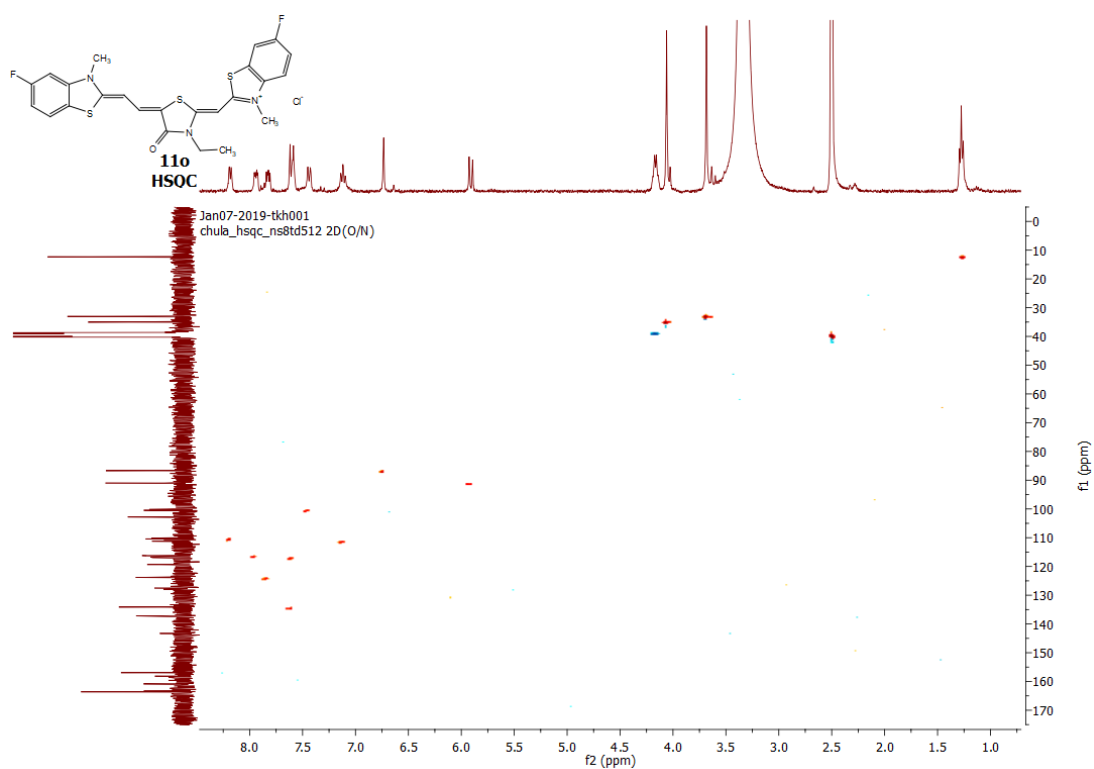


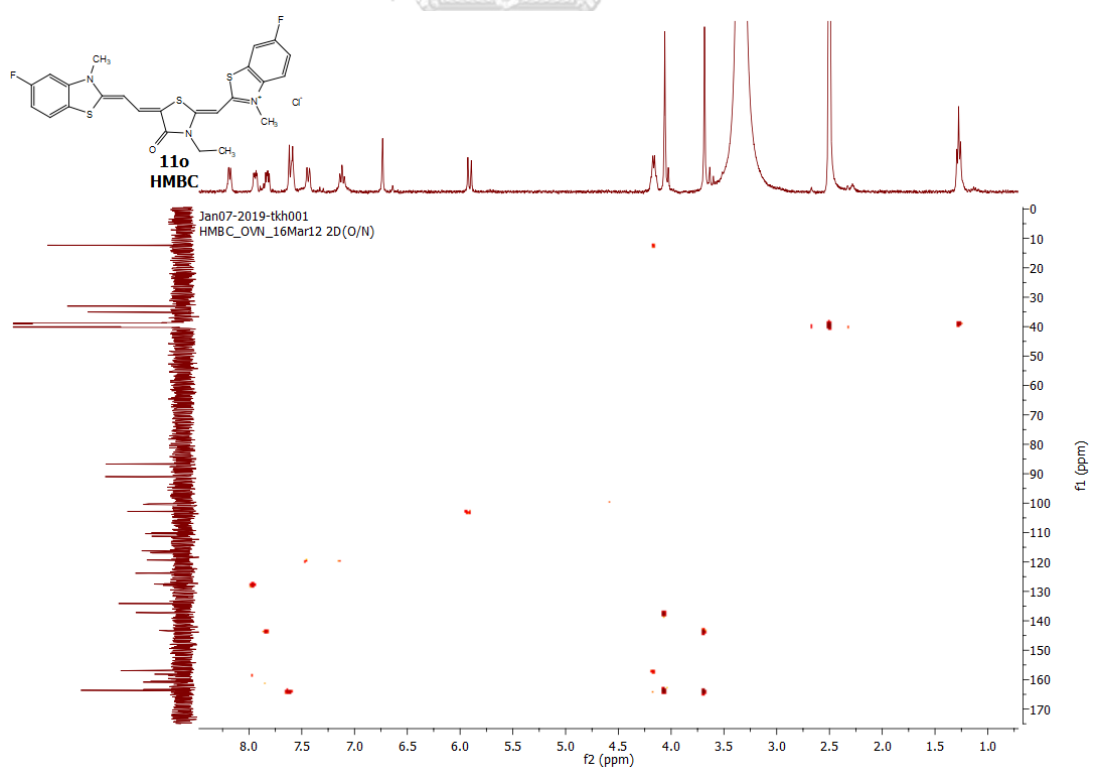
Figure 131 <sup>13</sup>C NMR spectrum of 11o

Figure 132 <sup>19</sup>F NMR spectrum of 11o

(b)



(c)

Figure 133 2D NMR spectra of **11o** (a) COSY; (b) HSQC; and (c) HMBC spectrum

## Mass Spectrum List Report

### Analysis Info

Analysis Name D:\Data\Data Service\190813\TL-B39-P1\_RA8\_01\_2876.d  
Method nv\_pos\_6min\_profile\_wguardcol\_190624.m  
Sample Name TL-B39-P1  
Comment

Acquisition Date 8/13/2019 4:33:05 PM

Operator CU.  
Instrument / Ser# micrOTOF-Q II 10335

### Acquisition Parameter

Source Type	ESI	Ion Polarity	Positive	Set Nebulizer	3.0 Bar
Focus	Not active	Set Capillary	4000 V	Set Dry Heater	200 C
Scan Begin	100 m/z	Set End Plate Offset	-500 V	Set Dry Gas	8.0 l/min
Scan End	1500 m/z	Set Collision Cell RF	250.0 Vpp	Set Divert Valve	Waste

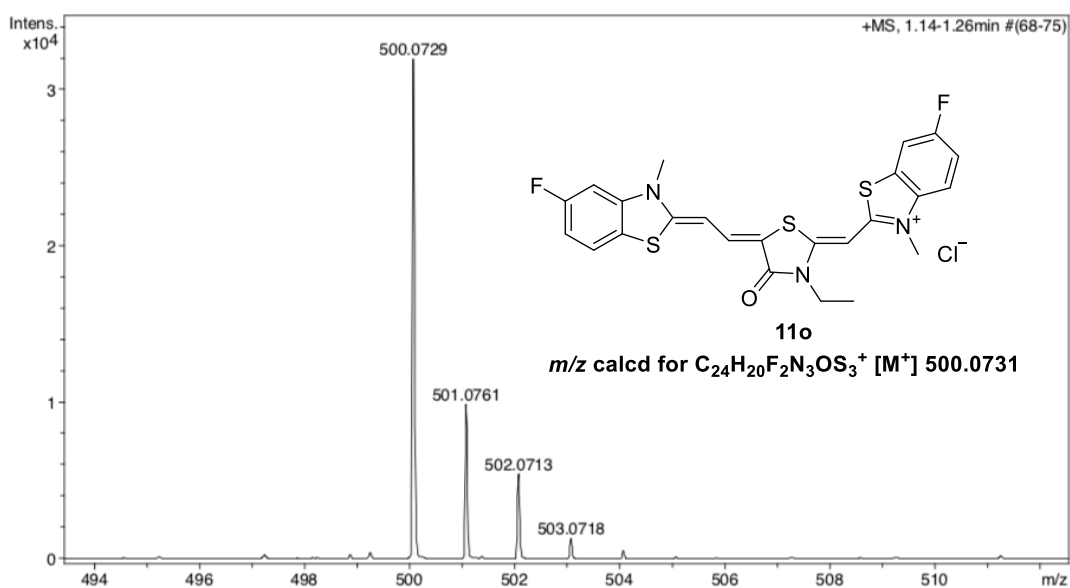


Figure 134 HRMS spectrum of 11o



2-(3-Ethyl-5-(2-(6-fluoro-3-methylbenzo[d]thiazol-2(3H)-ylidene)ethylidene)-4-oxothiazolidin-2-ylidene)methyl)-5-fluoro-3-methylbenzo[d]thiazol-3-ium chloride (11p)

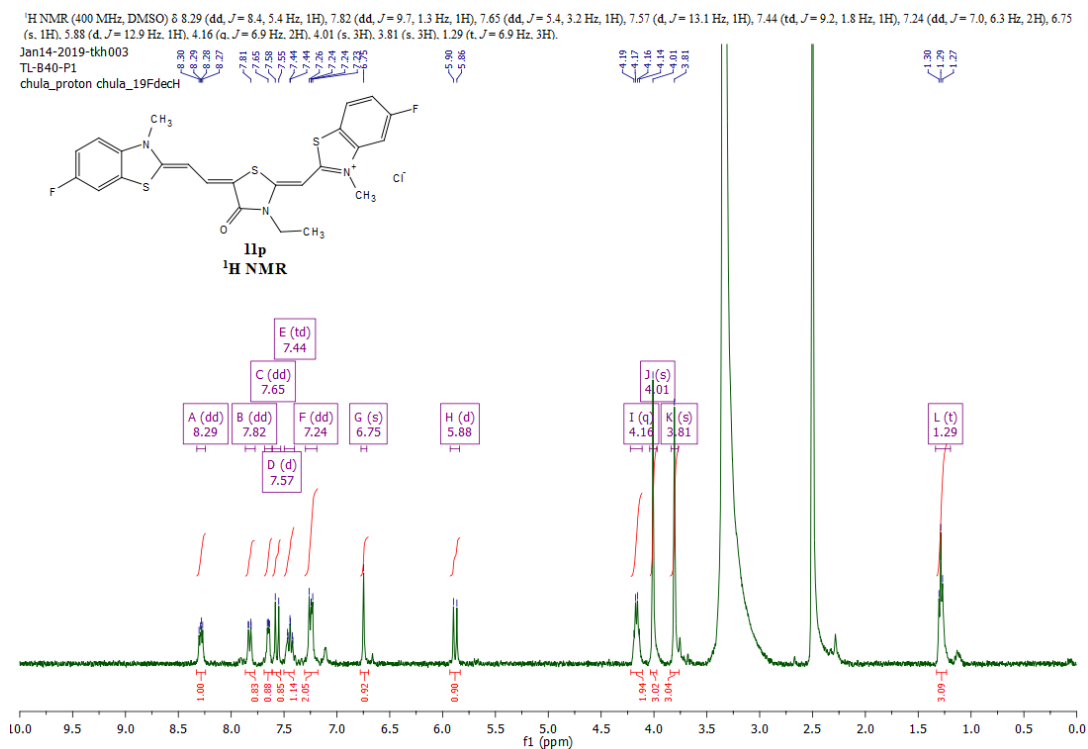


Figure 135 <sup>1</sup>H NMR spectrum of 11p

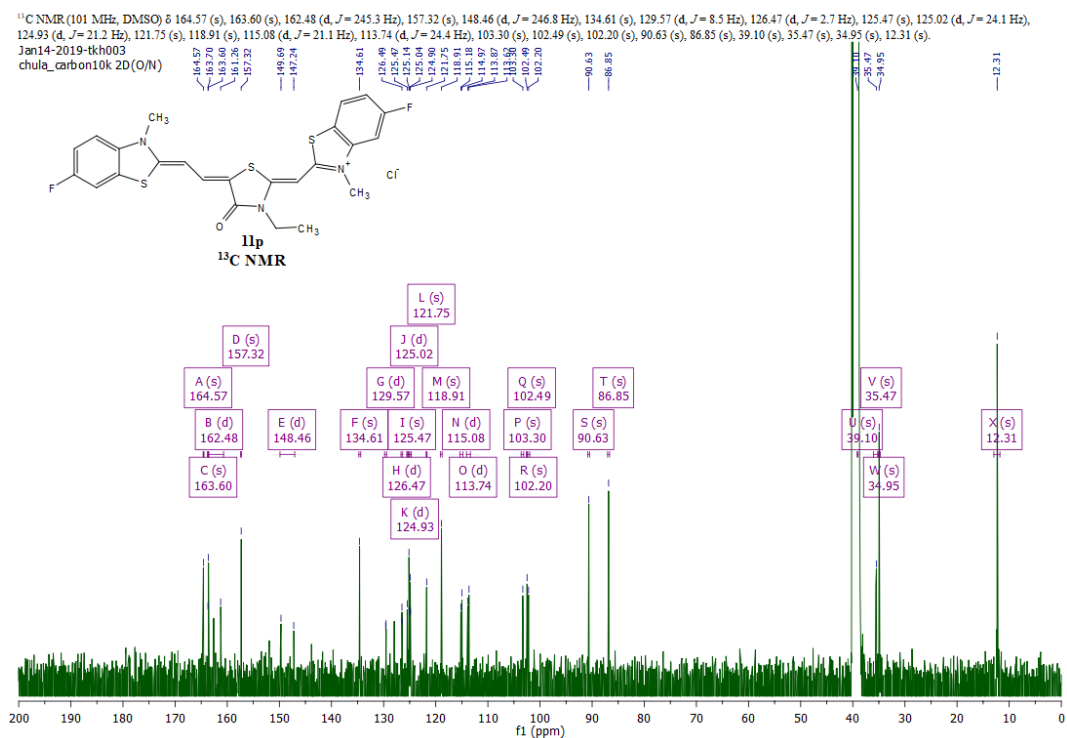
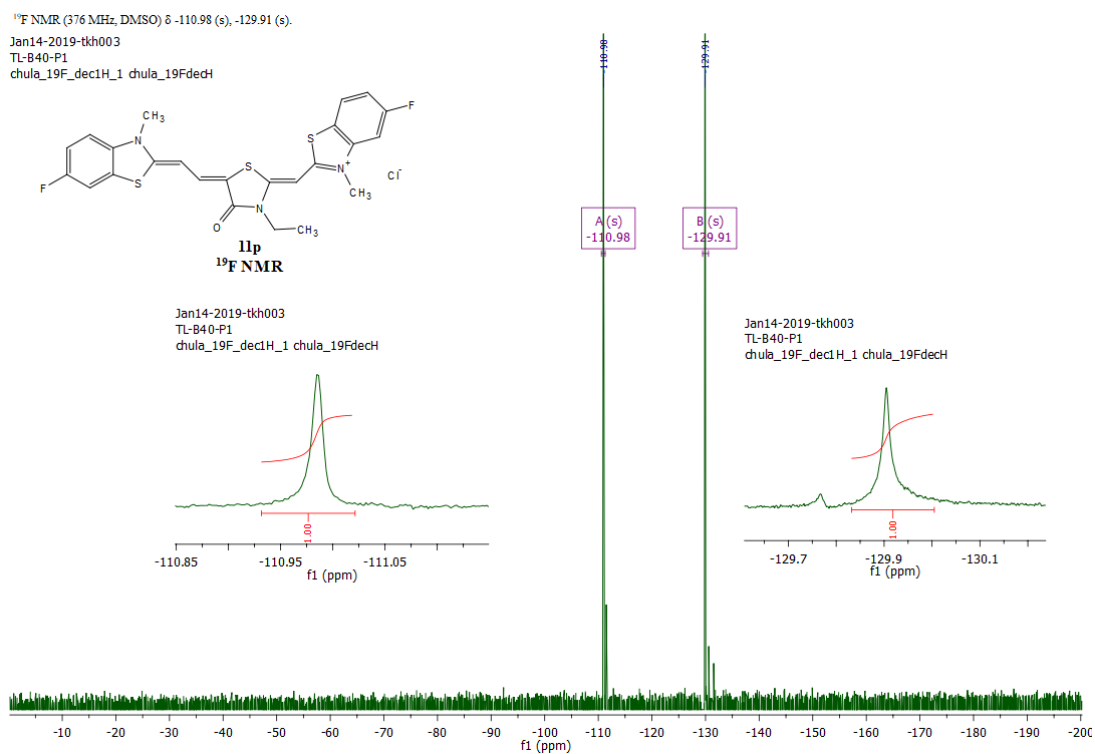
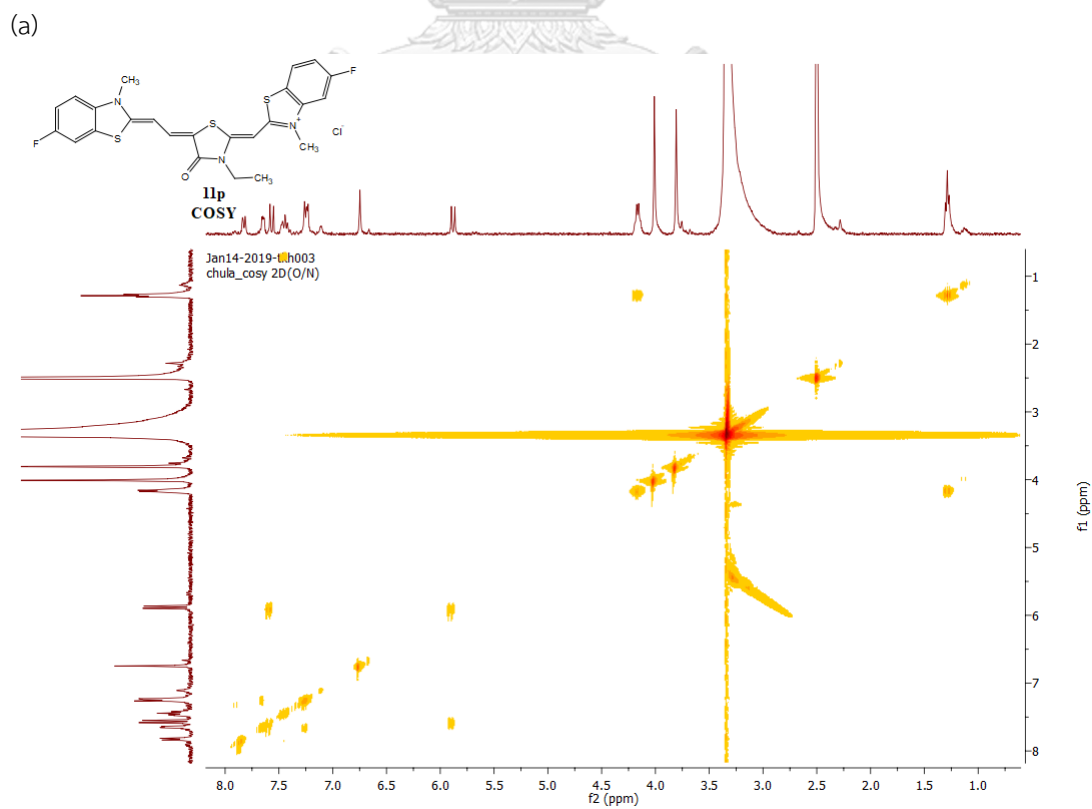
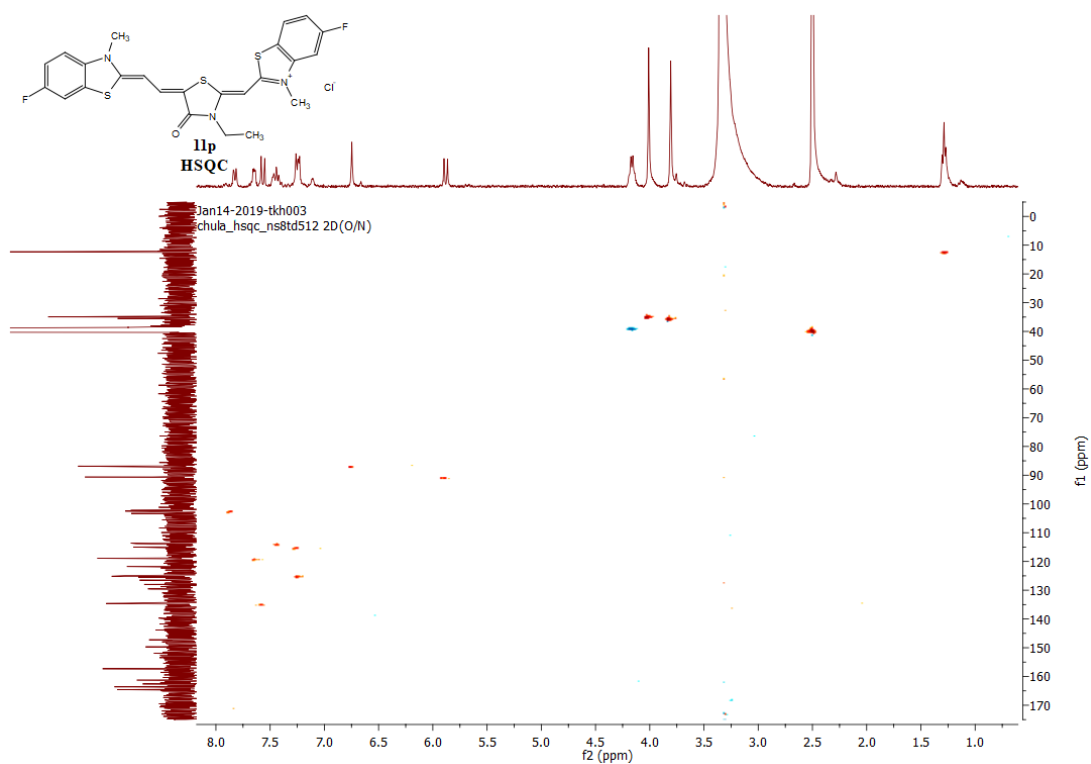


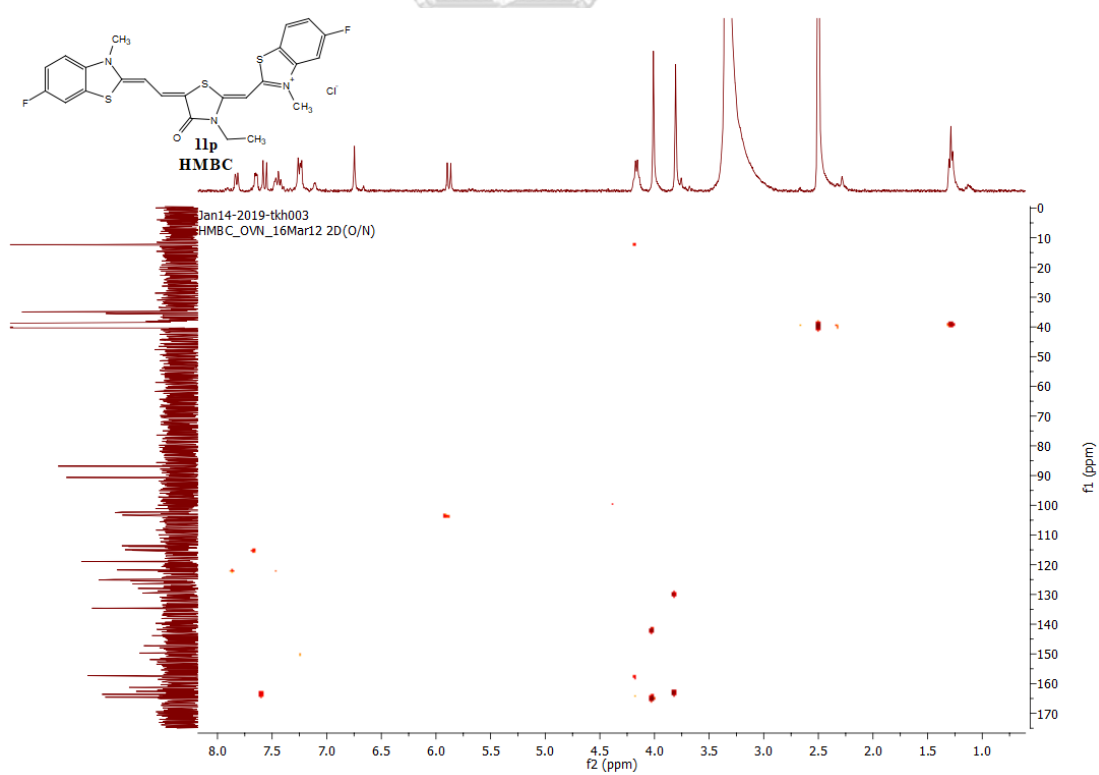
Figure 136 <sup>13</sup>C NMR spectrum of 11p

Figure 137 <sup>19</sup>F NMR spectrum of 11p

(b)



(c)

Figure 138 2D NMR spectra of **11p** (a) COSY; (b) HSQC; and (c) HMBC spectrum

## Mass Spectrum List Report

**Analysis Info**  
Analysis Name D:\Data\Data Service\190318\TL-B40-P1\_RD6\_01\_2349.d  
Method nv\_pos\_5min\_profile\_190214.m  
Sample Name TL-B40-P1  
Comment  
Acquisition Date 3/18/2019 10:37:47 PM  
Operator CU.  
Instrument / Ser# micrOTOF-Q II 10335

**Acquisition Parameter**

Source Type	ESI	Ion Polarity	Positive	Set Nebulizer	3.0 Bar
Focus	Not active	Set Capillary	4000 V	Set Dry Heater	200 °C
Scan Begin	100 m/z	Set End Plate Offset	-500 V	Set Dry Gas	8.0 l/min
Scan End	1500 m/z	Set Collision Cell RF	250.0 Vpp	Set Divert Valve	Waste

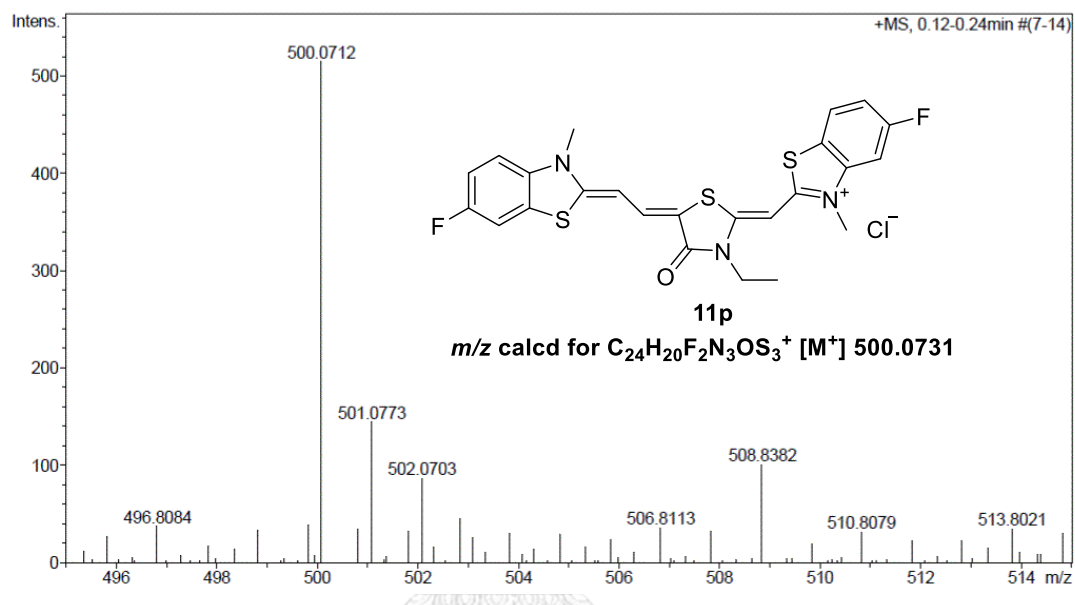


Figure 139 HRMS spectrum of 11p

2-(3-Ethyl-5-(2-(3-methyl-6-(trifluoromethyl)benzo[d]thiazol-2(3H)-ylidene)ethylidene)-4-oxothiazolidin-2-ylidene)methyl)-5-fluoro-3-methylbenzo[d]thiazol-3-ium chloride (11q)

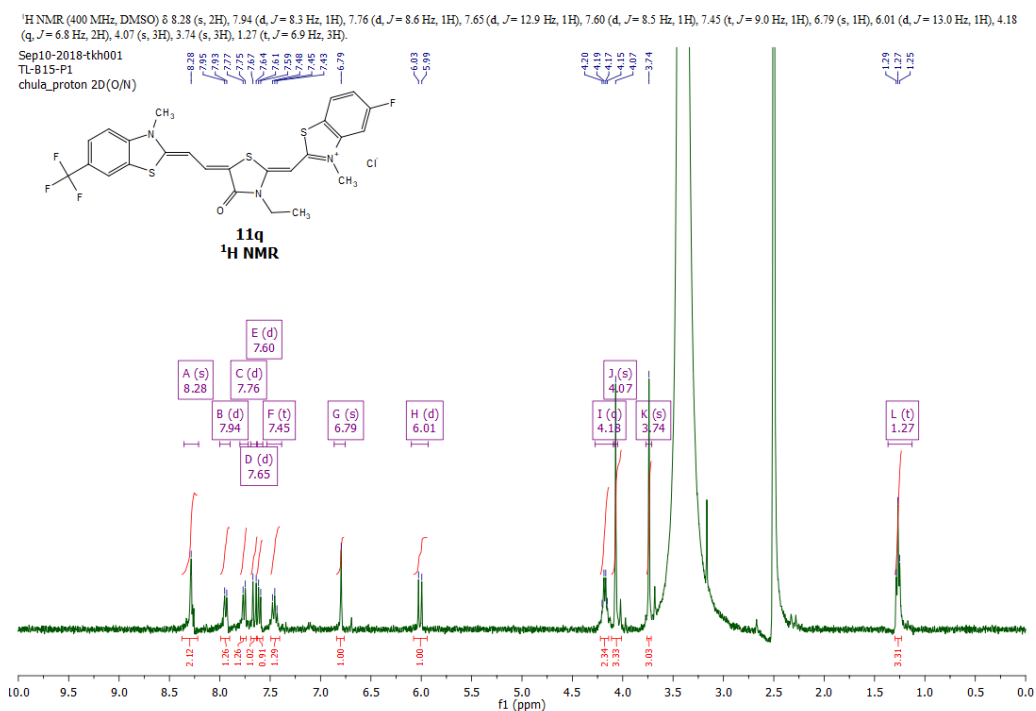


Figure 140 <sup>1</sup>H NMR spectrum of 11q

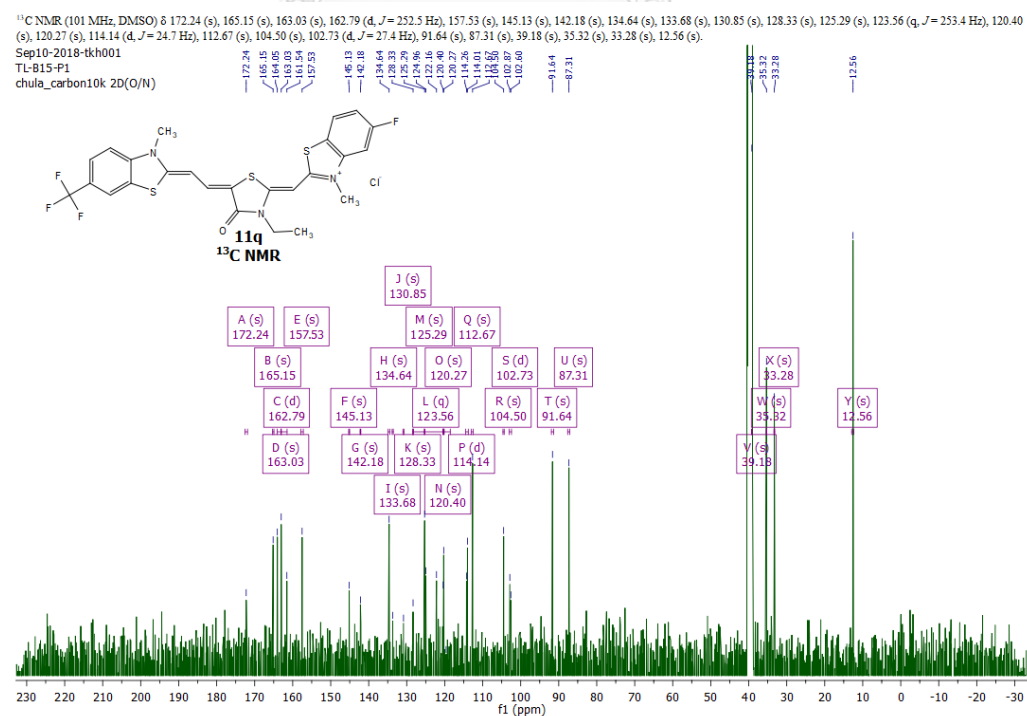
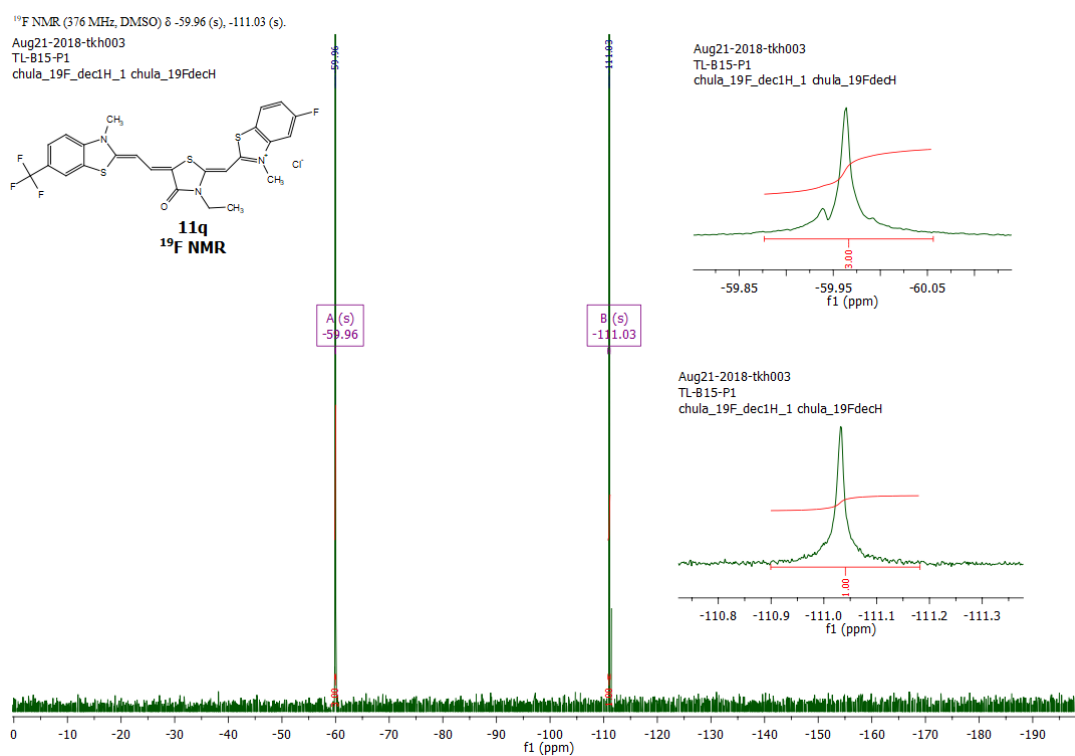
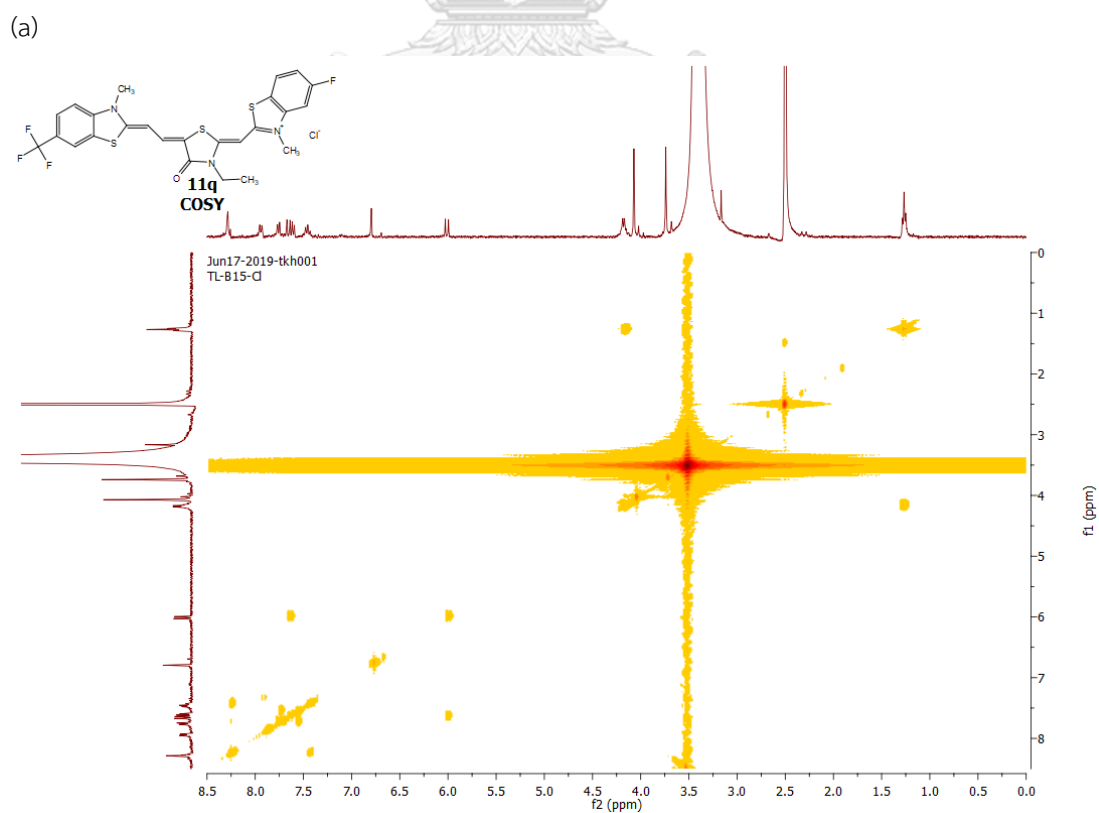
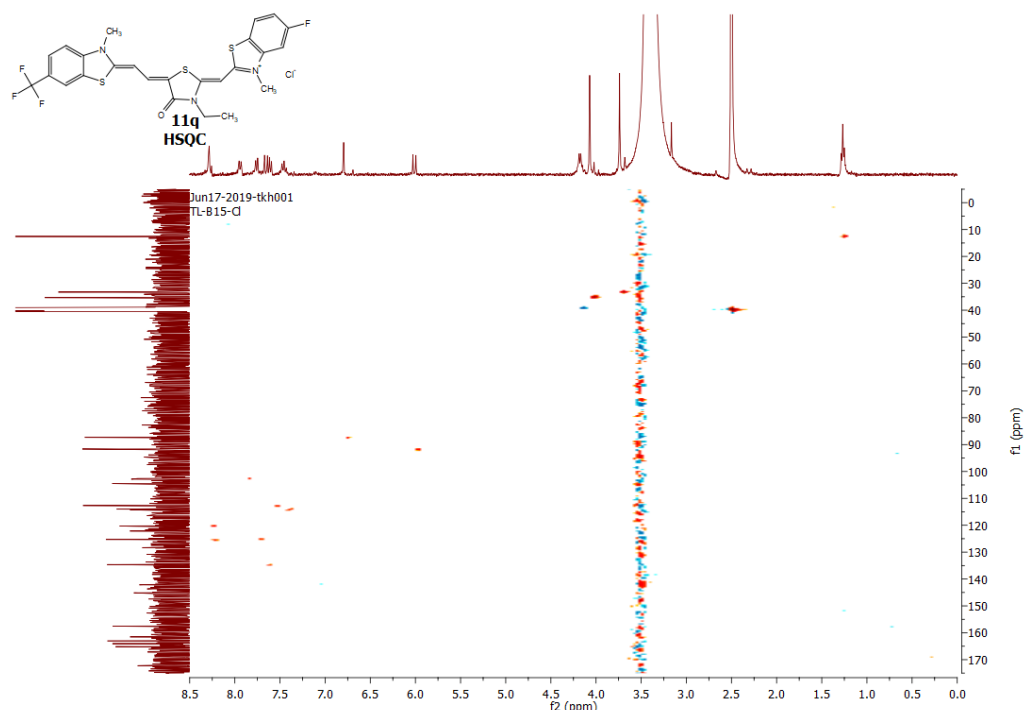


Figure 141 <sup>13</sup>C NMR spectrum of 11q

Figure 142 <sup>19</sup>F NMR spectrum of 11q

(b)



(c)

### Mass Spectrum List Report

Analysis Info		Acquisition Date	
Analysis Name	D:\Data\Data Service\190813\TL-B15-P1_RA7_01_2874.d	8/13/2019 4:20:15 PM	
Method	nv_pos_6min_profile_wguardcol_190624.m	Operator	CU.
Sample Name	TL-B15-P1	Instrument / Ser#	micrOTOF-Q II 10335
Comment			

Acquisition Parameter					
Source Type	ESI	Ion Polarity	Positive	Set Nebulizer	3.0 Bar
Focus	Not active	Set Capillary	4000 V	Set Dry Heater	200 °C
Scan Begin	100 m/z	Set End Plate Offset	-500 V	Set Dry Gas	8.0 l/min
Scan End	1500 m/z	Set Collision Cell RF	250.0 Vpp	Set Divert Valve	Waste

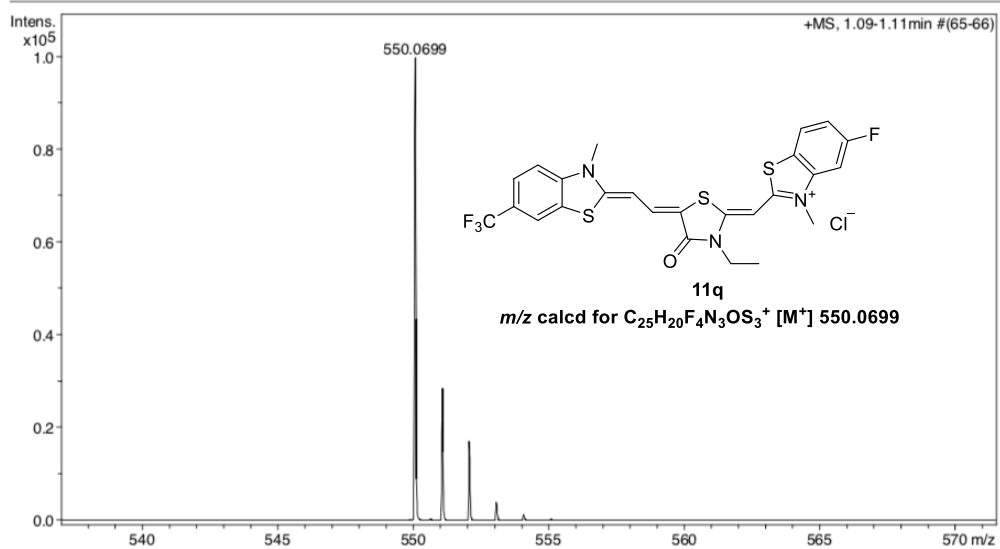


Figure 143 2D NMR spectra of **11q** (a) COSY; and (b) HSQC spectrum; and (c) HRMS spectrum

## VITA

**NAME** Thitiya Lasing

**DATE OF BIRTH** 12 April 1995

**PLACE OF BIRTH** Phetchabun, Thailand

**INSTITUTIONS ATTENDED** Bachelor of Science (B.Sc.) in Chemistry, Faculty of Science, Naresuan University, Thailand

**HOME ADDRESS** 68/1 Village No.9, Thadang Sub-district, Nongphai District, Phetchabun Province, Thailand 67140

**PUBLICATION** Lasing, T., Phumee, A., Siriyasatien, P., Chitchak, K., Vanalabhpatana, P., Mak, K.-K., Hee Ng, C.; Vilaivan, T., Khotavivattana, T. 2019. Synthesis and antileishmanial activity of fluorinated rhodocyanine analogues: the 'fluorine-walk' analysis. *Bioorganic & Medicinal Chemistry*, 115187. doi:<https://doi.org/10.1016/j.bmc.2019.115187>